Biogeomorphic feedback drives dune development along nourished coastlines

Corjan Nolet

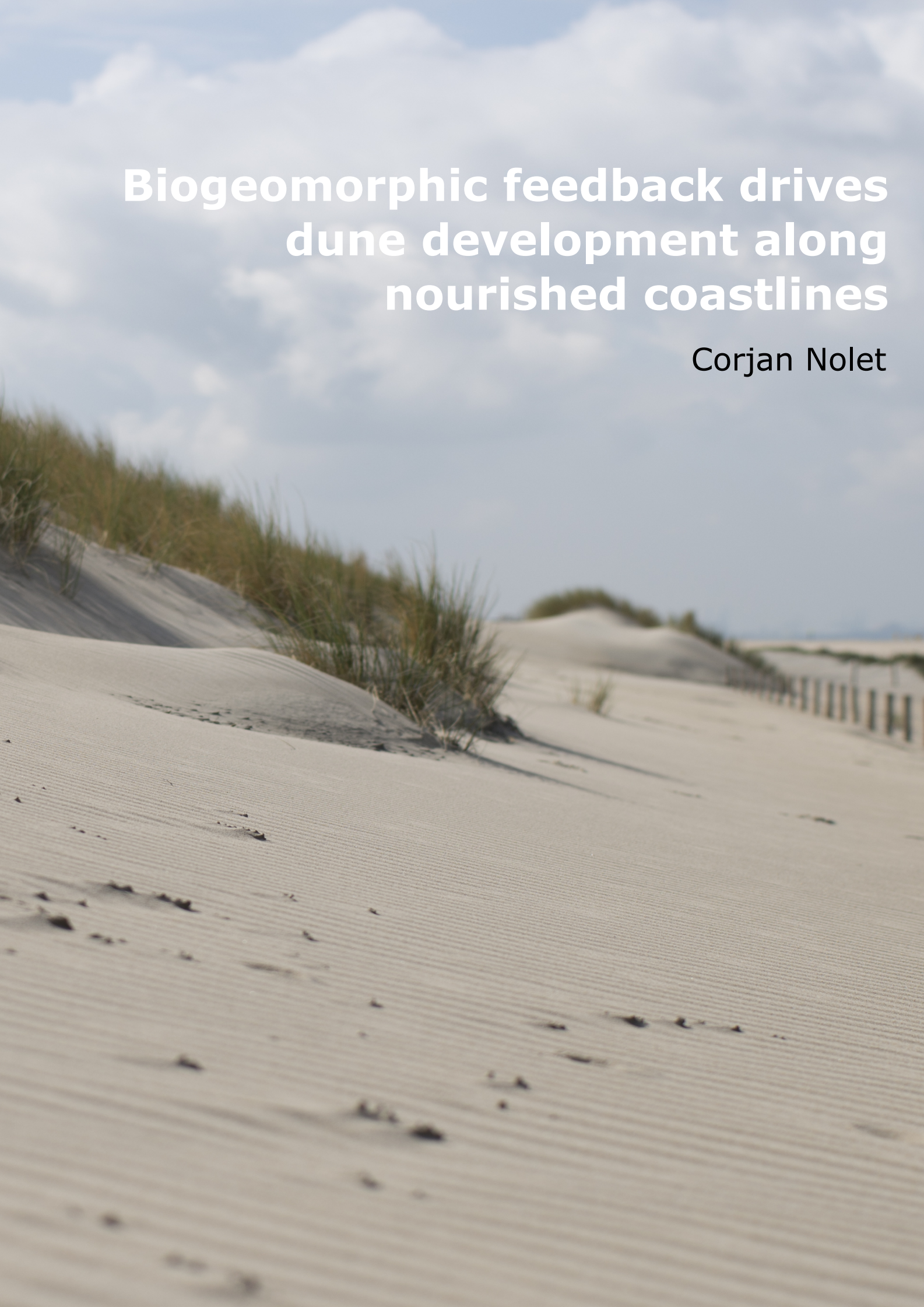

Propositions

1. In the Netherlands, the capacity of coastal dunes to provide coastal safety solely depends on the positive biogeomorphic feedback between wind-blown sand and growth response of European marram grass.
   (this thesis)

2. In nourished coastal environments, the saltation mass flux is better explained by a quadratic than a cubic dependence to shear velocity.
   (this thesis)

3. Scientists are better off focusing on medium resolution data because the highest resolution datasets are often riddled with noise and variability.

4. *Natura non facit saltus* ('nature does not make jumps') has been an influential but ultimately incorrect principle of natural philosophy.

5. Contrary to popular belief, future conflicts will occur over access to sand instead of freshwater resources.

6. A three-month long Covid-19 lockdown makes you realize that home is not an office.

Propositions belonging to the thesis, entitled

Biogeomorphic feedback drives dune development along nourished coastlines

Corjan Nolet
Wageningen, 3 December 2020

Biogeomorphic feedback drives dune development along nourished coastlines

Corjan Nolet

Thesis committee

Promotor:
Prof. Dr C.J. Ritsema
Professor of Soil Physics and Land Management Group
Wageningen University & Research

Co-promotors:
Dr. M.J.P.M. Riksen
Assistant Professor, Soil Physics and Land Management Group
Wageningen University & Research

Other members:
Prof. Dr J. Wallinga, Wageningen University & Research
Prof. Dr D. Van der Wal, Twente University, Enschede
Prof. Dr I. Delgado-Fernandez, Edge Hill University, Ormskirk, UK
Dr A.C.W. Baas, King's College London, UK

This research was conducted under the auspices of the C.T. de Wit Graduate School of Production Ecology & Resource Conservation (PE&RC)

Biogeomorphic feedback drives dune development along nourished coastlines

Corjan Nolet

Thesis
submitted in fulfilment of the requirements for the degree of doctor
at Wageningen University
by the authority of the Rector Magnificus
Prof. Dr A.P.J. Mol,
in the presence of the
Thesis Committee appointed by the Academic Board
to be defended in public
on Thursday 3 December 2020
at 11:00 a.m. in the Aula.

Corjan Nolet
Biogeomorphic feedback drives dune development along nourished coastlines,
135 pages.

PhD thesis, Wageningen University, Wageningen, NL (2020)
With references, with summary in English

ISBN 978-94-6395-567-6
DOI 10.18174/532101

Contents

Chapter 1

Introduction

1.1 Context

1.1.1 Coastal systems in a changing world

Human settlement has long been drawn to coastal areas because of their rich supply of (subsistence) resources and access points to marine trade and transport (McGranahan et al., 2007). The development and utilization of coastal zones has greatly increased over the last decades and coasts are undergoing enormous socioeconomic and environmental changes. Population density is already significantly higher in coastal areas compared to inland areas and there is an ongoing trend of coastal migration associated with global demographic changes (Martínez et al., 2007; Neumann et al., 2015). The low-lying coastal zones, situated below 10 m of elevation, constitutes 2% of the world's land area but contains approximately 10% of the world's population (600 million) based on estimates from the year 2000. And about 65% of the world's large cities, with populations greater than 5 million, are located within the coastal zone (McGranahan et al., 2007).

The high concentration of people and economic activities on and near the coast has had serious environmental consequences. Urban systems have radically altered the flows of water, energy and materials, transforming the pre-existing ecosystems. Onshore and offshore coastal ecosystems are among the most productive in the world but also among the most threatened by human settlement: an estimated one-third of coastal mangrove forests and one-fifth of coral reefs have already been lost due to negative urban impact (McGranahan et al., 2007). Urban development, at the same time, expose coastal populations to an increased risk from flooding, particularly when high tides combine with storm surges and/or high river flows. Water drains more rapidly from built-up land, increasing peak flows and flood risk, particularly if drainage systems are not adapted accordingly. Draining wetlands to accommodate urban expansion is also a common practice, effectively removing an important buffer against tidal floods. Moreover, delta regions across the world are subjected to land compaction and subsidence due to groundwater withdrawal and, often simultaneously, experience reductions in the rate of sediment delivery from their rivers due to large-scale engineering infrastructures (Koster et al., 2020). Besides creating various other problems, these processes lead, in effect, to a relative rise in sea-levels and increasing flood risk.

Due to sea level rise (SLR), low-lying coastal zones across the globe are also increasingly confronted with adverse impacts related to climate change, such as coastal erosion due to (temporary) flooding and inundation as well as permanent submergence of previously subaerial land (Wong et al., 2014; Haasnoot et al., 2020). Global sea levels are rising due to thermal expansion as the oceans warm, together with (increasing amounts of) meltwater coming off glaciers, icecaps, and ice sheets of Greenland and Antarctica. Regional variations in the rate of rise occur because of ocean circulation patterns and glacial isostatic rebound and tectonic movement (e.g., Nicholls and Cazenave, 2010; Zhang and Church, 2012). Global mean sea levels, according to assessment by the Intergovernmental Panel on Climate Change (IPCC), are projected to rise significantly under the greenhouse gas emission scenarios RCP 4.5 and 8.5 (with RCP for Representative Concentration Pathway, see Fig. 1.1). Under the high emission scenario RCP 8.5 a global mean SLR up to 1.1 m for 2100 is projected, with an increasing

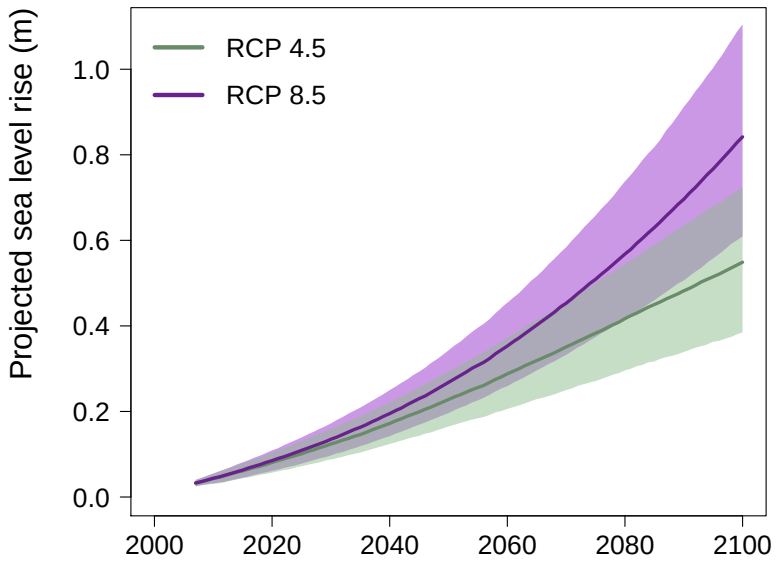

Figure 1.1: Projected global mean sea level rise (m) with uncertainty bands up to the year 2100 under Representative Concentration Pathway (RCP) 4.5 and 8.5

probability that SLR will be even higher due to accelerated ice sheet melting (e.g., DeConto and Pollard, 2016; Bakker et al., 2017). The magnitude and rate of this rise will strongly depend on changes in global and regional temperature, altered oceanographic dynamical patterns near Antarctica and the corresponding response of the Antarctica ice cap, which are all closely linked to greenhouse gas emissions (Haasnoot et al., 2020).

About one third of the low-lying coastal zones is constituted of sandy beaches, barrier islands, and associated sand dunes. Globally an estimated 30-35% of the ice-free coastal shorelines are therefore considered sandy (e.g., Hardisty, 1994; Luijendijk et al., 2018). Even though sandy coastal systems often exhibit distinct seasonal changes, beaches and dunes across the world have in general undergone net erosion over the past century or longer (e.g. see Bird (2011) for an overview), due to cumulative impacts arising from human activities and climate-related drivers (Crain et al., 2009; Wong et al., 2014). Coastal systems may either undergo landward retreat under rising sea levels or experience so-called 'coastal squeeze' when the eroding shoreline approaches hard, immobile structures such as artificial seawalls or natural cliffs. Sandy beaches, in these instances, will narrow due to the resulting sediment deficit and produce adverse impacts such as habitat destruction for benthic organisms in the littoral zone (Jackson and McIlvenny, 2011). Ultimately, sand dunes may get completely removed as the beach continues to erode and narrow during storm surges, exposing the hinterland to inundation and flooding if recovery does not occur before the next storm occurs or the adverse impacts are not counteracted by intervention measures such as sand replenishment (e.g., Claudino-Sales et al., 2008; Stronkhorst et al., 2018)

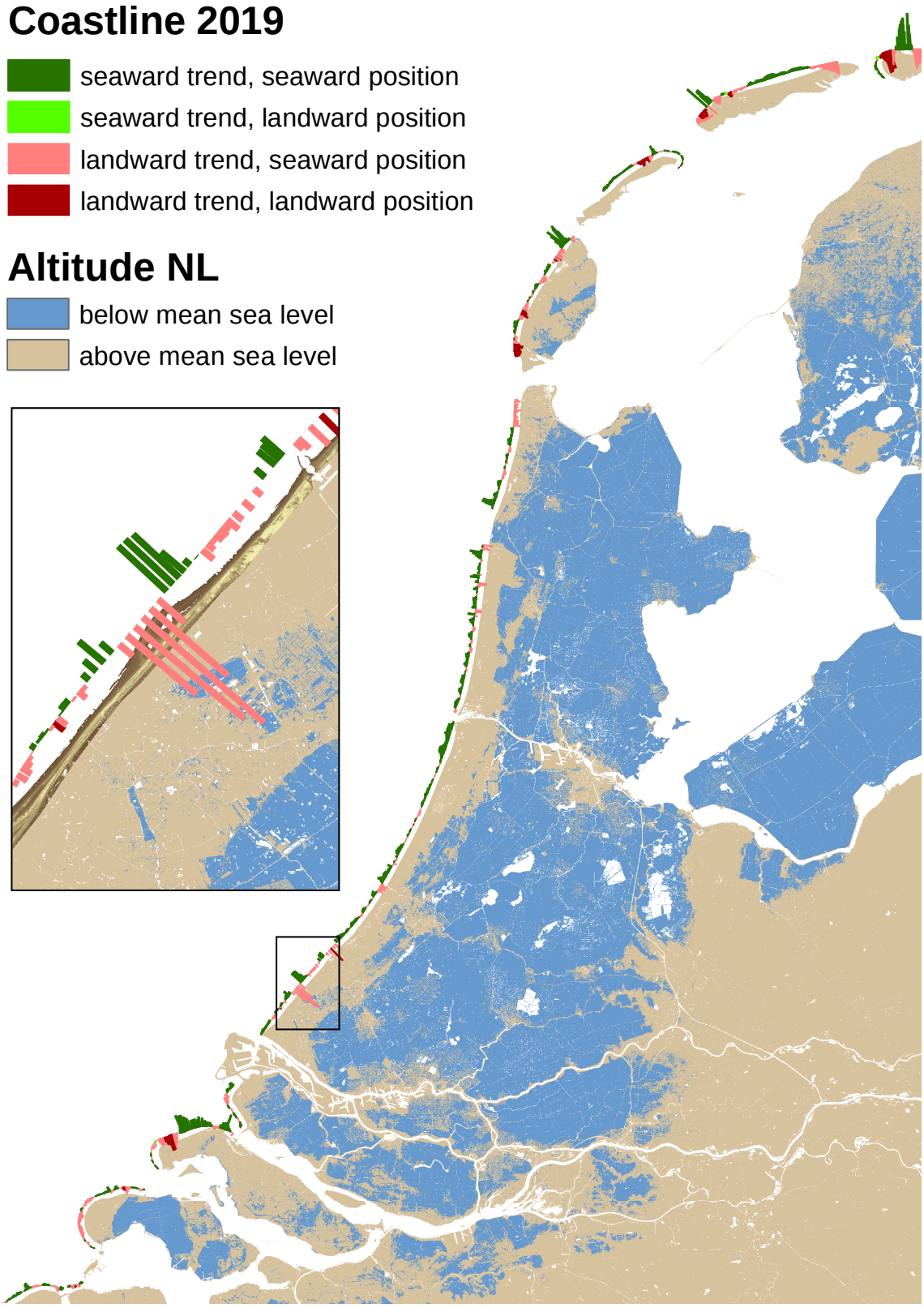

Figure 1.2: Position and trend of the Dutch coastline in relation to a defined reference position. Insert shows the Delfand coast including the mega-scale beach nourishment *Zandmotor*.

1.1.2 Coastal protection in the Netherlands

The Netherlands is situated in the low-lying Rhine-Meuse delta along the North Sea coast. Apart from a number of artificial sea barriers, the approximately 500 km long Dutch coastline can generally be characterized by sandy beaches and dune areas (see also Fig. 1.2). About half of the sandy coastline, however, is subject to structural marine erosion (De Vriend et al., 2015). And with 26% of its area well below mean sea level, the country is particularly susceptible to large scale coastal and river flooding, making flood risk management and adaptation to sea level rise essential for its existence. The focus of Dutch coastal policy has traditionally been on safety from flooding, which was guaranteed by large structures such as sea dikes, groins and other artificial barriers. Nowadays, however, the focus has widened to also include preserving the spatial quality and natural values of the coastal zone (Van Slobbe et al., 2013). It was recognized that coastal dunes, apart from flood defense, also represent unique ecological and recreational values and often serve as an important source for drinking water supply (e.g., De Jong et al., 2014; Keijsers et al., 2015b). By acknowledging sand as 'the carrier of all coastal functions' the principal management practice since 1990 has been to nourish the coastline with sand whenever it was about to retreat beyond a defined reference position (Van Koningsveld et al., 2007). A key component of such a dynamic preservation of the coastline involves utilizing natural processes to further redistribute the sand. By allowing marine and aeolian forces to gradually help shape the coastline, the aim of this building-with-nature engineering strategy is to counteract a negative sediment balance while minimizing adverse effects to the coastal ecosystem (Van Slobbe et al., 2013).

Sand nourishment is now generally the preferred method to compensate for marine erosion in sandy coastal areas. Speybroeck et al. (2006) defines sand nourishment as 'the process of mechanically or hydraulically placing sand on or just in front of an eroding shore to restore or form, and subsequently maintain, an adequate protective or desired recreational beach'. The application as a standard means of coastal protection is a fairly recent phenomenon; in Europe and North America the first large projects were executed only about 50 years ago (Speybroeck et al., 2006). Initially these nourishments were implemented as traditional beach and dune nourishments, where sand is directly placed on the sub-aerial beach and/or the dunes, but at present the majority of the nourishments are implemented as shoreface nourishments (Stive et al., 2013a). By feeding the shoreface with sand the surf zone processes are modified in order to achieve a non-eroding or accretive beach. It is nowadays often favored over beach nourishments as the sand gets exposed to hydrodynamic reworking due to wave action (Grunnet and Ruessink, 2005). This leads to a more natural sorting of the nourishment sand which reduces unwanted effects such as beach armoring and/or cementation (Van der Wal, 2004; Speybroeck et al., 2006), causing a drop in (potential) aeolian and hydrodynamic transport. In contrast to hard protection structures, sand nourishments generally produce smaller disturbances in the dynamics of both sediment and water and thus a natural equilibrium is reached again sooner (Peterson et al., 2000; Speybroeck et al., 2006). Sand nourishments, however, have been shown to significantly reduce the diversity of near-shore benthic fauna (e.g., Van Duin et al., 2004; Van Egmond et al., 2018) and the nourishment have to be applied every 4-5 years to remain effective against marine erosion, which coincides with the time it takes for benthic communities to recover to pre-nourishment conditions (Baptist et al., 2008). Another

negative aspect are the higher costs, as a consequence of the need of replenishment every few years, and the lower applicability on beaches with high wave energy (Stronkhorst et al., 2018).

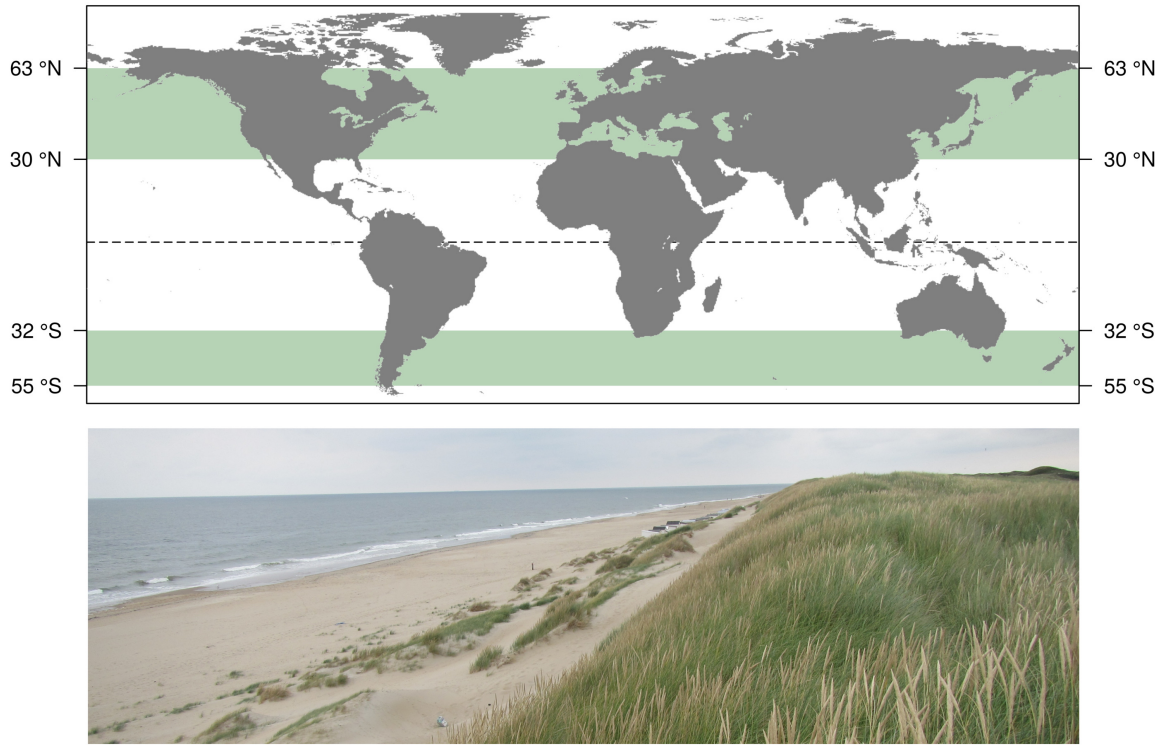

Figure 1.3: Coastal foredunes along the Dutch coast are created and stabilized by European Marram grass (*Ammophila arenaria*). This dune-building grass species thrives in temperate regions in across the world, but is often considered a harmful invasive species outside of Europe.

Due to sea level rise, the annual average sand nourishment volumes on the Dutch coast have increased from 0.4 M m^3yr^{-1} during the period 1952 until 1990, to 2.5 M m^3yr^{-1} between 1991 and 2000, and from 5 to approximately 12 M m^3yr^{-1} between 2001 until now, at an annual cost of around 25 million euro. Except for a few weak links, this nourishment volume currently ensures an overall positive sediment budget for the Dutch coast (see Fig 1.2 and has caused the coastline and dune foot to slowly advance by approximately 0.5 – 1 m^{-1} (Giardino et al., 2011). Recent sea level rise observations and projections, however, have raised concerns about a possible strong acceleration of SLR after 2050 due to rapid mass-loss of the Antarctic ice sheet, which is not accounted for in the current SLR assessments on which Dutch coastal policy relies for its adaptation strategies (Haasnoot et al., 2020). Thus, as SLR accelerates, it is anticipated that sand nourishments need to increase in volume or frequency to combat erosion and maintain the sandy coast. Estimates of required nourishment volumes, however, vary considerably (ranging from 80 up to 280 M m^3yr^{-1}) due to the increasing uncertainty in SLR projections over larger time horizons (e.g., Kabat et al., 2009; Stive et al., 2013a; Haasnoot et al., 2020).

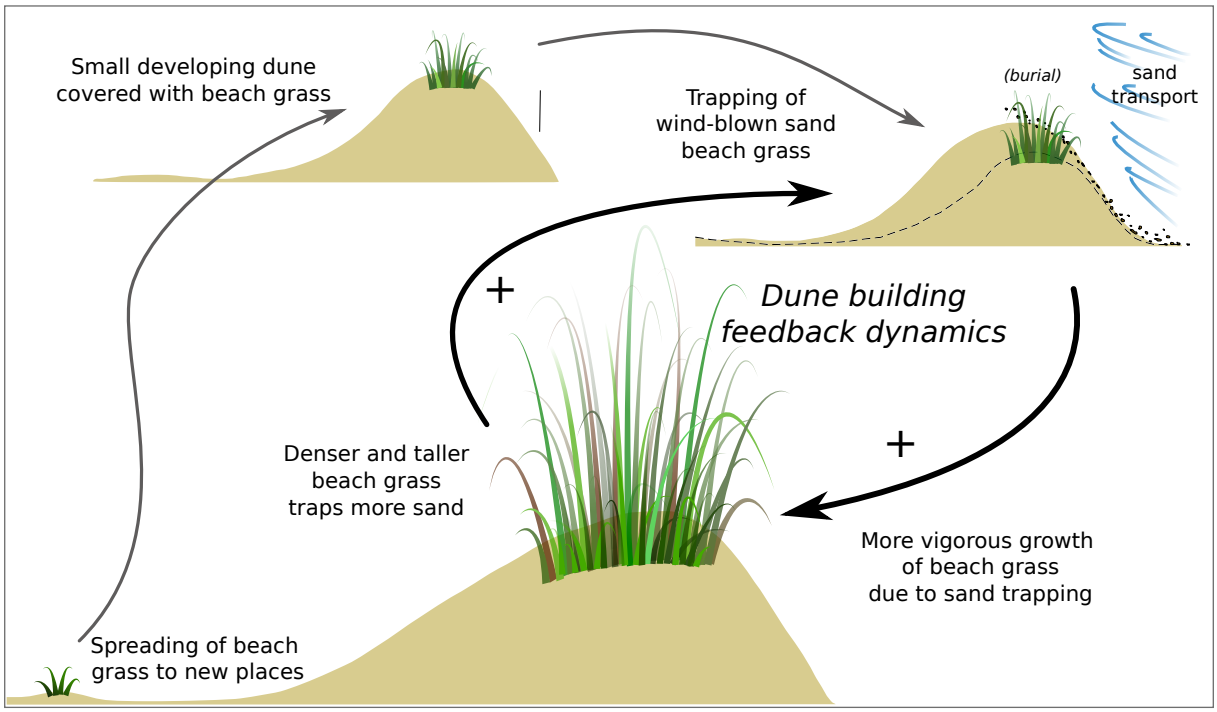

Figure 1.4: Coastal dunes in the Netherlands develop through a positive feedback interaction between aeolian sand deposition and dune-building vegetation. European marram grass (*Ammophila arenaria*) in particular combines two unique advantages for dune-building: a very high tolerance to sand burial and more vigorous growth because of trapping of wind-blown sand. (Illustration by C. Carranza)

1.1.3 Coastal (fore)dune development

Present-day Dutch coastal safety policy in particular prioritizes creating favorable conditions for natural dune development, as over 75% of the Dutch coastline relies on its vegetated foredunes (the most seaward facing dune ridge parallel to the coastline, see Fig 1.3) as the first line of flood defense against the sea (Hardisty, 1994; Van Koningsveld and Mulder, 2004). Coastal dunes are formed through a complex interaction between wind, waves, sand and vegetation (Hesp, 1989; Keijsers et al., 2016) and have the capacity (1) to reduce hydrodynamic impact from storm surges and (2) to keep up with sea-level rise by accumulating and stabilizing wind-blown sand (Temmerman et al., 2013). As a result, coastal dunes are often essential for flood protection and ensuring coastal safety (De Jong et al., 2014; Keijsers et al., 2015b; Poortinga et al., 2015a). Coastal dunes typically form above the high tide line and landward of the sandy beach. Three essential requirements must be met for dune formation on a beach: (1) a prevailing onshore wind above the critical wind velocity for aeolian sand transport (2) a continuous supply of sand, and (3) an obstacle to reduce the velocity of the wind to encourage deposition and prevent remobilization of the sediment (e.g., Hesp, 2002; Maun, 2009). Aeolian sand supply is typically highest on gently sloping (dissipative) beaches, where wide intertidal areas store large volumes of sand that are well sorted by wave action (e.g., Hesp, 1989; Sarre, 1989b; Anthony, 2013). Dune development is initiated when discrete clumps of incipient (embryo) dunes form by sand deposition around plants or obstacles such as flotsam

and driftwood. Embryo dunes require support by perennial plants in order to persist and are considered transient when formed around nonliving obstructions or annual plant species. When a beach experiences progradation, e.g. due to a positive sand budget, embryo dunes can grow and merge into continuous and shore-parallel foredune ridges that extend in a seaward direction (Hardisty, 1994; Hesp, 1989, 2002). Established foredunes are typically 5–20 m high and 30–50 m wide, but (as is the case in the Netherlands) human interference can inflate foredune heights to 30–35 m through sand nourishment and the installation of sand fencing (Arens, 1996b; Arens et al., 2001).

An essential element to coastal building-with-nature in the Netherlands is the utilization of European marram grass (*Ammophila arenaria*, see Fig. 1.4) to help stabilize and build up the foredunes (Keijsers et al., 2015b). Compared to other (native) coastal pioneer psammophytes that thrive on sandy soils, this beach grass is most effective at dune building because not only can it trap high amounts of wind-blown sand between its leaves and keep it in place with its roots, but it will in fact grow much more vigorously because of regular burial in sand (e.g., Disraeli, 1984; Van der Putten et al., 1988; Hesp, 1991). This introduces a reinforcing biogeomorphic feedback crucial to coastal dune development: trapping of wind-blown sand encourages marram grass to grow, which in turn enhances the capacity of marram grass to trap sand and build dunes (Maun, 1998; Zarnetske et al., 2012). This trait, combined with the ability of clonal growth through rhizome fragments (Konlechner et al., 2013), enables marram grass to help create and maintain high vegetated foredunes critical to coastal safety (Ranwell, 1972; Keijsers et al., 2015b). Moreover, because of the frequent sand nourishments, positive plant-sand feedback dynamics are (up to a certain extent) enabling the Dutch foredunes to grow in pace with rising sea levels (Temmerman et al., 2013).

1.2 Motivation

1.2.1 Mega-scale beach nourishment 'Zandmotor'

Within this context, to downscale the frequency and increase the lifespan of sand nourishments, an unprecedented mega-scale beach nourishment of 21.5 Mm^3 termed *Zandmotor* (Dutch for 'Sand Motor', see Fig. 1.5), was constructed in 2011 along the Delfland coast just south of the city The Hague (Stive et al., 2013b). The overall purpose of this mega-nourishment experiment is to test whether its benefits in terms if coastal safety, spatial quality and ecological values outweigh the extra costs involved and to determine to what extent such an approach can help cope with expected changes in the global climate (e.g., Mulder and Tonnon, 2011; Stive et al., 2013b; De Schipper et al., 2016). The *Zandmotor* has a hook-shaped design that aims to mirror the natural onshore migration of an intertidal sandbar. Just after construction it had a surface area of about 28 ha, extending 2.5 km along the coastline and protruding 1 km into the sea. Natural processes have since then been working to redistribute the sand, causing the base to flatten and the sand to spread in alongshore directions (De Schipper et al., 2016). With an expected lifespan over 20 years, it is expected that this type of large scale intervention will be beneficial to marine biodiversity by allowing longer recovery times (Van Egmond et al., 2018).

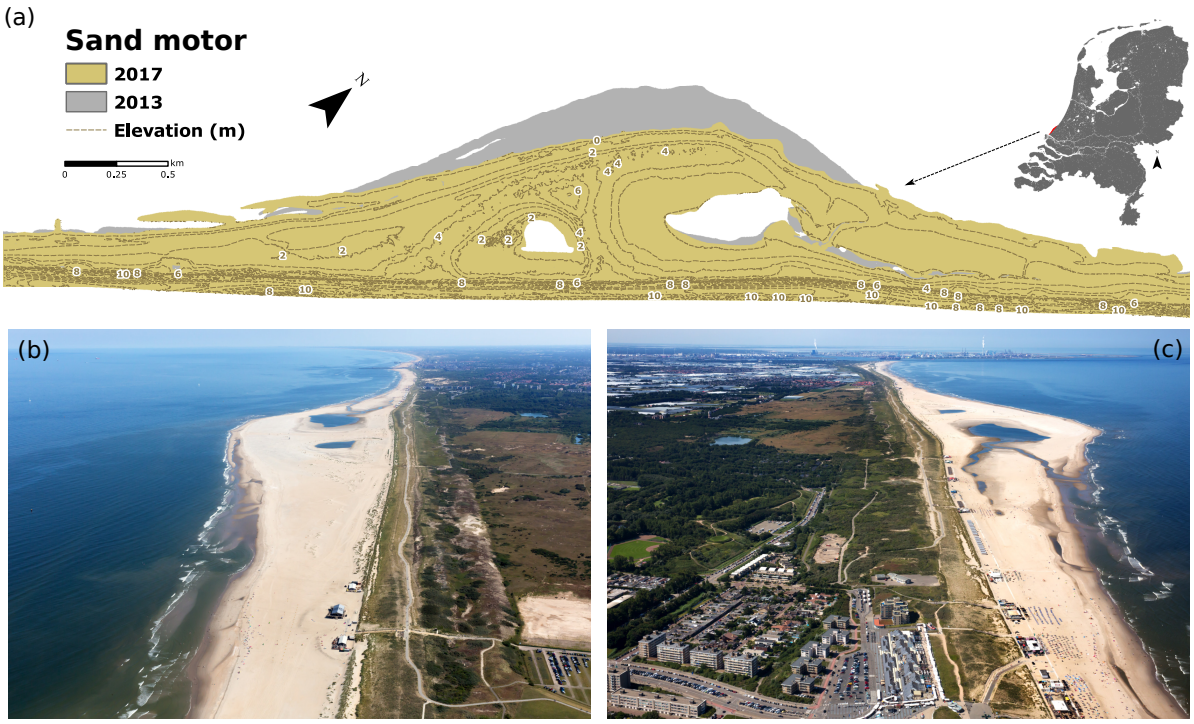

Figure 1.5: The *Zandmotor* (sand motor), an experimental mega-scale beach nourishment located along the Delfland coast in the Netherlands. Its design mirrors the onshore migration of an (intertidal) sandbar and aims to provide coastal safety by redistributing its sand along the coastline by wave and wind action. The aerial photographs (taken July 2017) are facing north (B) towards The Hague and south (C) towards the harbor of Rotterdam.

1.2.2 Dune-building dynamics

In line with the building-with-nature approach of Dutch coastal policy (De Vriend and Van Koningsveld, 2012), natural dynamics are encouraged to redistribute the sand of the *Zandmotor* along the coastline, thereby broadening the adjacent foredunes and beach. Specifically, a main objective was defined as 'Encouraging natural dune growth, primarily in width, in the coastal cell between the cities Rotterdam and The Hague. This creates a larger sand buffer to cope with rising sea level as well as more space for nature and recreation and a larger freshwater lens under the dunes' (Fiselier, 2010; Van Slobbe et al., 2013). Based on an empirical relation between beach width and dune foot migration, a preliminary modeling study estimated that after 20 years the *Zandmotor* would broaden the dunes along the Delfland coast by about 33 ha (Mulder and Tonnon, 2011). However, because of its novel and experimental nature, the long-term effects of such a mega-scale beach nourishment on dune-building dynamics is unknown.

For instance, a distinct feature that sets the *Zandmotor* apart from more traditionally nourished or natural coastlines, is the locally very high construction height. Most of the base is constructed at a height of around 5 m above mean sea level (a.m.s.l), while just north of a small dune lake the *Zandmotor* reaches a height of 7 m a.m.s.l. This is well above the current

maximum storm surge level of about 3 m a.m.s.l (Radermacher et al., 2018), so reworking of sand on the subaerial surface of the *Zandmotor* is almost exclusively due to aeolian forcing (Hoonhout and de Vries, 2017a). As a consequence, while may provide established dunes sheltering from storm surges, Van Puijenbroek (2017) concluded that this high construction height is likely to impede the establishment of new embryo dunes as rhizome dispersal by tide and wave action is absent on parts of the *Zandmotor*. At the same time, the high shell content and heterogeneous grain size distribution of the dredged sand used to create the *Zandmotor*, has been observed to lead to beach armoring due to aeolian sorting processes (Hoonhout and de Vries, 2017a) and cementation. Cementation is a process of lithification, in which chemical precipitates form in the pores of a sediment or rock, binding the grains together (Speybroeck et al., 2006). Although these processes are generally common occurrences on nourished beaches (Van der Wal, 2004), they may significantly reduce the erosivity of the *Zandmotor* in particular, thus reducing the potential for aeolian sand transport.

In fact, there are numerous factors in the coastal environment that limit the supply of sand to the aeolian transport system (e.g., Davidson-Arnott and Law, 1996; Sherman et al., 1998). Under these conditions the saltation mass flux, the principal mechanism of aeolian transport for sand-sized particles, does not saturate to a constant (or expected) saltation density for a given shear velocity (Nickling and Neuman, 2009). Shear velocity is an expression for the erosive force (shear stress) of near-surface winds in terms of a velocity. Surface moisture, in particular, is known to greatly increase the resistance of sand to entrainment, by binding sand grains together through cohesive and adhesive forces (Chepil and Woodruff, 1963; Belly, 1964; Cornelis and Gabriels, 2003a). Since wetting and drying processes are governed by complex hydraulics (i.e. tidal and wave action, groundwater and capillary flow, evaporation and precipitation), the control surface moisture exerts on sand particles is highly variable in time and space. While considerable effort has been undertaken to parameterize saltation equations to coastal environments (e.g., Bauer and Davidson-Arnott, 2003; Bauer et al., 2009b), the spatial-temporal complexity of surface moisture and numerous other supply-limiting factors (e.g. vegetation growth, shell layers, algae crusts, local topography) have been shown to significantly hamper their predictive quality (Arens, 1996a; Sherman et al., 1998; De Vries et al., 2014). Accurate and synchronous empirical measurements of aeolian sand transport and wind-forcing in coastal field experiments are very challenging to obtain (Barchyn et al., 2011; Baas, 2019) and as a result long-term continuous records of aeolian transport rates are not readily available. The challenge is to combine the advantages of passive trapping methods, i.e. direct measurement and long-term deployment (Goossens et al., 2000), with the advantages of active sensor-based methods, i.e. automated operation at (very) high temporal resolutions (Sherman et al., 2011; Poortinga et al., 2015b).

If accurate estimates of aeolian transport rates and subsequent estimates of available sand supply for dune building on the *Zandmotor* cannot be given, adequate predictions of dune development are also not possible. Moreover, relatively little empirical data are available on the mutually reinforcing dune-building interaction between marram grass and sand deposition (Keijsers, 2015). Positive feedback between the growth response of marram grass and burial by wind-blown sand is well documented (Huiskes, 1979; Disraeli, 1984; Maun and Lapierre, 1984; Van der Putten et al., 1988; Hesp, 1991; Maun, 1998) and recognized to be fundamental to

Figure 1.6: Artificial foredune ridge created just prior to construction of the *Zandmotor* (photo taken Oct. 2012). After completion the 40 m long stoss slope of the foredune (15° at its steepest) was manually planted with marram grass.

coastal dune development in temperate regions around the world (e.g., Baas and Nield, 2010; Durán and Moore, 2013; Keijsers et al., 2016). Field data, however, on plant response to sand burial, optimal burial levels and capacity to deal with adverse conditions are scarce. As a result, studies that model coastal dune development by incorporating positive feedback (i.e., Baas, 2002; Nield and Baas, 2008; Baas and Nield, 2010; Keijsers et al., 2016) may be hampered by burial response growth functions that are not validated by empirical measurement.

Further, it is worth mentioning that most of the foredunes adjacent to the *Zandmotor* were in fact also artificially created, by broadening them in a seaward direction (up to about 100 m) with a sand nourishment of approximately 20 Mm^3 over a length of 12 km. After completion (see Fig. 1.6) the newly created foredune ridge ranged between 4 and 12 m above mean sea level (a.m.s.l) from toe to crest. For stabilization, the approximately 15° stoss slope was manually planted with shoots of marram grass in a regular pattern of about 7-9 small tussocks per m^2. About 75% of the Delfland coastline has been reinforced in this manner between 2009 and 2011, thus prior to construction of the *Zandmotor*. Since these dunes were not established by natural bio-geomorphological processes, it remains unclear how they will respond to the

intended sand-feeding dynamics of the *Zandmotor*. Finally, while providing coastal safety is an important objective, the *Zandmotor* is also meant to serve a wide range of socioeconomic functions related to recreation and leisure. However, activities arising from these functions are often in direct conflict with coastal safety objectives (e.g., Jackson and Nordstrom, 2011; Lithgow et al., 2013). Dune development on and along the *Zandmotor* may, as a result, not reach the potential as foreseen by looking at bio-geomorphological processes alone.

1.3 Research questions and thesis outline

Because of its novel and experimental nature, the long-term effects of the *Zandmotor* mega-scale beach nourishment on dune-building dynamics is unknown and thus need to be established. The development of coastal dunes relies on a positive biogeomorphic feedback between aeolian sand deposition and dune-building grass species. This objective of this research is to provide field-based evidence and insight into how such reinforcing feedback controls dune morphology on the *Zandmotor* in particular and along nourished coastlines in general. To do this we aim to find an answer the following questions:

1. How does the design of mega-scale beach nourishment the *Zandmotor* impact coastal dune development on the beach and along the adjacent coastline? (Ch.2)
2. How do aeolian sand transport model estimates compare to field measurements on the *Zandmotor* and what are the implications for (predicting) coastal dune development? (Ch.3)
3. How does surface moisture impact coastal aeolian dynamics and how can it be measured at high spatial-temporal resolutions? (Ch.4)
4. How does aeolian sand deposition affect the growth rate of European marram grass and how does this impact dune development on and along the *Zandmotor*? (Ch.5)

Considering the coastal aeolian transport-dune system, research question 1 focuses on the boundary conditions for dune development on the *Zandmotor*. Research question 2 and 3 focus on supply-limited aeolian sand dynamics and research question 4 focuses on biogeomorphic dune building dynamics. Chapter 6 reflects on the main findings related to the research questions and discusses the implications and limitations of these answers and their contribution to science and society.

Chapter 2

Accommodation space indicates dune development potential along an urbanized and frequently nourished coastline

This chapter is based on:

Nolet, C. and Riksen, M. J. (2019). Accommodation space indicates dune development potential along an urbanized and frequently nourished coastline, *Earth Surface Dynamics* 7, 129–145

Abstract

With densely populated areas well below mean sea level, the Netherlands relies heavily on its dunes to ensure coastal safety. About half of the sandy coastline, however, is subject to structural marine erosion and requires frequent sand nourishment as a counteractive measure. A key component of present-day coastal safety policy is creating favorable conditions for natural dune development. These conditions essentially involve (1) a steady supply of wind-blown sand towards (2) wide accommodation space where sand can accumulate and dunes are sheltered from frequent storm surge impacts. This paper examines to what extent an experimental mega-scale beach nourishment (termed *Zandmotor* in Dutch) has contributed to creating accommodation space favorable for dune development. Using publicly available airborne lidar data and Sentinel-2 satellite imagery, favorable accommodation space is identified by comparing recent changes in coastal morphology against dune vegetation-cover dynamics. With a focus on European marram grass (*Ammophila arenaria*) as the most prominent dune-building species, this paper demonstrates that the *Zandmotor* supports an especially high potential for incipient (embryo) dunes to develop as most of its favorable accommodation space is located on the beach. However, considering the conditions required for successful marram grass establishment as well as persistent anthropogenic disturbances arising from recreation and nature management practices, it is not likely that dune development along this urbanized coastline reaches its full potential.

2.1 Introduction

Vegetated coastal foredunes, the most seaward facing dune ridge parallel to the coastline, often form the first and foremost line of flood defense against the sea (Hardisty, 1994). This is certainly true for the Netherlands, a country where the most densely populated areas are situated well below mean sea level. And, although widely known for its hydraulic engineering structures, over 75% of the Dutch coastline relies on its foredunes to ensure coastal safety (Van Koningsveld and Mulder, 2004). About half of that sandy coastline, however, is subject to structural marine erosion and requires frequent nourishment of dredged-up sand as a counteractive measure (Van der Wal, 2004). Subsequently, while the foredunes in the Netherlands are considered natural landscape elements, they are so strongly modified by human intervention that they too could be considered a feat of hydraulic engineering (De Vriend et al., 2015).

The focus of Dutch coastal policy has traditionally been on safety from flooding, which was guaranteed by large structures such as sea dikes, groins and other artificial barriers. Nowadays, however, the focus has widened to also include preserving the spatial quality and natural values of the coastal zone (Van Slobbe et al., 2013). It was recognized that coastal dunes, apart from flood defense, also represent unique ecological and recreational values and often serve as an important source for drinking water supply (e.g., De Jong et al., 2014; Keijsers et al., 2015b). By acknowledging sand as 'the carrier of all coastal functions' the principal management practice since 1990 has been to nourish the coastline with sand whenever it was about to retreat beyond a defined reference position (Van Koningsveld et al., 2007). A key component of such a dynamic preservation of the coastline involves utilizing natural processes to further redistribute the sand. By allowing marine and aeolian forces to gradually help shape the coastline, the aim of this building-with-nature engineering strategy is to counteract a negative sediment balance while minimizing adverse effects to the coastal ecosystem (Van Slobbe et al., 2013).

An essential element to building with nature in the Netherlands is the utilization of European marram grass (*Ammophila arenaria*) to help stabilize and build up the foredunes (Keijsers et al., 2015b). Compared to other (native) coastal pioneer psammophytes that thrive on sandy soils, this beach grass is most effective at dune building because not only can it trap high amounts of wind-blown sand in its leaves and roots, but it will in fact grow much more vigorously because of regular burial in sand (e.g., Disraeli, 1984; Van der Putten et al., 1988; Hesp, 1991; Nolet et al., 2018). This introduces a reinforcing feedback crucial to coastal dune development: trapping of wind-blown sand encourages marram grass to grow, which in turn enhances the capacity of marram grass to trap sand and build dunes (Maun, 1998; Zarnetske et al., 2012). This trait, combined with the ability of clonal growth through rhizome fragments (Konlechner et al., 2013), enables marram grass to help create and maintain high vegetated foredunes critical to coastal safety (Ranwell, 1972; Keijsers et al., 2015b). Moreover, because the Dutch shoreline is frequently nourished with dredged-up sand, positive plant-sand feedback dynamics enable the adjacent foredunes to grow in pace with sea-level rise due to changes in the global climate (Temmerman et al., 2013).

Figure 2.1: The *Zandmotor* (sand motor), an experimental mega-scale beach nourishment located along the Delfland coast, the Netherlands. **2.1A**. The design of the *Zandmotor* mirrors the onshore migration of an (intertidal) sandbar and aims to provide coastal safety by redistributing its sand along the coastline, thereby broadening the beach and dunes. **2.1B-C**. Aerial photographs of the *Zandmotor* and Delfland coast taken on July 9 2017, facing north (B) towards The Hague and south (C) towards the harbor of Rotterdam. The Delfland coast maintains relatively wide and natural dune areas, but in some places the dunes are no more than a narrow foredune ridge directly bordered by urbanized areas.

For that reason, present-day Dutch coastal safety policy in particular prioritizes creating favorable conditions for natural dune development. These conditions, essentially, involve (1) a steady supply of wind-blown sand towards (2) wide accommodation space (Jervey, 1988) where sand has the potential to accumulate and developing dunes are sheltered from frequent storm surge impacts (e.g., Ruggiero et al., 2001; Claudino-Sales et al., 2008; Montreuil et al., 2013; Van Puijenbroek et al., 2017a). Although a predominantly landward wind regime is required, the morphology of the beach arguably exerts the largest control on foredune development conditions (Short and Hesp, 1982). Aeolian sand supply, for example, is typically highest on gently sloping (i.e. dissipative) beaches, where wide intertidal areas store large volumes of sand that are well sorted by wave action (e.g., Hesp, 1989; Anthony, 2013). Wide accommodation space for foredune development is subsequently provided when such a dissipative coastline is supported by a wide supratidal beach that is high enough to offer protection from frequent storm surge impacts (e.g., Sallenger Jr, 2000; Suanez et al., 2012; Houser et al., 2008). Foredune development is initiated when discrete clumps of incipient dunes (i.e. embryo dunes) form after marram grass establishes itself on the beach through dispersal of seeds and rhizome fragments by wind and water (Konlechner and Hilton, 2009; Hilton and Konlechner,

2011). Over time, and under the right conditions, these individual embryo dunes can merge into continuous and shore-parallel foredune ridges that extend in a seaward direction (Hardisty, 1994; Hesp, 1989, 2002).

Creating favorable conditions for dune development is an important goal for the *Zandmotor* (Dutch for 'sand motor', see Fig. 2.1), an unprecedented mega-scale beach nourishment of 21.5 Mm^3 constructed in 2011 just south of The Hague (Stive et al., 2013b). The overall purpose of this mega-nourishment experiment is to test whether its benefits in terms if coastal safety, spatial quality and natural values outweigh the extra costs involved and to determine to what extent such an approach can help cope with expected changes in the global climate (e.g., Mulder and Tonnon, 2011; Stive et al., 2013b; De Schipper et al., 2016). In line with the building-with-nature approach, natural dynamics are encouraged to redistribute the sand of the *Zandmotor* along the coastline, thereby broadening the adjacent foredunes and beach. Specifically, the main objective of the project was defined as 'Encouraging natural dune growth, primarily in width, in the coastal cell between the cities Rotterdam and The Hague. This creates a larger sand buffer to cope with rising sea level as well as more space for nature and recreation and a larger freshwater lens under the dunes' (Fiselier, 2010; Van Slobbe et al., 2013).

However, while the Delfland coast partly maintains relatively wide and natural dune areas, the aerial photos in Fig. 2.1 clearly show that in some places the dunes are not more than a narrow foredune ridge that is directly bordered by urban areas. Because the region is densely populated, the coastline (including the *Zandmotor*) faces persistent pressure from anthropogenic disturbances. Even though the Delfland coast is meant to serve a wide range of socioeconomic functions related to recreation and leisure, activities arising from these function are often in direct conflict with the objectives related to coastal safety and natural values (e.g., Jackson and Nordstrom, 2011; Lithgow et al., 2013). Within this context, this paper examines to what extent the *Zandmotor* has contributed to creating accommodation space favorable for dune development, i.e., accommodation space that is sheltered from frequent storm impacts and experiencing a steady accumulation of wind-blown sand. This favorable accommodation space is identified, using publicly available remote-sensing data, by (1) comparing the presence of existing dunes against recent morphology of the Delfland coast and by (2) comparing recent coastal morphological changes against changes in dune cover by marram grass. Then, by taking into account the existing dunes and the conditions required for successful marram grass establishment, the identified favorable accommodation space is used to indicate the full potential for dune development along this urbanized and frequently nourished coastline.

2.2 Material and methods

2.2.1 Regional setting

The *Zandmotor* is located along the Delfland coast, an approximately 15 km long stretch of coastline that runs between Rotterdam and The Hague parallel to the dominant south-western wind direction. The Delfland coast has a long history of coastal erosion: early 17th century

maps make it clear that the coastline, compared with today, experienced a significant ($>$ 1.5 km) landward retreat (Van der Meulen et al., 2014). In the late 19th century the Delfland coast was fortified by groynes, but that only slowed down coastal erosion to a landward retreat of about 1 my^{-1} on average. Therefore from the early 1980s onward, well before it became central policy, the Delfland coast has been frequently replenished with sand nourishment of varying volumes (Van Koningsveld et al., 2007). Still, in 2002 the Delfland coast was labeled a 'weak link' as it did not meet stricter coastal safety standards that reflected expected increases in storm surge frequency and magnitude due to climate change (Keijsers et al., 2015b). Between 2009 and 2011, to guarantee that the Delfland coast could withstand hydraulic boundary conditions with a recurrence period of once every 10.000 years, most of the existing foredunes were broadened in a seaward direction (up to about 100 m) with a sand nourishment of approximately 20 Mm^3 over a length of 12 km. This included construction of a new dune area in the south (called *Spanjaardsduin* in Dutch) to compensate for loss of natural values because of expansion of the Rotterdam harbor (Van der Meulen et al., 2014). After completion the newly created foredune ridge ranged between 4 and 12 m above mean sea level (a.m.s.l) from toe to crest. For stabilization, the approximately 15° stoss slope was manually planted with shoots of marram grass in a regular pattern of about 7-9 small tussocks per square meter. About 75% of the Delfland coastline has been reinforced in this manner between 2009 and 2011. The newly created foredune ridge stretches landward approximately until the paved bike path (gray line in Fig. 2.1) that runs along its crest.

Once the new safety standards were met, the Delfland coast was considered an appropriate location to conduct the *Zandmotor* mega-nourishment experiment. As can be seen in Fig. 2.1, the *Zandmotor* has a hook-shaped design that aims to mirror the natural onshore migration of an intertidal sandbar. Just after construction it had a surface area of about 28 ha, extending 2.5 km along the coastline and protruding 1 km into the sea. Natural processes have since then been working to redistribute the sand, causing the base to flatten and the sand to spread in alongshore directions (De Schipper et al., 2016). Based on an empirical relation between beach width and dune foot migration, a preliminary modeling study estimated that after 20 years the *Zandmotor* would broaden the dunes along the Delfland coast by about 33 ha (Mulder and Tonnon, 2011). A distinct feature that sets the *Zandmotor* apart from more traditionally nourished or natural coastlines, is the locally very high construction height. Most of the base is constructed at a height of around 5 m a.m.s.l, while just north of a small dune lake the *Zandmotor* reaches a height of 7 m a.m.s.l. This is well above the current maximum storm surge level of about 3 m a.m.s.l, so reworking of sand on the *Zandmotor* is almost exclusively due to aeolian forcing (Hoonhout and de Vries, 2017a). As a consequence, while beneficial to already established dunes, Van Puijenbroek (2017) concluded that this high construction height may also impede the establishment of new embryo dunes as rhizome dispersal by tide and wave action is absent on parts of the *Zandmotor*. The semidiurnal tidal dynamics along the Delfland coast are characterized by a spring (neap) tidal amplitude around 2.0 m (1.5 m), generating alongshore currents with a velocity up to 0.5 ms^{-1} (Luijendijk et al., 2017).

Table 2.1: Sentinel-2A bands in VIS and NIR used for linear spectral unmixing procedure

Band	Central wavelength (nm)	Bandwidth (nm)	Pixel size (m)
2 - Blue	496.6	98	10
3 - Green	560.0	45	10
4 - Red	664.5	38	10
8 - NIR	835.1	145	10

2.2.2 Vegetated coastal dune dynamics

Data on the presence of dunes along the Delfland coast and changes in dune cover by marram grass were obtained using Sentinel-2A multispectral satellite imagery provided by the European Space Agency (ESA). Sentinel-2 images are acquired in 13 spectral bands in the visible (VIS), near-infrared (NIR) and shortwave infrared (SWIR) spectrum. Two level-1C images were downloaded from the Copernicus open-access hub (https://scihub.copernicus.eu, last access: 11 January 2018), with acquisition dates in the autumn of 2016 (September 11) and 2017 (October 12), when above-ground biomass of marram grass is highest (Nolet et al., 2018). With applied radiometric calibration and geometric correction, level 1C images contain top of atmosphere (TOA) reflectance in cartographic geometry (Drusch et al., 2012). Out of the 13 available bands, the 4 bands with the highest spatial resolution (10 meter pixel size) were selected for further analysis. Table 2.1 lists the characteristics of the bands, which are in the visible (blue, green, red) and near-infrared part of the spectrum. To illustrate the Sentinel-2 imagery used for analysis, Fig. 2.2 shows an image of the *Zandmotor* indicating the Normalized Difference Vegetation Index (NDVI) (Rouse Jr et al., 1974; Tucker, 1979). This ratio takes advantage of the contrasting reflection of photosynthetically active vegetation at visible and near-infrared wavelengths and is widely used for detection and classification of vegetated areas (e.g., Pettorelli et al., 2005; Nolet et al., 2018).

Linear spectral unmixing

The four selected bands were stacked into a new multispectral data cube and a linear spectral unmixing procedure was applied. This was done to derive sub-pixel proportions of dune cover by marram grass, the most prominent and abundant dune-building species. Linear spectral unmixing is an approach to determine the relative abundance of user-specified ground cover components (endmembers) in multispectral (or hyperspectral) imagery based on its spectral characteristics (e.g., Smith et al., 1985; Settle and Drake, 1993; Theseira et al., 2003). It has successfully been applied before by Lucas et al. (2002) and Zhang and Baas (2012) in mapping the abundance of vegetation, including marram grass, in coastal dune environments. The reflectance at each pixel of the image is assumed to be a linear combination of the reflectance of the endmembers present within the pixel:

$$R_i = \sum_{k=1}^{n} (f_k \; R_{ik}) + e_i, \tag{2.1}$$

where $i = 1, ..., m$ are the number of spectral bands, R_i is the reflectance of band i of each pixel, $k = 1, ..., n$ are the number of endmembers, f_k is the proportion of endmember k within each pixel, R_{ik} the spectral reflectance of endmember k within each pixel on band i, and e_i is the residual error term (Lu et al., 2003). Here, two endmembers were specified (see Fig. 2.2). The first endmember was made up by a group of pixels ($\sim$ eight) containing only beach sand, the second endmember by a similarly sized group of pixels fully covered by marram grass. The spectra of the two endmembers were obtained for each Sentinel-2 image separately, and maps containing subpixel proportions of beach sand and marram grass were derived using ENVI version 4.8 (Exelis Visual Information Solutions, Boulder, Colorado). The subpixel proportions of marram grass were subsequently interpreted as a percentage dune cover within each 10 m pixel. Older established dunes (with NDVI values above 0.6 in Fig. 2.2) were excluded from the analysis as they are minimally exposed to marine forces and mostly covered with vegetation species other than marram grass. Further, all artificial structures on the beach related to coastal safety (e.g., groynes) and leisure and recreation were masked from the imagery before the linear spectral unmixing procedure was executed.

Changes in dune cover by marram grass along the Delfland coast were obtained by subtracting the percentages of dune cover calculated for the 2016 Sentinel-2 image from the snapshot of 2017. Changes in dune cover between 2016 and 2017 were expressed for every 10 m pixel but also as an alongshore change in cover area ($m^2m^{-1}yr^{-1}$). This was done for better interpretation of dune dynamics along the Delfland coast and was calculated by multiplying the surface area of each pixel (100 m^2) by its fractional cover change. The linear spectral unmixing procedure was validated against a high-resolution orthomosaic of a stretch of foredune directly adjacent to the *Zandmotor* (see also Fig. 2.3). The georeferenced orthomosaic (5 cm pixel size) was obtained by an unmanned aerial vehicle (UAV) during a flight on September 1 2016, so 10 days before the acquisition date of the 2016 Sentinel-2 image. Using a k-means clustering algorithm (Hartigan and Wong, 1979), the individual 5 cm pixels of the orthomosaic were classified either as beach sand or marram grass. The accuracy of the algorithm was confirmed by visual inspection; for more details about acquisition and processing of the UAV-derived data the reader is referred to Nolet et al. (2018). The orthomosaic was subsequently resampled to match the 10 m pixel size resolution of the Sentinel-2 imagery and dune cover depicted in the orthomosaic was calculated as the proportion of the (former) 5 cm pixels classified as marram grass contained within each newly aggregated 10 m pixel.

2.2.3 Coastal morphology

Data on the morphology and morphological changes of the Delfland coast were obtained from digital terrain models (DTM) provided by Rijkswaterstaat, the executive agency of the Ministry of Infrastructure and Water Management. The 2 m pixel size DTMs are produced every year (since 1996) for coastline monitoring purposes by airborne lidar and have been made public under a Creative Commons Zero (CC0) statement. The contractor responsible for the lidar flights guaranteed a minimum density resolution of 1 laser point per square meter, with a systemic vertical error equal to or less than 2.6 cm and standard deviation equal to or less than $\pm$ 2.0 cm. Five yearly DTMs of the Delfland coast were used for analysis, ac-

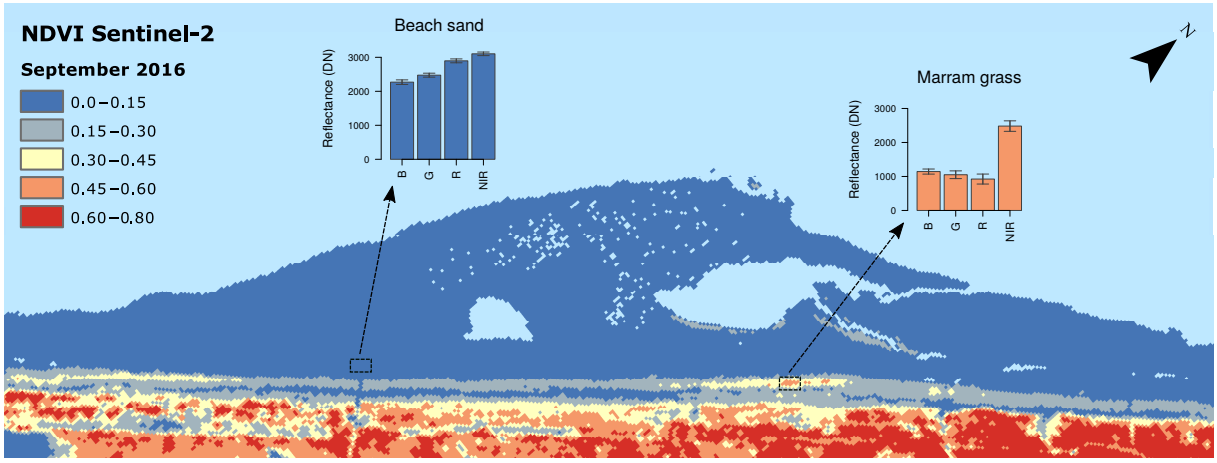

Figure 2.2: Map of the *Zandmotor* indicating Normalized Difference Vegetation Index (NDVI), and to illustrate the Sentinel-2 imagery and selection of endmembers (user-specified ground cover components) for the linear spectral unmixing procedure. Subpixel proportions of beach sand and marram grass (for every 10 m pixel) were derived using endmember reflectance spectra for four bands in the visible and near-infrared spectral ranges.

quired in spring 2013 until spring 2017. Changes in coastal morphology were first expressed by average change in height per year (m yr^{-1}), which was calculated per consecutive time step: $t_{5-1} = (t_{2-1} + t_{3-2} + t_{4-3} + t_{5-4})/4$. This was done to better consider temporal variations within each year and to account for yearly changes of the shoreline. Coastal morphological changes were also expressed as an average (alongshore) change in sand volume per year (m^3yr^{-1} or $m^3m^{-1}yr^{-1}$). Sand volume changes were likewise calculated per consecutive time step and obtained by multiplying the surface area of each pixel (4 m^2) by its yearly change in height. The quality of the DTMs were verified by comparing the height of features along the coastline that remained unchanged between 2013 and 2017 (e.g. parking lots, paved roads, building rooftops). The average standard deviation of the vertical component of the five DTMs (using $\approx$ 100 samples) was determined to be $\pm$ 2.4 cm. Data are available at: https://rijkswaterstaat.nl/apps/geoservices/geodata/dmc (last access: 16 January 2018). The Delfland coast considered in the analysis covers a subaerial area of about 500 ha and extends in the landward direction until the older established dunes. This approximately coincides with the paved bike-path (gray line in Fig. 2.1) running along the crest of the newly created foredune ridge. In order to compare the morphology and morphological changes in the Delfland coast against the presence of dunes and changes in dune cover by marram grass, the 2 m resolution DTMs were resampled using bilinear interpolation to match the 10 m pixel size of the Sentinel-2 imagery.

2.3 Results

Figure 2.3 shows the results of validating the linear spectral unmixing procedure on the Sentinel-2 images. The dune cover calculated from the orthophoto and the two Sentinel-2 images are plotted against each other in Fig. 2.3B. It is clear that deriving subpixel proportions

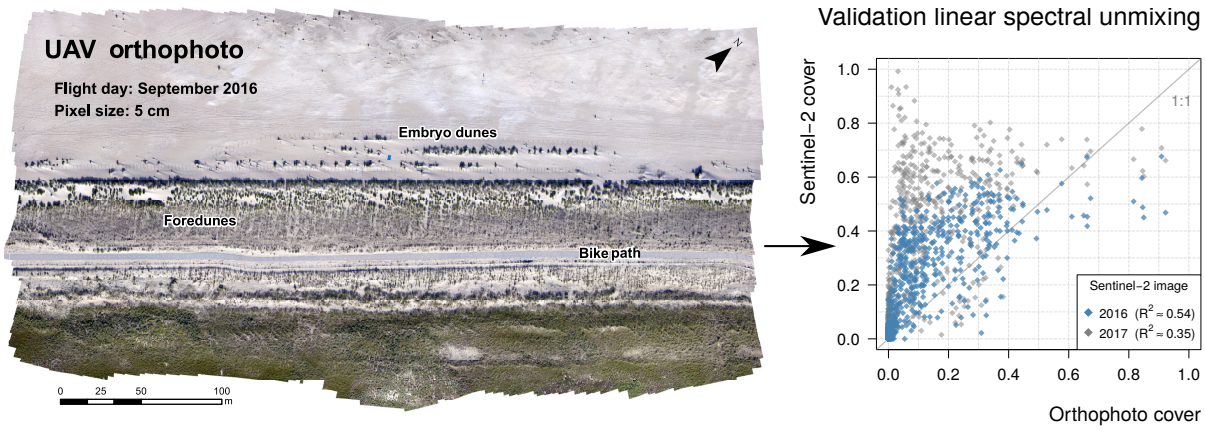

Figure 2.3: Validating the linear spectral unmixing procedure on the Sentinel-2 images using an orthophoto (5 cm pixel size) derived in September 2016 by an unmanned aerial vehicle (UAV). Linear spectral unmixing produces a systematic overestimation of subpixel proportions of marram grass cover compared to the cover values calculated from the orthophoto. A positive linear regression model explains 54% of the variance for the 2016 Sentinel-2 image and 35% of the variance for the 2017 image.

of dune cover using linear spectral unmixing results in an overestimation of dune cover by marram grass. Even though 54% of the variance for the 2016 Sentinel-2 image can be explained by a positive linear regression model, most of the data points deviate from the 1:1 identity line because of higher dune cover values calculated by the Sentinel-2 image. This trend, however, appears to be systematic to the linear spectral unmixing procedure since the data points from the 2017 Sentinel-2 image deviate even further from the identity line. This lower correlation ($R^2 \approx 0.35$) is in line with expectation as dune cover by marram grass was observed to have increased at this location between 2016 and 2017. So even though the linear spectral unmixing procedure overestimates the subpixel proportions of dune cover, the derived marram grass cover values for each Sentinel-2 image appear to be comparable relative to each other.

Figure 2.4 shows the derived maps used to identify favorable accommodation space for dune development.The first map (Fig. 2.4A) gives an overview of the morphological features, including the *Zandmotor*, during early spring 2017. The beach ranges between 0 and 6 m a.m.s.l. in height and this is where new embryo dunes have either formed or expanded since 2011. The foredunes are exclusively covered by marram grass and stretch fully along the coastline, albeit at variable widths, at heights between 6 - 14 m a.m.s.l. This indicates that the toe of the foredunes, compared to their construction height in 2011, have been raised by about 2 m due to aeolian deposition. The second map (Fig. 2.4B) shows how the subaerial coastal morphology changed between 2013 and 2017, expressed by the average yearly change in height (m yr^{-1}). It is clear that the most seaward part of the *Zandmotor* experienced strong erosion due to marine forcing, while most of the foredunes and particularly the beach just south and north of the *Zandmotor* experienced accretion due sand spreading-effects. The base of the *Zandmotor* with its high construction height either remained relatively stable or experienced moderate erosion. These morphological dynamics are more distinctly reflected in graph 2.4C,

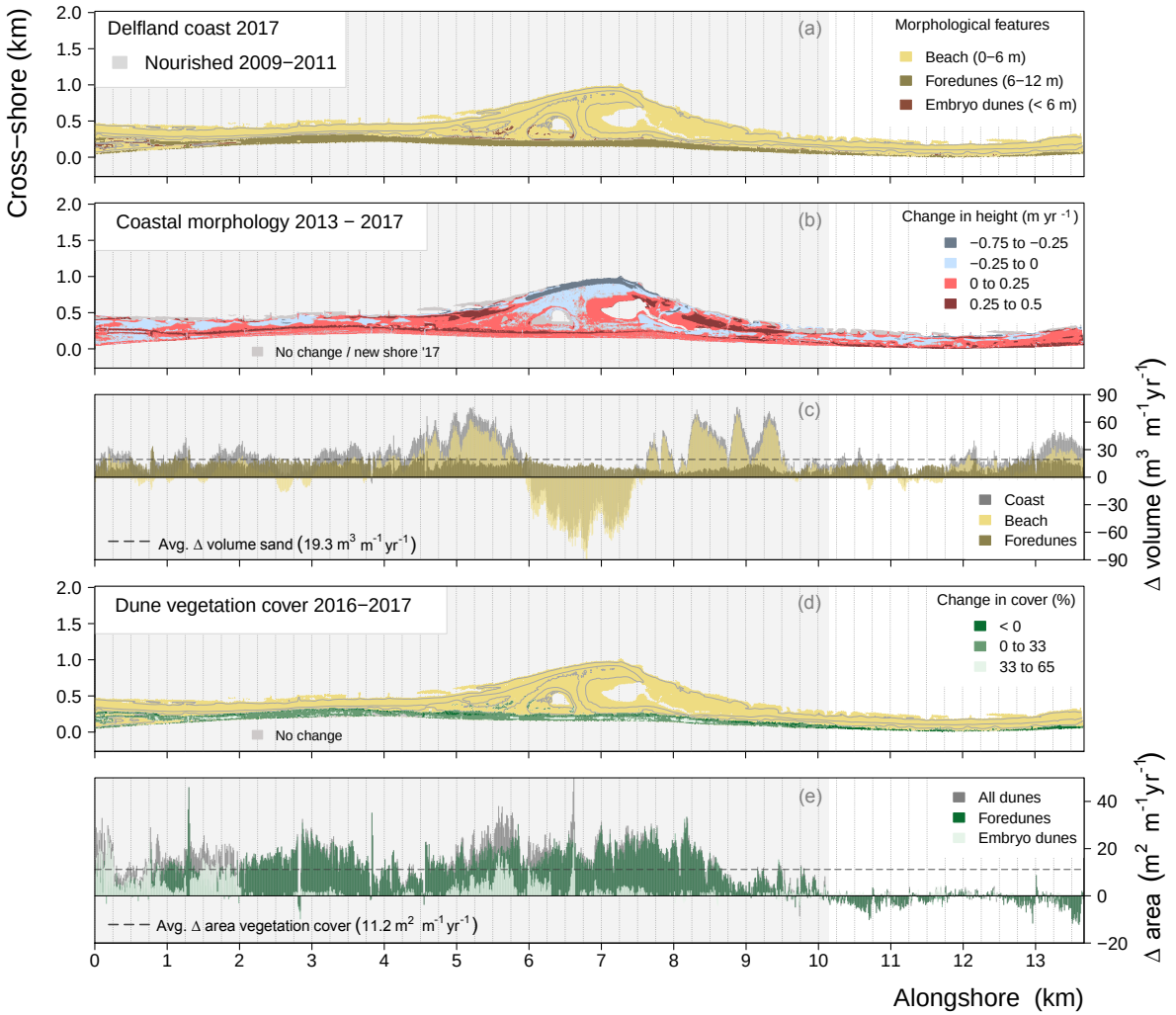

Figure 2.4: Morphological changes and dune vegetation-cover dynamics of the Delfland coast. **2.4A**. Map of the considered domain including the relevant morphological features (beach, foredunes, embryo dunes) in 2017. **2.4B**. Map of subaerial coastal morphological changes between 2013 and 2017, expressed average change in height per year (m yr^{-1}). **2.4C**. Average alongshore changes in coastal sand volumes ($m^3m^{-1}yr^{-1}$) between 2013 and 2017 for the Delfland coast and differentiated by the beach (embryo dunes included) and foredunes. **2.4D**. Map of changes in dune cover by marram grass between 2016 and 2017, expressed as percentage per 10 m pixel. **2.4E**. Alongshore changes in marram grass dune cover ($m^2m^{-1}yr^{-1}$) between 2016 and 2017, with differentiation between the foredunes and embryo dunes.

which shows the average alongshore change in coastal sand volumes ($m^3m^{-1}yr^{-1}$) between 2013 and 2017. On average the Delfland coastline has been accretive, at a rate of 19.3 $m^3m^{-1}yr^{-1}$, but it is clear that there has been a high alongshore variability in sand accretion and erosion rates. This can be attributed to the anticipated behavior of the *Zandmotor*: the accretive areas on its flanks gained approximately 2.8 10^5 m^3yr^{-1} of sand, while the erosive areas on its base lost about 1.7 10^5 m^3yr^{-1} of sand. Further, the foredunes experienced accretion of sand at relatively stable alongshore rates. In total, at an average rate of 11 $m^3m^{-1}yr^{-1}$, the foredunes along the Delfland coast gained approximately 1.6 10^5 m^3yr^{-1} of sand between 2013 and 2017.

The third map (Fig. 2.4D) shows how the dune cover by Marram grass (expressed as percentage per 10 meter pixel) changed along the Delfland coast between the acquisition dates of the two Sentinel-2 images. Using changes in marram grass cover as a proxy for dune development potential, it appears that in most places the dunes along the coastline have been expanding over the course of a year. This observation, however, must be considered with some reservation, as observed changes in marram grass cover may also have been due to denser or taller growth of marram grass and not because of actual lateral expansion. Having said that, Fig. 2.4D suggests that particularly the embryo dunes have been expanding, from 3 to 5 ha between 2016 and 2017. As a result, in 2017 about 17% of the dunes along the Delfland coast could be considered embryo dunes, of which most developed naturally along the coastline. The foredunes, in contrast, appear to have experienced more spatial variation in marram grass cover changes. Figure 2.4D suggests that, along most of the Delfland coast, the foredunes have been expanding between 2016 and 2017. However, especially at the dune toe and just leeward of the dune crest, the foredunes appear to have declined somewhat in cover. This decline is most apparent north of the *Zandmotor*, which is clearly reflected in the second graph (Fig. 2.4E) that shows the alongshore yearly change in dune cover ($m^2m^{-1}yr^{-1}$) between 2016 and 2017. This northerly foredune decline will be examined in more detail in the discussion, but it can likely be attributed to anthropogenic disturbances (due to recreational activities as well as nature management practices) and to the fact that this stretch of coastline has not been nourished with sand when the Delfland coast was reinforced between 2009 and 2011. All in all, data from Sentinel-2 imagery suggests that the dunes along the Delfland coast have been expanding between 2016 and 2017 at an average rate of about 11.2 $m^2m^{-1}yr^{-1}$. For the foredunes, this amounted to an increase in dune cover of 42 to 54 ha. Although, as stated before, this may be an exaggerated number as increase in dune cover by marram grass has likely not been due to lateral growth alone.

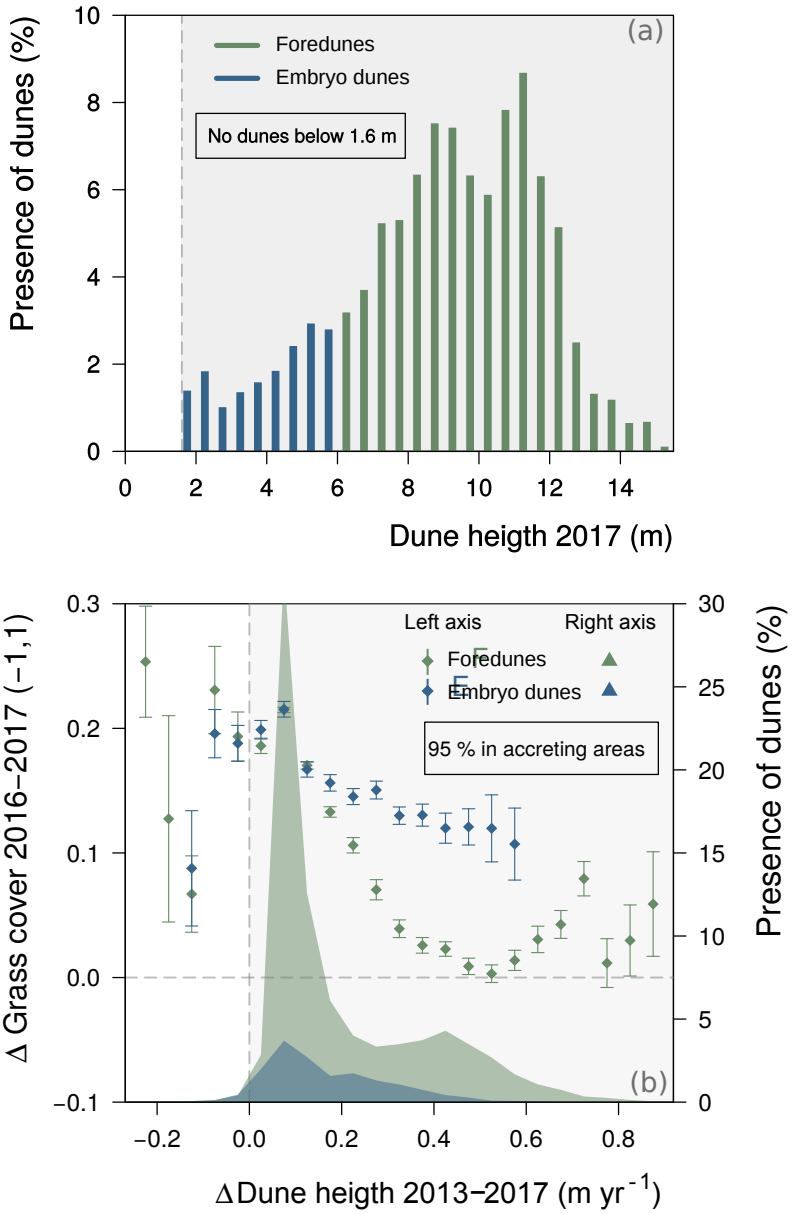

Figure 2.5: Identifying favorable accommodation space for dune development (both foredunes and embryo dunes) along the Delfland coast **2.5A**. Comparing the presence of dunes in 2017 to its elevation: no dunes present below 1.6 m a.m.s.l. **2.5B**. Comparing the changes in dune cover by marram grass from 2016 to 2017 to the average yearly change in dune height between 2013 and 2017: most dunes were present in accreting areas (right axis) and almost all dunes increased in cover by marram grass between 2016 and 2017 (left axis).

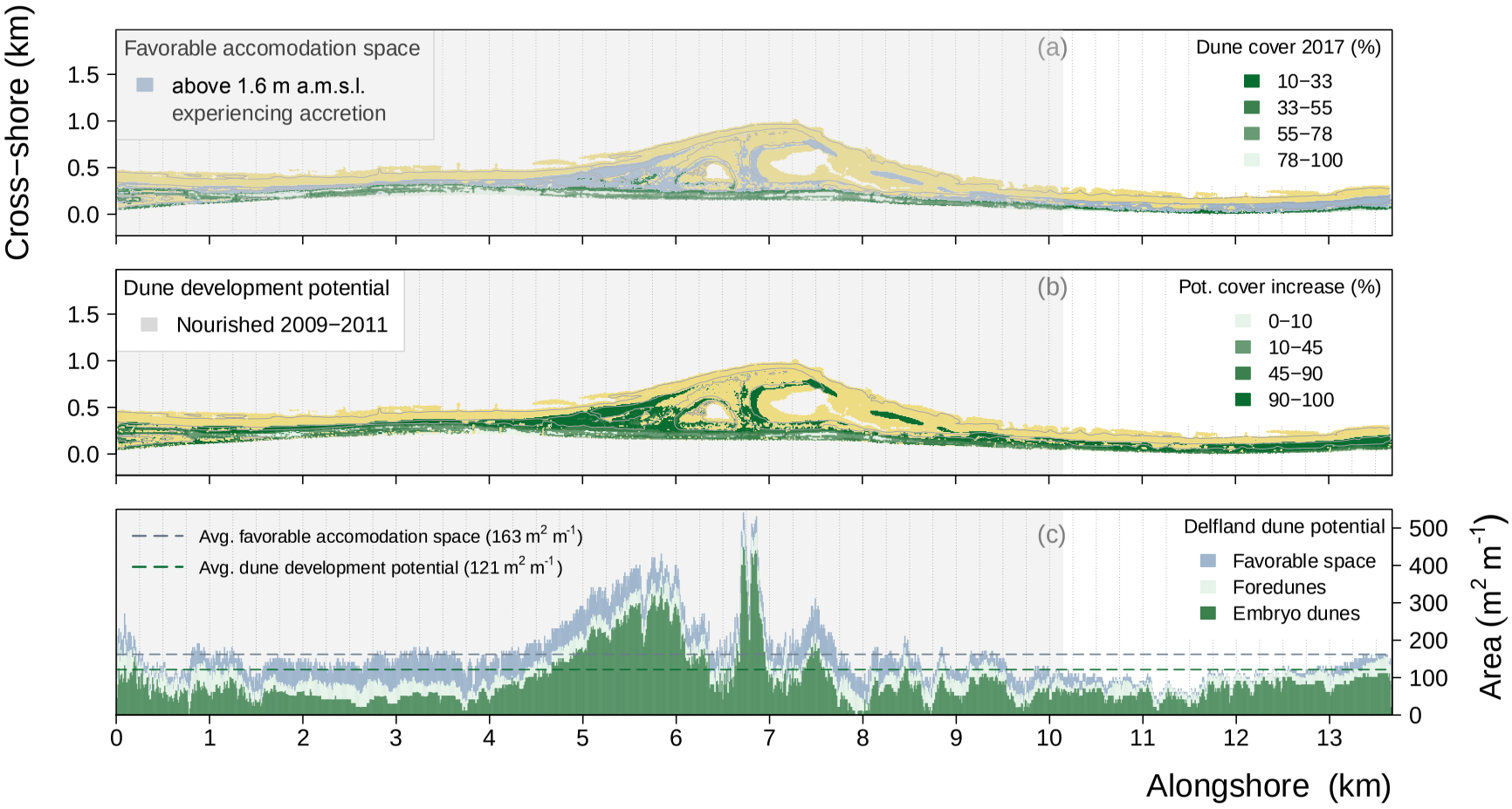

Figure 2.6: Favorable accommodation space to indicate dune development potential along the Delfland coast. **2.6A**. Map of dune cover (%) by marram grass in 2017 and accommodation space favorable for dune development: located above 1.6 m a.m.s.l. and experiencing an accretion of sand. **2.6B**. Map indicating Delfland coast dune development potential, calculated as the potential of marram grass to increase in cover (%) based on the accommodation space favorable for dune development and taking into account the dune cover already present in 2017. **2.6C**. Alongshore variation of favorable accommodation space and potential for dune development along the Delfland coast (m^2 m^{-1}), differentiated for foredunes and embryo dunes.

Accommodation space is considered favorable for dune development when it is (1) sheltered from frequent storm impacts and (2) experiencing a steady accumulation of wind-blown sand. The first (boundary) condition is identified by comparing the presence of dunes along the Delfland coast in 2017 to the height at which they were located. As Fig. 2.5A demonstrates, in 2017 there were no dunes present below a height of 1.6 m a.m.s.l. All embryo dunes were located on the beach between 1.6 and 6 m a.m.s.l., while the foredunes were located at heights between 6 and 14 m a.m.s.l.. This suggests, at least for 2017, that dunes along the Delfland coast were sheltered from storm impacts above a height of 1.6 m a.m.s.l. Accommodation space, as a result, is considered favorable for dune development above this boundary height. The second condition is identified (or verified as the positive effect of sand burial on marram grass vigor is well documented) by comparing the changes in dune cover by marram grass between 2016 and 2017 to the average yearly change in dune height between 2013 and 2017 (see Fig. 2.5B). Several observations can be drawn from that comparison but, most importantly, it demonstrates that 95% of all dunes along the Delfland coast in 2017 (both embryo dunes and foredunes) were present in areas that experienced on average a continuous accretion of sand from 2013 to 2017. This indicates that favorable accommodation space for dune development can indeed be characterized by a steady accumulation of sand. And since all dunes in 2017 were located above a height of 1.6 m a.m.s.l., it is reasonable to assume that this accumulation of sand occurred predominantly by aeolian forcing. In addition, Fig. 2.5B shows that almost all dunes increased in cover by marram grass between 2016 and 2017. Overall this increase in cover was most pronounced for the embryo dunes, as the foredunes showed limited increase and even some decrease in dune cover towards higher changes in dune height. The largest increase in dune cover between 2016 and 2017, however, coincided with the same change in dune height ($\sim$ 0.1 m yr^{-1}) for both the embryo dunes and the foredunes.

The identified accommodation space favorable for dune development (i.e. located above 1.6 m a.m.s.l. in height and experiencing a steady accumulation of wind-blown sand) is shown in Fig. 2.6A. Including the parts that were already covered by marram grass, it is clear that large areas along the Delfland coast were favorable for dune development in 2017. Especially the sheltered and accreting southern and middle part of the *Zandmotor* stood out for its large favorable accommodation space for dunes to develop. This is reflected more clearly by Fig. 2.6C, which shows the favorable accommodation space along the Delfland coast (in m^2 m^{-1}) as well as the potential for new dune development. As Fig. 2.6B shows, this potential is calculated by subtracting the dune cover already present in 2017 from the total favorable accommodation space. Fig. 2.6C makes it clear that dune development potential along the Delfland coast is mainly reserved for embryo dune development, as most of the favorable accommodation space is located on the beach. Further, Fig. 2.6C highlights the overall importance of the *Zandmotor* for dune development along the Delfland coast: by providing the largest favorable accommodation space the *Zandmotor* supports the highest potential for new dunes to develop. Most of this potential is allocated to embryo dune development, as most of the favorable areas are located on the beach. The existing foredunes show a limited development potential as they are already quite densely covered by marram grass. Still, of the considered 500 ha domain of the Delfland coast, in 2017 an estimated two-thirds ($\sim$ 165 ha) appears to have provided favorable accommodation space for dunes to develop.

2.4 Discussion

This paper examined to what extent the Zandmotor has contributed to creating accommodation space favorable for dune development along the Delfland coast. The results indicate that the *Zandmotor* itself provides the most favorable accommodation space, for it has large areas located above 1.6 m a.m.s.l. that on average experience a continuous accretion by wind-blown sand. As such, the results highlight that the *Zandmotor* supports an especially high potential for new embryo dunes to develop as most of its accommodation space is located on the beach. This section examines the merit of the identified conditions for when accommodation space is considered favorable for dune development, as well as the merit of using favorable accommodation space to indicate dune development potential. The latter is examined in relation to the design and intended dynamical nature of the *Zandmotor*, the conditions required for successful establishment of marram grass and the persistent anthropogenic disturbances along the Delfland coast arising from recreation and nature management practices.

2.4.1 Conditions indicating favorable accommodation space for dune development

Accommodation space is considered favorable for dune development when it is sheltered from storm impacts and experiences a steady accumulation of wind-blown sand. The latter condition is not disputed, as the reinforcing feedback between the growth response of marram grass and burial by wind-blown sand is well documented (Huiskes, 1979; Disraeli, 1984; Maun and Lapierre, 1984; Van der Putten et al., 1988; Hesp, 1991; Maun, 1998) and recognized to be fundamental to coastal dune development in temperate regions around the world (e.g., Baas and Nield, 2010; Durán and Moore, 2013; Keijsers et al., 2016; Nolet et al., 2018). The positive feedback mechanism originates from a trait that all beach grasses of the genus *Ammophila* possess, namely potentially unlimited horizontal and vertical growth through its rhizomes (Gemmell et al., 1953; Ranwell, 1972). Whether marram grass grows horizontally or vertically subsequently depends on the amount of wind-blown sand, which makes it so particularly advantageous to dune building. After establishment, by seed or rhizome dispersal, marram grass first produces leafy shoots along newly developing horizontal rhizomes. When wind-blown sand is trapped by the leafy shoots, the immediate sand surface is raised and a small embryo dune is formed (Hesp, 1989). The leafy shoots are capable of growing up through a moderate thickness of sand by elongation of individual leaves. If, however, a leafy shoot is overwhelmed by sand deposition, one or more of its axillary buds develop into a vertical rhizome that will continue to grow until the surface is reached. Adventitious roots are produced from the nodes of the vertical rhizome and the horizontal rhizomes gradually die, so that the vertical rhizomes become independent of one another. This process may be repeated as long as aeolian supply is abundant and marram grass continues to trap sand. The capacity to trap sand, as noted before, is enhanced by the growth response of marram grass to sand trapping, which introduces the positive feedback mechanism driving coastal dune development (Gemmell et al., 1953; Ranwell, 1972). Using very high-resolution data, Nolet et al. (2018) showed that marram grass on foredunes along the *Zandmotor* appears to thrive best under a sand trapping rate of approximately 0.3 meter of sand per growing season and

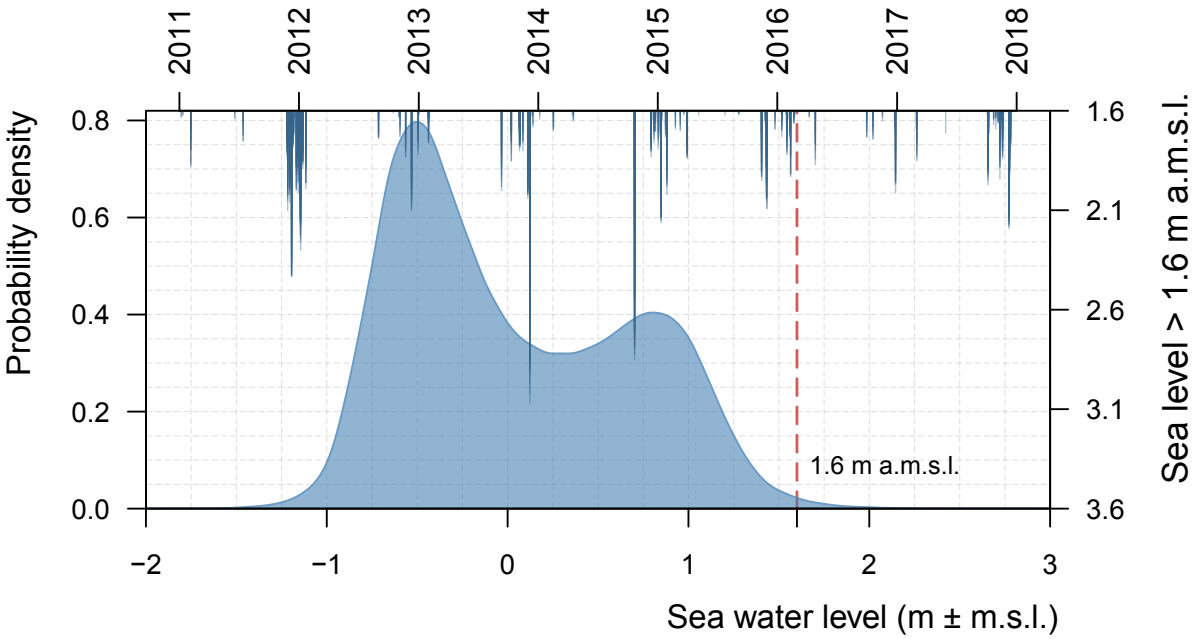

Figure 2.7: Bimodal probability density curve of sea water levels (in m ± a.m.s.l) measured by a buoy near Scheveningen since the construction of the *Zandmotor* in 2011 until 2017. Included are the instances when sea water level exceeded the 1.6 m a.m.s.l boundary height for dune development along the Delfland coast.

that marram grass can withstand sand burial of up to 1 meter of sand. However, while this demonstrates how positive plant-sand feedback steers dune development, it must be noted that the physical size of a developing dune and predominant wind regime also controls its morphology (Davidson-Arnott et al., 2018). As dunes grow, for example, a limit is imposed on its height because the wind force required to transport sand upslope increases significantly (e.g., Arens et al., 1995; Arens, 1996b; Keijsers et al., 2015a). Coastal foredunes therefore tend to expand in width rather than height, which emphasizes the importance of the wide favorable accommodation space the *Zandmotor* provides for foredune development.

The condition that accommodation space is considered favorable when it is sheltered from storm impacts warrants closer inspection, because the impact of a storm surge depend both on the magnitude of the storm as well as the geometry of the beach (Houser et al., 2008). Wind stress due to atmospheric pressure differences drive storm surge levels and offshore wave conditions, but the vertical dimension of the beach profile, in particular, exerts great control on shoreline parameters such as wave setup, swash and run-up (e.g., Stockdon et al., 2006; Sallenger Jr, 2000; Ruggiero et al., 2001). This is significant because the dissipation of kinetic energy of breaking waves is responsible for the highest rates of coastal erosion and dune decline (e.g., Vellinga, 1982; Short and Hesp, 1982). However, while empirical models can calculate wave run-up levels and wave breaking energy from parameters such as offshore wave conditions and beach profile (see Stockdon et al. (2006) and Sallenger Jr (2000) for details), those relations only return approximations as often not all required model input is available or because of inherent model uncertainties. Having said that, the results suggest

that dunes along the Delfland coast are sheltered from storm impacts above a beach height of 1.6 m a.m.s.l. This finding is examined in relation to offshore sea water levels measured by a buoy in close proximity to the *Zandmotor* mega-scale beach nourishment. Figure 2.7 shows the probability density curve (which is bimodal because of tidal dynamics) of those sea water levels (in m $\pm$ a.m.s.l.), measured every 10 minutes from 2011 until 2017. Included are the instances when sea water levels exceeded the apparent 1.6 m a.m.s.l. boundary height for dunes to be sheltered from storm impacts. It is clear from fig. 2.7 that this did not occur frequently, only during about 0.4% of the measurements. Those measurements, however, were relatively clustered together, meaning that the boundary height was exceeded over (relatively) prolonged periods of time. Although, over the course of 6 years this happened for no more than 10 full days. On average the exceedance was about 20 cm up to a sea water level of 1.8 m a.m.s.l., but on a few occasions sea water levels almost doubled compared to the boundary height to 3.10 m a.m.s.l.. This is excluding the wave run-up onto the beach, which can be significant for natural beaches in the Netherlands. Dependent on whether the beach profile is dissipative or reflective, both Stockdon et al. (2006) and Poortinga et al. (2015a) show that wave run-up may reach to heights from 0.85 to 1.45 m above still water level, which is the level that would occur in the absence of waves. This implies that, since the construction of the *Zandmotor* in 2011, the Delfland coast may have experienced coastal erosion by storm surge levels reaching heights up to at least 4 m a.m.s.l.

The observation that in 2017 quite a large number of embryo dunes were present on the beach at heights well below the maximum experienced storm surge levels, points to the capacity of established dunes to withstand and recover from hydrodynamic storm impacts as well as to the pivotal role marine dispersal of rhizome fragments likely plays to dune establishment processes. As remarked by various researchers (e.g., Suanez et al., 2012; Feagin et al., 2015; Houser et al., 2015; Van Puijenbroek et al., 2017a,b), the ability of embryo dunes to recover from storm impacts largely depends on the extent to which the above- and belowground structural integrity of marram grass remains intact after a storm event. This depends, in turn, on the severity of the storm impacts on the dune, which can be caused by wave erosion (scarping and overwash) and swash inundation (Sallenger Jr, 2000; Hesp and Martínez, 2007). Wave erosion may completely remove all sand from an embryo dune (so it is no longer raised from the beach surface) and have an abrasive effect on the leaves of marram grass, causing either minor damage or complete removal of all aboveground biomass. Most of the belowground root system of marram grass, however, has been observed to largely remain intact after wave scarping or overwash (Feagin et al., 2015). Potential damage of swash inundation to marram grass depends on the duration of the inundation period, but as Vergiev et al. (2013) demonstrate, marram grass displays no visible decomposition of stems, roots or rhizomes after being immersed with sea water for 20 days. This is well beyond the period a beach will be inundated after a storm event, which implies that inundation has a limited, if any, negative effect on the structural integrity of marram grass. Given that storm events occur more frequently in winter, it has been observed that embryo dunes on dissipative beaches undergo a classic seasonal cycle of erosion during the winter and accretion during the summer (Montreuil et al., 2013; Van Puijenbroek et al., 2017b). Their presence on the beach, however, would remain persistent throughout the year and often show a yearly net growth when aeolian supply was sufficient (Anthony et al.,

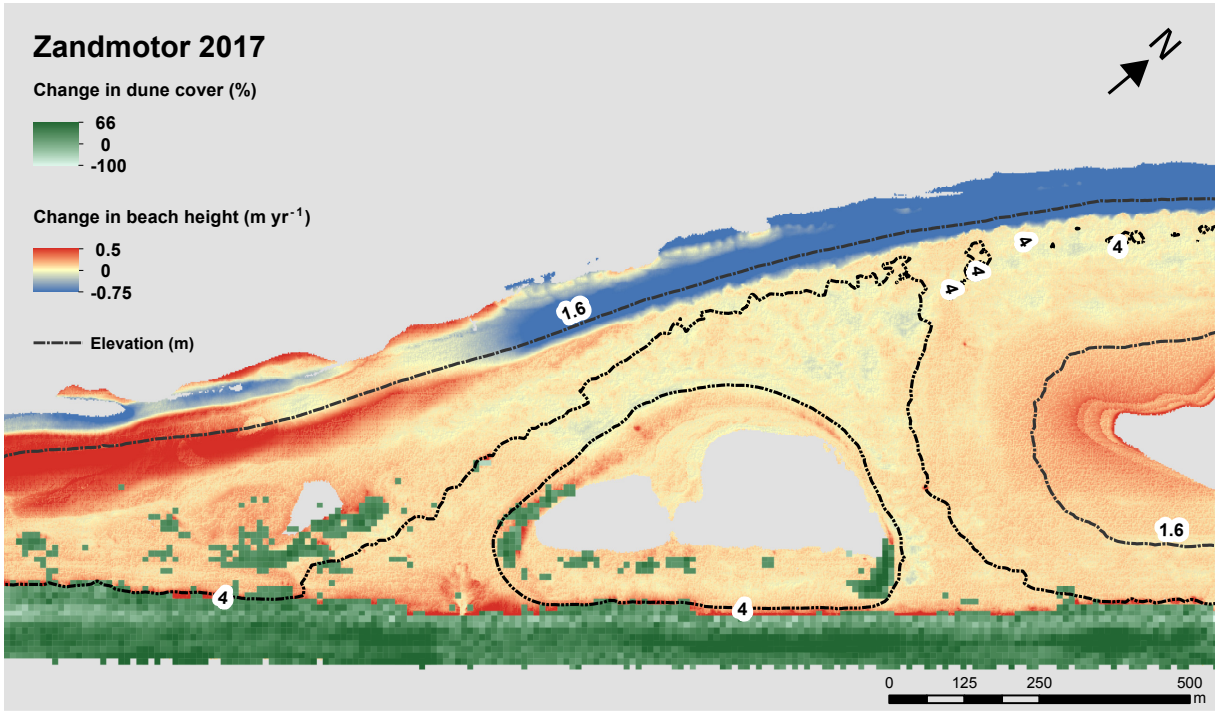

Figure 2.8: The distribution of (embryo) dunes on the *Zandmotor*, suggesting a correlation to marine dispersal of rhizome fragments as a large number of embryo dunes are present between the identified boundary height of 1.6 m a.m.s.l. and the (current) maximum expected storm surge height of 4 m a.m.s.l.

2007; Suanez et al., 2012). This not only indicates that embryo dunes have the capacity to withstand storm impacts and quickly recover to prestorm conditions, but also that the above- and belowground structure of marram grass often remains largely intact after a storm event. Marine forcing, at the same time, has been shown to be an important agent in the dispersal of marram grass rhizome fragments and subsequent dune establishment via clonal growth (Konlechner and Hilton, 2009; Hilton and Konlechner, 2011).

The distribution of (embryo) dunes on the southern part of the *Zandmotor*, as shown in close-up in Fig. 2.8, suggests a correlation to marine dispersal of rhizome fragments as a large number of embryo dunes are present between the identified boundary height of 1.6 m a.m.s.l. and the (current) maximum expected storm surge height of 4 m a.m.s.l. The embryo dunes around the small dune lake, while technically located in the same elevation zone, have likely mostly established by seed germination as the high constructed base of the *Zandmotor* has completely blocked all storm surge impacts until now. Over the years there has been a steady build-up of a freshwater lens under the *Zandmotor* and the salinity of the dune lake has significantly decreased as a result (Huizer et al., 2016). This fresh water availability, in combination with moderate burial dynamics, have been shown by Konlechner et al. (2013) to be beneficial to marram grass seed germination and subsequent dune establishment. The specific distribution of embryo dunes around the dune lake may therefore correlate best to seed dispersal by wind coming from the dominant south-western wind direction, either pushing the seeds over the lake

towards the north-east corner of the lake or depositing it on the south-west lee side where the beach slopes downwards towards the lake. In effect, Fig. 2.8 illustrates that, even though the *Zandmotor* may provide wide favorable accommodation space and thus a high potential for dune development, the conditions required for successful (natural) dune establishment must also be considered. Having said that, Van Puijenbroek (2017) showed in a field transplant experiment that planted marram grass (consisting of a rhizome fragment with one shoot) thrived on most parts of the *Zandmotor* except when exposed to direct wave action. This suggests that conditions that limit marram grass growth and subsequent dune development (e.g. high salinity, drought, low nutrient status) are mostly absent on the *Zandmotor* and likely along the entire Delfland coast.

2.4.2 Dune development potential in relation anthropogenic impacts

The results highlight the overall importance of the *Zandmotor* for dune development along the Delfland coast. First, this is because its beach provides very wide favorable accommodation space that therefore supports a high potential for new embryo dune development. And second, because of its sand-feeding effects, the *Zandmotor* has likely contributed to creating more favorable accommodation space for dune development along the entire Delfland coast. The coastline directly north of the *Zandmotor*, for example, experienced a significant accumulation of sand between 2013 and 2017 even though it has not been nourished with sand in the years before. Although the amount of sand accumulation was less compared to the coastline that has been nourished between 2009 and 2011, the overall positive sand budget illustrates the intended dynamical nature of the *Zandmotor*, where its sand is redistributed along the coastline causing a seaward broadening of the beach and dunes. In fact, graph 2.6C suggests that the unnourished northern part of the Delfland coastline supports a higher potential for dune development compared to the nourished southern coastline. In part this may be due to the fact that the Delfland coast is characterized by a net northward sediment transport regime (Van Rijn, 1997), which is reflected in the sand-feeding budget of the *Zandmotor*. In the first 18 months after its completion, De Schipper et al. (2016) for example show that up to 40% more sand of *Zandmotor* was transported in a northward direction rather than southward towards Rotterdam harbor. At the same time, because the 2009 – 2011 nourishment strategy consisted (for a large part) of foredune reconstruction that included plantings of marram grass, the created favorable accommodation space along the nourished coastline may not accommodate much new dune development. As such, even though the coastline south of the *Zandmotor* has been reinforced with sand nourishment, it is quite possible for the unnourished northern Delfland coastline to experience more pronounced dune development in the years to come.

Interestingly, however, the positive effect of the *Zandmotor* on the northern Delfland coastline, in terms of sand accretion, is not reflected in the changes in cover by marram grass between 2016 and 2017. Even though it is shown that the coastline north of the *Zandmotor* provides ample favorable accommodation space, it appears that the potential for dune development is currently not being realized. There are two main anthropogenic impacts that may hamper dune development along this urbanized coastline, namely persistent disturbances arising from

recreation and leisure as well as a (increasingly prevalent) nature management practice that is aimed at remobilizing the dune landscape. Figure 2.9 gives an overview of total alongshore changes in dune cover by marram grass between 2016 and 2017 (in $m^2m^{-1}yr^{-1}$) and aims to relate it to anthropogenic activities that may impact (both positively and negatively) dune development along the Delfland coast. In the broadest sense, the coastline can be divided first according to whether or not it has recently been nourished with sand and what type of sand nourishment has been implemented. A distinction can be made between the sand nourishment that was carried out between 2009 and 2011 to reinforce most of the Delfland coastline, the nature compensation project *Spanjaardsduin* implemented at the same time and, finally, the *Zandmotor* mega-scale beach nourishment that was completed at the end of 2011. Further, within the nourished coastline there is a zone where the dune development appears to lag behind compared to the rest of the nourished coastline. This zone, as Fig. 2.9B illustrates, can be characterized by a higher concentration of disturbances arising from recreation and leisure. Then, finally, there is the northern part of the Delfland coastline that has not been nourished with sand in recent years. Within this zone, as Fig. 2.9C shows, relatively large dune areas have been excavated between 2011 and 2013 aimed at rejuvenating the dune landscape by reinitiating aeolian dynamics. In the following paragraphs, each identified zone of the Defland coast and how dune development potential may be impacted by the various anthropogenic activities are discussed.

As Fig. 2.9C shows, the overall positive effect of the three sand nourishment schemes on dune development is clearly reflected in the changes in marram grass cover between 2016 and 2017. Within the nourished zone, however, there are three clear dips where the dune cover appears to have decreased over the course of a year. Upon closer inspection it seems that each dip coincides with a beach entrance where the public can enter the beach. A number of natural processes and human activities may be involved here in the observed decline in marram grass cover. First of all, as Fig. 2.9B shows, the seaward side of a beach entrance is commonly paved with concrete slabs and cuts relatively deep into the stoss slope of the foredune. This, effectively, mimics a through foredune blowout (e.g., Hesp, 2002), in which wind erosion is enhanced because of local wind speed acceleration and pronounced turbulent flow structures such as corkscrew vortices (Hesp and Martínez, 2007). Because the floor is paved, these wind-driven forces will in particular erode (i.e., widen) the slopes of the beach entrance and this susceptibility to lateral erosion may have lead to the observed decline in marram grass cover. Second, as can also be seen in Fig. 2.9B, there is often a hospitality establishment (e.g., a beach bar or restaurant) directly beside a beach entrance. And although their placement on the beach is often seasonal, their presence is numerous. In the summer of 2017, for example, only 3 of the 23 beach entrances along the Delfland coast did not have one or more hospitality establishments directly placed besides it. Perhaps not coincidentally, two of those three entrances gave access to the more isolated parts of the *Zandmotor*. The presence of hospitality establishments puts additional pressure on the dunes as people may flock around the beach entrances and motorized vehicles are more common, e.g., to resupply the establishment. Even though walking or driving in the foredunes is prohibited along the Delfland coast, several studies (e.g., Andersen, 1995; Anders and Leatherman, 1987) show that vehicles and people on the beach may have a significant negative effect on dune development.

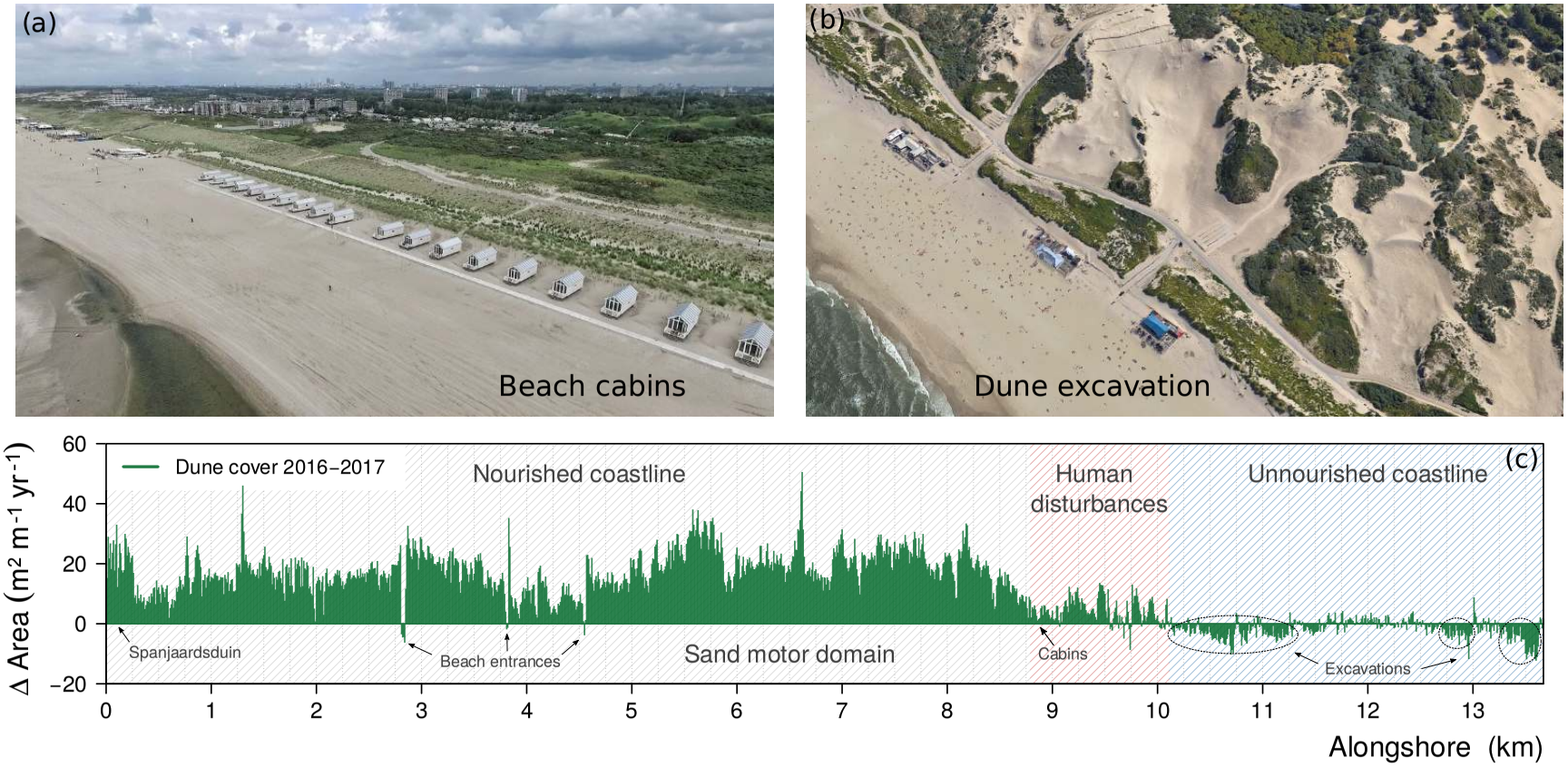

Figure 2.9: Overview of total alongshore changes in dune cover by marram grass between 2016 and 2017 (in $m^2m^{-1}yr^{-1}$) in relation to anthropogenic activities that impact (positively and negatively) dune development along the Delfland coast. Aerial photographs courtesy of René Oudshoorn (**2.8A**) and Google Maps (**2.8B**).

At the same time, as laid out in more detail by Jackson and Nordstrom (2011), the structure of the hospitality establishment itself may alter (i.e. block) aeolian transport from the beach and retard foredune development. This plays an even larger role in the nourished zone north of the *Zandmotor* where, besides a large number of hospitality establishments, a high amount of seasonal beach cabins are also placed along the toe of the foredunes from March until October (from 2016 onward). Their placement close together, as Fig. 2.9A shows, has the additional effect that the airflow can constrict and accelerate between the beach cabins, which increases the likelihood of local scour resulting in aeolian deposition farther landward (Nordstrom, 2004). Although in some instances this may actually be beneficial to the foredunes, the clear decline in cover by marram grass (see Fig. 2.9C) indicates that the placement of beach cabins had an overall negative impact on dune development between 2016 and 2017. And while the beach cabins were in fact raised slightly from the surface ($\sim$ 50 cm), Nordstrom and McCluskey (1984) show that such a modest height may not have been sufficient to minimize interference with the wind flow and resultant aeolian dynamics. Further, another important anthropogenic disturbance with a highly negative impact to dune development is that the beach directly north of the *Zandmotor* is mechanically raked during the summer to remove wrack line material and human litter. Even though it is a common practice to accommodate beach recreation (Jackson and Nordstrom, 2011), this severely hampers embryo dunes from establishing themselves on the beach. Not only can the machinery destroy any sprouting seedlings or rhizomes of marram grass, the removal of wrack deposits also deprives marram grass from potential hospitable locations to establish itself on the beach (Kelly, 2014). As a result, these anthropogenic disturbances combined have likely contributed to reduced dune development compared to the rest of the nourished Delfland coastline.

Then, as Fig. 2.9C and Fig. 2.4E show, the decrease in marram grass cover along the unnourished northern part of the Delfland coastline suggests that the foredunes have been in decline between 2016 and 2017. This is unexpected considering the positive sand-feeding effect of the *Zandmotor* on this stretch of coastline. Upon closer inspection, the main candidates for the observed foredune decline are a number of dune excavations aimed at rejuvenating the dune landscape. When the focus of Dutch coastal policy widened, to also include preserving the spatial quality and natural values of the coastal zone, it was recognized that traditional flood safety measures had led to over-stabilized dune systems that were characterized by a markedly reduced biodiversity compared to younger and more dynamic dune systems (e.g., van Dorp et al., 1985; Provoost et al., 2011). For that reason, in places where coastal safety could be guaranteed, remobilizing dune systems by removal of dune vegetation and topsoil has become a key management practice for maintaining a high biodiversity in the dune landscape. Reinitiating aeolian dynamics is hereto essential, as deflation and deposition zones creates habitat diversity and renewed opportunities for specialized pioneer vegetation species (e.g., Arens et al., 2013). Nowadays, in order to maintain or even increase dune mobility, the rejuvenated dune systems are often connected to the beach and foredunes through the excavation of foredune notches. This has been shown to result in a sustained input of wind-blown calcareous beach sand and more diverse living conditions for pioneer vegetation, e.g due to higher levels of sand burial, wind speeds or salt spray (Riksen et al., 2016; Ruessink et al., 2018). However, as Fig. 2.9C shows, dune excavation practices appear to adversely affect foredune development.

While there were no foredune notches explicitly excavated along the Delfland coast, Fig. 2.9B shows that the paved beach entrances may similarly act as conduits for aeolian transport into the dune excavations. As a result it is quite possible that the narrow foredunes in front of the excavated dune are experiencing a net deflation of sand that negatively affects the growth of marram grass (e.g. by root exposure). Sand deposition then likely occurs deeper landward where no marram grass is presently growing to benefit from an increase in sand burial. Marram grass cover, as a result, has been in decline between 2016 and 2017, indicating a decline in the foredunes as well. However, with the *Zandmotor* feeding the coastline and providing an effective flood defense, this localized foredune decline should not pose an imminent threat to coastal safety.

2.5 Conclusions

This paper examined to what extent the *Zandmotor* has contributed to creating accommodation space along the Delfland coast favorable for dune development, i.e. accommodation space that is sheltered from frequent storm impacts and experiencing a steady accumulation of wind-blown sand. Comparing the presence of dunes in 2017 to its elevation indicates that dunes are sheltered from storm surges above a height of 1.6 m a.m.s.l. Comparing the changes in dune cover by marram grass from 2016 to 2017 to the average yearly change in dune height between 2013 and 2017 demonstrates that dunes were almost exclusively present in accreting areas. As such, even though its design may not be optimal for successful marram grass establishment, the results highlight the overall importance of the *Zandmotor* to dune development potential:

- Compared to the rest of the Delfland coast, the supratidal beach of the *Zandmotor* provides very wide favorable accommodation space and therefore supports a high potential for new embryo dunes to develop.
- Because of its sand-feeding effects, the *Zandmotor* will likely contribute to creating more favorable accommodation space for dune development along the entire Delfland coast.

However, because of persistent anthropogenic disturbances arising from recreation and nature management practices, dune development along this urbanized coastline may not reach its full potential. This should not be too alarming, though, as the *Zandmotor* mega-scale beach nourishment is set to ensure the safety of the Delfland coast for years to come.

Chapter 3

Synchronous long-term measurements to characterize aeolian transport dynamics on a mega-scale beach nourishment

This chapter is based on:

Nolet, C., Gooren, H. Peters, P. and Riksen, M. (2020, in prep). Synchronous long-term measurements to characterize aeolian transport dynamics on a mega-scale beach nourishment.

Abstract

Coastal foredunes are often of great importance to coastal safety. For that reason a good insight into aeolian dynamics is essential as wind-blown sand exerts direct control on foredune development. This insight, however, is challenged by a high degree of uncertainty in characterizing aeolian transport dynamics in the coastal environment. This is foremost due to a lack of consensus about whether steady-state saltation is best described by a quadratic or cubic dependence to wind shear velocity, but the saltation mass flux may often also not be in steady-state due to unsteady wind conditions or may not be saturated to expected capacity due to supply-limiting factors. By applying nonlinear quantile regression analysis to a synchronous long-term record of aeolian transport and wind forcing measurements, this paper assesses the impact of supply-limiting factors on aeolian dynamics in the coastal environment. Analysis of the data demonstrates that this impact, to a great extent, is determined by the physical description of steady-state saltation. Regression analysis shows that saltation mass fluxes generated in the coastal environment, under typical limiting conditions, may be up to two (for quadratic dependence) or three (for cubic dependence) orders of magnitude lower than saltation rates predicted by equations parameterized in wind tunnel experiments. Taking the impact of supply-limiting factors better into account can help ensue more realistic saltation mass flux predictions applicable to the coastal environment.

3.1 Introduction

Coastal foredunes, the most seaward facing dune ridge parallel to the coastline, often form the first and most critical line of flood defense against the sea (Hardisty, 1994). This is certainly true for the Netherlands, a country where the most densely populated areas are situated well below mean sea level and over 75% of the coastline relies on its foredunes to ensure coastal safety (Van Koningsveld and Mulder, 2004). More than half of the Dutch sandy coastline, however, is subject to marine erosion and requires periodic sand nourishments as a counteractive measure (Van der Wal, 2004). Changes in the global climate, with expected consequences as sea level rise and increase in storm surge intensity, will likely increase the importance of the foredunes in providing coastal protection (e.g., Hillen and Roelse, 1995). For that reason a clear insight into coastal aeolian dynamics is essential, as sand transport by wind exerts great control on the development of foredunes (Adriani and Terwindt, 1974; Kroon and Hoekstra, 1990; Arens, 1996b, 1997).

In his classic work, Bagnold (1941) was the first to identify saltation as the principal mechanism of aeolian transport for sand-sized particles. Central to the saltation process are the hopping ballistic trajectories of particles that, upon rebounding off the surface, produce a splash of newly ejected particles (e.g., Ungar and Haff, 1987; Werner, 1990; Martin and Kok, 2017). When saltation is initiated by wind shear stress (τ) at the surface, the number of particles in saltation first increases exponentially due to the multiplicative nature of this splashing process (Anderson and Haff, 1988; Shao and Raupach, 1992). The drag of particles in saltation then causes the wind to lose momentum and the shear stress decreases to a critical value (τ_c) which corresponds to the impact threshold, the lowest wind stress at which saltation can be sustained after it has been initiated (Owen, 1964; Ho et al., 2011). Through this negative feedback mechanism, after a certain distance and time, the saltation process enters a steady-state (Sauermann et al., 2001; Andreotti et al., 2010). During such conditions the (saturated) saltation mass flux q (kg m^{-1} s^{-1}) can be expressed by:

$$q = (\tau - \tau_c)\frac{l_{hop}}{u_{\downarrow} - u_{\uparrow}} \tag{3.1}$$

Where l_{hop} is the mean saltation hop length (m), while $u_{\downarrow}$ and $u_{\uparrow}$ are the mean horizontal speeds (m s^{-1}) of saltating particles due to splash impact and aerodynamic entrainment (e.g., Andreotti, 2004; Ho et al., 2011; Durán et al., 2011; Kok et al., 2012).

A common assumption made in steady-state saltation models is that the mean horizontal speed of a particle in saltation linearly scales to the wind shear velocity (u_*). As shear stress (τ) is related to shear velocity by $\tau = \rho\, u_*^2$ (with ρ the density of air), it is demonstrated by Kok et al. (2012) that this assumption yields a cubic dependence of the saltation mass flux to shear velocity ($q \propto u_*^3$). Many classic and often-used aeolian transport models, starting with Bagnold (1941), assume such cubic dependence (e.g., Kawamura, 1951; Zingg, 1953; Owen, 1964). Recent work, however, has put into question the linear scaling of mean particle speeds to the shear velocity. Instead it is argued that, during steady state, mean particle speed (and the saltation length) is almost exclusively determined by momentum transfer from splash

impact and not by aerodynamic entrainment (e.g., Ungar and Haff, 1987; Andreotti, 2004; Kok et al., 2012). Under these conditions, for saltation to maintain steady-state, numerical modeling has shown that this requires mean particle speeds to be almost invariant to the shear velocity (e.g., Anderson and Haff, 1988; Werner, 1990; Namikas, 2003), which yields a quadratic dependence of the saltation mass flux to shear velocity ($q \propto u_*^2$). Subsequent wind tunnel experiments (e.g., Iversen and Rasmussen, 1999; Creyssels et al., 2009; Ho et al., 2011) and field observations (Jackson and McCloskey, 1997; Martin et al., 2013; Martin and Kok, 2017) have demonstrated this quadratic dependence.

The concept, however, that mean horizontal particle speeds in steady-state saltation do not linearly scale to shear velocity, has been not been fully embraced by the aeolian research community. Consequently, as put forward more exhaustively by Sherman and Li (2012) and Kok et al. (2012), there is no consensus about whether the saltation mass flux is best described by a quadratic or a cubic dependence to shear velocity. This scientific disagreement about the physical description of steady-sate saltation, poses a first and fundamental challenge in characterizing coastal aeolian transport dynamics. A second challenge relates to the fact that, under natural conditions, the saltation mass flux may often (1) not be in steady-state due to unsteady wind conditions (e.g., Kok et al., 2012) or (2) not be saturated to constant (i.e. full) capacity due to supply-limiting factors (e.g., Nickling and Neuman, 2009). So-called transient-state saltation dynamics arises from the inherent turbulent nature of near-surface winds (Metzger et al., 2007). Turbulent flow structures in the atmospheric surface layer (e.g. bursts, vortices and eddies) lead to highly unsteady and fluctuating winds. Which, in turn, lead to transient transport responses such as intermittency (Stout and Zobeck, 1997), lags and overshoot (Shao and Raupach, 1992), streamers (Baas and Sherman, 2005) and (threshold) hysteresis (Martin et al., 2013). Steady-state saltation equations do not account for such turbulence-driven effects and their predictive quality is thus inherently compromised under field conditions (e.g., Butterfield, 1991; Sterk et al., 1998).

Moreover, especially in the coastal environment, there are numerous factors that limit the supply of sand to the aeolian transport system (e.g., Davidson-Arnott and Law, 1996; Sherman et al., 1998). Under these conditions the saltation mass flux, while reaching steady-state, does not saturate to a constant (or expected) saltation density for a given shear velocity (Nickling and Neuman, 2009). Surface moisture, in particular, is known to greatly increase the resistance of sand to entrainment, by binding sand grains together through cohesive and adhesive forces (Chepil and Woodruff, 1963; Belly, 1964; Cornelis and Gabriels, 2003a). Since wetting and drying processes are governed by complex hydraulics (i.e. tidal and wave action, groundwater and capillary flow, evaporation and precipitation), the control surface moisture exerts on particle entrainment (both splash impact and fluid lifting) is highly variable in time and space. As a result, the proportionality of the saltation mass flux to shear velocity (regardless whether it is quadratic or cubic) is not stable in time and space either. While considerable effort has been undertaken to parameterize steady-state saltation equations to coastal environments (e.g., Bauer and Davidson-Arnott, 2003; Bauer et al., 2009b), the spatial-temporal complexity of surface moisture and numerous other supply-limiting factors (e.g. vegetation growth, shell layers, algae crusts, local topography) have been shown to significantly hamper their predictive quality (Arens, 1996a; Sherman et al., 1998; De Vries et al., 2014).

These above-mentioned issues combined give rise to a high degree of uncertainty in characterizing coastal aeolian transport dynamics. This paper aims to address these uncertainties through analysis of a long-term record of direct aeolian saltation mass flux measurements at a high temporal resolution. Such records are not readily available because appropriate measurement equipment is lacking (Barchyn et al., 2011). The challenge is to combine the advantages of passive trapping methods, i.e. direct measurement and long-term deployment (Goossens et al., 2000), with the advantages of active sensor-based methods, i.e. automated operation at (very) high temporal resolutions (Sherman et al., 2011; Poortinga et al., 2015b). For that reason a new automated sand trap has been developed and deployed on a wide nourished beach in the Netherlands between May till November 2015. Using this new equipment, together with detailed shear velocity measurements, the primary aim of this paper is to characterize the overall impact of supply-limiting factors on coastal aeolian dynamics. Using nonlinear regression analysis, the issue addressed first is whether the saltation mass flux may be better described by a quadratic or cubic dependence to shear velocity. Quantile regression is an approach to account for (unmeasured and variable) limiting factors in the field that induce a response distribution of observations scattered beneath an upper limit. As a result, this paper aims to show that the physical description of steady-sate saltation, to a great extent, determines how supply-limiting factors impact coastal aeolian dynamics.

3.2 Material and methods

3.2.1 Regional setting

The research was conducted in the Netherlands at the *Zandmotor* (Dutch for 'Sand Motor', see Fig. 3.1), an experimental mega-scale beach nourishment of 21.5 Mm^3 constructed in 2011 for coastal protection (Stive et al., 2013b). Located just south of the city The Hague, the *Zandmotor* has a hook-shaped design that mirrors the natural onshore migration of an intertidal sandbar. Just after its construction it had a surface area of about 28 ha, extending 2.5 km along the coastline and protruding 1 km into the sea. The design of the *Zandmotor* reflects the 'building-with-nature' coastal management strategy (Van Slobbe et al., 2013), which aims to provide coastal safety by utilizing natural processes. Marine and aeolian forces are permitted to gradually redistribute the sand of the *Zandmotor* along the coastline, thereby reinforcing the adjacent beach and dunes against storm surges and sea level rise. As such, a net negative sediment balance is counteracted while adverse effects to the coastal ecosystem are minimized (De Schipper et al., 2016).

A distinct feature that sets the *Zandmotor* apart from more traditionally nourished or natural coastlines, is the locally very high construction height. Most of the beach is constructed at a height around 5 m above mean sea level (a.m.s.l.), but in some places the beach even reaches a height of 7 m a.m.s.l. This is well above the current maximum storm surge level of about 3 m a.m.s.l. (Radermacher et al., 2018), so reworking of sand on the *Zandmotor* is almost exclusively due to aeolian forcing. The high shell content and heterogeneous grain size distribution of the dredged sand used to create the *Zandmotor* has been observed to lead to beach armoring due to aeolian sorting (Hoonhout and de Vries, 2017a). This likely acts as an

Figure 3.1: The *Zandmotor* ('sand motor'), an experimental mega-scale beach nourishment constructed in 2011 for coastal protection. **3.1A**. The *Zandmotor* has a hook-shaped design that aims to mirror the onshore migration of an intertidal sandbar. Natural dynamics are encouraged to redistribute the sand of the along the coastline, causing the base to flatten and the sand to spread in alongshore directions. **3.1B-C**. Aerial photographs of the *Zandmotor* (taken May 2015) which shows its position along the Delfland coast facing north towards the city The Hague (B) and a close-up of the foredunes and small dune lake (C).

additional supply-limiting factor specific to *Zandmotor*, although it is a common occurrence on nourished beaches (Van der Wal, 2004). The semidurnal tidal dynamics are characterized by a spring / neap tidal amplitude around 2.0 / 1.5 meter, generating alongshore currents velocities up to 0.5 ms^{-1} (Luijendijk et al., 2017). Climate in the Netherlands is temperate humid, with strong seasonal contrasts (Arens et al., 1995). There is a clear year-round dominance of south-westerly winds, but those winds are strongest and most prevalent in the summer and winter. Current annual average rainfall in the Netherlands is around 880 mm and is distributed quite evenly throughout the year, although early spring is generally a dryer period (e.g., Daniels et al., 2014).

3.2.2 Saltation mass flux

The red box in Fig. 3.1A depicts the measurement location at the *Zandmotor* and Fig. 3.2A shows the employed measurement setup. Aeolian sand transport was measured by modified Leatherman traps. The Leatherman trap is a passive cylindrical and non-rotating vertical sand trap first developed by Leatherman (1978) and later improved by Rosen (1978). The simple and sturdy design has proven its worth in the harsh coastal environment (e.g., Sarre, 1988, 1989b; Greeley et al., 1996; Jackson, 1996; Sherman et al., 1998). In the modified version

used here, the part of the instrument that traps the sand closely follows the original design. The modification relates to the added capacity to digitally register the weight of the trapped sand. This allows for long-term deployment at user-defined temporal resolutions, which was not possible in previous designs. The Leatherman trap is a vertically integrating sampler and lacks information about the height of the saltation layer. Aeolian transport, therefore, is expressed as a horizontal saltation mass flux per meter width (kg m^{-1} s^{-1}).

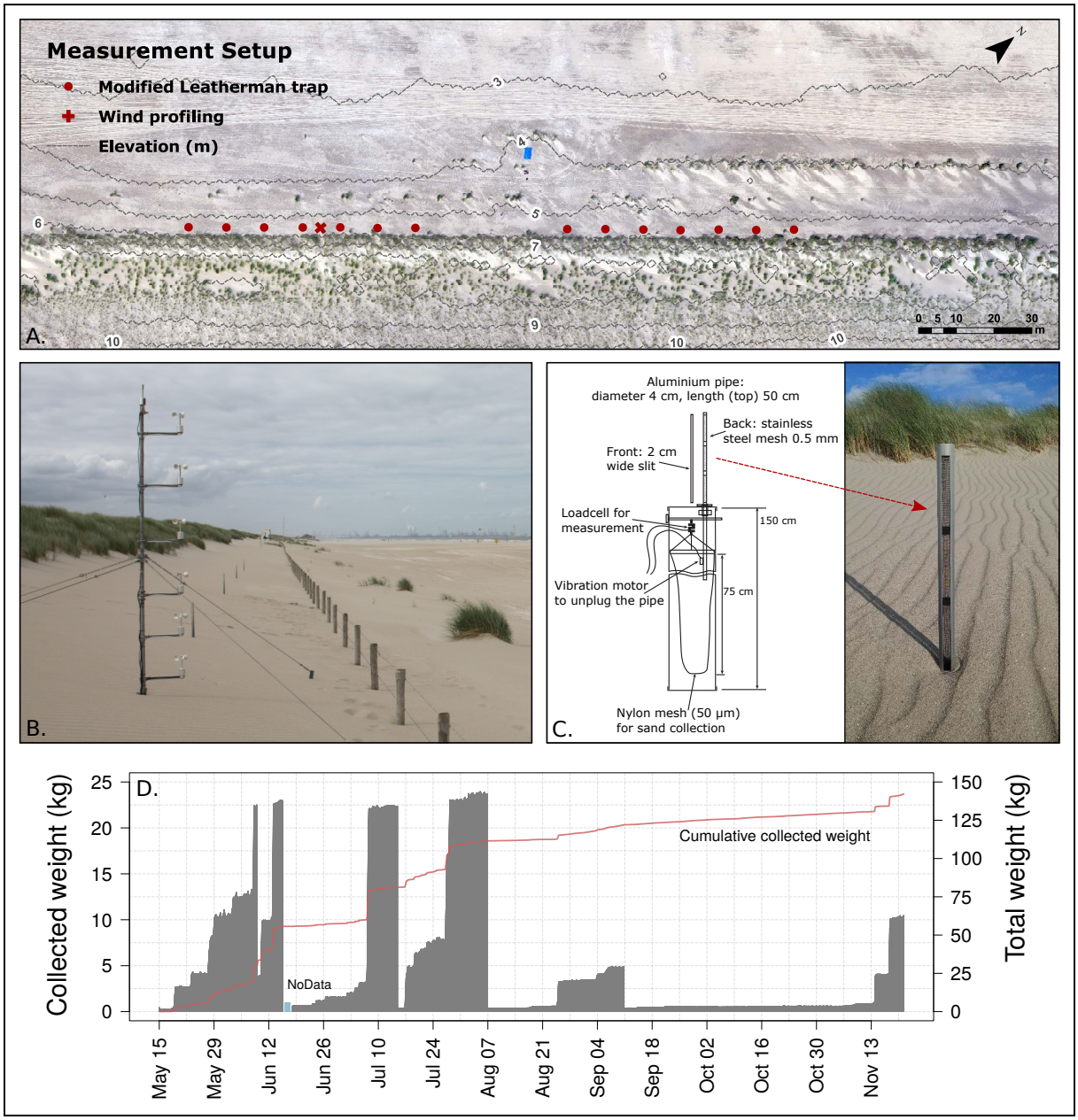

Figure 3.2: Measurement location and experimental set-up. **3.2A**. Saltation mass flux was measured by 14 modified Leatherman sand traps placed parallel in front of the foredunes. **3.2B**. Shear velocity was derived from a wind profile using 6 three-cup anemometers installed at discrete heights in a vertical profile. **3.2C**. Schematic of the modified Leatherman trap and its deployment in the field. **3.2D**. Example of raw data output of the modified Leatherman sand trap.

Figure 3.2C shows a schematic of the modified Leatherman trap and its deployment in the field. The part that traps the sand consists of a 4 cm diameter and 100 cm long aluminum pipe, which has two 50 cm long vertical slits at opposite sides that extend above the beach surface. The 2 cm wide front slit acts as a collection inlet for sand particles, while the 4 cm wide back slit allows for air to flow through the pipe. The back slit is covered by a 0.5 mm stainless steel mesh to block sand particles from being blown through the pipe. The aluminum pipe extends downward into a 20 cm diameter and 150 cm long PVC tube buried beneath the beach surface. The PVC tube houses a 75 cm long 50 μm nylon mesh bag for sand collection, which is suspended from a tension load cell with a rated capacity of 25 kg. Using a CR6 data logger (Campbell Scientific Ltd), the cumulative weight of the trapped sand could be measured with a 0.24 g resolution and was recorded at 10-minute intervals. To help prevent clogging up, for example by wet sand, the trap was fitted with a vibration motor that was activated for a few seconds every 30 minutes.

As shown in the measurement setup (Fig. 3.2A), two sets of 7 modified Leatherman traps were installed downwind of the prevalent wind direction, along the toe of the fore dunes at approximately 6 m a.m.s.l. To account for spatial variability, the traps were spaced 10 m apart from each other and the distance between the two sets was approximately 50 m. The measurement location was chosen (1) to measure the input of aeolian sand transport from the *Zandmotor* into the foredunes and (2) reduce the occurrence of transient-state saltation over (potential) long fetch distances (e.g., Owen, 1964; Gillette et al., 1996; Davidson-Arnott et al., 2005b). Also, from a practical standpoint, the placement of the equipment behind fencing (see Fig. 3.2A) provided protection against vandalism and ensured long-term field deployment. The front vertical inlets of the modified Leatherman traps were positioned parallel to the dune toe facing the shoreline at a 310° north-westerly orientation. Assuming a capacity to trap sand over an angle of 180°, the modified Leatherman traps were restricted to measuring aeolian sand transport coming from approximately 220° up to 40° angles in onshore wind direction. To illustrate the data collection procedure, figure 3.2D shows the raw data as measured by one modified Leatherman trap. With a maximum trapping capacity of 25 kg the traps had to be emptied out on a regular basis. Also, due to a technical problem in the field, there was a 2-day period in June (shown in blue) in which no data were collected. The measurement campaign was halted after a prolonged stormy period at the end of November 2015 damaged the solar panels that provided power to the measurement equipment.

To derive a saltation mass flux the collected cumulative weights were first expressed as a weight per 10-minute time step, by calculating the successive weight differences ($t_{diff} = t_2 - t_1$). Those weight registrations (kg 10 min^{-1}) were then converted to a saltation mass flux with standard units (kg m^{-1} s^{-1}), by taking into account the 0.02 m trap inlet width of the sampler and the 10 minute sampling duration. Because the modified Leatherman trap (in its current form) is non-rotating and does not orient itself to the prevailing wind direction, the effective trap inlet width of the sampler was adjusted according to the angle of incident saltation. For each 10-minute measurement interval the angle of saltation incidence was determined from the average wind direction. Then, with w the 0.02 m inlet width of the modified Leatherman trap and α the angle of incident saltation, the effective trap inlet width was determined by:

$$w_{eff} = w\ sin\ \alpha \tag{3.2}$$

Subsequently, during shore-perpendicular winds (coming from a 310° wind direction) the incident saltation angle equaled 90° and the effective trapping width equaled the full 0.02 m trap inlet width. During oblique winds the incident angle decreased and the effective trapping width of the sampler was adjusted accordingly. To avoid unrealistically high saltation fluxes during almost shore-parallel winds, a lower bound of 10° was set for the incident saltation angle. The trapping efficiency of the modified Leatherman trap was determined to be approximately 97% during a field study by Goossens et al. (2018). For that reason no additional scaling was applied to correct for the trapping efficiency. Further, while the beach towards the measurement location was slightly sloping upward, any type of slope correction was not deemed necessary because of its limited impact for gentle ($< 15°$) slope angles (Sherman et al., 1998).

3.2.3 Shear velocity

A wind profile mast was set up in between the modified Leatherman traps at the southern location (Fig. 3.2B). Wind speed (m s^{-1}) was measured every 20 seconds and the min, max and average wind speed was recorded every minute. Six three-cup anemometers (A100R Windspeed Ltd.) were installed at discrete heights in a vertical profile. The anemometers were installed at an initial height of 0.3, 0.7, 1.1, 1.6, 2.1 and 2.6 m with respect to the sand surface. Over the course of the measurement period the anemometer heights were effectively lowered by about 0.04 m because the surface was gradually raised by sand deposition. For that reason the height of the lowest anemometer (w.r.t. the sand surface) was measured during each field visit and during analysis the heights of the six anemometers were calculated for each 1-minute time step using linear interpolation. Wind direction (0-360°) was measured every minute with a windvane (W200P Windspeed Ltd.) installed at 2.7 meter height. Rainfall (mm), not depicted in Fig 3.2, was measured with a 0.2 mm resolution tipping bucket raingauge (ARG100 Environmental Measurements Ltd.) and recorded every 10 minutes.

The 1-minute average wind speeds recorded by each anemometer at the six different heights (w.r.t. the sand surface at the time of the measurement) were used to estimate the shear velocity u_* and roughness length z_0 via the Law of the wall (Von Kármán, 1930), which states a logarithmic increase in velocity with height:

$$u_z = \frac{u_*}{k} \ln\left(\frac{z}{z_0}\right) \tag{3.3}$$

Where u_z is the wind speed (m s^{-1}) at height z above the surface (m), u_* is the shear velocity (m s^{-1}), k is the Von Kármán's constant (0.4) and z_0 is the roughness height (m) where the wind speed approaches zero. Rearranging Eq. 3.3 into $u_z = a \ln z + b$ and using nonlinear regression analysis, the shear velocity and roughness length were calculated by $u_* = ka$ and $z_0 = e^{-b/m}$, respectively (Bergeron and Abrahams, 1992). To account for measurement errors (e.g. due to a malfunctioning anemometer) it was decided, in line with the procedure outlined by Sherman et al. (1998), that a 95% confidence level (corresponding to a goodness of fit

$R^2 \gtrsim 0.92$) was required for any wind profile to be included in further analysis. The calculated shear velocities were subsequently averaged to match the 10-minute time step of the modified Leatherman trap.

3.2.4 Quadratic and cubic aeolian transport model

To assess whether the saltation mass flux may be better described by a quadratic or a cubic dependence to shear velocity, two aeolian sand transport equations were selected:

$$q = \begin{cases} b\ u_{*t}\ (u_*^2 - u_{*t}^2) & \text{if} \quad q \propto u_*^2 \\ b\ (u_* - u_{*t})\ (u_* + u_{*t})^2 & \text{if} \quad q \propto u_*^3 \end{cases} \tag{3.4}$$

Where parameter b and the impact threshold shear velocity u_{*t} are taken as regression parameters. Parameter b incorporates three variables related to each other by $b = C\frac{\rho}{g}$, where C is an empirically derived saltation flux scaling parameter related to the transported material, g the gravitational acceleration (9.81 m s^{-2}) and ρ the (standard) density of air (1.23 kg m^{-3}). The quadratic function (Eq. 3.4-top) has been proposed by Kok et al. (2012) as the most promising candidate to relate the saltation mass flux to shear velocity. Parameter b in this equation's original form takes the value of 0.63 (with $C = 5.0$). The cubic function (Eq. 3.4-bottom) has been proposed by Kawamura (1951) and was the first to extend the equation of Bagnold (1941) by including an explicit term for the (impact) threshold shear velocity. Compared to other cubic steady-state saltation relationships (e.g., Zingg, 1953; Owen, 1964; Lettau, 1978), the equation of Kawamura (1951) describes the upper range of predictions for aeolian transport rates at higher shear velocities. In this equation's original form the parameter b takes the value of 0.35 (with $C = 2.78$), though later work by White (1979) suggests that a value of $C = 2.61$ may be more appropriate. In that case regression parameter b takes a value 0.33.

Figure 3.3A illustrates the performance of the quadratic and cubic function as well as the difference between them. The cubic function predicts higher saltation mass fluxes for a given shear velocity, but its performance is less sensitive to changes in the (impact) threshold shear velocity u_{*t}. Estimates for the impact threshold shear velocity u_{*t} are derived using Bagnold (1936): $u_{*t} = A\sqrt{gd\frac{\rho_s - \rho_a}{\rho_a}}$, with 0.08 for constant A, 2650 kg m^{-3} for sand density ρ_s, and d the grain size diameter. Grain size analysis using laser diffraction yielded an average grain size diameter of 255, 429 and 656 μm for the D10, D50 and D90 cumulative mass percentages of the trapped sand. Both the quadratic and cubic function have in common that a change in the impact threshold shear velocity affects the rate of saltation mass flux. But, as can be seen Fig. 3.3A, the performance of the quadratic function is significantly more impacted by such a change than the cubic function.

3.2.5 Nonlinear quantile regression analysis

The quadratic and cubic transport functions were fitted to the data using nonlinear quantile regression, as described by (Koenker and Bassett Jr, 1978) and implemented in the R-package

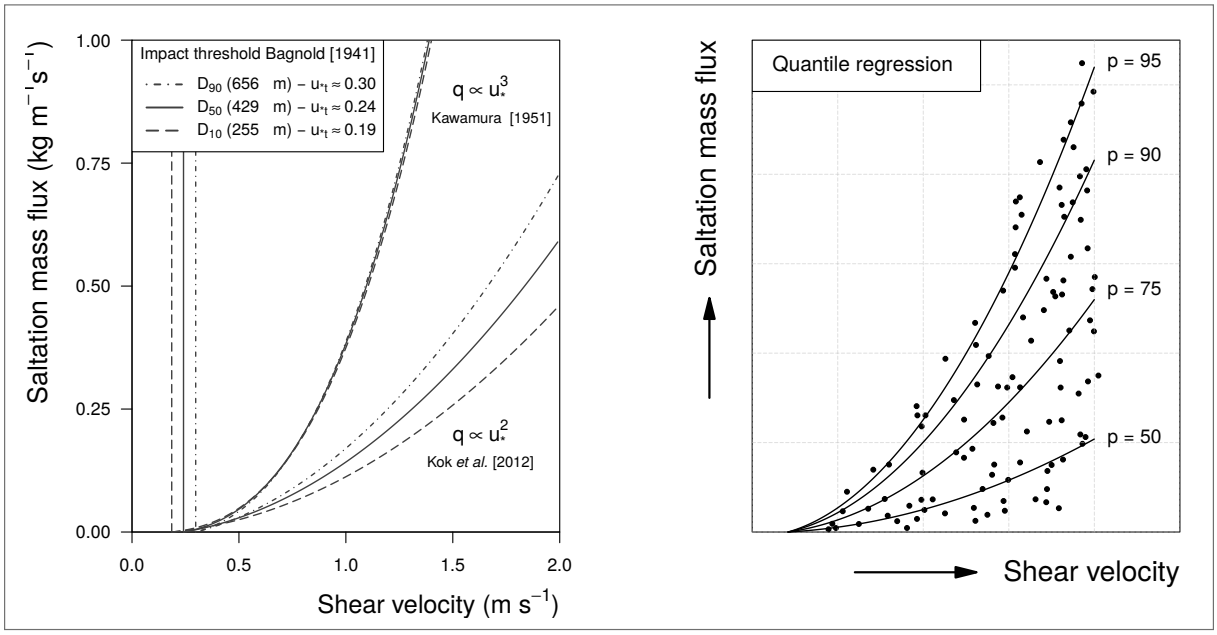

Figure 3.3: Performance of the saltation mass flux equations (Eq. 3.4) and the procedure of quantile regression analysis. **3.3A**. The cubic function of Kawamura (1951) predicts a higher saltation mass flux in response to shear velocity, but is less sensitive to changes in the impact threshold shear velocity u_{*t} than the quadratic function of Kok et al. (2012). **3.3B**. Demonstration of how the saltation mass flux may be related to shear velocity using nonlinear quantile regression. Fitting the same equation to different percentiles of the response distribution yields different rates of saltation mass flux in response to shear velocity.

Quantreg Koenker et al. (2018). Quantile regression is a method to estimate function parameters that model the conditional median or other percentiles (p) of a response variable. It is a method to describe relationships that are not represented effectively by least-squares regression of mean responses. It was popularized in the field of ecology (e.g., Huston, 2002; Cade and Noon, 2003; Austin, 2007), but has found widespread applications across many fields of science (Yu et al., 2003). The strength of quantile regression is that it is an approach to account for (often unmeasured) factors that pose an active limiting constraint on the process under investigation (Cade et al., 1999).

For this study, the underlying idea for its application is that highly variable supply-limiting factors act to obscure the 'true' relationship between the saltation mass flux and shear velocity, whether it is cubic or quadratic, by inducing a response distribution of observations scattered beneath an upper limit (e.g., Cade et al., 1999; Cade and Noon, 2003). At this upper limit the relationship between the saltation mass flux and shear velocity is thus expected to be least affected by limiting factors (Austin, 2007) and to be most in agreement with physical theory and wind tunnel observations (e.g., Creyssels et al., 2009; Ho et al., 2011; Durán et al., 2011; Kok et al., 2012). Wind tunnel experiments are typically performed under non-limiting conditions, i.e. during homogeneous wind flow over a surface composed of dry, loose and uniform sand. Transient-state saltation dynamics are thus minimized and the saltation mass flux is saturated to full and constant capacity. Both the quadratic equation of Kok et al.

(2012) and the cubic equation of Kawamura (1951) were parameterized using wind tunnel experiments and are therefore expected to describe the upper limit of saltation flux rates if that flux was measured in the field under limiting conditions. In other words, fitting the quadratic and cubic function of Eq. 3.4 to the upper percentiles of the response distribution obtained under field conditions, would approximate non-limiting wind tunnel conditions and be informative on whether the saltation mass flux is best described by a quadratic or a cubic dependence to shear velocity.

At the same time, fitting the functions to the median of the response distribution would be informative on how supply-limiting factors most typically impact coastal aeolian dynamics on nourished beaches. To illustrate this notion and the quantile regression approach, figure 3.3B shows how the quadratic function (Eq. 3.4-top) proposed by Kok et al. (2012) may be fitted through randomly generated data at some (hypothetical) percentiles. The uppermost line is generated using the equation's original value of 5.0 for flux scaling parameter C and can be thought to fit for example at the 95th percentile of the response distribution. The remaining three lines are generated using lower values for C, which may be a consequence of fitting the quadratic function to lower percentiles of the response distribution. At the median response distribution, where the saltation mass flux is impacted by the most typically occurring supply-limiting conditions, the value obtained for scaling parameter C may deviate significantly from its original value. This deviation, effectively, provides a model parameterization to account for the overall impact of supply-limiting factors on coastal aeolian dynamics.

3.3 Results and Discussion

3.3.1 Long-term record of coastal aeolian transport dynamics

From May till November 2015 a long-term synchronous record of coastal aeolian transport dynamics on the *Zandmotor* has been constructed. Figure 3.4A shows the 10-minute interval time series of data when the (non-rotating) modified Leatherman traps were able to register aeolian transport, i.e. when saltation mass fluxes were generated by onshore winds. Approximately 15.000 measurement records (60% of total) satisfied this condition. The saltation mass fluxes are color-coded according to the number of traps registering aeolian transport and the shear velocity measurements are color-coded according to whether or not rainfall was registered, which occurred during about 4% of all measurement records. Color-scaling to distinguish between rainfall intensity was not practical as the amount of rainfall for almost half of these records was not more than 0.2 mm. The polar plots in Fig. 3.4A show the wind direction during the shear velocity and saltation mass flux observations. It is clear that the strongest and most prevalent winds came from a west to south-westerly direction, which is also reflected in the frequency and magnitude of the associated saltation fluxes. Approximately 50% of all measurement records originated from that wind direction, including the top 1% highest measured saltation fluxes (> 0.05 kg m^{-1} s^{-1}).

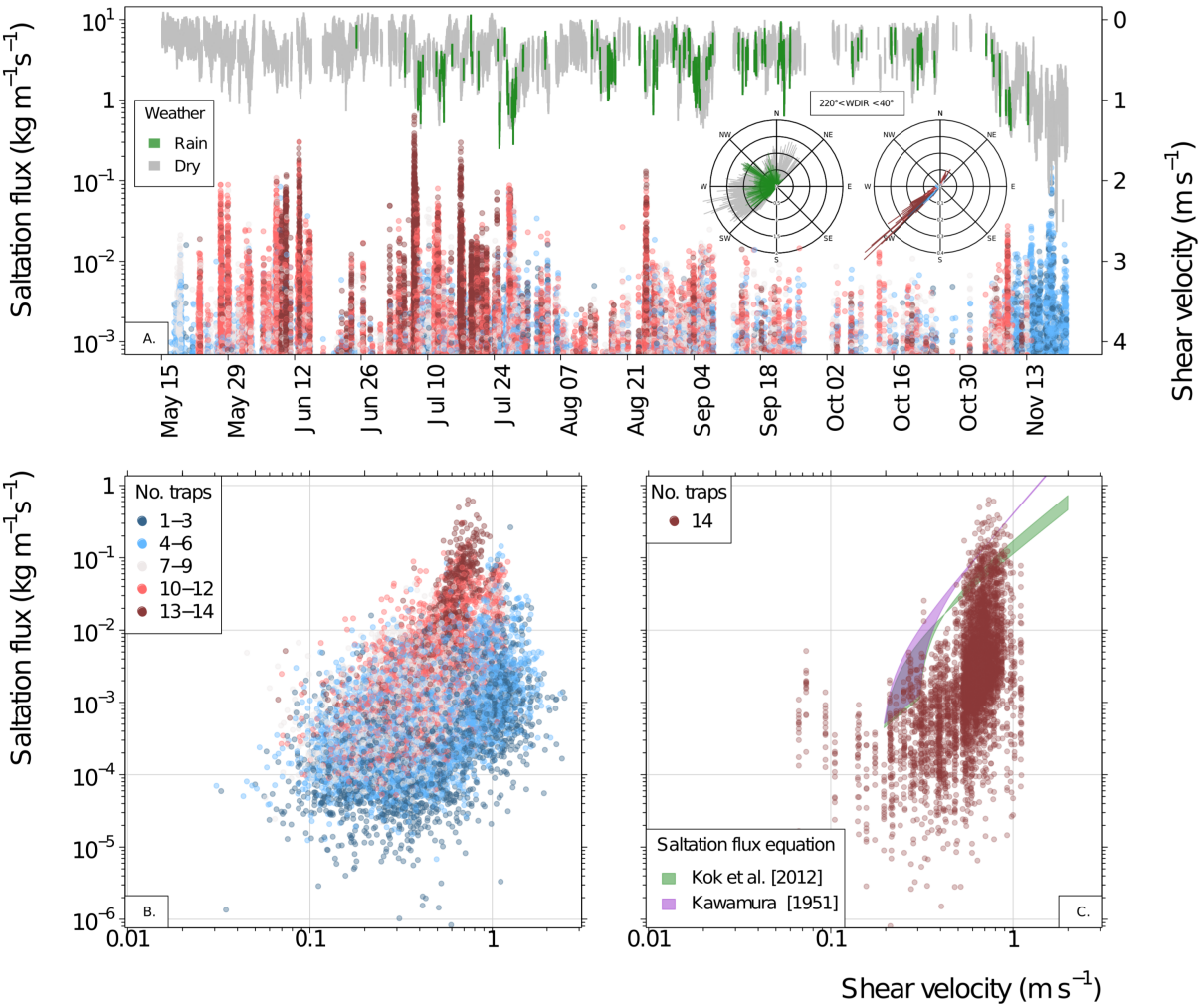

Figure 3.4: Long-term synchronous record of coastal aeolian transport dynamics on the *Zandmotor* From May till November 2015 during onshore winds between 220° up to 40° in direction. The saltation mass fluxes (kg m^{-1} s^{-1}) are color-coded according to the number of modified Leatherman sand traps registering aeolian transport and shear velocities (m s^{-1}) are color-coded according to whether or not rainfall was recorded during each time step.

Several observations can be made by examining the time series of shear velocity and saltation mass flux measurements. Most importantly, regarding the frequency and magnitude of measured saltation fluxes, it appears that aeolian transport at the measurement location occurred more frequently with higher saltation fluxes in the spring and summer of 2015 than in the autumn and (early) winter of that year. The differences in saltation frequency appear to be due to more prevalent offshore winds in the autumn and winter (which can be inferred by the gaps in the times series data) and may not be representative for aeolian transport dynamics on the *Zandmotor* as a whole. Due to the choice of the measurement location and positioning of the non-rotating inlets of the modified Leatherman traps, potential saltation fluxes generated by offshore winds between 40° and 220° angles could not be measured. Considering the differences in saltation flux magnitude during the measurement period, it is striking that

the measured saltation fluxes are considerably higher during the spring and summer 2015. Although not explicitly measured, this is likely due to drier surface conditions because of higher solar irradiance levels. As a result, with less control of surface moisture on particle entrainment, saltation mass fluxes may have developed more easily. This notion is supported by the fact that more modified Leatherman traps simultaneously registered aeolian transport during these high saltation flux transport events, suggesting a more homogeneously developed horizontal saltation layer. Similarly, wetter surface conditions limiting particle entrainment may explain the lower than expected measured saltation fluxes during a severe storm on November 18-19 2015, when the highest shear velocities of the entire time series were measured. Although equipment failure during these severe weather conditions can not be ruled out (e.g. clogging up of the trap inlet by wet sand), it is possible that surface moisture conditions limited the supply of sand to the aeolian transport system. This notion is supported by the fact that only a limited amount of modified Leatherman traps registered aeolian transport during this high shear velocity event.

Figure 3.4B shows the full distribution of measured saltation mass fluxes in response to shear velocity. Two general trends can be observed: (1) a direct relationship between number of sand traps registering aeolian transport and magnitude of the saltation mass flux, and (2) an inverse relationship between number of sand traps registering aeolian transport and the number of saltation mass flux observations. In other words, when more traps registered aeolian transport the saltation mass flux was higher but the measurements were fewer. These two trends reinforce the notion that coastal aeolian dynamics occur most of the time under supply-limiting conditions, preventing the saltation mass flux to saturate to a constant (or expected) saltation density. But it also suggests that, when more sand traps are simultaneously registering aeolian transport, that the wind profile may be more steady and the resultant saltation mass flux may be regulated less by transient-state transport responses. Under these circumstances it is conceivable that supply-limiting factors also exert less control, adding to the horizontal homogeneity of the saltation layer as result. Following this reasoning, to isolate those observations made under optimal field conditions, figure 3.4C shows the response distribution of the saltation mass flux when all 14 modified Leatherman traps registered aeolian transport during each 10-min time-step. A total of 325 records (2% of full record) satisfied this condition, yielding 4550 saltation mass flux observations considered to be least affected by unsteady wind conditions and supply-limiting conditions. What stands out is that the majority of these observations ($\sim$ 90%) were made during the summer of 2015 from June till August. For reference the saltation mass flux equations of Kok et al. (2012) and Kawamura (1951) are included. The impact threshold shear velocity was allowed to range between 0.19 - 0.30 m s^{-1}, which was calculated using the D10 and D90 grain size mass percentages (255 and 656 μm respectively) of the trapped sand. This was done to visualize how changes in the impact threshold shear velocity affects the saltation mass flux rates predicted by the equations of Kok et al. (2012) and Kawamura (1951).

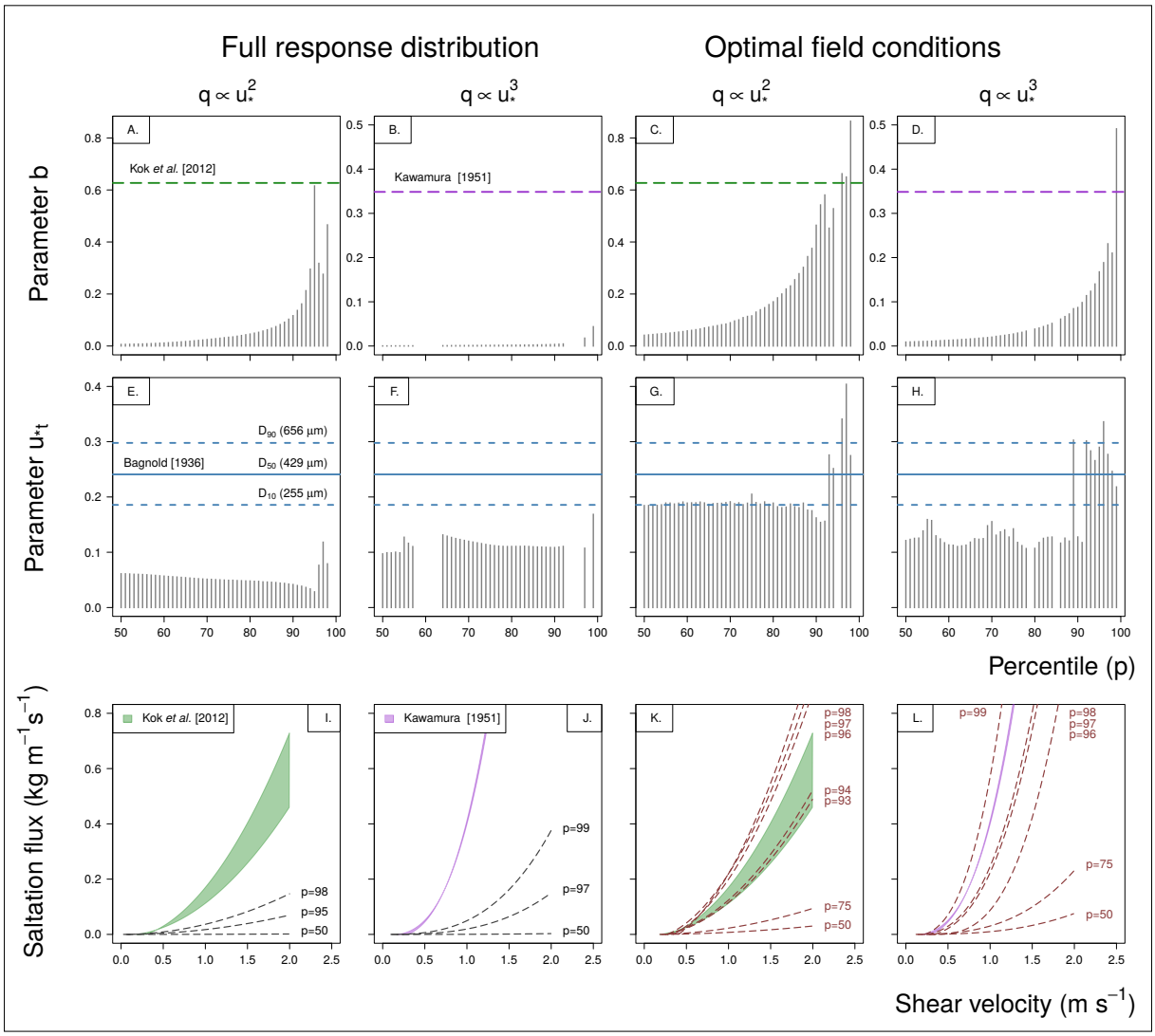

Figure 3.5: Nonlinear quantile regression analysis to saltation mass flux observations in response to shear velocity. The quadratic and cubic functions of Eq. 3.4 were fitted to the full response distribution impacted by supply-limiting factors and to the observations obtained under optimal field conditions during the summer of 2015. The progression of regression parameters estimates for b (**3.5A-D**) and the impact threshold shear velocity u_{*t} (**3.5E-H**) from percentile 50 to 99. The regression lines for the quadratic fits (**3.5I-J**) and cubic fits (**3.5K-L**) to various percentiles, in relation to the original quadratic and cubic saltation equations of Kok et al. (2012) and Kawamura (1951) respectively.

3.3.2 Quadratic or cubic dependence of saltation flux to shear velocity

The question whether the saltation mass flux is better described by a quadratic or cubic dependence to shear velocity is examined using nonlinear quantile regression. The quadratic and cubic functions of Eq. 3.4 are fitted to the full response distribution of saltation mass fluxes (see Fig. 3.4B) and to the observations obtained under optimal field conditions (see Fig. 3.4C). The top and middle panel of Figure 3.5 shows how the regression parameters b

and u_{*t} vary according to which percentile of the response distribution the quadratic and cubic function were fitted. As only the upper part of the response distribution is of interest, the regression analysis was performed starting at the median (50th percentile) up to the upper most 99th percentile, at 1-percentile intervals. For reference the parameter values for b as employed in the original saltation flux equations of Kok et al. (2012) and Kawamura (1951) are denoted in the panels as well. Likewise, this is done for the impact threshold velocity u_{*t} as calculated using the equation of Bagnold (1936) and average grain size diameters of 255, 429 and 656 μm for the D10, D50 and D90 cumulative mass percentages of the trapped sand. The bottom panel of Fig. 3.5 shows the saltation mass flux rates as predicted by the quadratic and cubic function when fitted to the considered percentiles of the two response distributions. The original saltation mass flux equations are again included for reference. Note that the quadratic and cubic function could not be fitted to every considered percentile, which is apparent by a number of missing values in the graphs for the obtained parameter values of b and u_{*t}.

Focusing first on the quadratic and cubic fit to the full saltation mass flux distribution, several observations stand out. As stated before, measurements at or just below the upper limit can be considered as least affected by limiting factors. Fitting the quadratic and cubic functions to this part of the distribution would, therefore, yield parameter values closer to those obtained by wind-tunnel studies where supply-limiting conditions are minimized or absent. Regarding values for parameter b (Fig. 3.5A-B), it is clear that this concept only holds when the quadratic function is fitted to the data. From the median (percentile 50) upward, while not consistently at the highest percentiles, the values for parameter b increase almost exponentially per increasing percentile. At the 95th percentile the regression parameter b of the quadratic fit takes a value of 0.62, which almost exactly matches the original parameter value for b of 0.63 as employed in the equation of Kok et al. (2012). Parameter b values obtained by fitting the cubic function, in contrast, fail to reach the value of 0.35 for parameter b as employed in the equation of Kawamura (1951). In fact, at the upper percentiles where the cubic function could be fitted (97th and 99th percentile), parameter b takes a value of 0.018 and 0.044 respectively which are thus about an order of magnitude lower than the value for parameter b employed by Kawamura (1951). On the other hand, regarding obtained values for parameter u_{*t} (Fig. 3.5E-F), it is clear that both the quadratic and cubic function fit below the theoretical impact threshold velocity calculated using the equation of Bagnold (1936) and average grain size distribution of the trapped sand. Fitting the quadratic function of Kok et al. (2012) to the full response distribution yields a maximum value of 0.12 m s^{-1} for parameter u_{*t} at the 97th percentile. Similarly, fitting the cubic function of Kawamura (1951) yields a maximum value of 0.17 m s^{-1} for parameter u_{*t} at the 99th percentile. Note, because the quadratic function is particularly sensitive to changes in the impact threshold shear velocity, that the low estimates for u_{*t} at the upper percentiles causes the saltation mass flux rate to be below rates predicted by the equation of Kok et al. (2012) even though parameter b estimates for the quadratic fit almost match the value employed in the original equation.

Focusing on the saltation mass flux observations obtained under optimal field conditions, it is clear that fitting the quadratic and cubic function to increasing percentiles of this distribution result in a more comparable progression of parameter b values (Fig. 3.5C-D). Now the regres-

sion estimates for parameter b increase almost exponentially per increasing percentile for both functions and, moreover, both the quadratic and cubic fits reach the values for b as employed in the original equations of Kok et al. (2012) and Kawamura (1951). Fitting the quadratic function to the upper quantiles of the observations obtained under optimal field conditions, however, yield more values for parameter b closer to the original value of 0.63 employed by Kok et al. (2012). At the 96th and 97th percentile, for example, parameter b for the quadratic fit takes a value of 0.66 and 0.64 respectively. The cubic fit, in contrast, only reaches (and overshoots) the original value for b as employed in Kawamura (1951) at the 99th percentile. There parameter b takes a value of 0.49, but at the 98th and 97th percentile the value for b already sharply drops to 0.21 and 0.23 respectively. Regarding parameter u_{*t} values for the quadratic and cubic fit to the optimal field data (Fig. 3.5I and 3.5J), what directly stands out is that the values for u_{*t} are higher overall at each percentile compared to the values for u_{*t} obtained by fitting the quadratic and cubic function to the full response distribution. The quadratic fit, however, consistently yields higher values for u_{*t} compared to the cubic fit. Between percentiles 50 - 89 the quadratic fit yields parameter values for u_{*t} very close to the impact threshold shear velocity calculated using Bagnold (1936) and the D10 grain size mass percentage. At the upper percentiles, after a slight dip, the values for u_{*t} then quickly increase to reach (and exceed) the impact threshold shear velocity values calculated for the D50 and D90 grain size mass percentages. Although at the upper percentiles (89, 92-99) the cubic fit also yields parameter values for u_{*t} in the range calculated by Bagnold (1936) and the D10 to D90 grain size mass percentages, at lower percentiles the cubic fit yields considerably lower values for the impact threshold shear velocity than for the quadratic fit and calculated using Bagnold (1936).

3.3.3 Quantifying the impact of supply-limiting factors

The bottom panel of figure 3.5 and table 3.1 summarize the results of fitting the quadratic and cubic function of Eq. 3.4 to the full response distribution impacted by supply-limiting factors and to the observations obtained under optimal field conditions. Considering first the full response distribution, it is clear that both the quadratic and cubic fit (Fig. 3.5I-J) result in a strong underprediction of the saltation mass flux in response to shear velocity at every considered percentile, compared to saltation rates predicted by the equations of Kok et al. (2012) and Kawamura (1951). The regression lines at the 50th percentile for both the quadratic and cubic fit appear as a horizontal line ($q = 0$) at the depicted scale and at the upper most percentile, where the functions could be fitted, the regression lines are still far below the rates predicted by Kok et al. (2012) or Kawamura (1951). It is also clear, though, that fitting the cubic function to the full response distribution results in a stronger underprediction of the saltation mass flux compared to the quadratic function. To assess how much stronger the cubic fit underpredicts the saltation mass flux, the flux scaling parameter C as incorporated in the regression parameter b (via $b = C\rho/g$) is calculated and listed in table 3.1 for the quadratic and cubic fits at the percentiles depicted in bottom panel of Fig. 3.5. Also listed are the values of 5.0 and 2.78 for C employed by the equations of Kok et al. (2012) and Kawamura (1951) respectively, which were obtained by wind-tunnel experiments where supply-limiting conditions are either minimized or absent. Interestingly, but presumably coincidental, table 3.1 shows

Table 3.1: Values for flux scaling parameter C employed in the saltation flux equations of Kok et al. (2012) and Kawamura (1951) and impact threshold shear velocity u_{u*t} obtained using nonlinear quantile regression analysis. The (theoretical) impact threshold velocity range is given as reference and was calculated using the equation of Bagnold (1936) and average grain size distribution of the trapped sand.

	Full response distribution				Optimal field conditions			
	$q \propto u_*^2$		$q \propto u_*^3$		$q \propto u_*^2$		$q \propto u_*^3$	
Parameter	C	u_{*t}	C	u_{*t}	C	u_{*t}	C	u_{*t}
Kawamura (1951)	-	-	**2.78**	0.19 - 0.30	-	-	2.78	0.19 - 0.30
Kok et al. (2012)	**5.0**	0.19 - 0.30	-	-	5.0	0.19 - 0.30	-	-
p = 99	-	-	0.35	0.17	-	-	3.92	0.22
p = 98	3.71	0.08	-	-	6.89	0.27	1.68	0.25
p = 97	2.20	0.12	0.14	0.11	5.18	0.40	1.84	0.28
p = 96	2.53	0.08	-	-	5.28	0.34	1.50	0.35
p = 95	4.91	0.03	-	-	-	-	-	-
p = 94	2.36	0.03	-	-	4.21	0.25	1.12	0.26
p = 93	1.70	0.04	-	-	3.61	0.28	0.99	0.28
p = 75	0.27	0.05	0.01	0.11	0.92	0.20	0.22	0.14
p = 50	**0.05**	0.06	**0.00278**	0.10	0.33	0.18	0.07	0.12

that flux scaling parameter C at the 50th percentile takes a value of 0.05 for the quadratic fit and 0.00278 for the cubic fit to the full response distribution. In other words, based on values for C at the median response distribution where the observed saltation rates are impacted by the most typically occurring supply-limiting conditions, the quadratic fit appears to underestimate the saltation mass flux by exactly two orders of magnitude compared to the equation of Kok et al. (2012) and the cubic fit by exactly three orders of magnitude compared to the equation of Kawamura (1951). It must be noted that this comparison only holds true when the same values for the impact threshold velocity u_{*t} are used. Because the performance of the quadratic function is more sensitive to changes in the impact threshold shear velocity then the cubic function, the lower estimates for u_{*t} compared to those calculated by Bagnold (1936) causes the quadratic fit to stronger underpredict the saltation mass flux than based on the value for the flux scaling parameter C alone. The underprediction, nonetheless, is still in the range of two orders of magnitude rather than three as for the cubic fit.

At higher percentiles of the full response distribution, where supply-limiting conditions are less prevalent, the underestimation of the saltation mass flux by the quadratic and cubic fit are less striking. At the 98th percentile, based on both the estimates for C and u_{*t}, the quadratic fit predicts saltation rates that are about a factor 3 lower compared to the equation of Kok et al. (2012) and the cubic fit at the 99th percentile predicts saltation rates that are about a factor 8 lower compared to Kawamura (1951). Regarding the response distribution obtained under optimal field conditions, what stands out is that at the 50th percentile the estimates for C for both the quadratic and cubic fit are still much lower than the values employed by Kok et al. (2012) and Kawamura (1951). This suggests that, under the most typical optimal conditions

(i.e. dry weather in summer), there may still be a considerable impact by supply-limiting factors. At the median response distribution, taking both the estimates for C and u_{*t} into account, the quadratic fit predicts saltation mass flux rates that are about a factor 20 lower compared to rates predicted by Kok et al. (2012) while the cubic fit predicts rates that are about a factor 40 lower compared to Kawamura (1951). Under optimal field conditions the underestimation for the quadratic and cubic fit are thus both in the same order of magnitude, but the cubic fit underpredicts the saltation mass flux twice stronger than the quadratic fit for a given shear velocity. This difference diminishes for increasingly higher percentiles, suggesting that at the upper percentiles of the optimal response distribution the impact of supply-limiting factors on aeolian dynamics are increasingly minimized or become completely absent. It must be noted though that only a very small number of saltation mass flux observations comprise the upper percentiles of the optimal response distribution. Thus, caution should be exercised when inferring any conclusions from them as they could be outliers of the distribution.

3.3.4 Uncertainties in field observations

A drawback of the modified Leatherman sand trap, in its current form, is that the trap is non-rotating and can therefore not orient itself to the prevailing wind-direction. This may have lead to a bias in calculating the saltation flux in standard units (kg m^{-1} s^{-1}) because the inlet width (w) of the trap effectively changes depending on the angle of incident saltation. To account for this bias the effective trap inlet width of the sampler (w_{eff}) was adjusted according by $w_{eff} = w\ sin\ \alpha$, where the angle of saltation (α) was taken as the average wind direction during each 10-minute measurement interval. While this approach to correct the performance of the modified Leatherman trap is sound in theory, it is likely not a substitute to direct measurement by a rotating sampler that can orient itself to the prevailing wind direction. The pathway of saltating particles, as demonstrated by Sterk et al. (1998) and Baas and Sherman (2005) for example, do not necessarily follow the time-averaged velocity component of shear stress at the sand surface because of turbulent flow structures. While a rotating sampler may also not completely capture these saltation dynamics, the measurement uncertainty arising from turbulence driven effects is likely less compared to a non-rotating sampler. Moreover, the rather heterogeneous morphology of the *Zandmotor* upwind of the study area and the presence of small incipient dunes (during the experiment) in proximity of the measurement location (see Fig. 3.1) may also have resulted in a divergence in the direction of the incident saltation flux and average 10-minute wind direction. No reliable analysis, however, into the potential bias in measured saltation fluxes to different wind direction regimes could be performed in the field. For this study priority was given to long-term field deployment, but in future design the capacity to rotate (reliably over time) is recommended for the modified Leatherman trap. Otherwise its performance in measuring saltation mass fluxes over different incident angles needs to be investigated further.

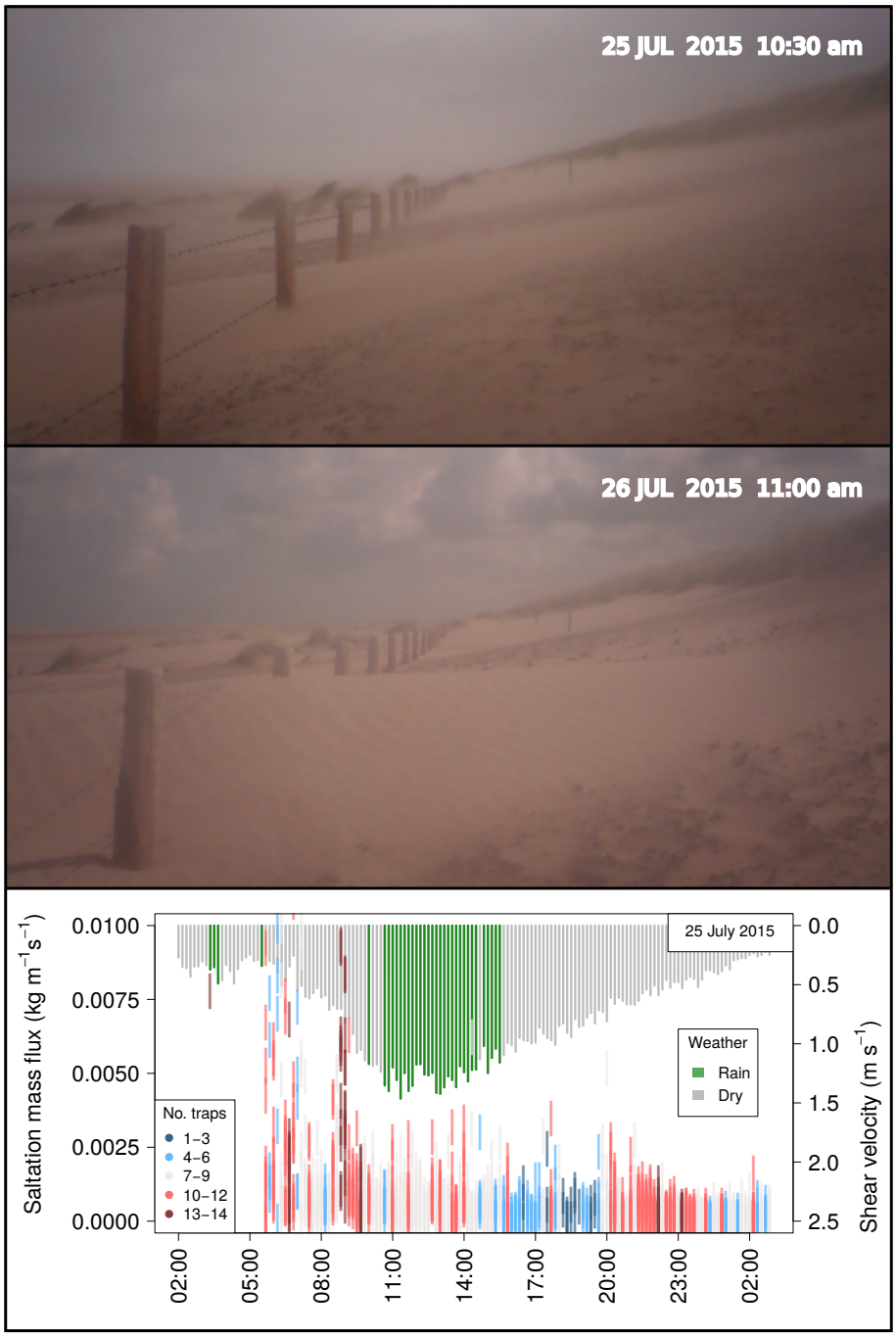

Figure 3.6: Aeolian dynamics and meteorolgical conditions on the *Zandmotor* during and just after a severe summer storm on July 25 2015.

What also stands out, as can most clearly be observed in Fig. 3.4C, are the higher than expected saltation fluxes measured at shear velocities below the impact threshold velocities calculated using Bagnold (1936) and average D10 to D90 grain size mass percentages of trapped sand. An explanation may be that the modified Leatherman trap is extra sensitive to intermittent saltation dynamics because the trap extends down completely to the surface.

Intermittent saltation arises when turbulent winds produce velocity (and direction) fluctuations just above and below the threshold for saltation (Stout and Zobeck, 1997). This, effectively, may lead to more prominent transient-state saltation responses around threshold velocities. Such dynamics can temporarily produce saltation fluxes that are (1) not accounted for by averaged 10-min shear velocity intervals and (2) not represented by steady-state saltation equations. Saltation overshoot due to exponential particle cascading, for example, is known to briefly produce higher fluxes than steady-state equations predict (e.g., Anderson and Haff, 1988; Shao and Raupach, 1992). Or hysteresis, the dependence of the saltation flux on both current and past shear velocities, (e.g., Poortinga et al., 2013) may also contribute to higher than expected fluxes. And while both increasing and decreasing shear velocities may affect the current saltation mass flux, it was shown by Martin et al. (2013) that the hysteresis pathway during decreasing velocities was significantly longer (t $\approx$ 5 sec.) than for increasing shear velocities (t $\approx$ 1 sec.). This may indicate that when saltation mass fluxes are affected by hysteresis they, effectively, more often increase than decrease in magnitude.

Further, as can be seen in Fig. 3.4B, at high shear velocities ($>$1 m s^{-1}) the measured saltation mass fluxes were often much lower than expected. It is likely that this may be attributed to equipment limitations during storm weather conditions, when high wind speeds are usually accompanied by heavy precipitation. Even though the modified Leatherman traps were fitted with a vibration motor to loosen up sand stuck in the trap, it has been observed that saltating wet sand could continue to clog up the inlet of the trap and render them inoperable. While surface moisture greatly increases the resistance of sand to entrainment by wind, it has been demonstrated that sand grains in the uppermost layer may still dry sufficiently due to direct wind exposure and get ejected into the air stream (e.g., Cornelis and Gabriels, 2003a; Poortinga et al., 2015a). The splash impact of those drier sand grains may subsequently dislodge wetter sand grains which then can also become part of the saltation cascade. High surface moisture content has also been shown to generate higher saltation heights as more impact energy is retained on wet surfaces (e.g., Neuman and Scott, 1998; Farrell et al., 2012). These dynamics combined may subsequently still give rise to considerable saltation fluxes during storm events with heavy precipitation. Because of the wetness of the sand, however, these fluxes remain very difficult to quantify by direct measurement. The newly developed modified Leatherman trap has also not been able to completely mitigate this challenge. This is illustrated by Fig. 3.6, which shows the aeolian dynamics and meteorolgical conditions on the *Zandmotor* during (and after) a severe summer storm on July 25 2015. In the bottom panel of Fig. 3.6 it appears that aeolian transport almost completely halted after rainfall started, while in reality the photographs clearly show that significant amounts of aeolian transport took place during this storm event.

Another obvious issue to address are the frequent low estimates for the impact threshold shear velocity u_{*t}, compared to the range of values of u_{*t} calculated by Bagnold (1936) and the D10 grain size mass percentages of the trapped sand. Fitting the quadratic and cubic function of Eq. 3.4 both yield parameter u_{*t} estimates that remain below this theoretical impact threshold velocity when fitted to the full response distribution impacted by supply-limiting factors. This can likely be attributed to transient-state saltation dynamics arising from turbulent flow structures but, as Stout (1998) argues, it may also be explained by the

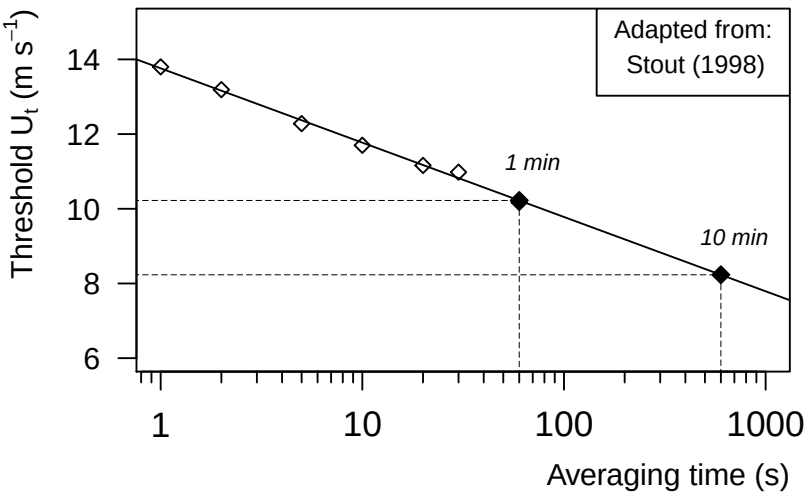

Figure 3.7: Inverse linear relationship of Stout (1998) between wind speed threshold and the logarithm of averaging time. Extrapolation of the regression line suggests that averaging time from 1 minute to 10 minutes may lead to an underestimation of the threshold velocity by about 20%. Extrapolation to $t_{avg} \rightarrow 0$ suggests that 10-minute averaged time intervals may underestimate the threshold shear velocity up to 40%.

effect that averaging time has on the apparent threshold for aeolian transport. It was shown that under field conditions, with typical gusty turbulent winds, long averaging times of wind velocity measurements would produce thresholds that were considerably lower than the true wind velocity at which saltation is initiated. Most importantly, as figure. 3.7 denotes, Stout (1998) found an inverse linear relationship between wind speed threshold and the logarithm of averaging time. Generally, the calculated threshold velocity for aeolian transport to initiate decreases as the averaging time increases. Applying this relationship here, by extrapolating the regression line of Stout (1998), suggests that averaging time from 1-min to 10-min intervals may lead to an underestimation of the threshold shear velocity by about 20%. And further still, as the averaging time approaches zero, extrapolation suggests that the threshold shear velocity obtained from averaging time to 10-min intervals may underestimate the actual threshold shear velocity up to 40%. This does not necessarily mean that the obtained estimates for impact threshold shear velocity u_{*t} should be scaled to account for the effect of averaging time, but it may offer an explanation for the lower than expected estimates for u_{*t} compared to the values predicted by the equation of Bagnold (1936) and the average grain size distribution of the trapped sand. Furthermore, small variability in the actual height placement of the anemometers (expressed by z in Eq. 3.3 to calculate the shear velocity) may also help explain the lower than expected estimates for impact threshold velocity. The sand surface directly below the wind profiler could, for example, have been raised temporarily in between field visits due to sand deposition. This may effectively have lead to a lower anemometer heights than assumed, resulting in a lower calculated shear velocity than actually occurred when the measurement was taken.

3.4 Conclusions

Field studies investigating coastal aeolian dynamics report that measured saltation mass fluxes are, almost without exception, much lower than predicted by traditional aeolian transport equations. While commonly attributed to supply-limiting factors, this study shows with nonlinear quantile regression that the failure to produce a strong correspondence between measured and predicted aeolian transport rates can also arise from the notion that the saltation mass flux may be better explained by a quadratic than a cubic dependence to shear velocity. Regression parameters obtained at the upper part of the response distribution are in line with parameters employed by the quadratic function of Kok et al. (2012), yielding more consistent saltation rates than predicted by the cubic function of Kawamura (1951). The main findings of this study are:

- Except during extreme storm conditions with high intensity rainfall, a newly developed automated sand trap is capable of constructing a continuous, long-term and high-resolution record of coastal saltation mass flux measurements
- Fitting the quadratic and cubic function to the median response distribution indicates that saltation rates generated in the coastal environment may typically be two (for quadratic dependence) or three (for cubic dependence) orders of magnitude lower than predicted by the transport equations of parameterized during wind tunnel experiments.
- While the obtained saltation mass flux rates correspond better to traditional transport equations when the quadratic and cubic function are fitted to the observations made under optimal field conditions, the still significantly lower saltation rates indicate that coastal aeolian dynamics are characterized by a persistent impact of supply-limiting conditions.

By parameterizing the flux scaling parameter C this study provides a measure to account for the overall impact of limiting factors, which can help ensue more realistic saltation mass flux predictions that are better applicable to conditions found on the *Zandmotor* and along (nourished) coastlines in general.

Chapter 4

Measuring and modeling the effect of surface moisture on the spectral reflectance of coastal beach sand

This chapter is based on:

Nolet, C., Poortinga, A., Roosjen, P., Bartholomeus, H., and Ruessink, G. (2014). Measuring and modeling the effect of surface moisture on the spectral reflectance of coastal beach sand, *PloS one* 9, e112 151

Abstract

Surface moisture is an important supply limiting factor for aeolian sand transport, which is the primary driver of coastal dune development. As such, it is critical to account for the control of surface moisture on available sand for dune building. Optical remote sensing has the potential to measure surface moisture at a high spatio-temporal resolution. It is based on the principle that wet sand appears darker than dry sand: it is less reflective. The goals of this study are (1) to measure and model reflectance under controlled laboratory conditions as function of wavelength (λ) and surface moisture (θ) over the optical domain of 350-2500 nm, and (2) to explore the implications of our laboratory findings for accurately mapping the distribution of surface moisture under natural conditions. A laboratory spectroscopy experiment was conducted to measure spectral reflectance (1 nm interval) under different surface moisture conditions using beach sand. A non-linear increase of reflectance upon drying was observed over the full range of wavelengths. Two models were developed and tested. The first model is grounded in optics and describes the proportional contribution of scattering and absorption of light by pore water in an unsaturated sand matrix. The second model is grounded in soil physics and links the hydraulic behaviour of pore water in an unsaturated sand matrix to its optical properties. The optical model performed well for volumetric moisture content $\theta < 24\%$ ($R^2 > 0.97$), but underestimated reflectance for θ between 24-30% ($R^2 > 0.92$), most notable around the 1940 nm water absorption peak. The soil-physical model performed very well ($R^2 > 0.99$) but is limited to $4\% > \theta < 24\%$. Results from a field experiment show that a short-wave infrared terrestrial laser scanner (λ=1550 nm) can accurately relate surface moisture to reflectance (standard error 2.6%), demonstrating its potential to derive spatially extensive surface moisture maps of a natural coastal beach.

4.1 Introduction

Every decade sea water level of the North Sea rises by 2-3 cm (Solomon, 2007). This is alarming for a country as the Netherlands considering large parts are already below sea level. It puts urgency on finding coastal defense strategies that are able to adapt to climate change (Keijsers et al., 2014a; De Jong et al., 2014; Bochev-Van der Burgh et al., 2011). In this context an unprecedented large nourishment of sand ('Sand Motor', www.zandmotor.nl) was laid down along a stretch of the Dutch coast in 2011. Its aim is to mimic the onshore migration of an intertidal sandbar, supplying the adjacent coast with a surplus of sand for years to come (Van Slobbe et al., 2013; Stive et al., 2013b). An important expected result is the transport of sand by wind over the beach towards the dunes, enabling the dunes to naturally grow in volume (Keijsers et al., 2014b; Poortinga et al., 2011).

Surface moisture is an important supply limiting factor for aeolian sand transport (Davidson-Arnott et al., 2005a; Bauer et al., 2009a; de Vries et al., 2014; Poortinga et al., 2014; Namikas and Sherman, 1995; Ellis et al., 2012). By binding sand grains together, through cohesive and adhesive forces, water significantly increases the resistance of the uppermost sand layer against wind erosion (Chepil, 1956; McKenna-Neuman and Nickling, 1989; Cornelis and Gabriels, 2003b). It has been suggested by Belly (1964) that the required wind force to initiate saltation grows exponentially with a linear increase of moisture content. Above a certain moisture content beach sand becomes inherently resistant to entrainment by most natural winds.

To accurately predict aeolian sand availability for dune building it is thus critical to account for the control of surface moisture. However, wetting and drying processes are governed by complex hydraulics of tidal and wave action, groundwater and capillary flow, and evaporation and precipitation (Atherton et al., 2001; Davidson-Arnott and Bauer, 2009; Namikas et al., 2010; Hugenholtz et al., 2009; Huisman et al., 2011). As a result, the distribution of surface moisture on a beach can vary greatly in space and time. Therefore, to estimate the control surface moisture exerts on aeolian sand transport, data at a high spatio-temporal resolution is required (Wiggs et al., 2004; Yang and Davidson-Arnott, 2005; Poortinga et al., 2013).

Optical remote sensing can be a viable solution for measuring surface moisture at a high spatio-temporal resolution. It is based on the principle that wet sand appears darker than dry sand: it is less reflective. This familiar reduction in reflectance is attributed to pore water surrounding the sand grains, causing a change in scattering and absorption of light. Scattering and absorption of sunlight occur at the same time, but their proportional contribution to reduction in reflectance depends on wavelength (λ) and moisture content (θ) (Bowers and Hanks, 1965; Lobell and Asner, 2002; Weidong et al., 2002). This holds true when other parameters affecting beach surface reflectance (e.g. mineral composition, grain size distribution, packing density, surface roughness (Leu, 1977; Shuchman and Rea, 1981) remain unchanged.

The potential of optical remote sensing of surface moisture, for aeolian research in the coastal environment, was first demonstrated by Mckenna Neuman and Langston (2003); McKenna Neuman and Langston (2006); Darke and McKenna Neuman (2008); Darke et al. (2009) and Delgado-Fernandez et al. (2009). Through a photographic methodology ($\lambda =$

400 – 700 nm), beach surface moisture content was related to a corresponding normalized surface reflectance. This relationship was applied to photographs of a beach, resulting in a time-series of surface moisture maps. The same principle was later tested by (Nield et al., 2011; Nield and Wiggs, 2011) and (Nield et al., 2014), where the reflective signal of a terrestrial laser scanner ($\lambda = 539$ nm) was related to beach surface moisture. It is a more convenient application since the reflected signal does not require a correction for changes in illumination. Another application of the principle was tested by Edwards et al. (2013b) and Edwards et al. (2013a), where point data on beach surface moisture was collected using a portable narrow band radiometer ($\lambda = 1940$ nm) and spectroradiometer ($\lambda = 970$ nm). At these wavelengths the correlation between surface reflectance and moisture content was shown to be higher than at visible wavelengths, due to stronger absorption of light in water.

In soil science, optical remote sensing is widely used to determine soil moisture content (Bowers and Hanks, 1965; Idso et al., 1975; Skidmore et al., 1975; Lobell and Asner, 2002; Knadel et al., 2014). However, the recent studies that relate reflectance to surface moisture in a coastal environment, show ambiguous results, as was also recognized by Edwards et al. (2013b) and Edwards et al. (2013a). It is in part due to the focus on a limited range of wavelengths in which measurements were taken (see overview in Figure 4.1-bottom). The goals of this study are (1) to measure and model reflectance under controlled laboratory conditions as function of wavelength (λ) and surface moisture content (θ) over the full optical domain of 350-2500 nm, and (2) to explore the implications of our laboratory findings for accurately mapping the distribution of surface moisture under natural conditions. A laboratory spectroscopy experiment is conducted to measure spectral reflectance (1 nm interval) under different surface moisture conditions using beach sand. Two models are developed and tested. The first model is grounded in optics and describes the proportional contribution of scattering and absorption of light by pore water in an unsaturated sand matrix. The second model is grounded in soil physics and links the hydraulic behavior of pore water in an unsaturated sand matrix to its optical properties. A field experiment is conducted to test the potential of a short-wave infrared terrestrial laser scanner (λ=1550 nm) to derive spatially extensive surface moisture maps with a high accuracy. As such, this study aims to support practical applications for optical remote sensing of surface moisture on a sandy coastal beach.

4.2 Background

4.2.1 Spectral reflectance

Elastic scattering of light is the re-directing of light by a medium without alteration of the wavelength. It encompasses the optical phenomena of reflection, refraction, and diffraction (Hecht, 2002; Bohren and Huffman, 2008; Hapke, 2012) which are determined by wavelength, angle of incidence and optical properties of the medium. Transmission of sunlight into opaque beach sand is in the order of a few sand grains thick (Leu, 1977; Shuchman and Rea, 1981; Tester and Morris, 1987; Ciani et al., 2005). Optical reflectance is thus strictly a surface phenomenon.

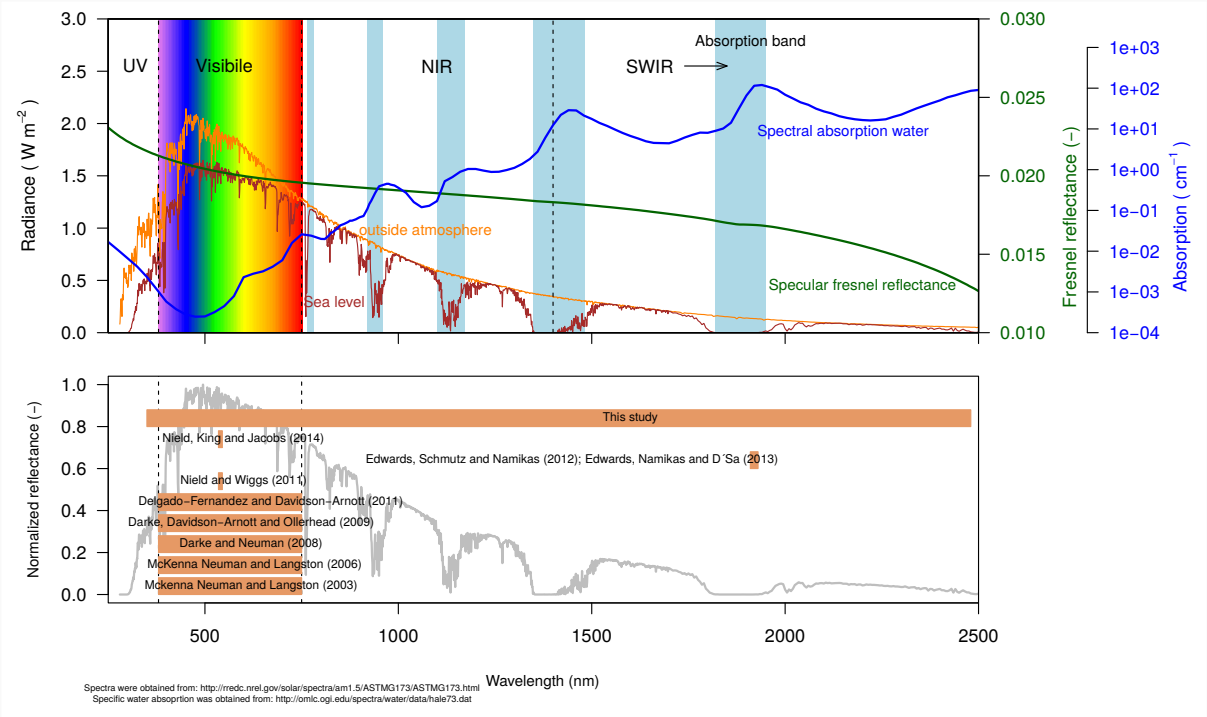

Figure 4.1: The spectral power distribution (SPD) of sunlight (in Wm^{-2}) over the optical domain of 350-2500 nm. Top panel: yellow line shows SPD of sunlight outside the atmosphere, brown line shows SPD of sunlight at sea level. Green line shows spectral Fresnel reflectance (-) for a water surface, blue line shows absorption coefficients (in cm^{-1}) for pure water. The blue bands indicate absorption peaks due to water. Bottom panel: overview of the studies (including this study) that demonstrate the potential of relating reflectance to surface moisture. The orange bars indicate the spectral range in which the measurements were taken.

With optics Ångström (1925) proposed an explanation for the familiar visual darkening of sand upon wetting, ascribing it to total internal reflection within water films surrounding the sand grains. In effect, sunlight at or exceeding the critical angle is reflected back to the surface at the liquid-air interface, increasing the likelihood of being absorbed by the sand grains. Assuming ideal diffuse reflection Ångström (1925) described the relation between wet (R_w) and dry (R_d) reflectance by:

$$R_w = \frac{R_d}{n^2(1 - R_d) + R_d} \tag{4.1}$$

With n the refractive index of water. Lekner and Dorf (1988) later modified this model to account for the fraction of sunlight that is not transmitted into the water film but reflects specularly (R_s) at the air-liquid interface:

$$R_w = \frac{(1 - R_s)R_d}{n^2(1 - R_d) + R_d} \tag{4.2}$$

$$R_s \approx \left(\frac{n_w - n_a}{n_w + n_a} \right)^2 \tag{4.3}$$

Specular reflectance R_s is approximated by Fresnel reflection of normal incident sunlight (Hecht, 2002), with n_w the refractive index of water and n_a the refractive index of air, taken as 1. How specular reflectance changes with wavelength is shown in Figure 4.1.

The process of absorption is also important to spectral reflectance. Absorption of sunlight is the uptake of light by conversion of its energy into thermal energy. It is strongly correlated to wavelength. Spectral absorption of sunlight is described by the Beer-Lambert law (Bohren and Huffman, 2008), stating an exponential decrease of reflectance as a function of the absorption coefficient $\alpha(\lambda)$ (cm^{-1}) and optical path length d (cm):

$$R = R_d e^{-\alpha d} \tag{4.4}$$

The spectral absorption coefficient describes the extent to which sunlight is absorbed as it passes through a medium. Figure 4.1 shows the absorption coefficients for pure water in the optical domain 350-2500 nm (data: (Segelstein, 1981)). It becomes clear that water is a strong absorber of sunlight at specific wavelengths. Notable absorption peaks all occur at near- and shortwave-infrared wavelengths, around 760, 970, 1200, 1470 and 1940 nm (Segelstein, 1981; Pope and Fry, 1997). At visible wavelengths the absorption coefficient is close to zero. Here, the penetration depth (i.e. inverse of absorption) of sunlight in water is high, which is why water appears transparent.

The effect of absorption of sunlight by water is illustrated by comparing the spectral power distribution (SPD) of sunlight (Wm^{-2}) outside the atmosphere to that at sea level (Fig. 4.1). Since water (vapour) is abundant in the atmosphere, certain wavelengths of sunlight are absorbed to such an extent that it may not reach the earth's surface. This is of consequence for collecting remotely sensed data. Passive methods, that depend on sunlight for acquiring information about an object, are 'short-sighted' or in fact blind in wavelengths strongly absorbed by water. This is true for wavelengths around the 1470 and 1940 nm absorption peaks. In these wavebands an active method must be employed, where data is collected using a light source other than the sun (Elachi and Van Zyl, 2006).

4.2.2 Surface moisture

The decrease of spectral reflectance upon wetting is non-linear, as is the hydraulic behaviour of water in an unsaturated sand matrix. Both processes can be linked conceptually, as is shown in Figure 4.2. At (and below) wilting point (Fig. 4.2.1) pore water is held tightly in the sand matrix as adsorbed water films around the sand grains. Here the optical path length in water (d) is close to zero, and the decrease of spectral reflectance is almost solely due to scattering. Approaching field capacity (Fig. 4.2.2) pore water proceeds to fill micro pores and form water wedges between sand grains. This increases the optical path length in water (d), with increasing absorption as result. When the sand matrix gets fully saturated (Fig. 4.2.3)

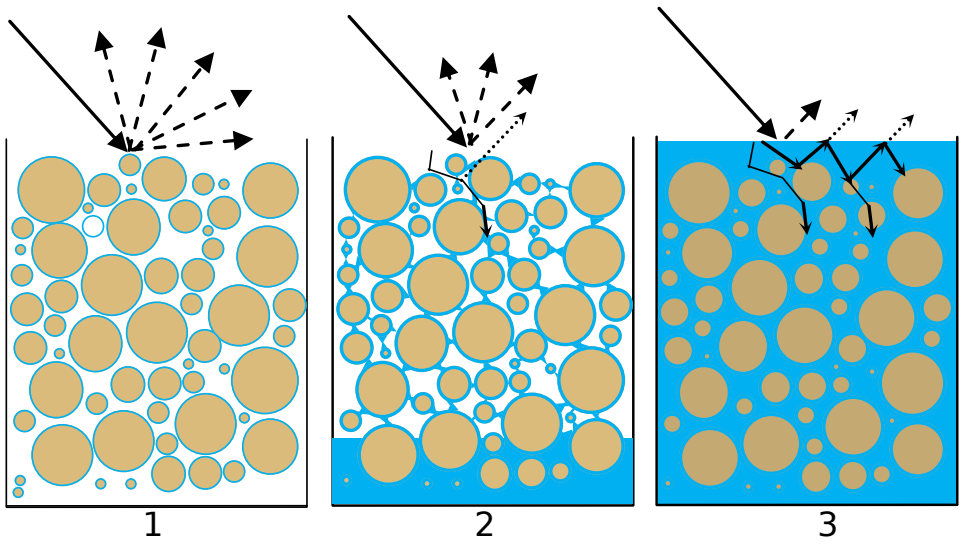

Figure 4.2: Conceptual representation of the non-linear decrease of spectral reflectance as moisture content in the sand matrix increases. At wilting point (1) there is almost no absorption of light in water as the optical path length (d) is close to zero. At field capacity (2) the optical path length in water (d) increases with increasing absorption as result. At saturation (3) the optical path length in water (d) is at its maximum and certain wavelengths may be completely absorbed.

all remaining air in the sand matrix is replaced with water and free water may appear at the surface. Now the optical path length in water (d) is at its maximum and certain wavelengths may be completely absorbed (Hillel, 1998; Lobell and Asner, 2002).

The hydraulic behaviour of water in an unsaturated sand matrix is described by the water retention curve (Fig. 4.3), relating volumetric water content θ to the water pressure head h in cm. Under unsaturated conditions the water pressure head is always negative, for cohesive and adhesive forces in the sand matrix reduce pore water potential relative to free water. A well-established empirical model to describe the water retention curve is the Van Genuchten equation (Eq. 4.5) of (Van Genuchten, 1980):

$$\theta_h = \theta_r + \frac{\theta s - \theta_r}{[1 + (a|h|)^n]^{1-1/n}} \tag{4.5}$$

With θ_r the residual water content and θ_s the saturated water content. At these water contents the gradient $d\theta/dh$ of the water retention curve becomes zero. Parameter a (cm^{-1}) approximately equals the inverse of the pressure head at the inflection point, where $d\theta/dh$ has its maximum value. It is interpreted as the air entry value. The dimensionless parameter n relates to the slope at the inflection point, thus reflecting steepness of the water retention curve. It is is interpreted as an indicator of pore-size distribution (Van Genuchten, 1980; Wosten and Van Genuchten, 1988). Note that moisture levels of $\theta < \theta_r$ and $\theta > \theta_s$ are beyond the range of Eq. 4.5.

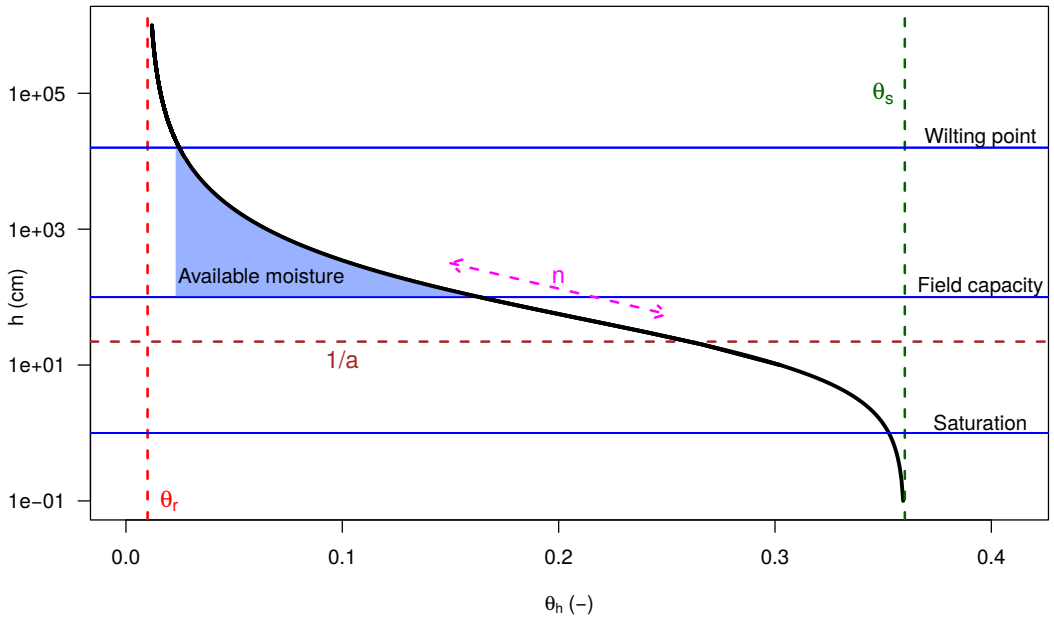

Figure 4.3: The water retention curve for a coarse grained sand matrix (M50 = 350-500 μm), created using Eq. 4.5. Shown in the graph are the residual water content (θ_r), saturated water content (θs), air entry value ($1/a$) at the inflection point, and (n) which is related to the slope at inflection point and indicates pore-size distribution. Data taken from (Wösten et al., 2001).

4.2.3 Surface moisture - spectral reflectance models

Two simple models are proposed to obtain a description of spectral reflectance under different moisture conditions. The first model (Eq. 4.6) is grounded in optics. Spectral reflectance R_θ as a function of volumetric surface moisture is described by:

$$R_\theta = f_s R_d e^{-\alpha d} \tag{4.6}$$

Where parameters f_s (fraction) and d (cm) at a certain wavelength and moisture content, are obtained by curve fitting. Parameter f_s describes the contribution of elastic scattering to reduction of spectral reflectance upon wetting, while parameter d (optical path length in water) describes the contribution of absorption to reduction of spectral reflectance upon wetting. Further, α denotes the wavelength dependent absorption coefficient for pure water, and R_d the dry spectral reflectance. The model is based on the approach of Philpot (2010), with omission of the fraction R_s as the contribution of specular reflectance to darkening upon wetting was shown by Philpot (2010) to be minimal. The model of Philpot (2010) is similar to the model of (Lobell and Asner, 2002), although the latter model takes the absorption coefficient α as a regression parameter.

The second model (Eq. 4.7) is grounded in soil physics. The Van Genuchten equation (Eq. 4.5) is modified by replacing pressure head h (cm) with spectral reflectance R_θ. Parameters a and n, at a certain wavelength, are obtained by curve fitting and become dimensionless as

spectral reflectance is a fraction. Volumetric moisture content θ_R as a function of spectral reflectance is described by:

$$\theta_R = \theta_r + \frac{\theta s - \theta_r}{[1 + (aR_\theta)^n]^{1-1/n}} \tag{4.7}$$

Where residual water content θ_r and the saturated water content θ_s are sand matrix constants. Note that the soil-physical model is fitted at a certain wavelength, whereas the optical model is fitted over all wavelengths in the optical domain.

Materials and Methods

Experimental setup

A laboratory spectroscopy experiment was conducted in duplo to observe spectral reflectance in the optical domain (350-2500 nm) under different moisture conditions. A representative sample of beach sand was collected from the 'Sand Motor' (GPS location: 52.052°N 4.184°E). A field permit was not required and sample collection did not involve endangered or protected species of flora or fauna. Before the experiment the sample was coarsely sieved (2 mm) to remove shells and constituents other than sand. The sand, composed of quartz with some feldspar, had a dry bulk density ρ_b of 1.655 gcm^{-3} with mean and median grain size of 324 and 288 μm respectively.

For each experiment, a sub-sample of the collected beach sand was placed in a matte black petridish (5 cm radius, 1.5 cm height), filling it up to the rim, and oven dried for 24h at 105 °C. The sample was, after measuring its initial weight, slowly saturated with distilled water. The water was let to distribute itself uniformly in the sample and excess free water was drained from the surface. The sample was placed on a data-logging weighing scale with milligram precision.

During the drying process the reflectance (correct terminology: biconical reflectance factors or BCRF's) of the sample were acquired using the spectroscopy facility of Wageningen University (Roosjen et al., 2012). The spectral reflectance was measured at 1 nm intervals using an ASD Fieldspec Pro spectrometer (Analytical Spectral Devices, Boulder, CO). A 40 x 40 cm white Spectralon panel (LabSphere, Inc., North Sutton, NH) was used to calibrate the spectrometer.

The spectrometer was fitted with a 1° FOV foreoptic which was directed at nadir at 40 cm distance from the sample. As an artificial light source, a 900 watt Quartz Tungsten Halogen (QTH) lamp was placed 70 cm from the sample at a 30° zenith angle (see Figure 4.4). At the time of the measurements the room temperature was kept stable at 23 °C and the humidity was kept constant at 50%. The spectrometer was programmed to take a measurement every 5 minutes. At the same time the weight of the sample was measured and stored. Data are publicly accessible at doi:10.4121/uuid:866135c2-2be3-4b74-8f9c-922505285a7b.

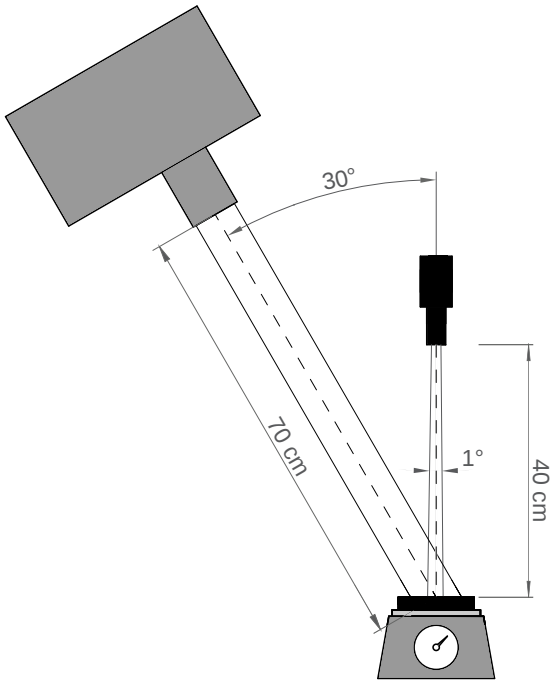

Figure 4.4: Measurement setup of the laboratory spectroscopy experiment. An ASD Fieldspec Pro spectrometer (Analytical Spectral Devices, Boulder, CO), fitted with a 1° FOV foreoptic, was directed at nadir at 40 cm distance from the sample. A 900 watt Quartz Tungsten Halogen (QTH) lamp was placed 70 cm from the sample at a 30° zenith angle. The spectral reflectance was measured over a range of 350-2500 nm, at 1 nm intervals.

Analysis method

For each sub-sample the laboratory spectroscopy experiment obtained five-minute interval measurements of spectral reflectance at a certain volumetric moisture content. Only wavelengths between 350 - 2100 nm were included in the analysis, as wavelengths $>$ 2100 nm were found to have a lower signal-to-noise ratio. Volumetric moisture content was calculated by:

$$\theta = \frac{m_w \rho_s}{m_s \rho_w} \tag{4.8}$$

With m_w and ρ_w the (decreasing) mass and density (0.997 gcm^{-3}) of water, and m_s and ρ_s the mass and dry bulk density (1.655 gcm^{-3}) of the sand sample. Equation 4.6 and 4.7 were fitted to the spectral reflectance measurements. Parameters f_s and d (Eq. 4.6) and a and n (Eq. 4.7) were optimized using a non-linear (weighted) least-squares regression algorithm (R Core Team, 2012). The spectrum of the air-dry sample was used for R_d and the spectrum for R_θ corresponded to a certain volumetric moisture content. The sand matrix constants θ_r and θ_s were determined manually, using the graphical relationship between spectral reflectance and volumetric moisture content.

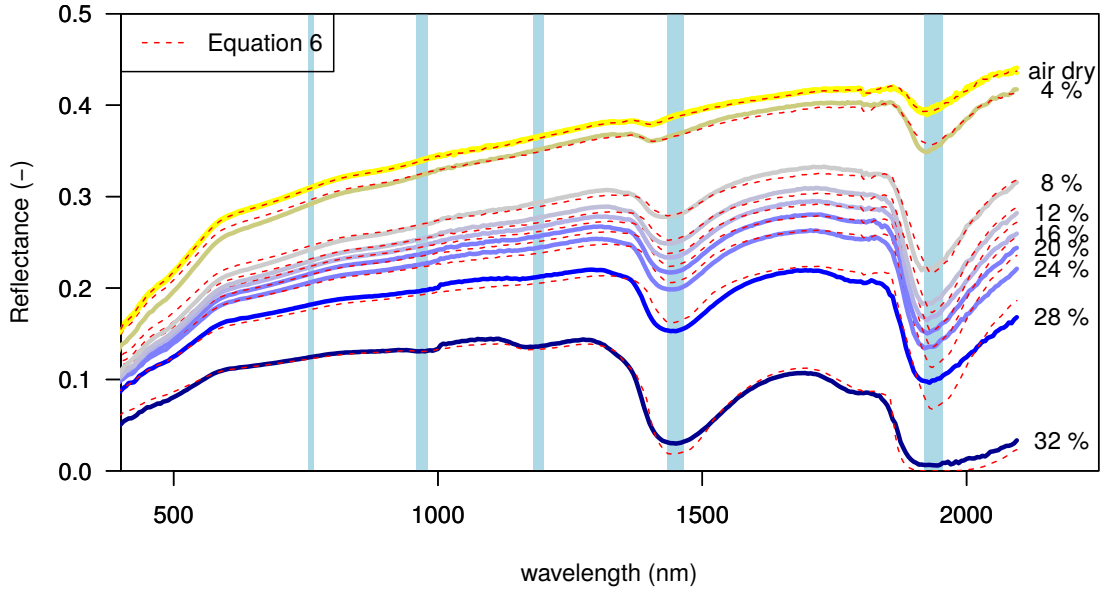

Figure 4.5: The measured spectral reflectance over a range of 350-2100 nm at 4% volumetric moisture content interval, between 32% (saturation) and $<$ 0.01% (air-dry). A non-linear decrease in reflectance upon wetting is observed over the full range of wavelengths. Notable dips in reflectance occur at water absorption peaks at 1470 and 1940 nm (blue bands). The dashed red lines show the spectral reflectance R_θ as calculated by fitting the optical model (Eq. 4.6) to measured spectral reflectance.

Results and Discussion

Laboratory experiment

The laboratory spectroscopy experiment was conducted in duplo to assess the variation in spectral reflectance of the beach sand as function of surface moisture content. The spectral reflectance curves of both experiments (interpolated to regular moisture intervals) showed minimal variation between 400-2100 nm ($R^2 > 0.997$). Therefore the dataset with most data points was selected for further analysis. A total of 300 spectral reflectance measurements were taken over a period of 25 hours. Volumetric surface moisture content varied between 32% (saturation) and $<$ 0.01% (air-dry).

Figure 4.5 shows measured spectral reflectance plotted at 4% moisture intervals. A non-linear decrease of reflectance, as moisture content increases, is observed over the full range of wavelengths. The shape of the air-dry spectral reflectance curve (top line Fig. 4.5) reflects the optical properties of the beach sand itself. Overall, at longer wavelengths, dry beach sand becomes more reflective but wet beach becomes less reflective. This is due to stronger absorption of light in water at near- and short-wave infrared wavelengths (see Fig. 4.1). Notable dips in reflectance are observed at the absorption peaks of 1470 and 1940 nm. The overall shape of the curve at visible wavelengths (400-700 nm) does not change greatly with increasing moisture content. This corresponds to the notion that soils darken when wet but with little apparent color change.

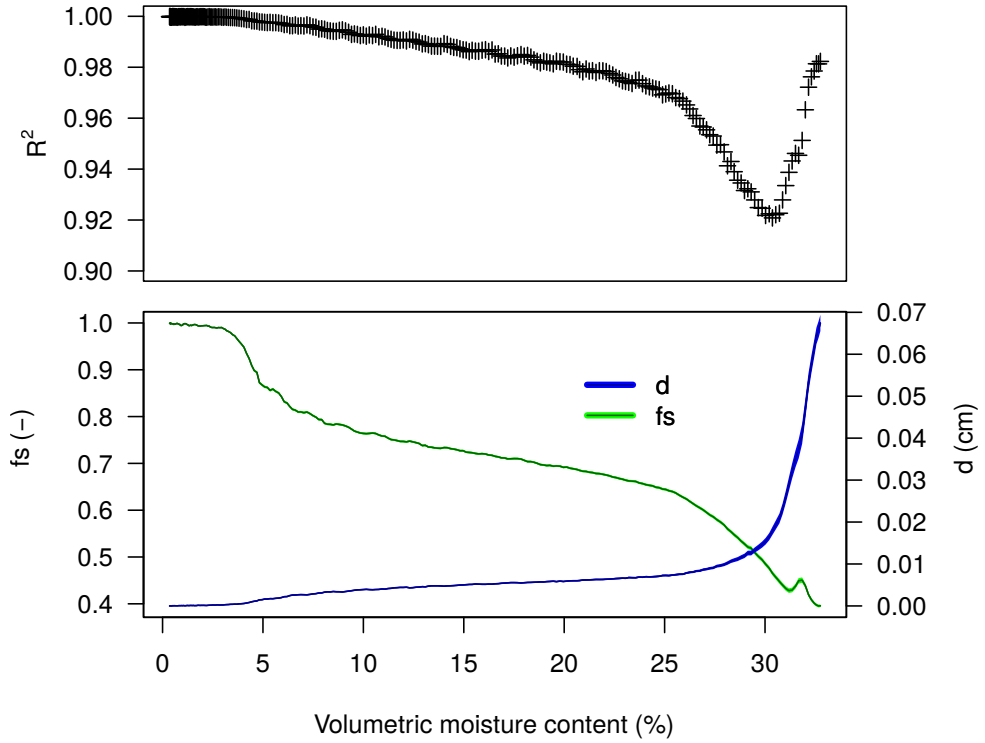

Figure 4.6: Performance of the optical model (Eq. 4.6). Top panel: goodness of fit R^2 of the optical model as function of volumetric moisture content. Bottom panel: trajectories of the regression parameters f_s and d of the optical model, describing the proportional contribution of scattering (fraction f_s) and absorption (optical path length in water d) as moisture levels increase. Shaded areas indicate 95 % confidence intervals.

The optical model (Eq. 4.6) was fitted to the spectral reflectance measurements and shown as dashed red lines in Figure 4.5. As can be seen in Figure 4.6 (top) the optical model performs well for surface moisture contents $\theta < 24\%$ ($R^2 > 0.97$), but gives an underestimation in reflectance for θ between 24-30% ($R^2 > 0.92$). This is most notable around the 1940 nm water absorption peak (see Fig. 4.5). A plausible explanation is that the absorption of light is not as effective in pore water since it is partially bound to the sand matrix. This notion is supported by the fact that at saturation ($\theta \geq 32\%$), where free water is present, model performance improves ($R^2 > 0.97$).

Figure 4.6 (bottom) shows the values of f_s (fraction) and d (cm) at corresponding moisture content. The trajectories of the regression parameters of the optical model describe the proportional contribution of elastic scattering (f_s) and water absorption (d) to spectral reflectance upon wetting. These trajectories are in agreement with the principle outlined in Figure 4.2. At air-dry conditions (Fig. 4.2.1) pore water is held tightly in the sand matrix. The optical path length in water (d) is close to zero as there is negligible absorption of light in water. Reflectance is thus almost solely due to scattering, and fraction f_s is close to 1. When pore water proceeds to fill micro pores and form water wedges between sand grains (Fig. 4.2.2), the contribution of absorption increases, while the contribution of scattering decreases. When the sand matrix gets fully saturated (Fig. 4.2.3) the optical path length in water (d) is at its max-

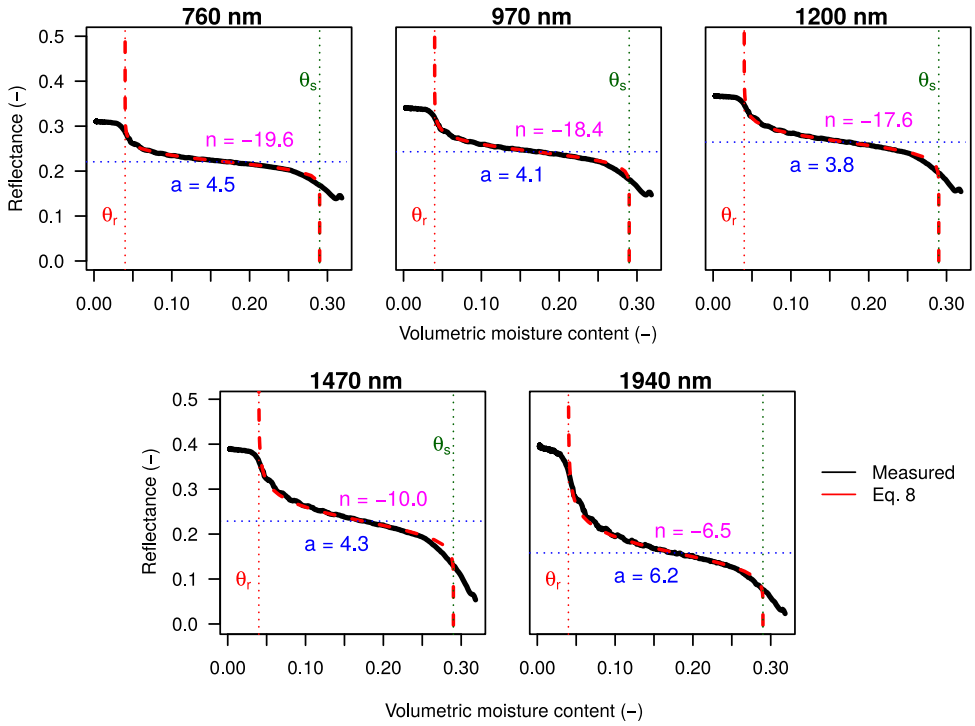

Figure 4.7: The measured spectral reflectance upon wetting at the water absorption peaks of 760, 970, 1200, 1470, and 1940 nm. The dashed red lines show volumetric moisture content θ_R as calculated by fitting the soil-physical model (Eq. 4.7). With sand matrix parameters $\theta_r = 0.04$ and $\theta_s = 0.29$. Non-linear regression parameters a and n are shown in the plot at corresponding wavelength.

imum, between 0.06 - 0.07 cm. This corresponds to a thickness of a few sand grains (median 288 μm). It is encouraging that the order of magnitude is within physical expectation.

Figure 4.7 (black lines) shows measured reflectance as a function of volumetric moisture content plotted for the five water absorption peaks at 760, 970, 1200, 1470, and 1940 nm. It can be seen that at longer wavelengths the air-dry reflectance increases and reflectance upon wetting decreases, resulting in greater contrast between wet and dry reflectance. Wavelengths at 1470 and 1940 nm are absorbed by water to such an extent that saturated reflectance approaches zero. Further, it becomes clear from Figure 4.7 that the shape of the spectral reflectance curves are very similar to the shape of the water retention curve calculated by Eq. 4.5 of Van Genuchten (1980) (Fig. 4.3). This suggests that spectral reflectance influenced by surface moisture content is linked to the hydraulic behaviour of water in an unsaturated sand matrix. This link is conceivable, as both processes share common drivers such as mineral composition and texture of the soil. The spectral reflectance upon wetting and water retention characteristics of beach sand can thus be described by the same empirical formulation.

The soil-physical model (Eq. 4.7) was fitted to the reflectance curves of Figure 4.7. Non-linear regression parameters a and n are shown in the plots at corresponding wavelength. The sand matrix parameters θ_r and θ_s were determined at 0.04 and 0.29 respectively. As a consequence, moisture levels of $\theta < 4\%$ and $\theta > 29\%$ are beyond the range of the soil-physical model. While

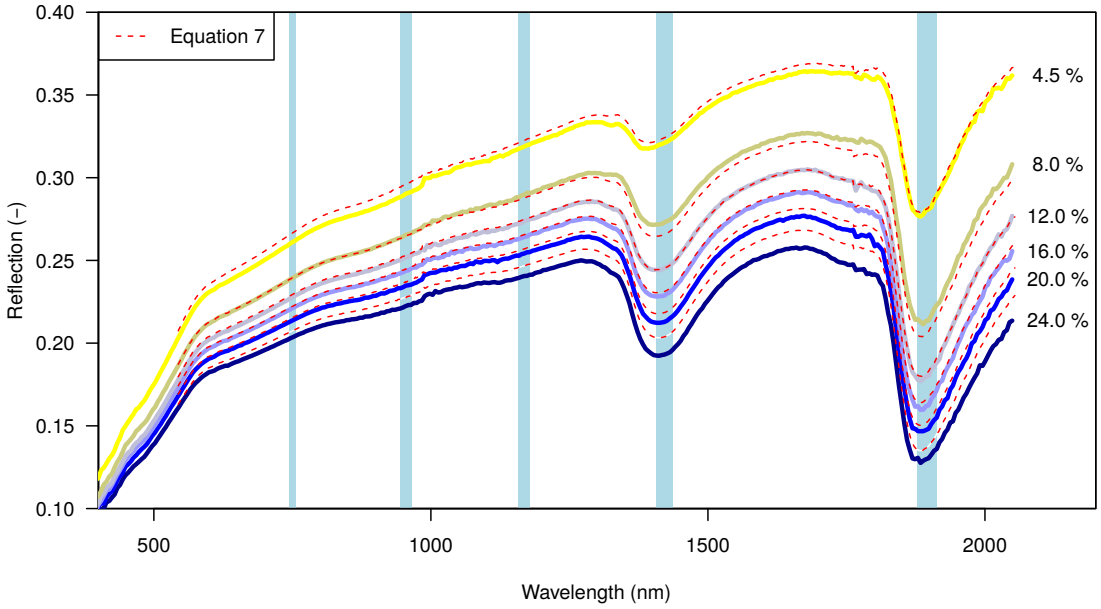

Figure 4.8: Spectral reflectance upon wetting (red dashed lines) obtained by fitting the soil-physical model (Eq.4.7) to measured spectral reflectance at 1 nm interval. The blue bands indicate spectral absorption peaks for water. Between 4.5-24% volumetric moisture content the spectral reflectance reconstructed with Eq. 4.7 has a goodness of fit of $R^2 > 0.99$.

knowledge of $\theta > \theta_s$ is not very relevant for aeolian coastal research, knowledge of $\theta < \theta_r$ is relevant. Even at low levels, surface moisture exerts a significant control on the aeolian entrainment of sand. As can be seen in Figure 4.7, the reflectance for $\theta < \theta_r$ at shorter wavelengths remain almost level and a differentiation between moisture levels $< \theta_r$ is not possible. At near- and short-wave infrared wavelengths, however, the reflectance does increase as moisture content decreases towards air-dry conditions. Here the approach of Wesseling et al. (2008) offers an alternative to the soil physical model, as it can describe the reflectance curve over the full moisture range using cubical spline approximations.

The soil-physical model (Eq. 4.7) was also fitted to measured spectral reflectance upon wetting over the full range of 350-2100 nm, at 1 nm interval. By obtaining the values for *a* and *n* for all optical wavelengths for the unsaturated sand matrix between θ_r and θ_s, it was possible to calculate the spectral reflectance as a function of volumetric moisture content (R_θ). Figure 4.8 shows the calculated (red dashed lines) and measured (continuous lines) spectral reflectance upon wetting between 4.5-24% volumetric moisture content plotted at 4% moisture content interval. Between these moisture levels the reconstructed spectral reflectance has an overall goodness of fit of $R^2 > 0.99$. A slight underestimation in spectral reflectance was found for higher surface moisture contents, most notable around the absorption peaks of 1470 and 1940 nm.

It becomes clear from Figure 4.9 that, at visible wavelengths averaged over 400-700 nm, there is a limited contrast between dry and wet reflectance of beach sand composed of quartz sand. The slope of the reflectance curve is, after an initial steep decline, close to zero for intermediate moisture levels ($\sim$ 5-25%). This suggests that, for quartz sand beaches at visible

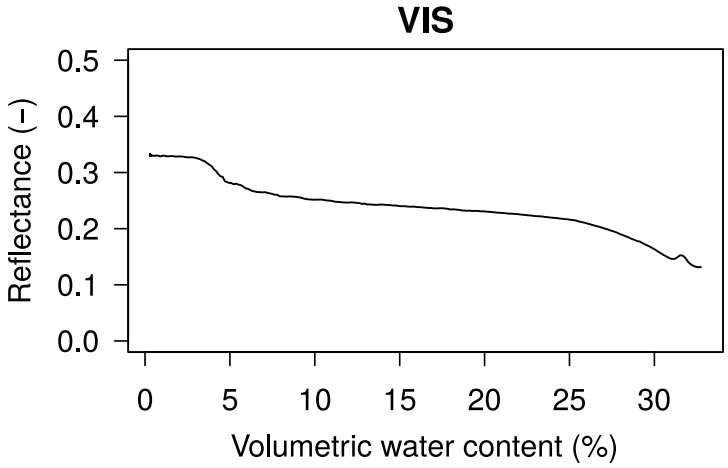

Figure 4.9: Averaged measured spectral reflectance upon wetting at visible wavelengths (400-700 nm), illustrating the limited contrast in reflectance between a dry and a wet beach composed of quartz sand.

wavelengths, only a distinction between a dry and a wet surface is practical. Differentiation of intermediate moisture levels would require very accurate radiometric calibration, also considering that other parameters affecting surface reflectance (e.g. mineral composition, grain size distribution, packing density, surface roughness) may vary under field conditions. This limited contrast is a plausible explanation for the weak correlation between beach surface moisture and reflectance found in the studies of Mckenna Neuman and Langston (2003); McKenna Neuman and Langston (2006); Darke and McKenna Neuman (2008); Darke et al. (2009); Delgado-Fernandez et al. (2009) and Nield et al. (2014, 2011); Nield and Wiggs (2011). A standard error of $\sim$ 10% moisture content is reported by Edwards et al. (2013b) and Edwards et al. (2013a) for the photographic method, while with the terrestrial laser scanner ($\lambda = 539$ nm) the standard error increases after 7-8% moisture to such an extent that the method becomes impractical.

Practical applications

The findings of our laboratory spectroscopy experiment imply that optical remote sensing of surface moisture is most effective when measuring in the near- and short-wave infrared. These wavelengths are strongly absorbed by water and provide sufficient contrast in the signal to differentiate intermediate moisture levels ($\sim$ 5-25%). The water absorption peaks of 1470 and 1940 nm are effective in particular. At these wavelengths there is enough contrast in the signal to also differentiate low moisture levels ($\sim$ 0-5%). Because of strong absorption by the atmosphere an active remote sensing technique is required, for example such as employed by (Ruessink et al., 2014) in a subsequent field experiment.

Ruessink et al. (2014) tested the applicability of a RIEGL VZ-400 3D terrestrial laser scanner to derive spatially extensive moisture maps of a natural beach. The wavelength of this TLS is in the short-wave infrared at $\lambda = 1550$ nm, hence on the wings of the absorption peak at 1470 nm. Ruessink et al. (2014) deployed their scanner from a tripod at Egmond Beach in The

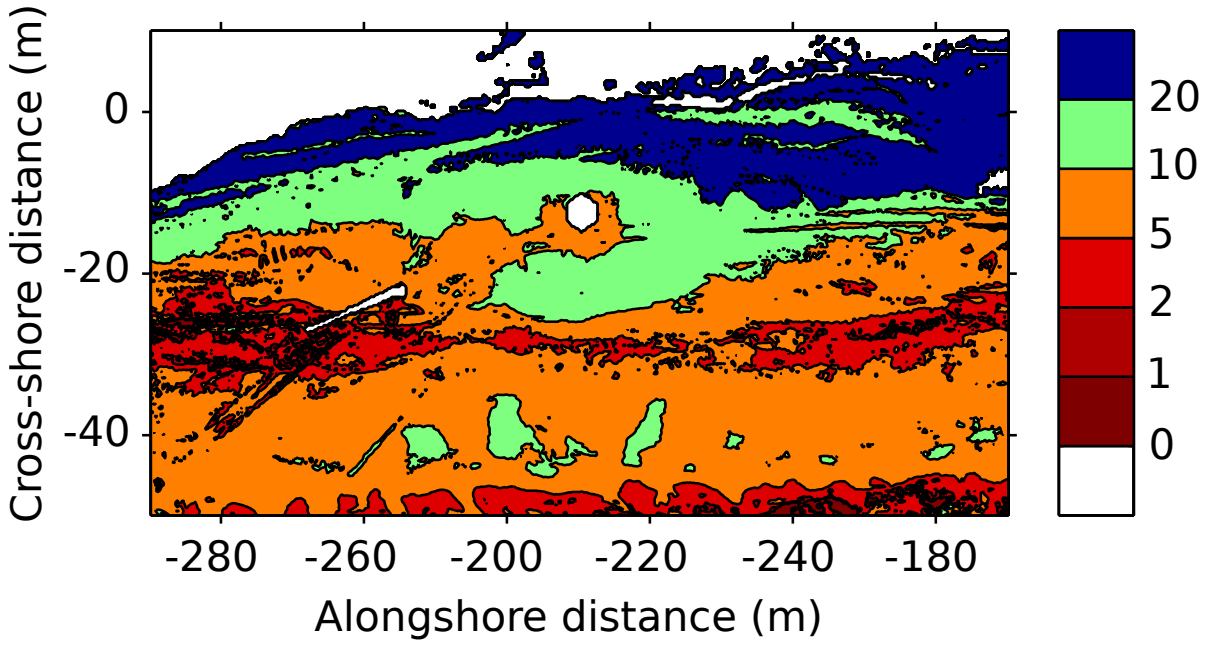

Figure 4.10: Example gravimetric moisture content (in %) map, estimated from the reflectance collected with a RIEGL VZ-400 3D terrestrial laser scanner at Egmond aan Zee, The Netherlands, from the upper dry beach (cross-shore distance $x \approx -50$ m) to the water line ($x \approx -10$ to 10 m) (Ruessink et al., 2014). The local co-ordinates are positive in the seaward direction and to the south. The scanner was located at $(x, y) \approx (-15, -230)$ m. The slightly drier sand immediately around the scanner position is an artifact of the conversion from intensity to reflectance; close to the scanner, as also noted by Nield et al. (2014), the imposed $1/r^2$ correction does not apply. The narrow bands with apparent lower moisture content (e.g. at alongshore y distances -200 to -180 m and $x \approx -15$ m) correspond to car tracks.

Netherlands and collected 9 panorama scans (360° in the horizontal, 100° in the vertical, with 0.002° resolution in the horizontal and vertical). Each scan took about 10 minutes to complete and resulted in a cloud of ∼35,000,000 points. Simultaneously, 69 surface scrapings (thickness of a few millimeters) were taken, which were later on processed into gravimetric moisture estimates using standard laboratory techniques. The RIEGL VZ-400 outputs reflectance in decibels, with a $1/r^2$ correction to account for the reduction of returned intensity with range r. For $r = 15 - 60$ m Ruessink et al. (2014) found a linear dependence between gravimetric surface moisture content and reflectance for the full range from dry to saturated sand. This confirms that the use of TLS with a wavelength near an absorption band is inherently more suitable to detect surface moisture over its full range than a TLS with a wavelength in the visible range (for example, (Nield et al., 2014)). The linear dependence is qualitatively consistent with Eq. (4.6), as decibel is a logarithmic unit. The standard error of their best-fit line amounted to about 2.6%, which is considerably lower than reported for the photographic method of Mckenna Neuman and Langston (2003); McKenna Neuman and Langston (2006); Darke and McKenna Neuman (2008); Darke et al. (2009); Delgado-Fernandez et al. (2009).

An example of a derived moisture map is provided in Figure 4.10. It illustrates the overall

increase in moisture content from the dunefoot to the waterline, with superimposed variability related to secondary morphological highs and lows, consistent with Namikas et al. (2010). The map also shows two narrow, approximately alongshore bands of apparent lower moisture content, which correspond to car tracks. While the sand in the car tracks may actually contain less pore water e.g. due to compaction, the collected reflectance could depend on surface roughness too. The rougher car tracks may increase the reflectance relative to a flat beach surface with the same moisture content. Nonetheless, the results of Ruessink et al. (2014) results illustrate the potential power of active remote sensing near a water absorption band to derive accurate surface moisture maps at a spatial and temporal resolution infeasible with other techniques. A future publication will describe and analyze the TLS data of Ruessink et al. (2014) more extensively.

Conclusions

In this study the effect of surface moisture content on spectral reflectance of coastal beach sand is measured and modeled for the the full optical domain of 350-2100 nm, to support practical applications for optical remote sensing of surface moisture. It is shown that:

- The effect of surface moisture on spectral reflectance of coastal beach sand can be described by an optical as well as a soil physical model.
- Near- and short-wave infrared wavelengths are most effective for relating surface moisture content to reflectance due to strong absorption of light in water.
- A terrestrial laser scanner operating at $\lambda = 1550$ nm can derive accurate surface moisture maps at a high spatio-temporal resolution.

Chapter 5

UAV-imaging to model growth response of marram grass to sand burial by wind: Implications for coastal dune development

This chapter is based on:

Nolet, C., van Puijenbroek, M., Suomalainen, J., Limpens, J., and Riksen, M. (2018). UAV-imaging to model growth response of marram grass to sand burial: Implications for coastal dune development, *Aeolian Research* 31, 50–61

Abstract

Vegetated coastal dunes have the capacity to keep up with sea-level rise by accumulating and stabilizing wind-blown sand. In Europe, this is attributed to marram grass (*Ammophila arenaria*), a coastal grass species that combines two unique advantages for dune-building: (1) a very high tolerance to burial by wind-blown sand, and (2) more vigorous growth due to positive feedback to sand burial. However, while these vegetation characteristics have been demonstrated, observational data has not been used to model a function to describe the growth response of *Ammophila* to sand burial. Studies that model coastal dune development by incorporating positive feedback, as a result, may be hampered by growth functions that are unvalidated against field data. Therefore, this study aims to parameterize an empirical relationship to model the growth response of *Ammophila* to burial by wind-blown sand.

A coastal foredune along a nourished beach in the Netherlands was monitored from April 2015 to April 2016. High-resolution geospatial data was acquired using an Unmanned Aerial Vehicle (UAV). Growth response of *Ammophila*, expressed by changes in Normalized Difference Vegetation Index (Δ NDVI) and vegetation cover (Δ Cover), is related to a sand burial gradient by fitting a Gaussian function using nonlinear quantile regression. The regression curves indicate an optimal burial rate for *Ammophila* of 0.31 meter of sand per growing season, and suggest (by extrapolation of the data) a maximum burial tolerance for *Ammophila* between 0.78 (for Δ Cover) and 0.96 meter (for Δ NDVI) of sand per growing season. These findings are advantageous to coastal management: maximizing the potential of *Ammophila* to develop dunes maximizes the potential of coastal dunes to provide coastal safety.

5.1 Introduction

Coastal dunes are prominent features along many of the world's sandy shorelines, covering about 34% of the world's ice-free coasts (Hardisty, 1994). They are the result of complex interactions between wind, waves, sand and vegetation (Hesp, 1989; Keijsers et al., 2016) and have the capacity (1) to reduce hydrodynamic impact from storm surges and (2) to keep up with sea-level rise by accumulating and stabilizing wind-blown sand (Temmerman et al., 2013). As a result, coastal dunes are often essential for flood protection and ensuring coastal safety (De Jong et al., 2014; Keijsers et al., 2015b; Poortinga et al., 2015a).

The capacity of coastal dunes to keep up with sea-level rise is attributed to the specialized morphology of coastal grass species covering the dunes. Especially European and American marram grass, *Ammophila arenaria* and *Ammophila breviligulata*, combine two unique advantages for dune-building, namely (1) very high tolerance to burial by wind-blown sand, reportedly up to 1 meter (Ranwell, 1972) or even 2 meter of sand per year (Baas and Nield, 2010), and (2) more vigorous growth under the right conditions of sand burial (e.g., Huiskes, 1979; Disraeli, 1984; Maun and Lapierre, 1984; Hesp, 1991; Van der Putten et al., 1988). This introduces a reinforcing feedback essential to dune development: adequate levels of wind-blown sand encourages *Ammophila* to grow, which in turn enhances *Ammophila's* capacity to accumulate and stabilize wind-blown sand (Maun, 1998; Zarnetske et al., 2012). As a result, dune development is directly related to the growth response of marram grass to sand burial (Keijsers et al., 2016), and throughout temperate climate zones in the world *A. arenaria* and *A. breviligulata* helped to create very high vegetated coastal dune landscapes (Ranwell, 1972).

However, while stimulated growth of *Ammophila* to sand burial has convincingly been demonstrated by aforementioned studies, the observational data has not been used to model a function to describe this response. Instead, the findings are reported primarily using inferential statistics based on a limited number of plant samples. Moreover, except in Disraeli (1984), results are drawn from experiments that relied on artificial sand burial treatments within a restricted burial range. The reported growth response of *Ammophila* to sand burial, therefore, may not have been fully representative for burial conditions due to natural coastal aeolian dynamics.

As a result, studies that aim to model coastal dune development by explicitly incorporating positive feedback, (i.e., Baas, 2002; Nield and Baas, 2008; Baas and Nield, 2010; Keijsers et al., 2016), may be hampered by an inadequate description of growth response of marram grass to sand burial under natural conditions. While the employed growth functions are deliberately simplistic to reduce model complexity, they are not validated against field data but rather based on anecdotal evidence and derived by trial-and-error model runs (Baas and Nield, 2010). Therefore, to help fill that gap, this study aims to parameterize an empirical relationship to model the growth response of *Ammophila* to burial by wind-blown sand. It builds on the conceptual model put forward by Maun (1998) and Maun and Perumal (1999), in which a 2^{nd} order polynomial is proposed for describing stimulated growth of *Ammophila* in response to sand burial, up to a maximum burial tolerance beyond which plants start to show a negative response.

To this end, a stretch of coastal foredune, along a nourished beach in the Netherlands, has been extensively monitored over the course of a year using an unmanned aerial vehicle (UAV). Rapid technological advances in platforms, sensors and software have positioned UAV's as a powerful low-cost tool to accurately derive very high-resolution geospatial data, at temporal resolutions defined by the end-user (Westoby et al., 2012; Hugenholtz et al., 2013; Mancini et al., 2013). Processing the aerial images using photogrammetric software is particularly advantageous, for it allows producing high quality digital elevation models and orthomosaics of the same area at the same time. The ability of UAV's to collect topographic and ecological data simultaneously holds invaluable promise for spatial biogeomorphology (Anderson and Gaston, 2013), and may prove to be essential to better quantify the growth response of *Ammophila* to burial by wind-blown sand.

This paper presents the results obtained by aforementioned monitoring study, focusing on a growing season of *Ammophila arenaria* from April 2015 till October 2015. Growth response of marram grass is expressed by temporal changes in Normalized Difference Vegetation Index (Δ NDVI) and spatial-temporal changes in vegetation cover (Δ Cover), while sand burial by wind is derived from changes in dune morphology due to aeolian dynamics (Δ dune height). It has been demonstrated by Disraeli (1984), Maun and Lapierre (1984) and Yuan et al. (1993) that plants subjected to regular burial in sand showed a higher total chlorophyll content and above-ground biomass than plants not subjected to sand burial. This suggests that changes in NDVI and vegetation cover are appropriate indicators for growth of *Ammophila* in response to a sand burial gradient.

As such, by modeling the growth response of *Ammophila arenaria* to burial by wind-blown sand using high-resolution geospatial data, this study aims to provide better insight into the role of this grass species to coastal dune development. This is of particular interest for a country as the Netherlands, considering large parts are situated below sea level. The Dutch coastline requires continuous maintenance by sand nourishment to mitigate the effects of coastal erosion (De Jong et al., 2014; Keijsers et al., 2015b; Poortinga et al., 2015a). An important aspect of this strategy is a steady supply of wind-blown sand towards the dunes, where *Ammophila* enables the dunes to naturally grow in volume and thus subsequently helps ensuring coastal safety.

5.2 Material and methods

5.2.1 Data acquisition

Study area

The research was conducted at the *Zandmotor* (i.e. Sand Motor, figure 5.1), an uniquely 21.5 Mm^3 large nourishment of sand laid down for coastal protection. It is designed from the viewpoint of 'Building with Nature' (Van Slobbe et al., 2013), a coastal management strategy that aims to provide coastal safety by utilizing natural processes. Through wave and wind action the *Zandmotor* is gradually releasing its sand along the coastline and re-enforcing the beach and dunes against storm surges and sea-level rise (Nolet et al., 2014; De Schipper et al.,

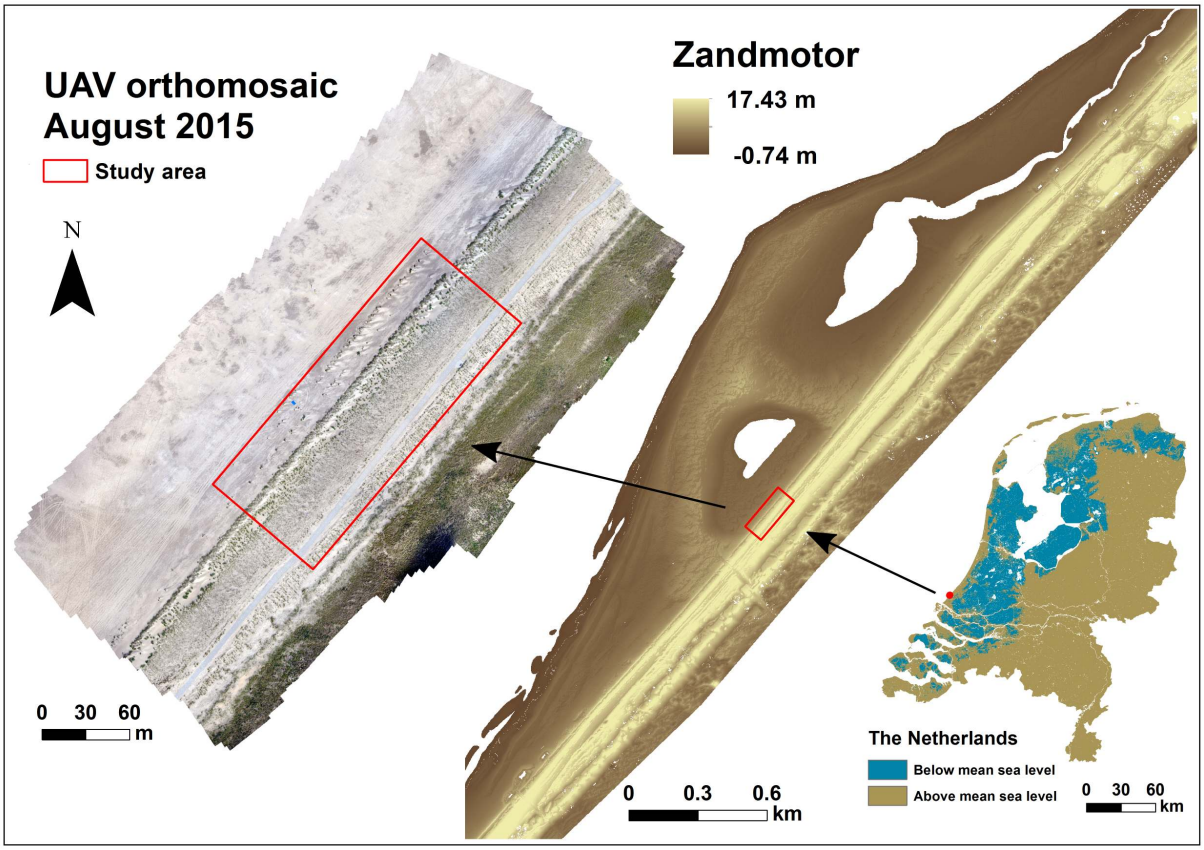

Figure 5.1: The study area (red box), a stretch of foredune that was artificially created in 2011 just prior to construction of the *Zandmotor*, an uniquely large nourishment of sand (21.5 Mm^3) located just south of The Hague along the Dutch coast. The studied foredune has a south-west to north-east orientation, parallel to the dominant south-western wind direction. Just after construction the ∼40 meter long stoss slope of the foredune (15° at its steepest) was manually planted with marram grass (*Ammophila arenaria*) in a regular grid of about 7-9 small tussocks per m^2. From dune toe to dune crest the stoss slope ranges between 4-12 m above mean sea level (MSL) and *Ammophila* grows between 7-12 m +MSL. Note the bike path running along the dune crest at 11.5 m +MSL and the incipient dunes in front of the dune toe at 4 m +MSL.

2016). As such, a net negative sediment balance is counteracted with minimal adverse effects to the coastal ecosystem (Stive et al., 2013b). The *Zandmotor* is located just south of the city The Hague, along the Delfland coast, and has a hook-shaped design that mirrors the natural onshore migration of an intertidal sandbar. Just after its construction in summer 2011 the *Zandmotor* had an surface area of about 28 ha, extending 2.5 km along the coastline and protruding 1 km into the sea. Natural processes have since then been working to re-distribute the sand at high rates (De Schipper et al., 2016).

The red box in figure 5.1 shows the study area, a stretch of foredune in direct proximity of the *Zandmotor*. The foredune has a south-west to north-east orientation, parallel to the dominant south-western wind direction. From dune toe to dune crest the stoss slope ranges between 4-12 meter above mean sea level (MSL). Along the stoss slope *Ammophila arenaria* grows

between 7-12 m +MSL. Note the bike path running along the dune crest at 11.5 m +MSL and the incipient dunes in front of the dune toe at 4 m +MSL. Gravimetric sampling showed that soil moisture conditions along the vegetated stoss slope are comparable up to a depth of 1.15 meter. Since the groundwater table at the dune toe is deep ($<$ 2 m from ground level) and the coarse dune sand has a high (unsaturated) hydraulic conductivity (Huiskes, 1979), the foredune is characterized by excellent drainage and very low capillary rise. As a result, *Ammophila* is purely rain-fed along the whole stoss slope of the studied foredune.

While principally selected to study the effect of the *Zandmotor* on subsequent dune development, this stretch of foredune is well suited to investigate the growth response of *Ammophila* to sand burial by wind. First, the foredune was artificially created just prior to construction of the *Zandmotor* and, therefore, the starting conditions in terms of dune morphology and vegetation state were known and uniform. Just after completion the $\sim$40 meter long stoss slope of the foredune (15° at its steepest) was manually planted with marram grass in a regular grid of about 7-9 small tussocks per m^2. Second, because of steady supply of wind-blown sand and complete shielding against storms, the morphology of the foredune has been shaped only by aeolian forces. The development of *Ammophila* has thus not been affected by marine erosion and, as a result, sand burial by wind has most likely been the dominant process affecting its growth.

Figure 5.2 shows the average cross-sectional development of the foredune since its construction in 2011 up to 2016. It is clear that, even though *Ammophila* acts to trap and stabilize wind-blown sand, the stoss slope exerts a great control on the spatial distribution of accumulation of wind-blown sand. Generally speaking, though coastal foredunes are known to deflect obliquely approaching winds towards a more crest-normal orientation (Hesp et al., 2015), sand has either accumulated at the dune toe due to oblique onshore winds or leeward of the dune crest due to perpendicular onshore winds (Arens, 1996b). Halfway the stoss slope the dune has accumulated little sand, due to local acceleration of the wind flow and steepness of the slope itself (Arens et al., 1995). All processes combined have resulted in an actively growing foredune, at a rate between 15-20 m^3 per meter alongshore per year. This corresponds well to rates reported by (Van der Wal, 2004) for nourished Dutch coasts. The accumulated dune sand, composed of quartz with some feldspar, has a dry bulk density ρ_b of 1.655 g/cm^3 and median grain size of 325 μm.

UAV-imaging

Monitoring of the foredune was carried out with aerial imaging using an Unmanned Aerial Vehicle (UAV). The purpose of the flights was to derive digital elevation models and orthomosaics using photogrammetric software. The digital elevation models (5 cm pixel size) provide information on dune morphology due to aeolian dynamics, while the orthomosaics (1 cm pixel size) provide information on vegetation characteristics, in this case Normalized Difference Vegetation Index (NDVI) and vegetation cover. Changes in dune morphology serve to indicate a sand burial gradient, while subsequent changes in NDVI and vegetation cover aim to express the growth response of *Ammophila* to sand burial. The data-set is made up of seven different flight days carried out over a period from April 2015 to April 2016, with emphasis on the

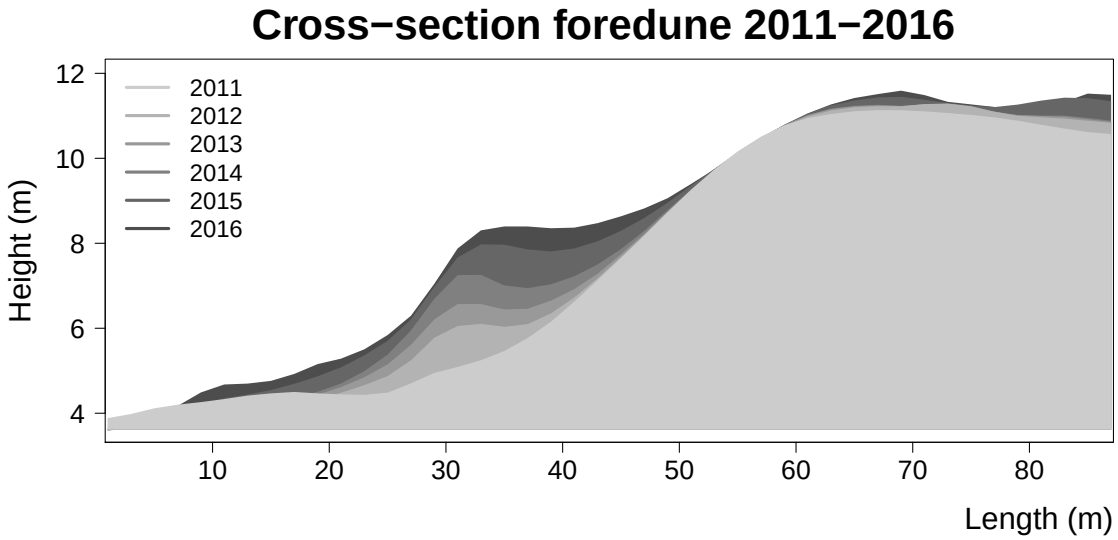

Figure 5.2: The averaged cross-sectional development of the studied foredune since its construction in 2011 up to 2016. Wind-blown sand has either accumulated at the dune toe due to oblique onshore winds, or leeward of the dune crest due to perpendicular onshore winds. Halfway the stoss slope the dune has accumulated little sand, due to local acceleration of the wind flow and steepness of the slope itself. All processes combined have resulted in an actively growing foredune, at a rate between 15-20 m^3 per meter alongshore per year. The figure is derived from freely available airborne Lidar data (2 meter pixel size).

growing season of *Ammophila* from April to October 2015.

The flights were carried out with an rotary octocopter UAV system (Aerialtronics Altura Pro AT8 v1) with a diameter of 0.85 m and weight of 3.0 kg. The platform has a fully autonomous flying functionality and can carry up to a 2 kg payload. The octocopter was equipped with a multi-spectral mapping system custom-built by the Unmanned Aerial Remote Sensing Facility (www.wur.eu/uarsf) of Wageningen UR. It consists of two Canon EOS 700D single-lens reflex cameras, both with 28 mm f/2.8 Voigtländer Color Scopar SL-II N objectives. One camera gives standard color (RGB) output, while the other camera has been modified to give false color output. Most distinctly, by replacing the standard infrared cut-off filter (ICF), the red channel of this camera has been converted to be sensitive in the near-infrared (NIR), with center point around 720 nm and full width at half maximum (FWHM) of about 80 nm. This enables indicating NDVI, ensuring enriched applicability for ecological monitoring.

Aerial images were acquired by auto-piloted flights at an altitude of 80 meter at 4-5 m/s velocity. The cameras were triggered synchronously using a Canon TC-80N3 intervalometer with modified dual output connector. Up to 300 RAW images per camera were collected per 5-10 minute flight. Four flights were needed to cover the study area, resulting in a maximum of 1200 image pairs per flight day. Nine ground control targets were permanently placed in the flight area and measured with RTK-GPS (Topcon HiPer Pro, accuracy H: 10 mm, V:15 mm).

5.2.2 Data processing

Radiometric calibration

In order to use the cameras as radiometric sensors, two calibration steps were applied following the procedure outlined in Suomalainen et al. (2014). First the output of each individual pixel of the sensor in the camera is calibrated. RAW digital number (DN) is converted into radiance (L) units using a pixel-wise dark current and flat field calibration according to Eq 5.1:

$$L = \frac{DN - DN_{darkcurrent}}{DN_{flatfield} - DN_{darkcurrent}} L_{flatfield} \tag{5.1}$$

Where DN is the intensity of an individual pixel (as recorded by the camera) in the image to be calibrated, $DN_{darkcurrent}$ is the intensity of the same pixel in a dark current calibration image, $DN_{flatfield}$ is the pixel intensity in a flat field calibration image (taken with same exposure and gain settings as the main image), and $L_{flatfield}$ is the flat field radiance at the central wavelength of the pixel. As absolute radiometric calibration is not required in this application, flat field radiance was set to $L_{flatfield} = 1$.

Second, each band of each individual image was separately calibrated to correct for changes in incident irradiance on (and during) different flight days. Calibrated radiances (L_{image}) are converted into a reflectance factors (R_{image}) using a Spectralon panel with known reflectance factor ($R_{reference}$) according to Eq 5.2.

$$R_{image} = \frac{L_{image}}{L_{reference}} R_{reference} \tag{5.2}$$

With values for R_{image} typically between 0-1. The reference radiance ($L_{reference}$) is the reflected radiance from the reference panel. It was measured during operation in the field, by taking a picture of the panel by both cameras, just before the first flight.

Normalized difference vegetation index

The calibrated images were subsequently converted into images indicating Normalized difference vegetation index (NDVI). This ratio (-1,1) takes advantage of a plant's contrasting reflection at visible and near-infrared wavelengths, and is indicative of the abundance of photosynthetically active vegetation (Rouse Jr et al., 1974; Tucker, 1979). NDVI near-linearly increases with increasing chlorophyll concentration, albeit up to threshold value after which it enters an asymptotic regime (Curran et al., 1991; Gamon et al., 1995). While this threshold value is variable, e.g. depending on vegetation type and leaf water content (Carlson and Ripley, 1997), the asymptotic behaviour is inherent to NDVI as it is bounded on an interval. Chlorophyll concentration, in its turn, is in a similar fashion as NDVI related to vegetation indicators such as leaf area index (LAI) or biomass per unit ground area (Filella and Penuelas, 1994). For this study a custom NDVI formulation was used, according to Eq 5.3:

$$NDVI = \frac{(NIR + G) - (2B)}{(NIR + G) + (2B)} \tag{5.3}$$

Where *NIR, G*, and *B* are the near-infrared, green and blue bands of the modified false color camera respectively. The sum of the NIR and green channel is used for the vegetation reflection, while the blue absorption channel is multiplied by two to compensate for the NIR and green being summed together. In this dataset small negative values were associated with man-made structures and were excluded by restricting NDVI-values between 0 and 1. The used custom NDVI formulation was recommended by the company that modified the sensor, due to the lack of a red band in the false color camera. Though not substantiated by peer-reviewed research, on their website (MaxMax.com) it was shown to be just as effective for green vegetation as the traditional NDVI formulation which uses the red band as the absorption channel.

Photogrammetric reconstruction

The auto-piloted UAV flight lines were designed to collect aerial images with at least 85% forward and 65% side-way overlap. This is a prerequisite for photogrammetric software to successfully correlate individual images into a 3D point cloud. The aerial images (with calibrated NDVI-layer) were processed into a 3D point cloud using Agisoft Photoscan Professional, through implementation of the Structure-from-Motion (SfM) and Multi-View Stereo (MVS) algorithms (Westoby et al., 2012; Fonstad et al., 2013). The correlated 3D points were georeferenced to match the ground control targets, and contain pixel intensity values of the input imagery. Due to advances in computing power, the point density resolution and vertical error distribution of data produced by UAV photogrammetry is equivalent to (or even better than) airborne lidar data (Mancini et al., 2013; Hugenholtz et al., 2013).

5.2.3 Data analysis

Gaussian response model

The conceptual model put forward by Maun (1998) and Maun and Perumal (1999), for describing the growth response of marram grass to burial by wind-blown sand, can be placed in a broader (ecological) context: response of a species to an environmental gradient often follows Shelford's Law of tolerance (Shelford, 1931). Each species thrives best around a particular value (its optimum) and cannot survive when this value is either too low or too high. Each species is thus confined to a limited range, or its ecological niche (Ter Braak and Prentice, 1988). In idealized form the response along an environmental gradient is symmetric and unimodal, approximating a normal distribution (Gauch and Whittaker, 1972; Austin and Smith, 1990; Oksanen and Minchin, 2002). This bell-shaped response curve, as shown in figure 5.3, is described by the Gaussian function:

$$f(x) = ae^{-\frac{1}{2}(x-b)^2/c^2} \tag{5.4}$$

Where, in this context, growth response of *Ammophila arenaria* (f) along sand burial gradient

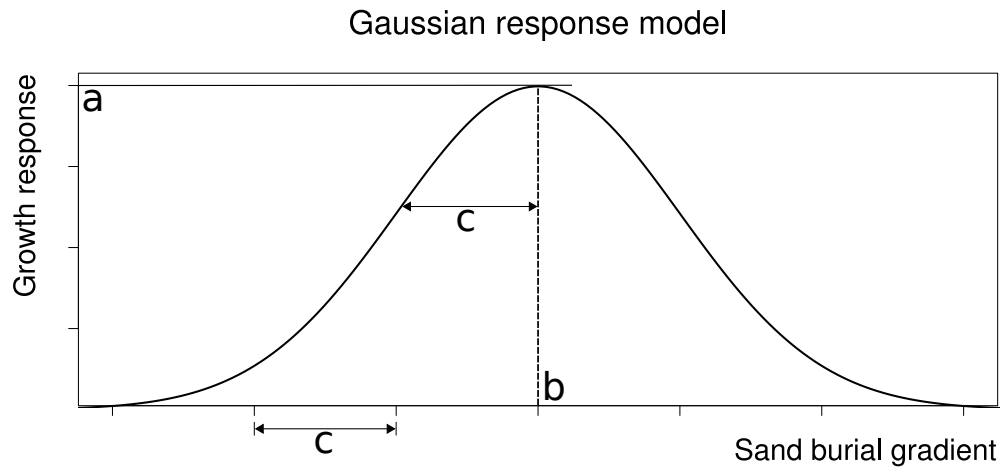

Figure 5.3: Gaussian response model to describe the growth response of *Ammophila arenaria* along a sand burial gradient (x). Gaussian response of *Ammophila* is characterized by three parameters: height (or maximum) of the response (a), position of optimum response (b) i.e. value of x for which the maximum is attained, and tolerance of the response (c) to gradient (x). The range of growth response of *Ammophila* to sand burial is about four times its tolerance c, with maximum tolerance to sand burial $\approx b + 2c$.

(x), is defined by three parameters: height (or maximum) of the response (a), position of optimum response (b) i.e. value of x for which the maximum is attained, and tolerance of the response (c) to gradient x. In general form parameter b controls the mode of the Gaussian response curve, while parameter c its standard deviation (Ter Braak and Looman, 1986). As can be seen in fig. 5.3, the range of Gaussian response is about four times its tolerance c (Ter Braak and Prentice, 1988). The maximum tolerance of *Ammophila* to sand burial by wind is thus approximately described by $b + 2c$.

Model variables

Figure 5.4 summarizes how the model variables for the Gaussian function were derived from the 3D point cloud. The sand burial gradient to which *Ammophila* responds is expressed by Δ dune height (m) over the growing season from April to October 2015. Changes in dune morphology were derived from Digital Terrain Models (DTM), thus without vegetation. Removal of *Ammophila* from the dune surface was done through classification using a k-means clustering algorithm (Hartigan and Wong, 1979). The algorithm was applied to the NDVI intensity values of the points in the 3D point cloud, to classify points pertaining to vegetation or bare dune sand. The DTM's were subsequently created by removing the vegetation points and interpolating the 3D point cloud using LAStools (rapidlasso GmbH). Change in dune height was calculated per consecutive time-step ($t_{4-1} = t_{2-1} + t_{3-2} + t_{4-3}$). This was done to consider temporal variation within the growing season.

The growth response of *Ammophila* to sand burial is expressed by Δ NDVI and Δ Cover, both of which can range between -1 and 1. To calculate (changes in) NDVI and vegetation cover

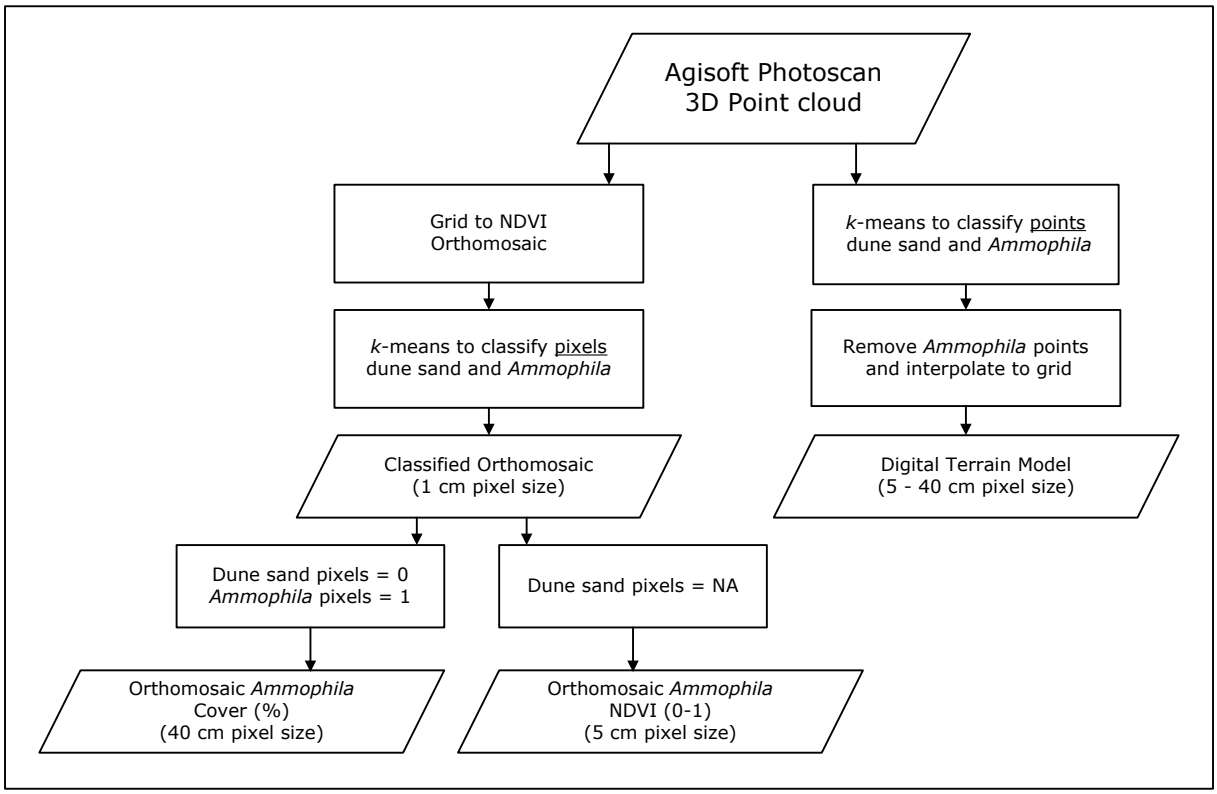

Figure 5.4: Extraction of Gaussian response model variables from the 3D point cloud derived by UAV-imaging. The sand burial gradient (Δ dune height) was calculated from Digital Terrain Models (DTM's), while the growth response variables Δ NDVI and Δ Cover were calculated from classified orthomosaics. A *k*-means clustering algorithm was used (1) to remove *Ammophila* points from the 3D point cloud and (2) to identify *Ammophila* pixels in the orthomosaics.

of *Ammophila*, the above mentioned *k*-means algorithm was also applied to the NDVI pixel values of the orthomosaics. To create the *Ammophila* NDVI orthomosaic, pixels classified as bare dune sand (NDVI $\lessapprox 0.1$) were removed from the orthomosaic (by setting them to NA), while the remaining pixels containing NDVI values for *Ammophila* were resampled to match the 5 cm pixel size of the digital terrain model. This was done by calculating the average NDVI value for *Ammophila* in every 5x5 cm grid and assigning that value to the resampled 5cm pixel. To create the *Ammophila* Cover orthomosaic, dune sand pixels were set to 0, while *Ammophila* pixels were set to 1. Cover was subsequently calculated as the number of pixels classified as *Ammophila* divided by the total number of pixels in a 40x40 cm grid. This grid size was chosen as analysis on spatial autocorrelation (Fortin and Dale, 2005) indicated a spatial dependency over a range of 40 cm for NDVI values within a tussock of *Ammophila*. A set of 40 cm pixel size DTM's were also interpolated, to match the resolution of the *Ammophila* Cover orthomosaics.

Both Δ NDVI and Δ Cover were calculated per consecutive time step in the same manner as for Δ dune height. An additional prerequisite for calculating Δ NDVI was for *Ammophila* to be present at each time-step at a particular location. The relation between changes in dune height and changes in NDVI and vegetation cover of *Ammophila* was investigated over the

growing season. Each data pair was sampled at the same location, meaning that the values for Δ dune height and Δ NDVI (from 5 cm pixels) as well as for Δ dune height and Δ Cover (from 40 cm pixels) were extracted from the same *xy*-pixel in the DTM or corresponding orthomosaic. To account for spatial autocorrelation, NDVI values of *Ammophila* were sampled with a 40 cm radius distance constraint. A total of 5600 NDVI values could be sampled for *Ammophila* within the study area, and at those locations also 5600 vegetation cover values were extracted.

Quantile regression

To parameterize the growth response of *Ammophila* to a sand burial gradient, the Gaussian function (Eq 5.4) is fitted to the data using non-linear quantile regression as implemented in the R-package *Quantreg* Koenker (2016). Quantile regression, introduced by Koenker and Bassett Jr (1978), aims to estimate function parameters that model the conditional median or other quantiles of a response variable. It is a method to describe relationships that are not represented effectively by least-squares regression of mean responses (Cade and Noon, 2003; Schröder et al., 2005). Which, arguably, is the case here too: during the growing season *Ammophila* will grow irrespective of response to sand burial, and NDVI and vegetation cover are expected to change regardless as well. Positive feedback by sand burial, consequently, will thus act to amplify the growth *Ammophila*. Quantile regression can capture this amplified response (Austin, 2007), by describing the maximum growth response that *Ammophila* can attain under different conditions of burial by wind-blown sand.

5.3 Results

The full data-set is made up of seven different flight days carried out over the course of 1 year from April 2015 to April 2016. Figure 5.5 shows the state of the foredune in August 2015, by the standard RGB orthomosaic along with contour lines and the NDVI orthomosaic of the same area. At certain parts the foredune *Ammophila* appears greener (fig. 5.5A) and is characterized by higher NDVI values (fig. 5.5B). This corresponds to areas with higher accumulation of wind-blown sand (as is shown in fig 5.2), which may be indicative of more vigorous growth of *Ammophila* due to sand burial by wind.

Figure 5.6 shows the temporal response and spatial variation of NDVI values of *Ammophila arenaria* per separate flight day over the full monitoring period. The temporal NDVI response suggests a seasonal trend, with increasing NDVI values from April up to (and peaking in) August 2015. From October 2015 onwards, the NDVI values decline again as *Ammophila* enters its resting phase. Based on this pattern the growing season was determined to range from April to October 2015. Subsequent analysis and results are therefore based on the four flight days during that period. It is clear from figure 5.6 that the variance of NDVI values is highest from June till October 2015, implying a higher spatial variation of NDVI values during the growing season than outside. The could be in part due to natural senescence above-ground biomass of *Ammophila* in the winter, as well as amplified growth response of *Ammophila* to sand burial during the growing season.

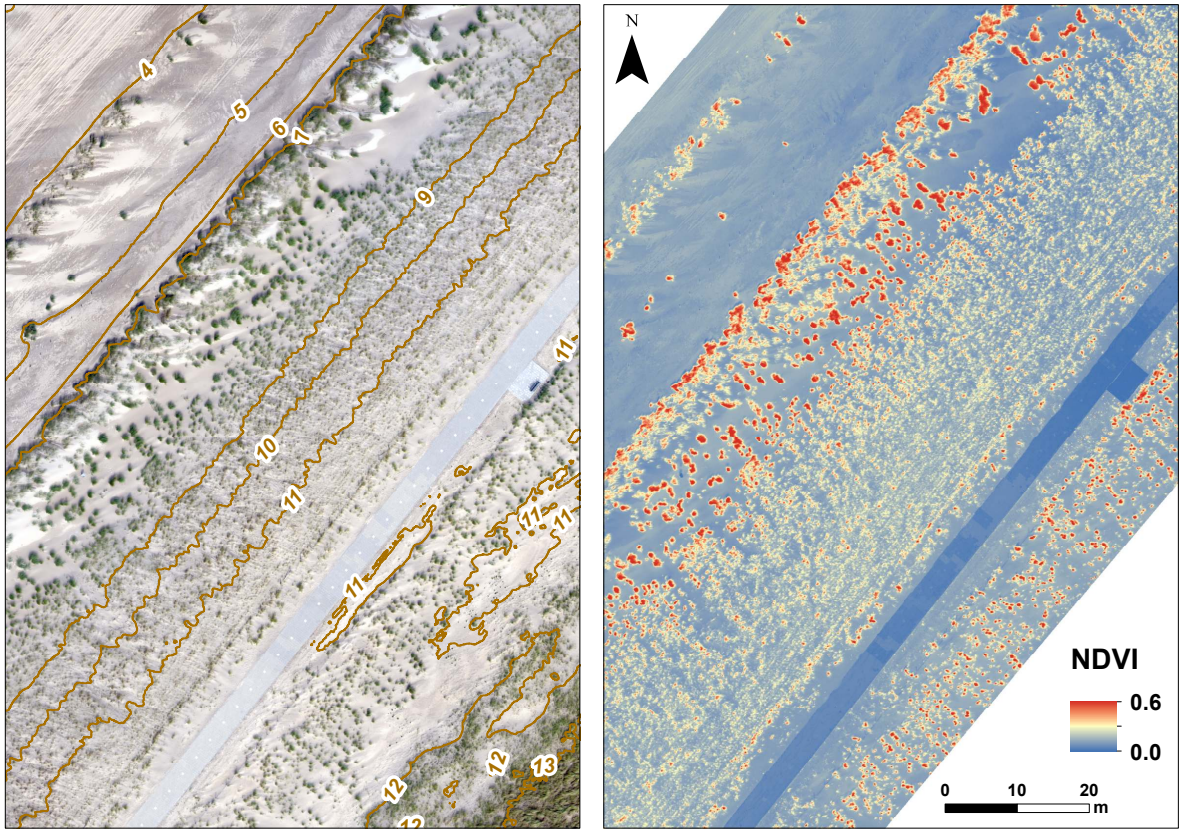

Figure 5.5: The studied foredune in August 2015, shown by the standard RGB orthomosaic with contour lines and the NDVI orthomosaic. Note the bike path running along the dune crest and the incipient dunes in front of the dune toe. At certain parts along the foredune *Ammophila* appears greener (fig. 5.5A) and is characterized by higher NDVI values (fig. 5.5B). This corresponds to areas with higher accumulation of wind-blown sand (see fig 5.2), which may be indicative of more vigorous growth of *Ammophila* due to sand burial by wind.

Figure 5.7 shows the spatial variation of Δ dune height as well as Δ NDVI and Δ Cover of *Ammophila* during the growing season. Note that, for visualization purposes, the NDVI values in figure 5.7B are shown at 40 cm pixel size instead of the 5 cm pixel size that was used for analysis. Examining the spatial variation of Δ dune height, Δ NDVI and Δ Cover in figure 5.7, what strikes is that the response variables appear spatially associated to the explanatory variable: higher changes in dune height correspond to higher changes in NDVI and vegetation cover of *Ammophila*, and vice versa. Moreover, the variation in Δ NDVI and Δ Cover appear spatially structured along the dune slope, in distinct zones parallel to the coastline corresponding to areas with a similar variation in Δ dune height. Which, more clearly than fig 5.5, reinforces the notion of more vigorous growth of *Ammophila* due to sand burial by wind.

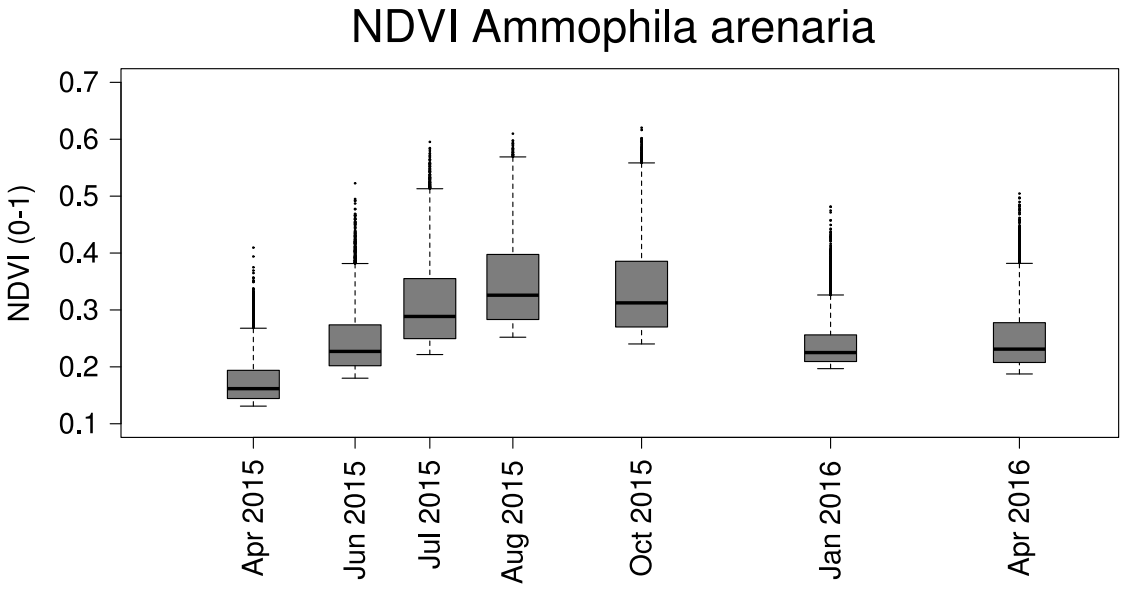

Figure 5.6: Temporal response of NDVI of *Ammophila arenaria* between April 2015 till April 2016. Data from seven different flight days indicate a seasonal trend, with NDVI values peaking in August 2015. The variance of NDVI values is highest from June till October 2015, suggesting a higher spatial variation in NDVI for marram grass during the growing season.

To parameterize the growth response of *Ammophila* to sand burial by wind under field conditions, changes in dune height are related to changes in NDVI and vegetation cover of *Ammophila* over the growing season from April till August 2015. Figure 5.8 shows the data distributions for Δ NDVI (fig 5.8A) and Δ Cover (fig 5.8B) along that sand burial gradient, together with their individual histograms. Comparing the distribution of both response variables, what strikes is that the growth responses Δ NDVI and Δ Cover of *Ammophila* seem to adhere to Shelford's Law of tolerance: over the growing season *Ammophila* shows stimulated growth response along a sand burial gradient up to a maximum, giving rise to (the outline of) a very similar Gaussian curve for both Δ NDVI and Δ Cover as the response variable. With noted difference that Δ Cover can attain negative values, while Δ NDVI values remain (mostly) positive. High burial rates, that overwhelm shoots of *Ammophila*, can account for the negative values of vegetation cover at the dune foot (see fig. 5.7B), while negative values mid-slope of the dune can be due to withering of *Ammophila* because of too low (or absent) sand burial rates. NDVI values remain positive since only pixels that consistently contained vegetation in each time-step were used in the analysis. It must be noted that over the growing season there has been some loss of sand (see fig. 5.7A), which gave rise to negative burial rates (i.e. deflation). While loss of sand undoubtedly affects the growth response of *Ammophila*, it is not reported on in this paper as there were not sufficient data to draw conclusions.

The Gaussian response model (Eq 5.4) is fitted to the data in figure 5.9A and 5.9B at four quantiles, the 3 upper quantiles (90^{th}, 95^{th} and 99^{th}) and the median 50^{th} quantile. Note that the range of sand burial rate at the x-axis has been expanded to show the full regression curves.

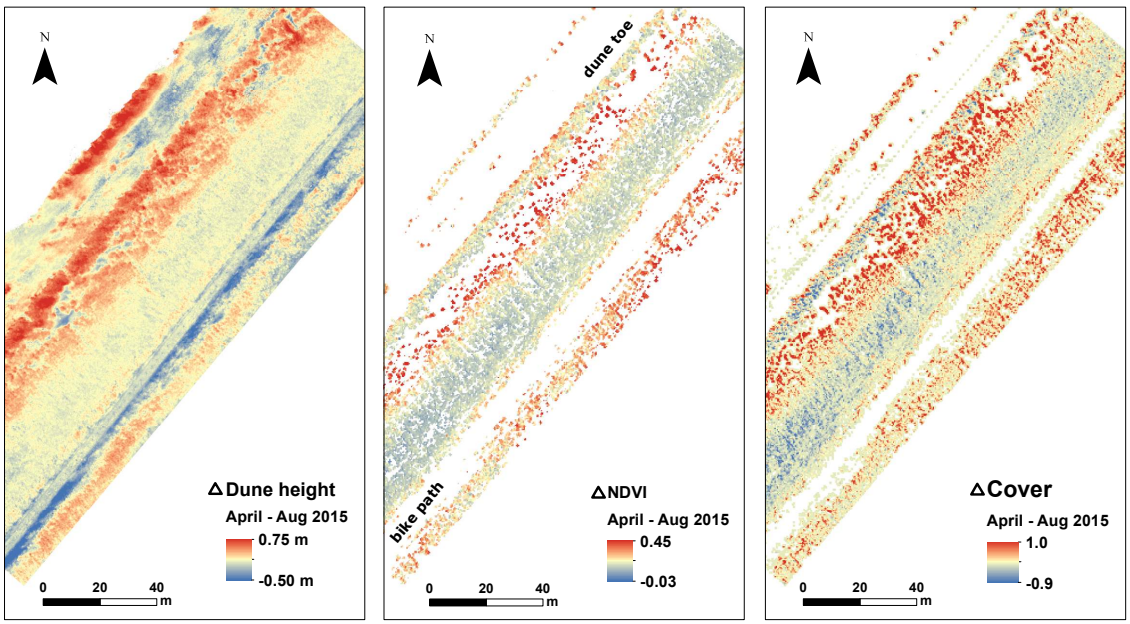

Figure 5.7: Spatial variation of Δ dune height (fig 5.7A), and Δ NDVI and Δ Cover of *Ammophila arenaria* (fig 5.7B-C) over the growing season period April - August 2015. The response variables Δ NDVI and Δ Cover of *Ammophila* appear spatially associated to the explanatory variable Δ dune height: higher changes in dune height correspond to higher changes in NDVI and vegetation cover of *Ammophila*, and vice versa. For spatial context, the position of the dune toe and the bike path running along the dune crest are depicted in fig 5.7B.

Because the Gaussian function is symmetrical, the median quantile regression curve closely resembles the least-squares regression curve of the mean response. It is added as reference only, since the interest is on the outer edge of the data distribution. The three upper quantiles describe the maximum growth responses *Ammophila* can attain under different conditions of sand burial. It becomes clear from figure 5.9 that the limit of the Gaussian function is 0 as sand burial $\rightarrow \infty$. As a result, values of Δ NDVI and Δ Cover < 0 are effectively omitted from the regression analysis. This is not a constraint as the growth response of *Ammophila* along a sand burial gradient is described only by response values ≥ 0.

The advantage of the Gaussian function is that its three parameters (a,b,c) have a clear ecological interpretation. Table 5.1 lists the values for the response of NDVI and vegetation cover of *Ammophila* to sand burial for each fitted quantile. An obvious effect of fitting the Gaussian function to higher quantiles of both growth response distributions, is that the regression curves move up through the distributions and become wider. Essentially, at higher quantiles, the maximum growth response (via parameter a) and the tolerance (via parameter c) of *Ammophila* to sand burial increases. What strikes is that, up to the 95^{th} quantile, the regression curves of both response variables asymptotically approach Δ NDVI $= 0$ and Δ Cover $= 0$ around the same values for sand burial. Though it is an extrapolation of the data, this suggests that the maximum tolerance of *Ammophila* to sand burial ($\approx b + 2c$) is

comparable over the different quantiles and for both response variables. For Δ NDVI and Δ Cover respectively, at the the 95th quantile, it is around 0.96 meter and 0.78 meter of sand burial per growing season. The small difference between both maxima could be because Δ Cover only accounts for lateral growth response, while sand burial may have led *Ammophila* to also invest in (unmeasured) vertical growth. The clear deviation of the Gaussian curve at the 99th quantile from the other quantiles suggests that discerning a maximum tolerance of *Ammophila* to sand burial at this quantile may not be realistic.

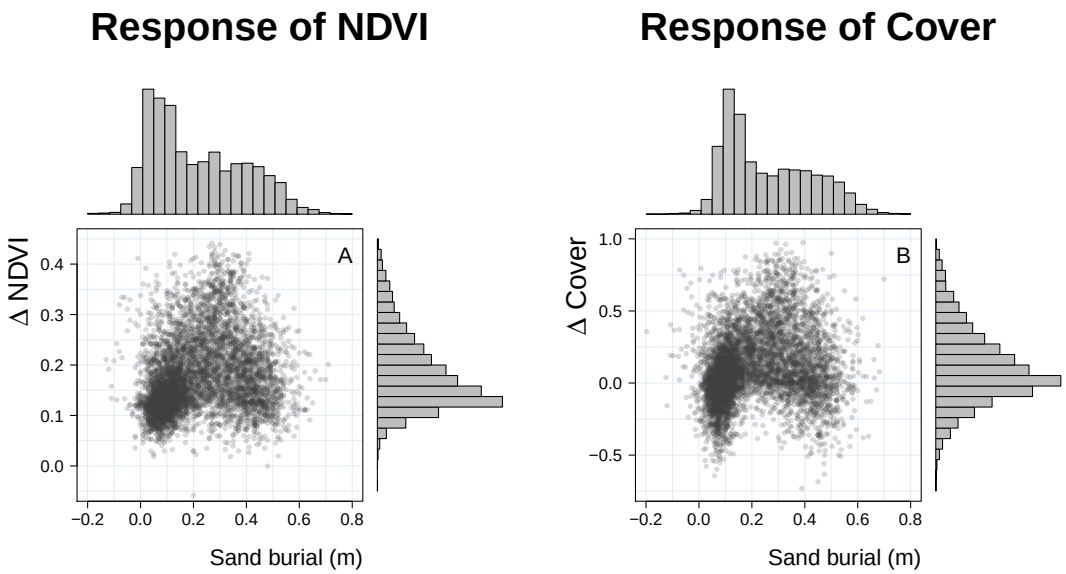

Figure 5.8: Distribution of growth response Δ NDVI (fig 5.8A) and Δ Cover (fig 5.8B) of *Ammophila arenaria* along a sand burial gradient over the growing season April - August 2015 (n = 5600). Data pairs were sampled with a 0.4m radius distance constraint to account for spatial autocorrelation. Shown in the plot margins are the histograms of the individual variables. Stimulated growth of *Ammophila* due to sand burial up to a maximum appears to give rise to (the outline of) a Gaussian curve for both Δ NDVI and Δ Cover as the response variable. Note that Δ Cover can attain negative values, while Δ NDVI values remain (mostly) positive.

Table 5.1: Parameters *a, b and c* of the Gaussian function fitted to the 50th, 90th, 95th and 99th quantile of the growth responses Δ NDVI and Δ Cover of *Ammophila arenaria* along a sand burial gradient over the growing season April - August 2015.

	Δ NDVI			**Δ Cover**		
Quantile	**Parameter**			**Parameter**		
	a	**b**	**c**	**a**	**b**	**c**
50th	0.202	0.317	0.261	0.272	0.268	0.079
90th	0.328	0.318	0.282	0.620	0.313	0.176
95th	0.359	0.314	0.322	0.710	0.325	0.228
99th	0.400	0.297	0.469	0.816	0.353	0.418

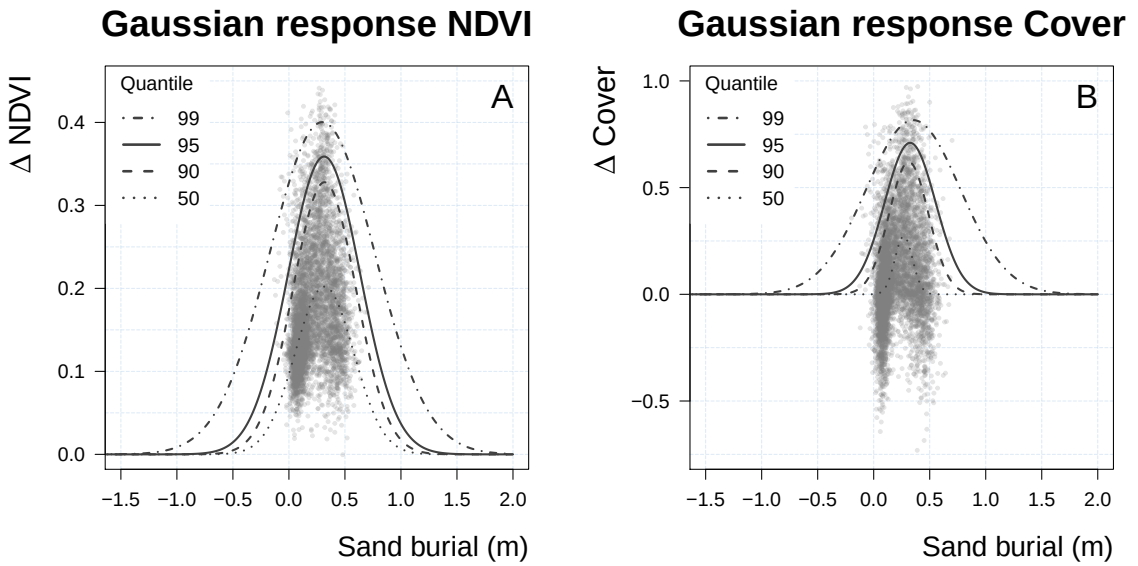

Figure 5.9: The regression curves ($p < 0.001$) of the Gaussian response model fitted to four quantiles (50^{th}, 90^{th}, 95^{th} and 99^{th} quantile) using nonlinear quantile regression. The limits of sand burial rate at the x-axis has been expanded to show the full regression curves. The regression curves indicate an optimal burial rate for *Ammophila arenaria* of 0.31 meter of sand per growing season, and suggest (by extrapolation) a maximum burial tolerance for *Ammophila* between 0.78 (for Δ Cover) and 0.96 meter (for Δ NDVI) of sand per growing season. Response values < 0 are omitted from the regression analysis as the growth response of *Ammophila* is described only by values ≥ 0.

Focusing on for which sand burial rate the optimum growth response is obtained, what stands out is that the values of parameter b (that indicate the optimum) remain quite stable over the different quantiles. This is most evident for the response of NDVI, where the optimum burial rate ranges between 0.30 to 0.32 meter (50^{th} to 99^{th} quantile) per growing season. For response of vegetation cover the optimum burial rate increases slightly from 0.27 to 0.35 meter, but remains in the same range as for the response of NDVI. Moreover, averaged over the different quantiles, the optimal burial rate for Δ NDVI and Δ Cover are both around 0.31 meter of sand per growing season.

It becomes clear from figure 5.9 that the growth response of *Ammophila* along a sand burial gradient is quite comparable when looking at the regression curves of either Δ NDVI or Δ Cover. Both response variables are independent vegetation characteristics: change in NDVI is calculated per individual pixel while vegetation cover is calculated as the total number of pixels classified as *Ammophila* in a 40x40 cm grid. They are, however, related as figure 5.10 shows: 58% of the variance between Δ NDVI and Δ Cover is explained by a linear (least-squares) regression model. Generally, a higher change in NDVI of *Ammophila* over the growing season is associated to a higher change in vegetation cover, and vice versa. This strong linear relationship may help to explain the similar findings for both response variables.

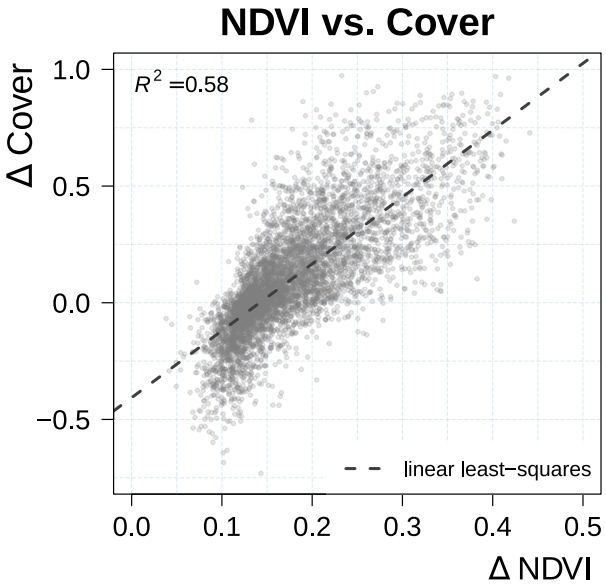

Figure 5.10: Linear least-squares regression between the growth response variables Δ NDVI and Δ Cover of *Ammophila arenaria* over the growing season April - August 2015. 58% of the variance is explained by the regression model.

5.4 Discussion

5.4.1 Growth function in context

Using UAV-acquired high-resolution geospatial data and nonlinear quantile regression, it has been demonstrated that the growth response of *Ammophila arenaria* to sand burial by wind can be described by a Gaussian response model. Two main results are highlighted by fitting the Gaussian function to the upper quantiles of the response distributions of Δ NDVI and Δ Cover. First, though maximum growth response (via parameter a) and the tolerance (via parameter c) of *Ammophila* increases at higher quantiles, extrapolating the regression curves suggest a maximum tolerance of *Ammophila arenaria* to sand burial between 0.78 (for Δ Cover) and 0.96 (for Δ NDVI) meter of sand per growing season. And second, regression analysis indicates that the optimal sand burial rate for which the growth response of *Ammophila arenaria* obtains its maximum (via parameter b), is around 0.31 meter of sand per growing season for both Δ NDVI and Δ Cover.

Aside from being parameterized under field conditions, the growth function presented here is different in two ways from the the growth functions that Baas (2002), Nield and Baas (2008), Baas and Nield (2010) and Keijsers et al. (2016) use to model coastal dune development by incorporating positive feedback due to sand burial. First, instead of a Gaussian function, the aforementioned modeling studies use a combination of linear functions to describe positive and negative response of *Ammophila* before and after an optimal sand burial rate. But this is of minor consequence as, depending on position of optimum and maximum burial tolerance, both approaches will give similar results. More importantly, due to the nature of the model algorithm, the growth functions in the modeling studies do not capture seasonality (Baas,

2002; Keijsers et al., 2016). While growth response of *Ammophila* can be evaluated after any number of iterations (with one iteration typically representing one month), the growth function itself remains the same. Moreover, the function parameters are tuned to yearly sand burial rates, using an optimal burial rate around 0.55 - 0.60 meter of sand per year and a maximum tolerance of *Ammophila* to sand burial up to 2 meter per year. As a result, positive feedback between sand burial and growth response of *Ammophila* is modeled throughout the year. Which, in all likelihood, is not realistic for this coastal grass species considering its zonation in temperate climates. When photosynthesis halters in winter, due to low temperatures and weak levels of solar irradiance (Maun, 2009), *Ammophila* will continue to trap sand (and contribute to dune development) but sand burial by wind does not result in an amplified growth response. Therefore, as was done in this study, restricting the growth function to a growing season may be a more accurate representation of growth response of *Ammophila* due to positive feedback to sand burial.

Due to the mismatch in timescales it is difficult to compare the burial rates used for parameterization in this study and the burial rates used in the modeling studies. Scaling the seasonal burial rates to yearly rates (or vice versa) is not trivial due to the inherent nonlinearity of coastal aeolian dynamics that control dune morphology. For example, due to favorable climatic conditions, aeolian transport in the Netherlands is most prevalent in the springtime and autumn (Jungerius et al., 1981). On larger timescales, however, it holds true that seasonal variation in aeolian dynamics is smoothened out into approximately linear relationships. On decadal scales, for example, dune growth in the Netherlands follows a strong linear trend (De Vries et al., 2012). And it was shown by Van der Weerd and Wijnberg (2016) and Hoonhout and de Vries (2017a) that aeolian deposition on and along the Zanmdotor are approximately linear on yearly scales. For the sake of comparison, while not wholly accurate, if the yearly burial rates of the modeling studies are linearly scaled to seasonal rates, an optimal burial rate of 0.23 – 0.25 meter of sand per growing season and a maximum burial tolerance up to 0.83 meter of sand per growing season is obtained. Which, though slightly more conservative, is in the same order of magnitude of the growth function parameters found in this study. So, even though year-round positive feedback response of *Ammophila* to sand burial is likely not realistic, the burial rates employed in the modeling studies are not far off from those observed under field conditions.

5.4.2 Significance to coastal management

It must be noted that the growth function parameters found in this study are site-specific and may not be used as rule-of-thumb for generic growth response of *Ammophila arenaria* to sand burial by wind. The unique experimental design of the *Zandmotor* has led to aeolian dynamics that deviate from dynamics found on unnourished or more conventionally nourished beaches. For instance, due to its unusual high construction height, much of the subaerial surface of the *Zandmotor* has seen minimal hydrodynamic reworking. This has led to extensive beach armoring by shell layers (Hoonhout and de Vries, 2017b) with a reduction in aeolian transport potential as result. Also, the irregular hooked shape of the *Zandmotor* and presence of a small dune lake give rise to higher spatial variation in aeolian transport. The dune lake, for

instance, acts as an sink area (Van der Weerd and Wijnberg, 2016), while the areas flanking the dune lake act as pathways for aeolian transport. As such, the foredunes adjacent to the *Zandmotor* have received wind-blown sand in locally varying rates, with varying burial rates for *Ammophila* as result.

Figure 5.11: Average yearly accretion of sand on and along the *Zandmotor* from 2012 until 2015. While average accretion rates vary alongshore, the foredunes have consistently received aeolian deposition around the optimal burial rate for *Ammophila* to thrive under. Defining a region for optimal growth ($\approx b \pm \frac{1}{2}c$), the stretch of foredune receiving favorable burial rates is extended upslope and unto the beach. Maximum observed aeolian sand deposition into the dunes is about half the (extrapolated) maximum burial tolerance for *Ammophila*. This suggests that the rate of foredune development could be higher still than currently observed at the *Zandmotor*.

The study area, however, has received sand at rates representative for Dutch nourished coasts (Van der Wal, 2004; De Vries et al., 2012) and the parameterized growth function for *Ammophila* may be representative for many of the dunes found along the Dutch coastline. The findings, therefore, can be advantageous to coastal safety in the Netherlands: in order to maximize natural dune development, coastal management strategies can aim for a regular input of wind-blown sand towards the dunes around the optimum burial rate for *Ammophila*

during the growing season and not exceed its maximum tolerance. The effect of the *Zandmotor* on the adjacent foredunes is illustrated in figure 5.11, which shows the average yearly (and continuous) subaerial accretion of sand on and along the *Zandmotor* from 2012 up to 2015. While average accretion rates vary alongshore (most notably north of the *Zandmotor*), the toe of the foredunes appear to have consistently received aeolian deposition around the optimal burial rate for *Ammophila* to thrive under. Although the same scaling issue arises here too, linearly scaling the yearly sand deposition to a deposition over a growing season amounts exactly to the optimal burial rate of 0.31 meter of sand. Which, not surprisingly, means that *Ammophila* grows most vigorously at the toe of the foredunes. And, when looking at a region for optimal growth ($\approx b \pm \frac{1}{2}c$), the stretch of foredune receiving sand at favorable burial rates is extended upslope and unto the beach. Over the last three years, though, the maximum observed aeolian sand deposition is about half the (extrapolated) maximum burial tolerance for *Ammophila*. This suggests that the rate of foredune development could be higher still than currently observed at the *Zandmotor* (Hoonhout and de Vries, 2017a).

Furthermore, although aeolian supply towards the foredunes is constrained which may hamper their development, the wide beach of the *Zandmotor* provides favorable conditions for new dunes to develop. Analysis by Keijsers et al. (2014b) on the influence of storminess and beach width on change in foredune volume (Δ V), showed that storminess (expressed by yearly maximum sea levels) and beach width is significantly correlated to Δ V for beaches less than 200 meter wide, while Δ V was positive for beaches wider than 200 meter irrespective of storminess. This implies that, for the foreseeable future, the foredunes directly adjacent to the *Zandmotor* will continue to develop uninterrupted by storm surges. And, though the very wide beach is no longer critically important for foredune development, it has allowed for new embryo dunes to develop. Which, as De Winter et al. (2015) and Van Puijenbroek et al. (2017a) show, may act as a supplementary buffer against storm surges and can thus help reinforce the foredunes against hydrodynamic erosion.

5.4.3 Justification of quantile regression

While the findings suggest that *Ammophila* may be an even better dune-builder, for it may thrive under and withstand even higher sand burial rates than previously reported (see Keijsers et al. (2016)), it does depend to which quantile of the response distribution the Gaussian function is parameterized. Although the primary reason to apply quantile regression was to capture the amplified growth response of *Ammophila* due to positive feedback, the technique can be placed in a broader ecological perspective. In ecology, quantile regression is used to account for unmeasured factors that may pose an active limiting constraint on the process under investigation. The justification is found in Liebig's law of limiting factors, a concept originally applied to plant growth. The law states that 'even if most chemical elements needed by plants are abundant, plant growth can still be limited if a single critical element is in short supply' (Huston, 2002). Essentially, plant growth is not controlled by the total amount of resources available, but by the resource that is most scarce (Cade et al., 1999; Austin, 2007).

In this context, the true (i.e. maximum) growth response of *Ammophila* under different

conditions of sand burial can only be quantified when sand burial is (1) either the active limiting resource and (2) all other factors occur at non-limiting levels. Which is, however, almost impossible to determine at field conditions. First, while spatial variation of sand burial is apparent from measured changes in dune height, the temporal variability of sand burial rates is not known. Measurements of aeolian processes that drive burial of *Ammophila* by sand are outside the scope of this study, so it cannot be determined if sand burial has been the active limiting factor for prolonged periods of time. While weather conditions in the Netherlands are generally calm during the growing seasons, it is often windy enough at the coast for aeolian transport to occur. Moreover, drier conditions in springtime and summer can help facilitate quicker entrainment of sand by wind. So sand burial may periodically have been the active limiting factor but this was likely not always the case.

And secondly, even if sand burial was the active limiting factor over time, it is unlikely that all other factors temporally occurred at non-limiting levels. While the cross-shore gradient of common stresses (e.g. salt spray, drought, temperature extremes, soil acidity, nutrient deficiency) can be considered to be low (since the studied foredune has a gentle slope and is less than 100m wide), the temporal variability can still be high. Salt spray and drought, for instance, depend on meteorological conditions which are variable over time. Moreover, a multitude of factors may interactively contribute to the observed positive feedback response of *Ammophila*, and thus collectively alter the conditions for *Ammophila* to grow under. Sand burial, for example, has been related to nutrient availability, ageing (lack of rhizome bud development) and competition capacity of *Ammophila*, as well as an decrease in harmful soil pathogens such as fungi and nematodes (Van der Putten et al., 1988, 1993). Any of these complex underlying mechanisms, at a certain point in time, may have been the active limiting factor and contributed to a response distribution with data points widely scattered beneath an upper limit. As a result, estimating changes near the upper extremes of the response distributions provides a more meaningful description of the expected response in case the observed factor is the active limiting resource (Thomson et al., 1996; Cade and Noon, 2003). Quantile regression, therefore, seems a justified approach to describe the amplified growth response of *Ammophila* due to sand burial by wind under field conditions.

5.5 Conclusions

Coastal dune development is directly related to the growth response of marram grass (*Ammophila arenaria*) due to positive feedback to sand burial. Maximizing the potential of *Ammophila* to grow and develop dunes thus, in turn, maximizes the potential of coastal dunes to provide coastal safety. With the use of UAV-acquired high-resolution geospatial data, this study is the first to parametrize an empirical relationship to model the growth response of *Ammophila* to sand burial by wind. This was done by fitting a Gaussian function to the response variables Δ NDVI and Δ Cover using nonlinear quantile regression. Though not generically applicable, the main findings from a foredune in direct proximity of the *Zandmotor* in the Netherlands are:

- Extrapolation of the Gaussian regression curves suggest a maximum tolerance of *Am-*

mophila arenaria to sand burial between 0.78 (for Δ Cover) and 0.96 (for Δ NDVI) meter of sand per growing season.

- The optimal sand burial rate for which the growth response of *Ammophila arenaria* obtains its maximum, is found to be around 0.31 meter of sand per growing season for both Gaussian response model variables Δ NDVI and Δ Cover.

Chapter 6

Synthesis

6.1 Main findings

This thesis provides field-based evidence and insight into how supply-limited aeolian transport and reinforcing biogeomorphic feedback controls dune development on and along the mega-scale beach nourishment the *Zandmotor*. This chapter reports the main findings related to the research questions defined in chapter 1 (see also Fig. 6.1) and discusses the implications and limitations of these answers and their contribution to science and society.

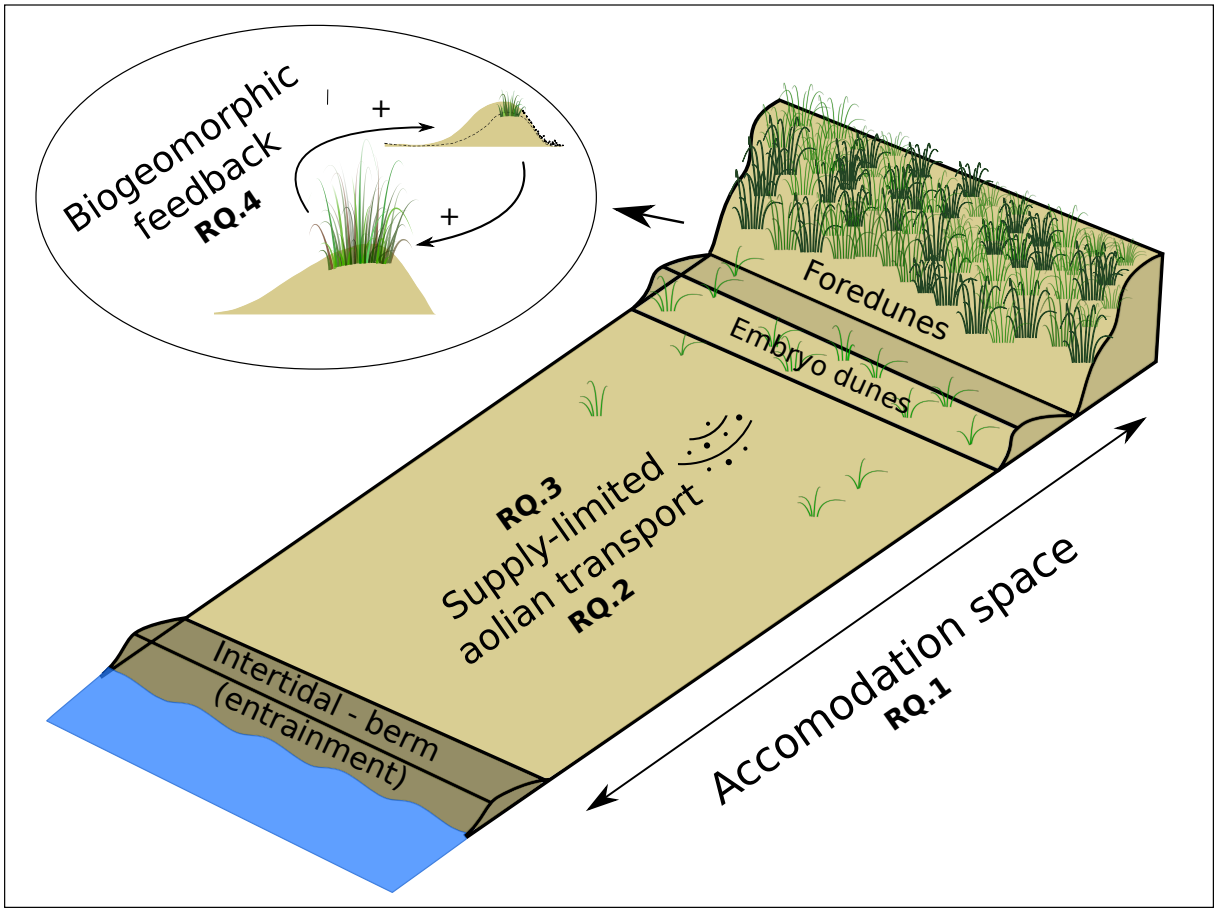

Figure 6.1: Schematic overview of the components of the aeolian beach-dune system, in relation to the research questions addressed in this thesis

1. How does the design of mega-scale beach nourishment the Zandmotor impact coastal dune development on the beach and along the adjacent coastline?

Chapter 2 examined to what extent the *Zandmotor* has contributed to creating accommodation space along the Delfland coast favorable for dune development, i.e. available space that is sheltered from frequent storm impacts and experiencing a steady accumulation of wind-blown sand. Comparing the presence of dunes in 2017 to its elevation indicates that dunes are sheltered from storm surges above a height of 1.6 m above mean sea level (a.m.s.l.). This is well below the maximum experienced storm surge levels (until 2017) up to at least 4 m a.m.s.l.,

which points to the capacity of established dunes to withstand and recover from hydrodynamic storm impacts. Comparing the changes in dune cover by marram grass (from 2016 to 2017) to the average yearly change in dune height (between 2013 and 2017) indicates that dunes were almost exclusively present in accreting areas. This demonstrates the significance of positive biogeomorphic feedback in steering dune development. As such, even though its high construction height may not be optimal for successful marram grass establishment, the results highlight the overall importance of the *Zandmotor* to dune development potential.

Compared to the rest of the Delfland coast, the supratidal beach of the *Zandmotor* provides very wide favorable accommodation space and therefore supports a high potential for new embryo dunes to develop. Because of its sand-feeding effects, which is also highlighted in chapter 3, the *Zandmotor* will likely contribute to creating more favorable accommodation space for dune development along the entire Delfland coast. However, because of persistent anthropogenic disturbances arising from recreation as well as nature management practices, dune development along this urbanized coastline may not reach its full potential. This should not be too alarming as the *Zandmotor* mega-scale beach nourishment is set to ensure the safety of the Delfland coast for years to come.

2. How do aeolian sand transport model estimates compare to field measurements on the Zandmotor and what are the implications for (predicting) coastal dune development?

Measured saltation mass fluxes in the coastal environment are, almost without exception, much lower than predicted by traditional aeolian transport equations, which is generally attributed to meteorological and surficial conditions that limit the supply of sand to the aeolian transport system. Chapter 3 presents an analysis on a synchronous long-term record of saltation mass flux and shear velocity measurements, constructed using a newly developed automated sand trap in conjunction with detailed wind forcing measurements. By applying nonlinear quantile regression, it shown that the failure to produce a strong correspondence between measured and predicted aeolian transport rates can also arise from the notion that the saltation mass flux may be better explained by a quadratic than a cubic dependence to shear velocity. Regression parameters obtained at the upper part of the response distribution are in line with parameters employed by the quadratic function of Kok et al. (2012), yielding more consistent saltation rates than predicted by the cubic function of Kawamura (1951).

Fitting the quadratic and cubic function to the median response distribution indicates that saltation rates generated in the coastal environment may typically be two (for quadratic dependence) or three (for cubic dependence) orders of magnitude lower than predicted by the transport equations of parameterized during wind tunnel experiments.The under-prediction of the saltation mass flux decreases when the quadratic and cubic function are fitted to the observations made under optimal field conditions, but the still lower observed saltation rates indicate that coastal aeolian dynamics on the *Zandmotor* may be characterized by a persistent impact of supply-limiting conditions. By parameterizing the flux scaling parameter C of the quadratic and cubic saltation flux equations, this study has provided a measure to account for the overall impact of limiting factors, which can help ensue more realistic saltation mass flux predictions

that are better applicable to conditions encountered on mega-scale beach nourishments and along nourished coastlines in general.

3. How does surface moisture impact coastal aeolian dynamics and how can it be measured at high spatial-temporal resolutions?

Surface moisture is an important supply limiting factor for aeolian sand transport. By binding sand grains together, through cohesive and adhesive forces, water significantly increases the resistance of the uppermost sand layer against wind erosion. It has been suggested by Belly (1964) that the required wind force to initiate saltation (i.e. threshold shear velocity) grows exponentially with a linear increase of moisture content. Above a certain moisture content beach sand becomes inherently resistant to entrainment by most natural winds. Since wetting and drying processes are governed by complex hydraulics (i.e. tidal and wave action, groundwater and capillary flow, evaporation and precipitation), the distribution of surface moisture on a beach and control it exerts on particle entrainment is also highly variable in time and space. To improve the applicability of aeolian transport equations to the coastal environment it is thus critical to account for the control of surface moisture. An approach to accomplish this is by making the threshold shear velocity dependent on surface moisture conditions. This study shows that, at particular wavelengths, optical remote sensing can be utilized to derive spatially extensive surface moisture maps with a high accuracy.

In chapter 4 it is shown that the effect of surface moisture on spectral reflectance of coastal beach sand can be described by an optical as well as a soil physical model. The first model is grounded in optics and describes the proportional contribution of scattering and absorption of light by pore water in an unsaturated sand matrix. The second model is grounded in soil physics and links the hydraulic behavior of pore water in an unsaturated sand matrix to its optical properties. Near- and short-wave infrared wavelengths are most effective for relating surface moisture content to reflectance due to strong absorption of light in water, in particular at water absorption peaks of 1470 and 1940 nm. At these wavelengths there is enough contrast in the signal to also differentiate low moisture levels ($\sim$ 0-5%). Because of strong absorption by the atmosphere an active remote sensing technique is required at these wavelengths. This research shows that a terrestrial laser scanner operating at $\lambda = 1550$ nm is capable of deriving accurate surface moisture maps at high spatio-temporal resolutions, which can help provide better insight into the control of surface moisture on coastal aeolian dynamics.

4. How does aeolian sand deposition affect the growth rate of European marram grass and how does this impact dune development on and along the Zandmotor?

Along sufficiently wide sandy beaches, vegetated coastal dunes have the capacity to keep up with sea-level rise by accumulating and stabilizing wind-blown sand. In Europe, this is attributed to European marram grass (*Ammophila arenaria*), a coastal grass species that possesses two traits advantageous for dune-building: (1) a very high tolerance to burial by wind-blown sand, and (2) more vigorous growth due to positive feedback to sand burial. Using high-resolution geospatial data (i.e. elevation models and near-infrared imagery) acquired

with an unmanned aerial vehicle (UAV) and nonlinear quantile regression analysis, chapter 5 demonstrates that the growth response of marram grass to sand burial by wind, expressed by changes in Normalized Difference Vegetation Index (Δ NDVI) and vegetation cover (Δ Cover), can be described by a Gaussian response model. The regression curves indicate an optimal burial rate for marram grass of 0.31 meter of sand per growing season, and suggest (by extrapolation of the data) a maximum burial tolerance between 0.78 (for Δ Cover) and 0.96 meter (for Δ NDVI) of sand per growing season.

The growth response parameters found in this research are specific to the *Zandmotor* and are likely not generically applicable to describe growth response of marram grass to sand burial by wind. The parameters may, however, be representative for many of the dunes found along the Dutch coastline, as the deposition rates on which the function parameters are based were representative for Dutch nourished coasts. The findings, therefore, can be advantageous to coastal safety in the Netherlands: in order to maximize natural dune development, coastal management strategies can aim for a regular input of wind-blown sand towards the dunes around the optimum burial rate for marram grass during the growing season and not exceed its maximum tolerance. Coastal dune development is directly related to the growth response of marram grass due to positive feedback to sand burial. Maximizing the potential of marram grass to grow and develop dunes thus, in turn, maximizes the potential of coastal dunes to provide coastal safety.

6.2 Discussion

6.2.1 Outlook on embryo dune development on the Zandmotor

A distinct feature that sets the *Zandmotor* apart from more traditionally nourished (or natural) coastlines, is the locally very high construction height. Most of the base is constructed at a height of around 5 m a.m.s.l, while just north of a small dune lake the *Zandmotor* reaches a maximum height of 7 m a.m.s.l. This is well above the current maximum storm surge level of about 3 m a.m.s.l, so reworking of sand on the subaerial parts of *Zandmotor* is almost exclusively due to aeolian forcing (Hoonhout and de Vries, 2017a). As a consequence, while beneficial to already established dunes, Van Puijenbroek (2017) concluded that this high construction height is likely to impede the establishment of new embryo dunes as marram grass rhizome dispersal by tide and wave action is mostly absent on the *Zandmotor*, limiting plant establishment sources to more environmentally sensitive germination of wind-carried seeds instead. The high beach elevation is also often accompanied by low soil moisture, which could slow down vegetation establishment as well.

The consequences of the high construction heights are in part reflected by the patterns of newly established embryo dunes on the *Zandmotor* as can be seen in the aerial photographs (taken May 2020) of Fig. 6.2. Embryo dunes on the highest parts of the *Zandmotor* are still mostly absent, while on the lower parts extensive embryo dune fields have been developing, especially along the south flank and the area around the dune lake. As discussed in more detail in chapter 2, this is likely due to the dispersal of rhizome fragments by sea and wind, as

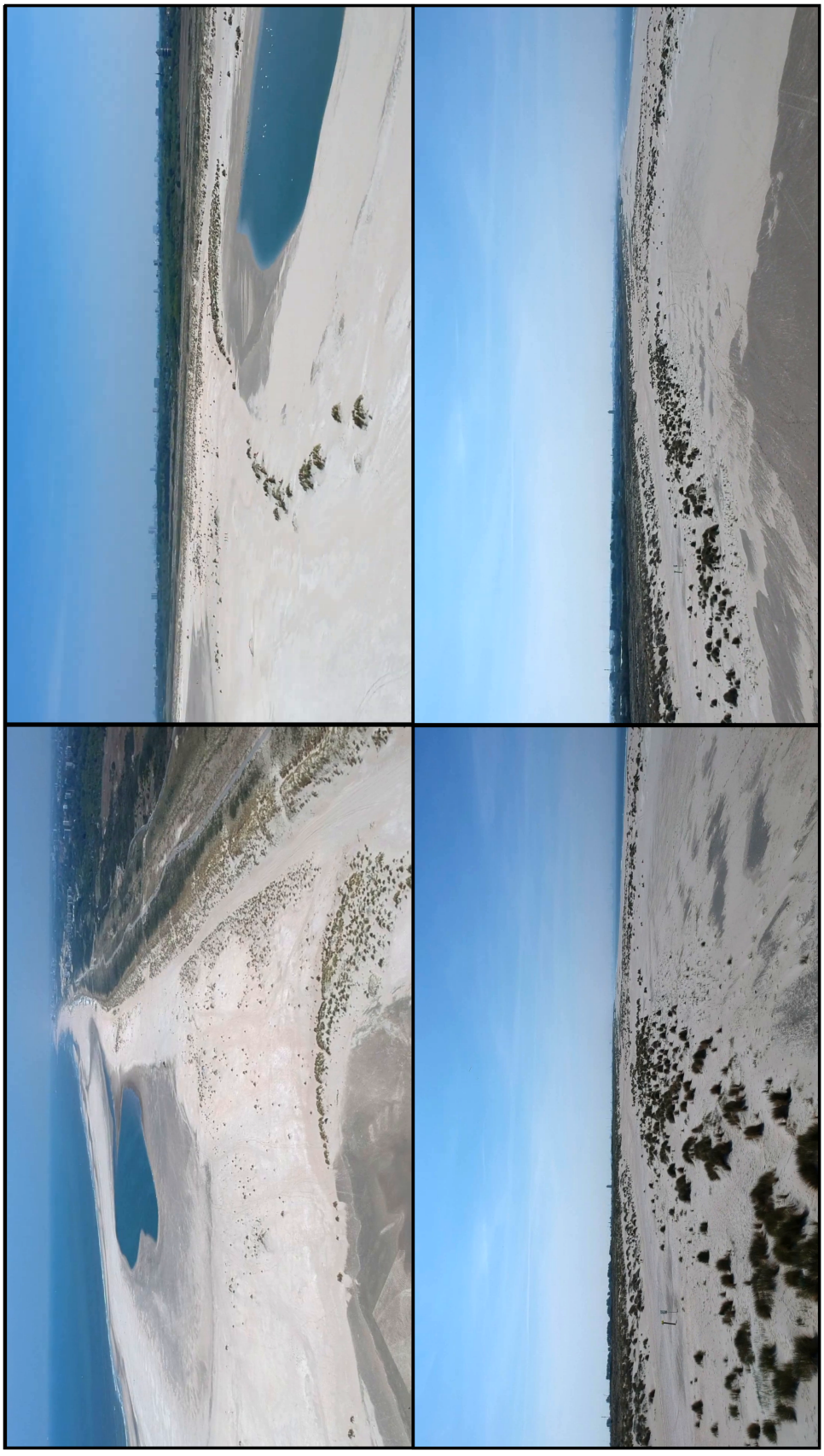

Figure 6.2: Aerial photographs of the *Zandmotor* (taken May 2020) showing extensive embryo dune fields, validating the notion that the wide accommodation space of *Zandmotor* supports a high potential for new dune development.

well as fresh water availability in combination with (moderate) burial dynamics. And these factors (or conditions) may become more significant (or prevalent) in the future. According to a long-term modeling study using different wave climate scenarios based on historical data, Arriaga et al. (2017) shows that the *Zandmotor* will display diffusive behavior with asymmetric feeding of the adjacent beaches and slow migration to a north-eastern direction. Specifically, results show that after 30 years the cross-shore amplitude of the *Zandmotor* perturbation will have decayed from the initial 960 m (immediately after construction) to about 350 m, which suggests a lifespan for the *Zandmotor* three times larger than projected during its design. Over the same time period, the shoreline of the adjacent beaches (2.5 km at each side) will have shifted seaward (on average) by about 100 m. Effectively, these long-term diffusion effects will probably reduce the high construction height and thus modify the *Zandmotor* to resemble a more traditional beach nourishment. The wide and max. 5 km long accretive beach that is created as a result will likely continue to provide accommodation space for embryo dunes to develop. The study of Arriaga et al. (2017), however, did not use model forcing under climate change, so the effect of future sea level rise and/or storm surge conditions are not considered, potentially leading to too optimistic modeling outcomes.

6.2.2 Outlook on foredune development along Zandmotor

Foredune sand budget analysis

Figure 6.3 shows the relationship between cumulative saltation flux (based on flux measurements presented in chapter 3 and changes in foredune height (based on the digital terrain models (DTM) presented in chapter 5). The cumulative saltation mass flux is expressed as a volume (m^3 m^{-1} t^{-1}) by dividing the obtained cumulative weight by the density of dry sand (taken as 1665 kg^3 m^3). The change in foredune (also expressed as m^3 m^{-1} t^{-1}) is calculated between nine successive UAV flights (from May 15 2015 until Sept 1 2016) and split along 1 m interval contour lines (based on 2011 elevation data), starting just in front of the developing embryo dunes (at 3 m height) up until the foredune crest at 12 m height. The vegetation line of (originally) planted marram grass starts in between the 6-7 m contour line (see also Fig. 5.5 for reference).

Essentially, Fig. 6.3 presents a sand budget analysis, in terms of how the saltation flux (i.e. aeolian supply) towards the reconstructed foredune along the *Zandmotor* relates to sand deposition. By dividing the sand deposition by aeolian transport (the ratio shown on the y-axis) a number of interesting observations can be made. Overall, with some exceptions, Fig. 6.3 suggests that only a relatively small fraction of windblown sand towards the foredune is actually deposited (or stabilized) into the foredune and thus available for dune building. The highest amount of deposition took place during during late summer 2015 (Aug-Oct), when on average about 40% of the aeolian supply was deposited across the foredune stoss slope. Late spring 2015 (May-June) and autumn 2015 / winter 2016 (Oct-Jan) also had relatively high deposition rates compared to available supply, about 30% and 20% respectively. The spring and summer periods of 2015 were characterized by warm, windy and (relatively) dry conditions (some isolated thunderstorms excepted), while late autumn 2015 was characterized by two severe storms (Nov 15 and Nov 26) with high wind speeds. During the other periods

the aeolian deposition into the foredune did not exceed 10% of the available supply, indicating that the overall meteorological conditions were not favorable for (i.e. limiting to) dune development. The contribution of the severe summer storm of July 25 2015 (see also Fig. 3.6 to dune development seems rather limited, as Fig. 6.3 suggests that only a small proportion of the windblown sand was actually deposited along the foredune. This seems to be contradicted by the photographic evidence of significant amounts of aeolian deposition at the foredune foot during the summer storm (Fig. 3.6). An explanation (from literature and personal observation) may be that those deposition patterns formed in the shadow zone (Hesp, 1981) of the developing embryo dunes and are in fact quite transient features subjected to changes in wind direction.

Looking more closely to the individual contour lines of the foredune stoss slope in Fig. 6.3, it is clear that limited or no aeolian deposition occurred at the base of the foredune (3-4 m and 4-5 m contour line). During three instances this zone even experienced (temporary) aeolian deflation, with the highest erosion taking place in the spring of 2016 when the wind regime was predominantly in a north-easterly offshore or shore-parallel direction. Other times this zone likely acted primarily as a throughput for wind-blown sand towards the foredune. The scattered embryo dunes were only just establishing in 2015 and likely did not yet contribute much (or only transiently) to aeolian deposition. Interestingly, during the last period (summer 2016) the most aeolian deposition took place along the lowest two contour lines, which may indicate the increasing capacity of the developing embryo dunes to trap and stabilize wind-blown sand. Further, the ratio of aeolian deposition to aeolian supply for the foredune foot (5-6 m contour line) is consistently positive for every time period and also often quite higher compared to the two lower contour lines. The relatively steep slope leading up to the vegetation front of marram grass may have acted as an boundary and prevented sand (in saltation during relatively low wind speeds) to be transported higher up the foredune, leading to a net accumulation of sand at the foredune foot. Arens (1996b) also observed that during oblique winds approaching the foredune, which were encountered on *Zandmotor* during the dominant south-westerly winds, wind-blown sand would typically accumulate at the foredune foot and not get transported higher up the foredune stoss slope. On the other hand, Davidson-Arnott et al. (2018) shows that during oblique winds the apparent slope of the foredune is effectively reduced, enabling more sand to be transported into the foredune than during perpendicular onshore winds. The fact that oblique winds can negate steeper slopes may help explain the positive deposition to supply ratios along the higher parts of the foredune stoss slope up to the crest (7-12 m). Relative to each other the ratios of the five contour lines between 7-12 m are quite stable over time, which suggests that the control the vegetated foredune stoss slope exerts on aeolian dynamics is quite stable too. The difference in magnitude of the ratios for the different time periods cannot be explained by wind direction (or wind speed); instead it likely arose because of supply-limiting transport conditions.

The ratio of aeolian deposition to aeolian saltation flux is consistently the highest for the 6-7 m contour line, coinciding with the seaward facing vegetation boundary of marram grass. This indicates that along this contour most aeolian supply is deposited, most likely due to sand trapping by the vegetation. This corresponds to Hesp (1989) where it was observed that saltation only continues up to a certain distance within the vegetation, depending on

vegetation density and wind speed. When the vegetation density is high, the seaward facing vegetation line of the foredune traps most of the incoming sand, causing the foredune to grow most along this front. For the May-June 2015 period the ratio aeolian deposition to aeolian supply is almost 1, suggesting that all windblown sand delivered to the dune is deposited here. For the period Aug-Oct 2015 it even appears as if the deposition was higher than the supply. This makes no physical sense and likely arose from an inaccuracy in deriving the digital terrain model from the digital surface model, which is the default output of UAV-derived elevation models. It may be assumed that during this period the ratio was in fact 1, so all wind-blown sand was trapped by the vegetation and made available for dune development. Interestingly, the Aug-Oct period coincides with the highest NDVI values for marram grass (see Fig 5.6), suggesting a highest amount of above ground biomass and thus the highest trapping capacity. In fact, it is likely that the high proportion of aeolian deposition for the May-June period can be attributed to vigorous growth that marram grass, like other perennial coastal grass species, typically experiences during spring regardless of positive feedback to burial. Several studies into foredune dynamics (e.g., Wal and McManus, 1993; Arens, 1997) also mention spring and autumn as the main periods for dune building, were the latter period was related a larger trapping capacity of vegetation at the end of the growing season.

As Arens (1997) remarks, most studies on coastal dune development either focus on measurements of transport processes at a short time scale (hours to days) (e.g., Sarre, 1989b; Lynch et al., 2008) or on measurement of changes in foredune elevation at longer timescales (months to years) (e.g., Davidson-Arnott and Law, 1996; Keijsers et al., 2014b). Few studies exist where aeolian transport and foredune evolution are simultaneously measured over the same time period (e.g., Davidson-Arnott et al., 2018), such that aeolian supply can be directly correlated to foredune growth. Changes in foredune elevation are most commonly related to a potential transport, using aeolian transport equations and wind data (Arens, 1997). The simplest sediment budget approach for modelling foredune development is based on the aeolian sand drift potential proposed by Fryberger et al. (1979) for desert environments, with the assumption that all sand delivered to the dune is deposited in the dune. As noted by Arens (1997) and Davidson-Arnott et al. (2018), among others, potential aeolian transport calculated from wind data usually results in amounts that far exceed the observed transport because of the involvement of supply-limiting factors. Additionally, Fig. 3.6 indicates that the assumption that all aeolian transport is deposited into the dunes also does not hold. The ratio of aeolian deposition to aeolian supply is generally well below below 1.0, meaning that only a fraction of aeolian supply is deposited persistently (i.e. stored) and thus available for dune development. Sherman (1995) attributed this to the propensity of foredune systems to 'leak' sand seaward due to wave erosion or landward through blowouts or parabolic dune migration, though this has not been the case for foredunes along the *Zandmotor*. Instead, because of the finding that the saltation mass flux may be better described by a quadratic than a cubic dependence to shear velocity, in the next section a case is made that the amount of geomorphic work accomplished by aeolian transport processes (Wolman and Miller, 1960) may commonly get overestimated, leading to an exaggerated effectiveness to coastal foredune development.

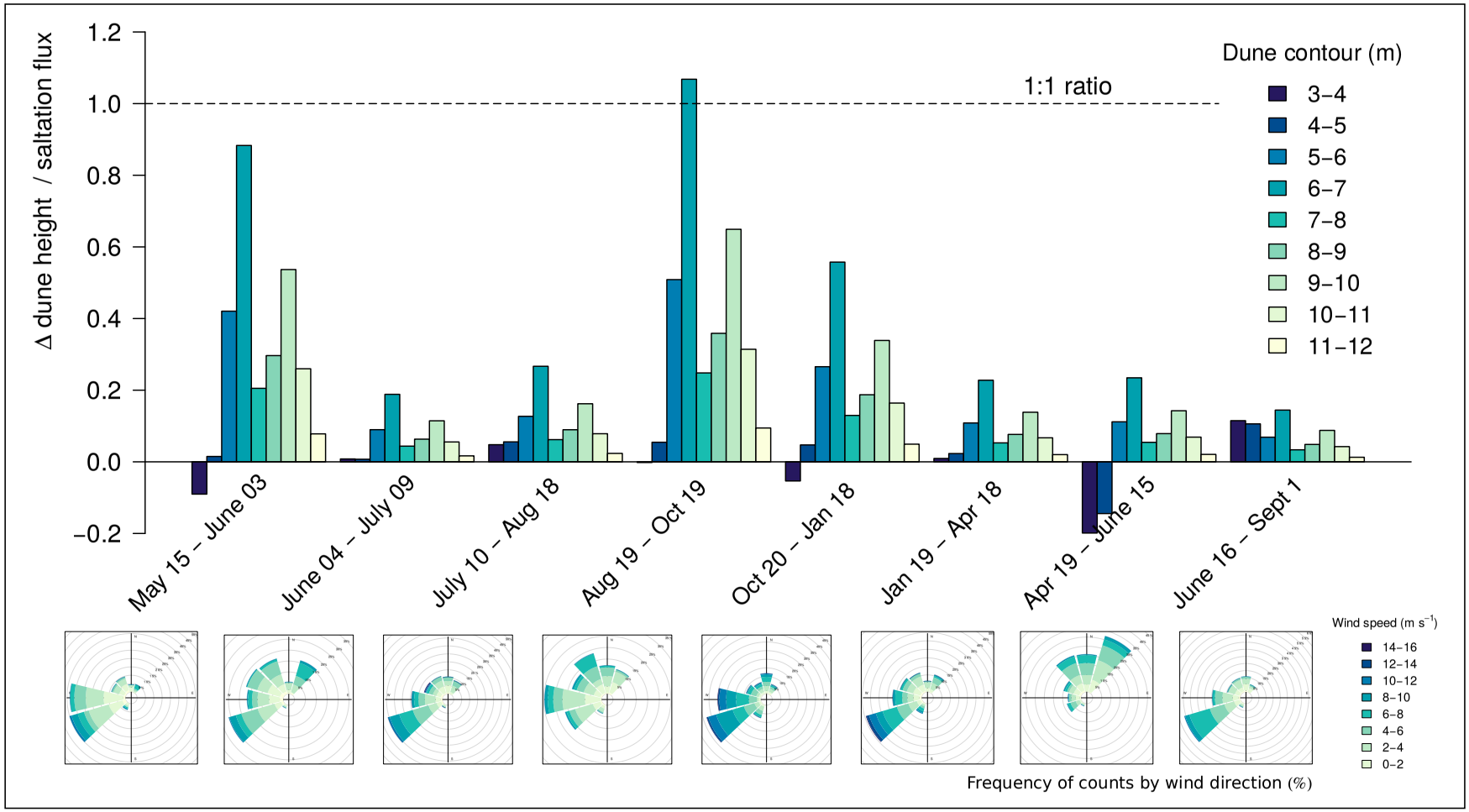

Figure 6.3: Sand budget analysis for a stretch of foredune adjacent to the *Zandmotor*. The ratio of aeolian deposition to the saltation flux suggest that generally only a fraction of aeolian supply is persistently 'stored' and made available for foredune development.

Implications of supply-limited quadratic aeolian transport

The combined effect of how supply-limiting factors and the physical description of steady state saltation regulate coastal aeolian transport dynamics, is perhaps best illustrated by the geomorphological frequency-magnitude concept (Fig. 6.4A) introduced by Wolman and Miller (1960) and shown to be applicable to coastal aeolian processes (i.e., Marston, 1986; Chapman, 1990; Jungerius et al., 1991; Arens, 1996a; Delgado-Fernandez, 2011). Because wind shear velocity under natural conditions is log-normally distributed and the resultant saltation mass flux is proportional to a power of shear velocity (either quadratic or cubic), Wolman and Miller (1960) showed that the product of shear velocity frequency and saltation mass flux magnitude attains a maximum. The effectiveness of an aeolian transport event to perform geomorphic work in the coastal environment, e.g. to shape the landscape by help forming dunes, depends thus both on its frequency of occurrence as well as its magnitude. The maximum geomorphic work, consequently, is accomplished by transport events of a moderate magnitude but which occur much more frequently than rare extreme events. Using the data and results presented in chapter 3, Fig 6.4B shows the different positions of maximum work calculated (per 0.01 m s^{-1} shear velocity intervals) using the quadratic and cubic fits to several percentiles of the response distribution fully impacted by supply-limiting factors (denoted in black, also depicted in Fig. 3.5I-J) and to the observations obtained under optimal field conditions (denoted in brown-red, selected from Fig. 3.5K-L). The positions maximum work calculated using the equation of Kok et al. (2012) and Kawamura (1951) are also included, as well as the empirical positions of maximum work (denoted in red) at the 50th, 95th and 99th percentile, which were derived by binning the saltation mass flux observations per 0.01 m s^{-1} shear velocity intervals.

Several observations stand out when presenting the data in this manner. First, with maximum recorded shear velocity ranging between 2 - 2.5 m s^{-1} (which occurred during 0.1% of the measurement period), the graph confirms that maximum geomorphic work is indeed accomplished at shear velocities of a moderate magnitude but with a higher frequency of occurrence. The position of the maximum geomorphic work, however, changes considerably with respect to the description for steady-state saltation and to which percentiles those functions are fitted. Figure 6.4B shows that when a quadratic dependence of saltation mass flux to shear velocity is considered, the maximum work occurs around a shear velocity of 0.6 m s^{-1}. However, when a cubic dependence of saltation mass flux to shear velocity is considered, then the position of maximum work shifts towards a shear velocity around 1.05 m s^{-1}. In other words, when a quadratic dependence is considered more relevance is assigned to lower shear velocities occurring at higher frequencies, while when a cubic dependence is considered more relevance is assigned to higher shear velocities that occur at a lower frequency. Considering the positions of maximum work obtained by fitting the quadratic and cubic function of Eq. 3.4 to different percentiles of both response distributions, it is clear that the saltation mass flux rate at each maximum reflects a similar pattern previously discerned by examining the flux scaling parameter C (see table 3.1) for the quadratic and cubic fit at the same percentiles. What stands out, though, is that the obtained empirical positions of maximum work at the upper 95th and 99th percentile closely match the position maximum work calculated using the equation of Kok et al. (2012). This strengthens the notion that the saltation mass flux is

likely better described by a quadratic than a cubic dependence to shear velocity and, at the same time, demonstrates the validity of nonlinear quantile regression analysis to examine the dependence of saltation mass flux to shear velocity.

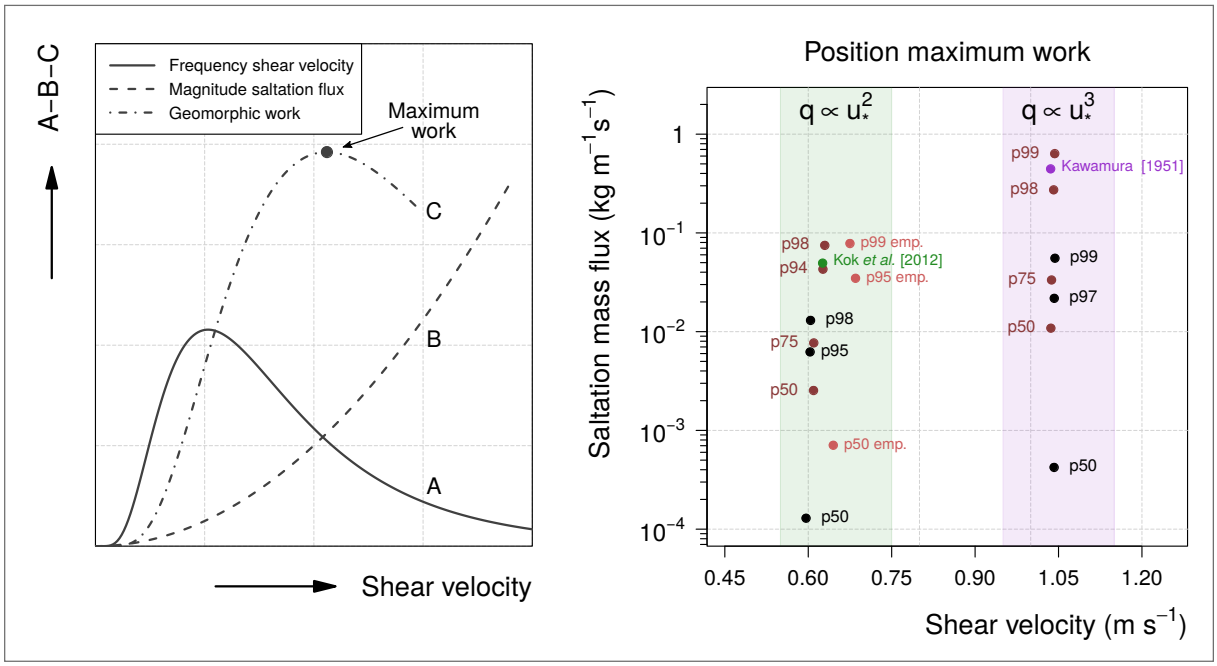

Figure 6.4: Relationship between frequency of shear velocity, magnitude of saltation mass flux and performed geomorphic work according to Wolman and Miller (1960). **6.4A**. Because shear velocity is log-normally distributed and the saltation mass flux is proportional to a power of shear velocity (regardless of a quadratic or cubic proportionality), their product attains a maximum. **6.4B**. Different positions of maximum work (both empirically derived (shown in red) as for the obtained fits depicted in Fig. 3.5I-J) show that a quadratic dependence of saltation flux to shear velocity assigns more relevance to lower shear velocities occurring at higher frequencies, while a cubic dependence assigns more relevance to higher shear velocities that occur at a lower frequency.

Furthermore, the maximum geomorphic work at lower shear velocities which is attained during supply-limited and quadratic aeolian transport, can help explain the typical pattern of seaward broadening of the foredunes observed along *Zandmotor* (see Fig 6.5). It is clear that (patterning of) aeolian transport is closely related to wind speed, which in turn is affected by foredune topography and vegetation density. Sarre (1989a) observed, for example, that aeolian transport decreases exponentially with increasing distance from the foredune foot and that negligible amounts of sand were transported inland beyond the foredune crest. Likewise, Arens (1996b) found that during wind speeds lower than 10 ms^{-1} (at 5 m above the surface), most of the sand would accumulate in front of the foredune foot before reaching the seaward facing vegetation boundary. Only when wind speed exceeded 10 ms^{-1} the sand was able to pass the vegetation boundary. During both oblique and perpendicular onshore winds Arens (1996b) observed as well that saltation fluxes diminished exponentially with increasing distance from the foredune foot. The gradient of change was found to depend on wind speed: during low wind speeds the gradient was steeper than during high wind speeds. So when a quadratic

dependence of saltation flux to shear velocity is considered, the maximum geomorphic work is accomplished during relatively low shear velocities that may typically lack the energy (of force) required to transport sand passed the vegetation boundary. As a result, sand will either accumulate in front of the foredune or may be entrained again into saltation when the wind direction changes. Thus, the effectiveness of aeolian transport events to perform geomorphic work in the coastal environment may commonly get overestimated, leading to exaggerated impact on coastal foredune development on the *Zandmotor* as well as nourished coastlines. The numerous supply-limited conditions, in turn, will likely only act to exacerbate this notion.

6.2.3 Outlook on positive biogeomorphic feedback in coastal dune development

Even though vegetation exerts a first-order control on aeolian sand dynamics and coastal dune development, it is usually the least considered component of the transport-dune system because of its complex (feedback) interactions with environmental conditions and physical processes involved in dune formation (Sherman, 1995). Vegetation is typically only seen to affect aeolian transport by (1) reducing the amount of bare surface available for transport and (2) by slowing down the airflow close to the ground, thus extracting momentum from the wind which is then no longer available to move sand (Baas, 2019). The latter effect is commonly expressed through the concept of shear stress partitioning (Raupach, 1992; Webb et al., 2014), in which the total surface shear stress is divided into two components, one acting on the vegetation and the other on the sand grains (Herrmann et al., 2008). Vegetation thus acts as a roughness element that absorbs part of the wind flow that would otherwise be transferred to the sand. The magnitude of momentum absorption depends strongly on the structure, porosity, geometry, size, and growth form of the vegetation as well as their spatial distribution, lateral density, and potential patterning relative to wind directions (Baas, 2019).

There is considerable interest in enhancing understanding of the controls on (fore)dune development and using these insights to improve morphological models of dune evolution under a range of (environmental and anthropogenic) forcing conditions (Davidson-Arnott et al., 2018). Broadly speaking, these models can be divided into two categories, with the first category comprising of conceptual models of dune evolution that link typical (fore)dune morphology to site-specific conditions (Keijsers, 2015). These models can be used to provide a first approximation of dune development in response to changes in one of these conditions, e.g. response of beach and dune sand budgets to change in vegetation cover (Psuty, 1988; Sherman and Bauer, 1993). Generally, the foredunes are found to follow the position of the shoreline; along an accreting coastline the foredunes tend to build seaward, but if the coastline recedes the dunes respond by retreating landward (Davidson-Arnott and Law, 1996; Hesp, 2002). A second category of models consists of (numerical) computer models that simulate one or several of the morphological processes involved in dune development. A primary objective of many of such models is to reproduce the complexities of the major controls on aeolian transport, deposition and erosion in order to enable real-world prediction of coastal dune evolution (e.g., Roelvink et al., 2009; Hoonhout and Vries, 2016; Fredriksson et al., 2017; Cohn et al., 2019). However, while a few of these simulation models explicitly include a vegetation

(growth) component (e.g. by shear stress partitioning) that affects the aeolian dynamics (e.g., Van Boxel et al., 1999; Durán and Herrmann, 2006; Durán and Moore, 2013; Vinent and Moore, 2015), they generally do not account for positive biogeomorphic feedback effects such as the enhanced growth response of marram grass to sand burial.

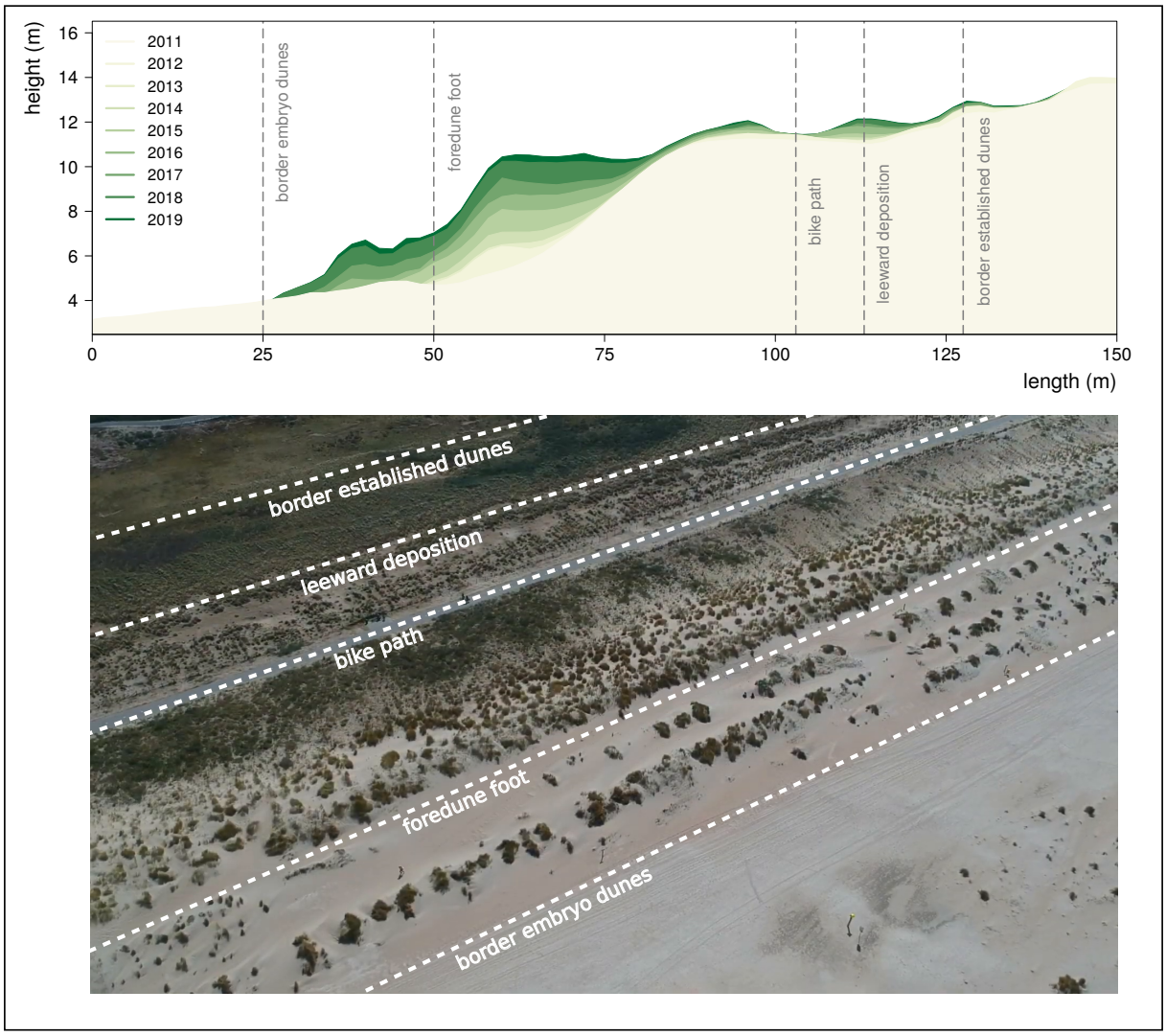

Figure 6.5: Average cross-sectional development of the foredune adjacent to the *Zandmotor* since its construction in 2011 up to 2019, showing a clear seaward broadening trend and embryo dune development along newly forming dune ridges. For reference a recent aerial photo (taken May 2020) is added.

Morphological dune development models that do include positive biogeomorphic feedback (in similar fashion as Fig. 6.6 illustrates) either build upon a cellular automaton model first developed by Werner and Fink (1993) (as already reviewed in chapter 5), or build upon the process-based numerical model introduced by Durán and Moore (2013). The latter model was modified by Moore et al. (2016) in order to capture the biogeomorphic feedback of American marram grass (*Ammophila breviligulata*) to sand deposition. (biogeomorphic feedback capabil-

ity was in fact already included in Durán and Moore (2013) but not utilized). A key modeling assumption in Moore et al. (2016) was a negative feedback between rhizome growth and local dune slope, such that steeper slopes slow the lateral growth of rhizomes, giving rise to incipient dune ridges in front of the foredune. At its core, the vegetation growth component takes the form of a reaction-diffusion equation (Murray, 2007), where the diffusion term models lateral growth (via rhizomes) and the reaction term models vertical growth (positive or negative depending on accretion or erosion). This type of equation is in fact more often employed for modeling spatial ecological processes in relation to abiotic conditions (e.g., Klausmeier, 1999; HilleRisLambers et al., 2001; Rietkerk et al., 2002). Vertical growth, considered as increase in cover fraction due to local biomass production, is modeled by the logistic growth function introduced by Verhulst (1838), i.e. an initial exponential growth followed by a saturation as the vegetation density reaches maximum cover (i.e. the carrying capacity). Following a typical response of dune–building plants to sand accretion, the intrinsic plant growth rate is allowed to linearly increase or decrease with the deposition or erosion rate respectively (Moore et al., 2016). Goldstein et al. (2017) later simplified the vegetation formulation to argue that foredune hummockiness (after Hesp (2002)) and coalescing time was controlled by lateral vegetation growth rates.

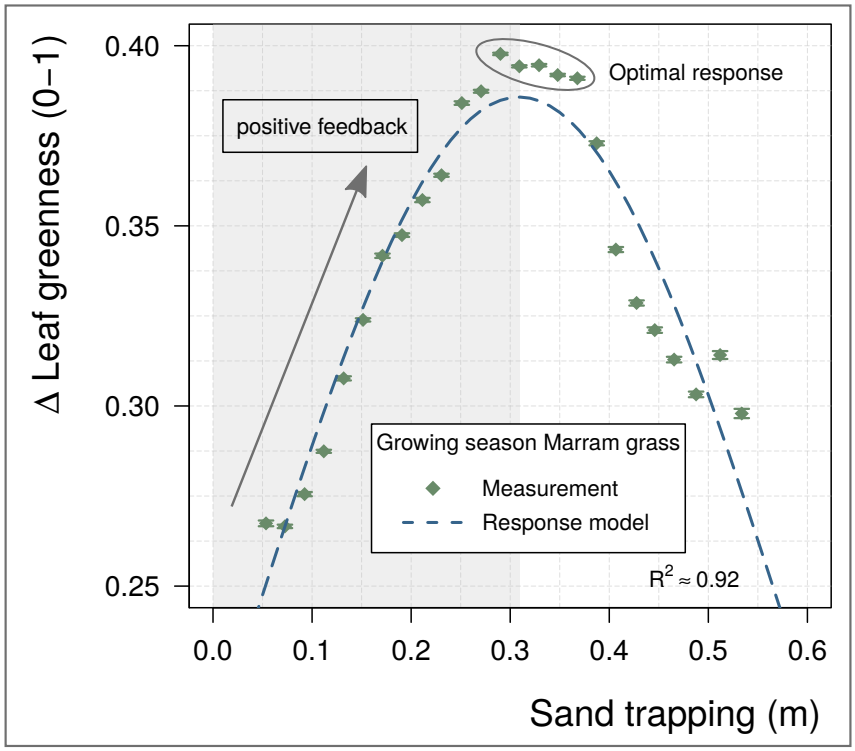

Figure 6.6: Positive feedback relationship between sand trapping of wind-blown sand and growth response of (Eurpean) Marram grass. Optimal growth (see also chapter 5) was found to occur around around 30 cm of sand trapping per growing season.

In a recent work by Davidson-Arnott et al. (2018) put into question the validity of some of the modeling assumptions (and subsequent model outcomes) of Durán and Moore (2013).

The authors specifically take issue with the assumption regarding an inherent limit to the sand supply to the foredune, due to the reduction in wind speed and transport potential at the base of a steep dune, so that a static equilibrium maximum dune height (H_{max}) is developed. Davidson-Arnott et al. (2018) argue that such natural limit to foredune height because of form-flow feedback must be considered an artefact of the assumptions in model of Durán and Moore (2013), particularly that of shore perpendicular flow against a 2D foredune. Due to prevalent oblique wind approach angles, Davidson-Arnott et al. (2018) conclude that sand supply to the foredune by aeolian processes can continue indefinitely as long as the littoral sediment budget can supply it, and assuming that changes in other controls (e.g. sea level, beach progradation, vegetation cover) do not exceed some critical limit. And because the concept of H_{max} has been incorporated in several follow-up papers (including Moore et al. (2016) and Goldstein et al. (2017)) Davidson-Arnott et al. (2018) argues that the results of those modelling efforts should be re-appraised.

While Davidson-Arnott et al. (2018) do not take issue with the biogeomorphic vegetation growth component included by Moore et al. (2016), the limit to foredune height imposed by Durán and Moore (2013) is (implicitly) incorporated in this model component as well and should perhaps also be re-appraised. As Goldstein et al. (2017) states, (H_{max}) is a function of several parameters, including the seaward vegetation growth limit. And Moore et al. (2016) states that lateral growth is limited by the stoss slope angle, which is dependent on (H_{max}). To address the critique of Davidson-Arnott et al. (2018) and to potentially advance the use of process-based morphological dune development models, an interesting approach might be utilizing a bi-logistic growth model (Meyer, 1994; Meyer and Ausubel, 1999). This idea was first proposed by Hugenholtz and Wolfe (2005) as an approach to model coastal dune fields that receive varying supply of sediment. The key concept in bi-logistic growth is that the carrying capacity is not a fixed upper boundary but instead also modeled as a logistic function of time. Subsequently, by dynamically increasing or decreasing the carrying capacity as a function of aeolian deposition and erosion, both the morphological and ecological feedback dynamics of coastal dune development can be captured. Essentially bi-logistic growth allows modeling of beach-dune systems that are not in dynamic equilibrium, which is true for the *Zandmotor* and nourished coastlines in general. Strikingly, but perhaps not related, the pattern that bi-logistic growth forms (with time on x-axis) looks in fact very similar to the cross-section of the foredune (see Fig. 6.5) along the *Zandmotor*.

6.3 General conclusion

As sea levels continue to rise, it is anticipated that sand nourishments need to increase in volume or frequency to combat erosion and maintain the sandy coast of the Netherlands. Within this context, the unprecedented mega-scale beach nourishment of 21.5 Mm^3 termed *Zandmotor* was constructed in 2011. The overall purpose of this mega-nourishment experiment is to test whether its benefits in terms if coastal safety, spatial quality and ecological values outweigh the extra costs involved and to determine to what extent such an approach can help cope with expected changes in the global climate. This objective of this research

is to provide field-based evidence about how reinforcing biogeomorphic feedback drives dune development on the *Zandmotor*. Insight into the growth response of European marram grass to sand burial is hereto essential, as is insight into prevailing coastal aeolian dynamics.

For this research, empirical measurements of aeolian transport and foredune evolution have been obtained synchronously, such that it has been possible to directly relate aeolian transport to coastal dune development. Sand budget analysis showed that typically only a small amount of sand blown towards the foredunes along the *Zandmotor* is deposited persistently and thus made available for dune development. The highest amount of deposition occurred around the seaward facing vegetation boundary of marram grass, highlighting the importance of marram grass accumulate and stabilize wind-blown sand. Further, observed aeolian transport rates were also much lower than predicted by traditional aeolian transport equations. While generally attributed to meteorological and surficial conditions that limit the supply of sand for aeolian transport in coastal environments, this research indicates that the lower transport rates may also arise from the notion that the saltation mass flux is better explained by a quadratic than a cubic dependence to shear velocity.

While positive biogeomorphic feedback between marram grass and aeolian dynamics may ultimately be the most important driver for coastal dune development, it is often also the least considered component of the coastal aeolian transport-dune system. For growth response of marram grass to sand burial, this research found an optimal burial rate around 0.3 m and a maximum burial tolerance around 1.0 meter of sand per growing season. While specific to the conditions on the *Zandmotor*, the growth parameters found in this research may be representative for Dutch nourished coasts and be advantageous to coastal management in the Netherlands: because dune development is directly related to the growth response of marram grass to sand burial, maximizing the potential of marram grass to grow maximizes the potential of coastal dunes to develop and provide coastal safety.

References

Adriani, M. J. and Terwindt, J. H. J. (1974). Sand stabilization and dune building, Tech. rep., Rijkswaterstaat.

Anders, F. J. and Leatherman, S. P. (1987). Effects of off-road vehicles on coastal foredunes at Fire Island, New York, USA, *Environmental Management* 11, 45–52.

Andersen, U. V. (1995). Resistance of Danish coastal vegetation types to human trampling, *Biological conservation* 71, 223–230.

Anderson, K. and Gaston, K. J. (2013). Lightweight unmanned aerial vehicles will revolutionize spatial ecology, *Frontiers in Ecology and the Environment* 11, 138–146.

Anderson, R. S. and Haff, P. K. (1988). Simulation of eolian saltation, *Science* 241, 820–824.

Andreotti, B. (2004). A two-species model of aeolian sand transport, *Journal of Fluid Mechanics* 510, 47–70.

Andreotti, B., Claudin, P., and Pouliquen, O. (2010). Measurements of the aeolian sand transport saturation length, *Geomorphology* 123, 343–348.

Ångström, A. (1925). The albedo of various surfaces of ground, *Geografiska Annaler* 7, 323–342.

Anthony, E. J. (2013). Storms, shoreface morphodynamics, sand supply, and the accretion and erosion of coastal dune barriers in the southern North Sea, *Geomorphology* 199, 8–21.

Anthony, E. J., Vanhée, S., and Ruz, M.-H. (2007). Embryo dune development on a large, actively accreting macrotidal beach: Calais, North Sea coast of France, *Earth Surface Processes and Landforms* 32, 631–636.

Arens, S. (1996a). Rates of aeolian transport on a beach in a temperate humid climate, *Geomorphology* 17, 3–18.

Arens, S. (1997). Transport rates and volume changes in a coastal foredune on a Dutch Wadden island, *Journal of Coastal Conservation* 3, 49–56.

Arens, S., Baas, A., Van Boxel, J., and Kalkman, C. (2001). Influence of reed stem density on foredune development, *Earth Surface Processes and Landforms* 26, 1161–1176.

Arens, S. M. (1996b). Patterns of sand transport on vegetated foredunes, *Geomorphology* 17, 339–350.

Arens, S. M., Kaam-Peters, V., and Van Boxel, J. H. (1995). Air flow over foredunes and implications for sand transport, *Earth Surface Processes and Landforms* 20, 315–332.

Arens, S. M., Mulder, J. P., Slings, Q. L., Geelen, L. H., and Damsma, P. (2013). Dynamic dune management, integrating objectives of nature development and coastal safety: examples from the Netherlands, *Geomorphology* 199, 205–213.

Arriaga, J., Rutten, J., Ribas, F., Falqués, A., and Ruessink, G. (2017). Modeling the long-term diffusion and feeding capability of a mega-nourishment, *Coastal Engineering* 121, 1–13.

Atherton, R., Baird, A., and Wiggs, G. (2001). Inter-tidal dynamics of surface moisture content on a meso-tidal beach, *Journal of Coastal Research* 17, 482–489.

Austin, M. P. (2007). Species distribution models and ecological theory: a critical assessment and some possible new approaches, *Ecological modelling* 200, 1–19.

Austin, M. P. and Smith, T. M. (1990). A new model for the continuum concept, in: Progress in theoretical vegetation science, pp. 35–47, Springer.

Baas, A. C. (2019). Grains in Motion, in: Aeolian Geomorphology: A New Introduction, pp. 27–60, John Wiley & Sons, Ltd Chichester, UK.

Baas, A. C. W. (2002). Chaos, fractals and self-organization in coastal geomorphology: simulating dune landscapes in vegetated environments, *Geomorphology* 48, 309–328.

Baas, A. C. W. and Nield, J. M. (2010). Ecogeomorphic state variables and phase-space construction for quantifying the evolution of vegetated aeolian landscapes, *Earth Surface Processes and Landforms* 35, 717–731.

Baas, A. C. W. and Sherman, D. (2005). Formation and behavior of aeolian streamers, *Journal of Geophysical Research: Earth Surface* 110.

Bagnold, R. (1936). The movement of desert sand, *Proceedings of the Royal Society of London. Series A, Mathematical and Physical Sciences* 157, 594–620.

Bagnold, R.: (1941). *The Physics of Windblown Sand*, Chapman and Hall, London, 265p.

Bakker, A. M., Wong, T. E., Ruckert, K. L., and Keller, K. (2017). Sea-level projections representing the deeply uncertain contribution of the West Antarctic ice sheet, *Scientific Reports* 7, 1–7.

Baptist, M., Tamis, J., Borsje, B., and Van der Werf, J. (2008). Review of the geomorphological, benthic ecological and biogeomorphological effects of nourishments on the shoreface and surf zone of the Dutch coast, Tech. rep., IMARES/Deltares.

Barchyn, T. E., Hugenholtz, C. H., and Ellis, J. T. (2011). A call for standardization of aeolian process measurements: moving beyond relative case studies, *Earth Surface Processes and Landforms* 36, 702–705.

Bauer, B., Davidson-Arnott, R., Hesp, P., Namikas, S., Ollerhead, J., and Walker, I. (2009a). Aeolian sediment transport on a beach: surface moisture, wind fetch, and mean transport, *Geomorphology* 105, 106–116.

Bauer, B., Davidson-Arnott, R., Hesp, P., Namikas, S., Ollerhead, J., and Walker, I. (2009b). Aeolian sediment transport on a beach: Surface moisture, wind fetch, and mean transport, *Geomorphology* 105, 106–116.

Bauer, B. O. and Davidson-Arnott, R. G. (2003). A general framework for modeling sediment supply to coastal dunes including wind angle, beach geometry, and fetch effects, *Geomorphology* 49, 89–108.

Belly, P.-Y.: (1964). *Sand movement by wind*, US Army coastal engineering research center.

Bergeron, N. E. and Abrahams, A. D. (1992). Estimating shear velocity and roughness length from velocity profiles, *Water Resources Research* 28, 2155–2158.

Bird, E. C.: (2011). *Coastal geomorphology: an introduction*, John Wiley & Sons.

Bochev-Van der Burgh, L., Wijnberg, K., and Hulscher, S. (2011). Decadal-scale morphologic variability of managed coastal dunes, *Coastal engineering* 58, 927–936.

Bohren, C. F. and Huffman, D. R.: (2008). *Absorption and scattering of light by small particles*, John Wiley & Sons.

Bowers, S. and Hanks, R. (1965). Reflection of radiant energy from soils, *Soil Science* 100, 130–138.

Butterfield, G. (1991). Grain transport rates in steady and unsteady turbulent airflows, in: Aeolian Grain Transport 1, pp. 97–122, Springer.

Cade, B. S. and Noon, B. R. (2003). A gentle introduction to quantile regression for ecologists, *Frontiers in Ecology and the Environment* 1, 412–420.

Cade, B. S., Terrell, J. W., and Schroeder, R. L. (1999). Estimating effects of limiting factors with regression quantiles, *Ecology* 80, 311–323.

Carlson, T. N. and Ripley, D. A. (1997). On the relation between NDVI, fractional vegetation cover, and leaf area index, *Remote sensing of Environment* 62, 241–252.

Carranza, C., Nolet, C., Pezij, M., and van der Ploeg, M. J. (2020). Estimating root zone soil moisture with Random Forests, journal of Hydrology X, accepted.

Chapman, D. M. (1990). Aeolian sand transport an optimized model, *Earth Surface Processes and Landforms* 15, 751–760.

Chepil, W. (1956). Influence of moisture on erodibility of soil by wind, *Soil Science Society of America Journal* 20, 288–292.

Chepil, W. and Woodruff, N. (1963). The physics of wind erosion and its control, *Advances in agronomy* 15, 211–302.

Ciani, A., Goss, K.-U., and Schwarzenbach, R. (2005). Light penetration in soil and particulate minerals, *European journal of soil science* 56, 561–574.

Claudino-Sales, V., Wang, P., and Horwitz, M. H. (2008). Factors controlling the survival of coastal dunes during multiple hurricane impacts in 2004 and 2005: Santa Rosa barrier island, Florida, *Geomorphology* 95, 295–315.

Cohn, N., Hoonhout, B. M., Goldstein, E. B., De Vries, S., Moore, L. J., Durán Vinent, O., and Ruggiero, P. (2019). Exploring marine and aeolian controls on coastal foredune growth using a coupled numerical model, *Journal of Marine Science and Engineering* 7, 13.

Cornelis, W. and Gabriels, D. (2003a). The effect of surface moisture on the entrainment of dune sand by wind: an evaluation of selected models, *Sedimentology* 50, 771–790.

Cornelis, W. M. and Gabriels, D. (2003b). The effect of surface moisture on the entrainment of dune sand by wind: an evaluation of selected models, *Sedimentology* 50, 771–790.

Crain, C. M., Halpern, B. S., Beck, M. W., and Kappel, C. V. (2009). Understanding and managing human threats to the coastal marine environment, *Annals of the New York Academy of Sciences* 1162, 39–62.

Creyssels, M., Dupont, P., El Moctar, A. O., Valance, A., Cantat, I., Jenkins, J. T., Pasini, J. M., and Rasmussen, K. R. (2009). Saltating particles in a turbulent boundary layer: experiment and theory, *Journal of Fluid Mechanics* 625, 47–74.

Curran, P. J., Dungan, J. L., Macler, B. A., and Plummer, S. E. (1991). The effect of a red leaf pigment on the relationship between red edge and chlorophyll concentration, *Remote Sensing of Environment* 35, 69–76.

Daniels, E., Lenderink, G., Hutjes, R., and Holtslag, A. (2014). Spatial precipitation patterns and trends in The Netherlands during 1951–2009, *International journal of climatology* 34, 1773–1784.

Darke, I. and McKenna Neuman, C. (2008). Field study of beach water content as a guide to wind erosion potential, *Journal of Coastal Research* 24, 1200–1208.

Darke, I., Davidson-Arnott, R., and Ollerhead, J. (2009). Measurement of beach surface moisture using surface brightness, *Journal of Coastal Research* 25, 248–256.

Davidson-Arnott, R. and Bauer, B. (2009). Aeolian sediment transport on a beach: thresholds, intermittency, and high frequency variability, *Geomorphology* 105, 117–126.

Davidson-Arnott, R., MacQuarrie, K., and Aagaard, T. (2005a). The effect of wind gusts, moisture content and fetch length on sand transport on a beach, *Geomorphology* 68, 115–129.

Davidson-Arnott, R., Hesp, P., Ollerhead, J., Walker, I., Bauer, B., Delgado-Fernandez, I., and Smyth, T. (2018). Sediment budget controls on foredune height: Comparing simulation model results with field data, *Earth Surface Processes and Landforms* 43, 1798–1810.

Davidson-Arnott, R. G. and Law, M. N. (1996). Measurement and prediction of long-term sediment supply to coastal foredunes, *Journal of Coastal Research* pp. 654–663.

Davidson-Arnott, R. G., MacQuarrie, K., and Aagaard, T. (2005b). The effect of wind gusts, moisture content and fetch length on sand transport on a beach, *Geomorphology* 68, 115–129.

De Jong, B., Keijsers, J. G., Riksen, M. J., Krol, J., and Slim, P. A. (2014). Soft Engineering vs. a Dynamic Approach in Coastal Dune Management: A Case Study on the North Sea Barrier Island of Ameland, The Netherlands, *Journal of Coastal Research* .

De Schipper, M. A., De Vries, S., Ruessink, G., De Zeeuw, R. C., Rutten, J., Van Gelder-Maas, C., and Stive, M. J. F. (2016). Initial spreading of a mega feeder nourishment: Observations of the Sand Engine pilot project, *Coastal Engineering* 111, 23–38.

De Vriend, H. J. and Van Koningsveld, M. (2012). Building with Nature: Thinking, acting and interacting differently .

De Vriend, H. J., van Koningsveld, M., Aarninkhof, S. G., De Vries, M. B., and Baptist, M. J. (2015). Sustainable hydraulic engineering through building with nature, *Journal of Hydro-environment research* 9, 159–171.

De Vries, S., Southgate, H., Kanning, W., and Ranasinghe, R. (2012). Dune behavior and aeolian transport on decadal timescales, *Coastal Engineering* 67, 41–53.

De Vries, S., de Vries, J. v. T., van Rijn, L., Arens, S., and Ranasinghe, R. (2014). Aeolian sediment transport in supply limited situations, *Aeolian Research* 12, 75–85.

de Vries, S., van Thiel de Vries, J., van Rijn, L., Arens, S., and Ranasinghe, R. (2014). Aeolian sediment transport in supply limited situations, *Aeolian Research* 12, 75–85.

De Winter, R., Gongriep, F., and Ruessink, B. (2015). Observations and modeling of alongshore variability in dune erosion at Egmond aan Zee, the Netherlands, *Coastal Engineering* 99, 167–175.

DeConto, R. M. and Pollard, D. (2016). Contribution of Antarctica to past and future sea-level rise, *Nature* 531, 591–597.

Delgado-Fernandez, I. (2011). Meso-scale modelling of aeolian sediment input to coastal dunes, *Geomorphology* 130, 230–243.

Delgado-Fernandez, I., Davidson-Arnott, R., and Ollerhead, J. (2009). Application of a Remote Sensing Technique to the Study of Coastal Dunes, *Journal of Coastal Research* 25.

Disraeli, D. J. (1984). The effect of sand deposits on the growth and morphology of Ammophila breviligulata, *The Journal of Ecology* pp. 145–154.

Drusch, M., Del Bello, U., Carlier, S., Colin, O., Fernandez, V., Gascon, F., Hoersch, B., Isola, C., Laberinti, P., Martimort, P., et al. (2012). Sentinel-2: ESA's optical high-resolution mission for GMES operational services, *Remote sensing of Environment* 120, 25–36.

Durán, O. and Herrmann, H. J. (2006). Vegetation against dune mobility, *Physical review letters* 97, 188 001.

Durán, O. and Moore, L. J. (2013). Vegetation controls on the maximum size of coastal dunes, *Proceedings of the National Academy of Sciences* 110, 17 217–17 222.

Durán, O., Claudin, P., and Andreotti, B. (2011). On aeolian transport: Grain-scale interactions, dynamical mechanisms and scaling laws, *Aeolian Research* 3, 243–270.

Edwards, B., Namikas, S., and D'Sa, E. (2013a). Simple infrared techniques for measuring beach surface moisture, *Earth Surface Processes and Landforms* 38, 192–197.

Edwards, B. L., Schmutz, P. P., and Namikas, S. L. (2013b). Comparison of surface moisture measurements with depth-integrated moisture measurements on a fine-grained beach, *Journal of Coastal Research* 29, 1284–1291.

Elachi, C. and Van Zyl, J. J.: (2006). *Introduction to the physics and techniques of remote sensing*, vol. 28, Wiley. com.

Ellis, J. T., Sherman, D. J., Farrell, E. J., and Li, B. (2012). Temporal and spatial variability of aeolian sand transport: Implications for field measurements, *Aeolian Research* 3, 379–387.

Farrell, E., Sherman, D., Ellis, J., and Li, B. (2012). Vertical distribution of grain size for wind blown sand,

Aeolian Research 7, 51–61.

Feagin, R. A., Figlus, J., Zinnert, J. C., Sigren, J., Martínez, M. L., Silva, R., Smith, W. K., Cox, D., Young, D. R., and Carter, G. (2015). Going with the flow or against the grain? The promise of vegetation for protecting beaches, dunes, and barrier islands from erosion, *Frontiers in Ecology and the Environment* 13, 203–210.

Filella, I. and Penuelas, J. . (1994). The red edge position and shape as indicators of plant chlorophyll content, biomass and hydric status., *International Journal of Remote Sensing* 15, 1459–1470.

Fiselier, J. (2010). Milieueffectrapportage Zandmotor Delflandse kust, *MER rapport door DHV in opdracht van provincie Zuid Holland* .

Fonstad, M. A., Dietrich, J. T., Courville, B. C., Jensen, J. L., and Carbonneau, P. E. (2013). Topographic structure from motion: a new development in photogrammetric measurement, *Earth Surface Processes and Landforms* 38, 421–430.

Fortin, M. J. and Dale, M. R. T.: (2005). *Spatial analysis: a guide for ecologists*, Cambridge University Press.

Fredriksson, C., Larson, M., and Hanson, H. (2017). Long-term modelling of aeolian transport and beach-dune evolution, *Proceedings of Coastal Dynamics 2017* pp. 715–726.

Fryberger, S. G., Dean, G., and McKee, E. (1979). Dune forms and wind regime, *A study of global sand seas* 1052, 137–170.

Gamon, J. A., Field, C. B., Goulden, M. L., Griffin, K. L., Hartley, A. E., Joel, G., Penuelas, J., and Valentini, R. (1995). Relationships between NDVI, canopy structure, and photosynthesis in three Californian vegetation types, *Ecological Applications* 5, 28–41.

Gauch, H. G. and Whittaker, R. H. (1972). Coenocline simulation, *Ecology* 53, 446–451.

Gemmell, A. R., Greig-Smith, P., and Gimingham, C. H. (1953). A note on the behaviour of Ammophila arenaria (L.) Link, in relation to sand-dune formation, in: Transactions of the Botanical Society of Edinburgh, vol. 36, pp. 132–136, Taylor & Francis.

Giardino, A., Mulder, J., Ronde, J. d., and Stronkhorst, J. (2011). Sustainable development of the Dutch coast: Present and future, *Journal of Coastal Research* pp. 166–172.

Gillette, D. A., Herbert, G., Stockton, P. H., and Owen, P. (1996). Causes of the fetch effect in wind erosion, *Earth Surface Processes and Landforms* 21, 641–659.

Goldstein, E. B., Moore, L. J., and Vinent, O. D. (2017). Lateral vegetation growth rates exert control on coastal foredune" hummockiness" and coalescing time, *Earth Surface Dynamics* 5, 417.

Goossens, D., Offer, Z., and London, G. (2000). Wind tunnel and field calibration of five aeolian sand traps, *Geomorphology* 35, 233–252.

Goossens, D., Nolet, C., Etyemezian, V., Duarte-Campos, L., Bakker, G., and Riksen, M. (2018). Field testing, comparison, and discussion of five aeolian sand transport measuring devices operating on different measuring principles, *Aeolian research* 32, 1–13.

Greeley, R., Blumberg, D. G., and Williams, S. H. (1996). Field measurements of the flux and speed of wind-blown sand, *Sedimentology* 43, 41–52.

Grunnet, N. M. and Ruessink, B. (2005). Morphodynamic response of nearshore bars to a shoreface nourishment, *Coastal Engineering* 52, 119–137.

Haasnoot, M., Kwadijk, J., Van Alphen, J., Le Bars, D., van den Hurk, B., Diermanse, F., van der Spek, A., Essink, G. O., Delsman, J., and Mens, M. (2020). Adaptation to uncertain sea-level rise; how uncertainty in Antarctic mass-loss impacts the coastal adaptation strategy of the Netherlands, *Environmental Research Letters* 15, 034 007.

Hapke, B.: (2012). *Theory of reflectance and emittance spectroscopy*, Cambridge University Press.

Hardisty, J. (1994). Beach and nearshore sediment transport, *Sediment transport and depositional processes.*

Blackwell, London, UK pp. 216–255.

Hartigan, J. A. and Wong, M. A. (1979). Algorithm AS 136: A k-means clustering algorithm, *Journal of the Royal Statistical Society. Series C (Applied Statistics)* 28, 100–108.

Hecht, E. (2002). Optics, Addison-Wesley, San Francisco, CA.

Herrmann, H. J., Durán, O., Parteli, E. J., and Schatz, V. (2008). Vegetation and induration as sand dunes stabilizators, *Journal of Coastal Research* 24, 1357–1368.

Hesp, P. (1981). The formation of shadow dunes, *Journal of Sedimentary Research* 51, 101–112.

Hesp, P. (2002). Foredunes and blowouts: initiation, geomorphology and dynamics, *Geomorphology* 48, 245–268.

Hesp, P. A. (1989). A review of biological and geomorphological processes involved in the initiation and development of incipient foredunes, *Proceedings of the Royal Society of Edinburgh. Section B. Biological Sciences* 96, 181–201.

Hesp, P. A. (1991). Ecological processes and plant adaptations on coastal dunes, *Journal of arid environments* 21, 65–61.

Hesp, P. A. and Martínez, M. L. (2007). Disturbance processes and dynamics in coastal dunes, *Plant disturbance ecology: the process and the response* pp. 215–247.

Hesp, P. A., Smyth, T. A., Nielsen, P., Walker, I. J., Bauer, B. O., and Davidson-Arnott, R. (2015). Flow deflection over a foredune, *Geomorphology* 230, 64–74.

Hillel, D.: (1998). *Environmental soil physics: Fundamentals, applications, and environmental considerations*, Academic press.

Hillen, R. and Roelse, P. (1995). Dynamic preservation of the coastline in the Netherlands, *Journal of Coastal Conservation* 1, 17–28.

HilleRisLambers, R., Rietkerk, M., van den Bosch, F., Prins, H. H., and de Kroon, H. (2001). Vegetation pattern formation in semi-arid grazing systems, *Ecology* 82, 50–61.

Hilton, M. and Konlechner, T. (2011). Incipient Foredunes Developed from Marine-dispersed Rhizome of Ammophilia arenaria, *Journal of Coastal Research* p. 288.

Ho, T. D., Valance, A., Dupont, P., and El Moctar, A. O. (2011). Scaling laws in aeolian sand transport, *Physical Review Letters* 106, 094 501.

Hoonhout, B. and de Vries, S. (2017a). Aeolian sediment supply at a mega nourishment, *Coastal Engineering* 123, 11–20.

Hoonhout, B. and de Vries, S. (2017b). Field measurements on spatial variations in aeolian sediment availability at the Sand Motor mega nourishment, *Aeolian Research* 24, 93–104.

Hoonhout, B. M. and Vries, S. d. (2016). A process-based model for aeolian sediment transport and spatiotemporal varying sediment availability, *Journal of Geophysical Research: Earth Surface* 121, 1555–1575.

Houser, C., Hapke, C., and Hamilton, S. (2008). Controls on coastal dune morphology, shoreline erosion and barrier island response to extreme storms, *Geomorphology* 100, 223–240.

Houser, C., Wernette, P., Rentschlar, E., Jones, H., Hammond, B., and Trimble, S. (2015). Post-storm beach and dune recovery: Implications for barrier island resilience, *Geomorphology* 234, 54–63.

Hugenholtz, C. and Wolfe, S. (2005). Biogeomorphic model of dunefield activation and stabilization on the northern Great Plains, *Geomorphology* 70, 53–70.

Hugenholtz, C., Wolfe, S., Walker, I., and Moorman, B. (2009). Spatial and temporal patterns of aeolian sediment transport on an inland parabolic dune, Bigstick Sand Hills, Saskatchewan, Canada, *Geomorphology* 105, 158–170.

Hugenholtz, C. H., Whitehead, K., Brown, O. W., Barchyn, T. E., Moorman, B. J., LeClair, A., Riddell, K., and Hamilton, T. (2013). Geomorphological mapping with a small unmanned aircraft system (sUAS): feature

detection and accuracy assessment of a photogrammetrically-derived digital terrain model, *Geomorphology* 194, 16–24.

Huiskes, A. H. L. (1979). Ammophila arenaria (L.) Link (Psamma arenaria (L.) Roem. et Schult.; Calamgrostis arenaria (L.) Roth), *Journal of Ecology* 67, 363–382.

Huisman, C. E., Bryan, K. R., Coco, G., and Ruessink, B. (2011). The use of video imagery to analyse groundwater and shoreline dynamics on a dissipative beach, *Continental Shelf Research* 31, 1728–1738.

Huizer, S., Oude Essink, G. H., and Bierkens, M. F. (2016). Fresh groundwater resources in a large sand replenishment, *Hydrology and Earth System Sciences* 20, 3149–3166.

Huston, M. A. (2002). Introductory essay: critical issues for improving predictions, *Predicting species occurrences: issues of accuracy and scale* pp. 7–21.

Idso, S., Jackson, R., Reginato, R., Kimball, B., and Nakayama, F. (1975). The dependence of bare soil albedo on soil water content, *Journal of Applied Meteorology* 14, 109–113.

Iversen, J. D. and Rasmussen, K. R. (1999). The effect of wind speed and bed slope on sand transport, *Sedimentology* 46, 723–731.

Jackson, A. and McIlvenny, J. (2011). Coastal squeeze on rocky shores in northern Scotland and some possible ecological impacts, *Journal of Experimental Marine Biology and Ecology* 400, 314–321.

Jackson, D. (1996). Potential inertial effects in aeolian sand transport: preliminary results, *Sedimentary Geology* 106, 193–201.

Jackson, D. W. and McCloskey, J. (1997). Preliminary results from a field investigation of aeolian sand transport using high resolution wind and transport measurements, *Geophysical Research Letters* 24, 163–166.

Jackson, N. L. and Nordstrom, K. F. (2011). Aeolian sediment transport and landforms in managed coastal systems: a review, *Aeolian research* 3, 181–196.

Jervey, M. (1988). Quantitative geological modeling of siliciclastic rock sequences and their seismic expression., *Sea-level changes: An integrated approach, Spec. Publ. SEPM* 42, 47–69.

Jungerius, P., Verheggen, A., and Wiggers, A. (1981). The development of blowouts in 'De Blink', a coastal dune area near Noordwijkerhout, The Netherlands, *Earth surface processes and landforms* 6, 375–396.

Jungerius, P., Witter, J., and Van Boxel, J. (1991). The effects of changing wind regimes on the development of blowouts in the coastal dunes of The Netherlands, *Landscape Ecology* 6, 41–48.

Kabat, P., Fresco, L. O., Stive, M. J., Veerman, C. P., Van Alphen, J. S., Parmet, B. W., Hazeleger, W., and Katsman, C. A. (2009). Dutch coasts in transition, *Nature Geoscience* 2, 450–452.

Kawamura, R. (1951). Study on sand movement by wind (Relationship between sand flow and wind friction, and vertical density distribution of sand), *Tokyo Daigaku Rikogaku Kenkyusho Hokoku,(Tokyo)* 5, 95–112.

Keijsers, J. (2015). *Modelling foredune dynamics in response to climate change*, Ph.D. thesis, Wageningen University.

Keijsers, J., De Groot, A., and Riksen, M. (2015a). Vegetation and sedimentation on coastal foredunes, *Geomorphology* 228, 723–734.

Keijsers, J., De Groot, A., and Riksen, M. (2016). Modeling the biogeomorphic evolution of coastal dunes in response to climate change, *Journal of Geophysical Research: Earth Surface* 121, 1161–1181.

Keijsers, J. G., Giardino, A., Poortinga, A., Mulder, J. P., Riksen, M. J., and Santinelli, G. (2014a). Adaptation strategies to maintain dunes as flexible coastal flood defense in The Netherlands, *Mitigation and Adaptation Strategies for Global Change* pp. 1–16.

Keijsers, J. G. S., Poortinga, A., Riksen, M. J. P. M., and Maroulis, J. (2014b). Spatio-temporal variability in accretion and erosion of coastal foredunes in the Netherlands: Regional climate and local topography, *PloS one* 9, e91 115.

Keijsers, J. G. S., Giardino, A., Poortinga, A., Mulder, J. P. M., Riksen, M. J. P. M., and Santinelli, G. (2015b). Adaptation strategies to maintain dunes as flexible coastal flood defense in The Netherlands, *Mitigation and Adaptation Strategies for Global Change* 20, 913–928.

Kelly, J. F. (2014). Effects of human activities (raking, scraping, off-road vehicles) and natural resource protections on the spatial distribution of beach vegetation and related shoreline features in New Jersey, *Journal of coastal conservation* 18, 383–398.

Klausmeier, C. A. (1999). Regular and irregular patterns in semiarid vegetation, *Science* 284, 1826–1828.

Knadel, M., Deng, F., Alinejadian, A., Wollesen de Jonge, L., Moldrup, P., and Greve, M. H. (2014). The Effects of Moisture Conditions – From Wet to Hyper dry – On Visible Near-Infrared Spectra of Danish Reference Soils, *Soil Science Society of America Journal* 78, 422–433.

Koenker, R. (2016). *quantreg: Quantile Regression*, r package version 5.29.

Koenker, R. and Bassett Jr, G. (1978). Regression quantiles, *Econometrica: journal of the Econometric Society* pp. 33–50.

Koenker, R., Portnoy, S., Ng, P. T., Zeileis, A., Grosjean, P., and Ripley, B. D. (2018). Quantile Regression; Package quantreg.

Kok, J. F., Parteli, E. J., Michaels, T. I., and Karam, D. B. (2012). The physics of wind-blown sand and dust, *Reports on Progress in Physics* 75, 106 901.

Konlechner, T. and Hilton, M. (2009). The potential for marine dispersal of Ammophila arenaria (Marram Grass) rhizome in New Zealand, *Journal of Coastal Research* pp. 434–437.

Konlechner, T. M., Hilton, M. J., and Orlovich, D. A. (2013). Accommodation space limits plant invasion: Ammophila arenaria survival on New Zealand beaches, *Journal of coastal conservation* 17, 463–472.

Koster, K., Stafleu, J., Vos, P. C., and Meulen, M. J. (2020). Can we elevate the subsiding coastal plain of the Netherlands with controlled sedimentation?, *Proceedings of the International Association of Hydrological Sciences* 382, 767–773.

Kroon, A. and Hoekstra, P. (1990). Eolian sediment transport on a natural beach, *Journal of Coastal Research* pp. 367–379.

Leatherman, S. (1978). A new aeolian sand trap design, *Sedimentology* 25, 303–306.

Lekner, J. and Dorf, M. C. (1988). Why some things are darker when wet, *Applied Optics* 27, 1278–1280.

Lettau, K. (1978). Experimental and micrometeorological field studies of dune migration, *Exploring in the World's driest climate* pp. 110–147.

Leu, D. J. (1977). Visible and near–infrared reflectance of beach sands: A study on the spectral reflectance/grain size relationship, *Remote Sensing of Environment* 6, 169–182.

Lithgow, D., Martínez, M., Gallego-Fernández, J., Hesp, P., Flores, P., Gachuz, S., Rodríguez-Revelo, N., Jiménez-Orocio, O., Mendoza-González, G., and Álvarez-Molina, L. (2013). Linking restoration ecology with coastal dune restoration, *Geomorphology* 199, 214–224.

Lobell, D. and Asner, G. (2002). Moisture effects on soil reflectance, *Soil Science Society of America Journal* 66, 722–727.

Lu, D., Moran, E., and Batistella, M. (2003). Linear mixture model applied to Amazonian vegetation classification, *Remote sensing of environment* 87, 456–469.

Lucas, N. S., Shanmugam, S., and Barnsley, M. (2002). Sub-pixel habitat mapping of a costal dune ecosystem, *Applied Geography* 22, 253–270.

Luijendijk, A., Hagenaars, G., Ranasinghe, R., Baart, F., Donchyts, G., and Aarninkhof, S. (2018). The state of the world's beaches, *Scientific reports* 8, 1–11.

Luijendijk, A. P., Ranasinghe, R., de Schipper, M. A., Huisman, B. A., Swinkels, C. M., Walstra, D. J., and Stive, M. J. (2017). The initial morphological response of the Sand Engine: A process-based modelling

study, *Coastal engineering* 119, 1–14.

Lynch, K., Jackson, D. W., and Cooper, J. A. G. (2008). Aeolian fetch distance and secondary airflow effects: the influence of micro-scale variables on meso-scale foredune development, *Earth Surface Processes and Landforms* 33, 991–1005.

Mancini, F., Dubbini, M., Gattelli, M., Stecchi, F., Fabbri, S., and Gabbianelli, G. (2013). Using unmanned aerial vehicles (UAV) for high-resolution reconstruction of topography: the structure from motion approach on coastal environments, *Remote Sensing* 5, 6880–6898.

Marston, R. (1986). Maneuver-caused wind erosion impacts, south central New Mexico, *Aeolian geomorphology* pp. 273–290.

Martin, R. L. and Kok, J. F. (2017). Wind-invariant saltation heights imply linear scaling of aeolian saltation flux with shear stress, *Science Advances* 3, e1602 569.

Martin, R. L., Barchyn, T. E., Hugenholtz, C. H., and Jerolmack, D. J. (2013). Timescale dependence of aeolian sand flux observations under atmospheric turbulence, *Journal of Geophysical Research: Atmospheres* 118, 9078–9092.

Martínez, M. L., Intralawan, A., Vázquez, G., Pérez-Maqueo, O., Sutton, P., and Landgrave, R. (2007). The coasts of our world: Ecological, economic and social importance, *Ecological economics* 63, 254–272.

Maun, M. A. (1998). Adaptations of plants to burial in coastal sand dunes, *Canadian Journal of Botany* 76, 713–738.

Maun, M. A.: (2009). *The biology of coastal sand dunes*, Oxford University Press.

Maun, M. A. and Lapierre, J. (1984). The effects of burial by sand on Ammophila breviligulata, *The Journal of Ecology* pp. 827–839.

Maun, M. A. and Perumal, J. (1999). Zonation of vegetation on lacustrine coastal dunes: effects of burial by sand, *Ecology Letters* 2, 14–18.

McGranahan, G., Balk, D., and Anderson, B. (2007). The rising tide: assessing the risks of climate change and human settlements in low elevation coastal zones, *Environment and urbanization* 19, 17–37.

Mckenna Neuman, C. and Langston, G. (2003). Spatial analysis of surface moisture content on beaches subject to aeolian transport, in: Proceedings of the Canadian Coastal Conference 2003, pp. 15–17.

McKenna Neuman, C. and Langston, G. (2006). Measurement of water content as a control of particle entrainment by wind, *Earth Surface Processes and Landforms* 31, 303–317.

McKenna-Neuman, C. and Nickling, W. (1989). A theoretical and wind tunnel investigation of the effect of capillary water on the entrainment of sediment by wind, *Canadian Journal of Soil Science* 69, 79–96, cited By (since 1996)112.

Metzger, M., McKeon, B., and Holmes, H. (2007). The near-neutral atmospheric surface layer: turbulence and non-stationarity, *Philosophical Transactions of the Royal Society of London A: Mathematical, Physical and Engineering Sciences* 365, 859–876.

Meyer, P. (1994). Bi-logistic growth, *Technological forecasting and social change* 47, 89–102.

Meyer, P. S. and Ausubel, J. H. (1999). Carrying capacity: a model with logistically varying limits, *Technological forecasting and social change* 61, 209–214.

Montreuil, A.-L., Bullard, J. E., Chandler, J. H., and Millett, J. (2013). Decadal and seasonal development of embryo dunes on an accreting macrotidal beach: North Lincolnshire, UK, *Earth Surface Processes and Landforms* 38, 1851–1868.

Moore, L. J., Vinent, O. D., and Ruggiero, P. (2016). Vegetation control allows autocyclic formation of multiple dunes on prograding coasts, *Geology* 44, 559–562.

Mulder, J. P. and Tonnon, P. K. (2011). Sand Engine: Background and design of a mega-nourishment pilot in the Netherlands, *Coastal Engineering Proceedings* 1, 35.

Murray, J. D.: (2007). *Mathematical biology: I. An introduction*, vol. 17, Springer Science & Business Media.

Namikas, S., Edwards, B., Bitton, M., Booth, J., and Zhu, Y. (2010). Temporal and spatial variabilities in the surface moisture content of a fine-grained beach, *Geomorphology* 114, 303 – 310.

Namikas, S. L. (2003). Field measurement and numerical modelling of aeolian mass flux distributions on a sandy beach, *Sedimentology* 50, 303–326.

Namikas, S. L. and Sherman, D. J. (1995). A review of the effects of surface moisture content on aeolian sand transport, in: Desert Aeolian Processes, pp. 269–293, Springer.

Neuman, C. M. and Scott, M. M. (1998). A wind tunnel study of the influence of pore water on aeolian sediment transport, *Journal of Arid Environments* 39, 403–419.

Neumann, B., Vafeidis, A. T., Zimmermann, J., and Nicholls, R. J. (2015). Future coastal population growth and exposure to sea-level rise and coastal flooding-a global assessment, *PloS one* 10, e0118 571.

Nicholls, R. J. and Cazenave, A. (2010). Sea-level rise and its impact on coastal zones, *science* 328, 1517–1520.

Nickling, W. G. and Neuman, C. M. (2009). Aeolian sediment transport, in: Geomorphology of desert environments, pp. 517–555, Springer.

Nield, J. M. and Baas, A. C. W. (2008). The influence of different environmental and climatic conditions on vegetated aeolian dune landscape development and response, *Global and Planetary Change* 64, 76–92.

Nield, J. M. and Wiggs, G. F. (2011). The application of terrestrial laser scanning to aeolian saltation cloud measurement and its response to changing surface moisture, *Earth Surface Processes and Landforms* 36, 273–278.

Nield, J. M., Wiggs, G. F., and Squirrell, R. S. (2011). Aeolian sand strip mobility and protodune development on a drying beach: examining surface moisture and surface roughness patterns measured by terrestrial laser scanning, *Earth Surface Processes and Landforms* 36, 513–522.

Nield, J. M., King, J., and Jacobs, B. (2014). Detecting surface moisture in aeolian environments using terrestrial laser scanning, *Aeolian Research* 12, 9 – 17.

Nolet, C. and Riksen, M. J. (2019). Accommodation space indicates dune development potential along an urbanized and frequently nourished coastline, *Earth Surface Dynamics* 7, 129–145.

Nolet, C., Poortinga, A., Roosjen, P., Bartholomeus, H., and Ruessink, G. (2014). Measuring and modeling the effect of surface moisture on the spectral reflectance of coastal beach sand, *PloS one* 9, e112 151.

Nolet, C., van Puijenbroek, M., Suomalainen, J., Limpens, J., and Riksen, M. (2018). UAV-imaging to model growth response of marram grass to sand burial: Implications for coastal dune development, *Aeolian Research* 31, 50–61.

Nordstrom, K. F.: (2004). *Beaches and dunes of developed coasts*, Cambridge University Press.

Nordstrom, K. F. and McCluskey, J. M. (1984). Considerations for control of house construction in coastal dunes, *Coastal Management* 12, 385–402.

Oksanen, J. and Minchin, P. R. (2002). Continuum theory revisited: what shape are species responses along ecological gradients?, *Ecological Modelling* 157, 119–129.

Owen, P. R. (1964). Saltation of uniform grains in air, *Journal of Fluid Mechanics* 20, 225–242.

Peterson, C. H., Hickerson, D. H., and Johnson, G. G. (2000). Short-term consequences of nourishment and bulldozing on the dominant large invertebrates of a sandy beach, *Journal of Coastal Research* pp. 368–378.

Pettorelli, N., Vik, J. O., Mysterud, A., Gaillard, J.-M., Tucker, C. J., and Stenseth, N. C. (2005). Using the satellite-derived NDVI to assess ecological responses to environmental change, *Trends in ecology & evolution* 20, 503–510.

Philpot, W. (2010). Spectral Reflectance of Wetted Soils, *Proceedings of ASD and IEEE GRS; Art, Science and Applications of Reflectance Spectroscopy Symposium* Vol II, 11pp.

Poortinga, A., Visser, S. M., Riksen, M. J., and Stroosnijder, L. (2011). Beneficial effects of wind erosion:

Concepts, measurements and modeling, *Aeolian Research* 3, 81–86.

Poortinga, A., Van Minnen, J., Keijsers, J., Riksen, M., Goossens, D., and Seeger, M. (2013). Measuring fast-temporal sediment fluxes with an analogue acoustic sensor: a wind tunnel study, *PloS one* 8, e74 007.

Poortinga, A., Keijsers, J. G., Maroulis, J., and Visser, S. M. (2014). Measurement uncertainties in quantifying aeolian mass flux: evidence from wind tunnel and field site data, *PeerJ* 2, e454, doi: 10.7717/peerj.454.

Poortinga, A., Keijsers, J. G. S., Visser, S. M., Riksen, M. J. P. M., and Baas, A. C. W. (2015a). Temporal and spatial variability in event scale aeolian transport on Ameland, The Netherlands, *GeoResJ* 5, 23–35.

Poortinga, A., van Rheenen, H., Ellis, J. T., and Sherman, D. J. (2015b). Measuring aeolian sand transport using acoustic sensors, *Aeolian Research* 16, 143–151.

Pope, R. and Fry, E. (1997). Absorption spectrum (380-700 nm) of pure water. II. Integrating cavity measurements, *Applied Optics* 36, 8710–8723.

Provoost, S., Jones, M. L. M., and Edmondson, S. E. (2011). Changes in landscape and vegetation of coastal dunes in northwest Europe: a review, *Journal of Coastal Conservation* 15, 207–226.

Psuty, N. P. (1988). Sediment budget and dune/beach interaction, *Journal of Coastal Research* pp. 1–4.

R Core Team (2012). *R: A Language and Environment for Statistical Computing*, R Foundation for Statistical Computing, Vienna, Austria, URL `http://www.R-project.org/`, ISBN 3-900051-07-0.

Radermacher, M., De Schipper, M., Price, T., Huisman, B., Aarninkhof, S., and Reniers, A. (2018). Behaviour of subtidal sandbars in response to nourishments, *Geomorphology* 313, 1–12.

Ranwell, D. S.: (1972). *Ecology of salt marshes and sand dunes*, vol. 258, Chapman and Hall London.

Raupach, M. (1992). Drag and drag partition on rough surfaces, *Boundary-Layer Meteorology* 60, 375–395.

Rietkerk, M., Boerlijst, M. C., van Langevelde, F., HilleRisLambers, R., de Koppel, J. v., Kumar, L., Prins, H. H., and de Roos, A. M. (2002). Self-organization of vegetation in arid ecosystems, *The American Naturalist* 160, 524–530.

Riksen, M. J., Goossens, D., Huiskes, H. P., Krol, J., and Slim, P. A. (2016). Constructing notches in foredunes: Effect on sediment dynamics in the dune hinterland, *Geomorphology* 253, 340–352.

Roelvink, D., Reniers, A., Van Dongeren, A., De Vries, J. V. T., McCall, R., and Lescinski, J. (2009). Modelling storm impacts on beaches, dunes and barrier islands, *Coastal engineering* 56, 1133–1152.

Roosjen, P. P., Clevers, J. G., Bartholomeus, H. M., Schaepman, M. E., Schaepman-Strub, G., Jalink, H., Van Der Schoor, R., and De Jong, A. (2012). A Laboratory Goniometer System for Measuring Reflectance and Emittance Anisotropy, *Sensors* 12, 17 358–17 371.

Rosen, P. (1978). An efficient, low cost, aeolian sampling system, *Geological Survey of Canada, Current Research, Part A* 78, 531–532.

Rouse Jr, J. W., Haas, R. H., Schell, J. A., and Deering, D. W. (1974). Monitoring vegetation systems in the Great Plains with ERTS, *NASA special publication* 351, 309.

Ruessink, B., Arens, S., Kuipers, M., and Donker, J. (2018). Coastal dune dynamics in response to excavated foredune notches, *Aeolian Research* 31, 3–17.

Ruessink, G., Brakenhoff, L., and Van Maarseveen, M. (2014). Measurement of surface moisture using infra-red terrestrial laser scanning, in: Geophysical Research Abstracts, Vol. 16, EGU2014-2797.

Ruggiero, P., Komar, P. D., McDougal, W. G., Marra, J. J., and Beach, R. A. (2001). Wave runup, extreme water levels and the erosion of properties backing beaches, *Journal of Coastal Research* pp. 407–419.

Sallenger Jr, A. H. (2000). Storm impact scale for barrier islands, *Journal of Coastal Research* pp. 890–895.

Sarre, R. (1988). Evaluation of aeolian sand transport equations using intertidal zone measurements, Saunton Sands, England, *Sedimentology* 35, 671–679.

Sarre, R. (1989a). The morphological significance of vegetation and relief on coastal foredune processes,

Zeitschrift für Geomorphologie. Supplementband 73, 17–31.

Sarre, R. D. (1989b). Aeolian sand drift from the intertidal zone on a temperate beach: potential and actual rates, *Earth Surface Processes and Landforms* 14, 247–258.

Sauermann, G., Kroy, K., and Herrmann, H. J. (2001). Continuum saltation model for sand dunes, *Physical Review E* 64, 031 305.

Schröder, H. K., Andersen, H. E., and Kiehl, K. (2005). Rejecting the mean: Estimating the response of fen plant species to environmental factors by non-linear quantile regression, *Journal of Vegetation Science* 16, 373–382.

Segelstein, D. (1981). *The complex refractive index of water*, Master's thesis, University of Missouri, Kansas City.

Settle, J. and Drake, N. (1993). Linear mixing and the estimation of ground cover proportions, *International Journal of Remote Sensing* 14, 1159–1177.

Shao, Y. and Raupach, M. (1992). The overshoot and equilibration of saltation, *Journal of Geophysical Research: Atmospheres* 97, 20 559–20 564.

Shelford, V. E. (1931). Some concepts of bioecology, *Ecology* 12, 455–467.

Sherman, D. J. (1995). Problems of scale in the modeling and interpretation of coastal dunes, *Marine Geology* 124, 339–349.

Sherman, D. J. and Bauer, B. O. (1993). Dynamics of beach-dune systems, *Progress in Physical Geography* 17, 413–447.

Sherman, D. J. and Li, B. (2012). Predicting aeolian sand transport rates: A reevaluation of models, *Aeolian Research* 3, 371–378.

Sherman, D. J., Jackson, D. W., Namikas, S. L., and Wang, J. (1998). Wind-blown sand on beaches: an evaluation of models, *Geomorphology* 22, 113–133.

Sherman, D. J., Li, B., Farrell, E. J., Ellis, J. T., Cox, W. D., Maia, L. P., and Sousa, P. H. (2011). Measuring aeolian saltation: a comparison of sensors, *Journal of Coastal Research* pp. 280–290.

Short, A. and Hesp, P. (1982). Wave, beach and dune interactions in southeastern Australia, *Marine geology* 48, 259–284.

Shuchman, R. A. and Rea, D. K. (1981). Determination of beach sand parameters using remotely sensed aircraft reflectance data, *Remote Sensing of Environment* 11, 295–310.

Skidmore, E., Dickerson, J., and Schimmelpfennig, H. (1975). Evaluating surface-soil water content by measuring reflectance, *Soil Science Society of America Journal* 39, 238–242.

Smith, M. O., Johnson, P. E., and Adams, J. B. (1985). Quantitative determination of mineral types and abundances from reflectance spectra using principal components analysis, *Journal of Geophysical Research: Solid Earth* 90.

Solomon, S.: (2007). *Climate change 2007-the physical science basis: Working group I contribution to the fourth assessment report of the IPCC*, vol. 4, Cambridge University Press.

Speybroeck, J., Bonte, D., Courtens, W., Gheskiere, T., Grootaert, P., Maelfait, J.-P., Mathys, M., Provoost, S., Sabbe, K., Stienen, E. W., et al. (2006). Beach nourishment: an ecologically sound coastal defence alternative? A review, *Aquatic conservation: Marine and Freshwater ecosystems* 16, 419–435.

Sterk, G., Jacobs, A., Boxel, J., et al. (1998). The effect of turbulent flow structures on saltation sand transport in the atmospheric boundary layer, *Earth Surface Processes and Landforms* 23, 877–887.

Stive, M. J., de Schipper, M. A., Luijendijk, A. P., Aarninkhof, S. G., van Gelder-Maas, C., van Thiel de Vries, J. S., de Vries, S., Henriquez, M., Marx, S., and Ranasinghe, R. (2013a). A New Alternative to Saving Our Beaches from Sea-Level Rise: The Sand Engine, *Journal of Coastal Research* 29, 1001–1008.

Stive, M. J., De Schipper, M. A., Luijendijk, A. P., Aarninkhof, S. G. J., Van Gelder-Maas, C., Van Thiel de

Vries, J. S. M., de Vries, S., Henriquez, M., Marx, S., and Ranasinghe, R. (2013b). A new alternative to saving our beaches from sea-level rise: The sand engine, *Journal of Coastal Research* 29, 1001–1008.

Stockdon, H. F., Holman, R. A., Howd, P. A., and Sallenger Jr, A. H. (2006). Empirical parameterization of setup, swash, and runup, *Coastal engineering* 53, 573–588.

Stout, J. and Zobeck, T. (1997). Intermittent saltation, *Sedimentology* 44, 959–970.

Stout, J. E. (1998). Effect of averaging time on the apparent threshold for aeolian transport, *Journal of Arid Environments* 39, 395–401.

Stronkhorst, J., Huisman, B., Giardino, A., Santinelli, G., and Santos, F. D. (2018). Sand nourishment strategies to mitigate coastal erosion and sea level rise at the coasts of Holland (The Netherlands) and Aveiro (Portugal) in the 21st century, *Ocean & Coastal Management* 156, 266–276.

Suanez, S., Cariolet, J.-M., Cancouët, R., Ardhuin, F., and Delacourt, C. (2012). Dune recovery after storm erosion on a high-energy beach: Vougot Beach, Brittany (France), *Geomorphology* 139, 16–33.

Suomalainen, J., Anders, N., Iqbal, S., Roerink, G., Franke, J., Wenting, P., Hünniger, D., Bartholomeus, H., Becker, R., and Kooistra, L. (2014). A lightweight hyperspectral mapping system and photogrammetric processing chain for unmanned aerial vehicles, *Remote Sensing* 6, 11 013–11 030.

Temmerman, S., Meire, P., Bouma, T. J., Herman, P. M. J., Ysebaert, T., and De Vriend, H. J. (2013). Ecosystem-based coastal defence in the face of global change, *Nature* 504, 79–83.

Ter Braak, C. J. F. and Looman, C. W. N. (1986). Weighted averaging, logistic regression and the Gaussian response model, *Vegetatio* 65, 3–11.

Ter Braak, C. J. F. and Prentice, I. C. (1988). A theory of gradient analysis, *Advances in ecological research* 18, 271–317.

Tester, M. and Morris, C. (1987). The penetration of light through soil, *Plant, Cell & Environment* 10, 281–286.

Theseira, M., Thomas, G., Taylor, J., Gemmell, F., and Varjo, J. (2003). Sensitivity of mixture modelling to end-member selection, *International Journal of Remote Sensing* 24, 1559–1575.

Thomson, J. D., Weiblen, G., Thomson, B. A., Alfaro, S., and Legendre, P. (1996). Untangling multiple factors in spatial distributions: lilies, gophers, and rocks, *Ecology* 77, 1698–1715.

Tucker, C. J. (1979). Red and photographic infrared linear combinations for monitoring vegetation, *Remote sensing of Environment* 8, 127–150.

Ungar, J. and Haff, P. (1987). Steady state saltation in air, *Sedimentology* 34, 289–299.

Van Boxel, J., Arens, S., and Van Dijk, P. v. (1999). Aeolian processes across transverse dunes. I: Modelling the air flow, *Earth Surface Processes and Landforms: The Journal of the British Geomorphological Research Group* 24, 255–270.

Van der Meulen, F., Van der Valk, B., Baars, L., Schoor, E., and Van Woerden, H. (2014). Development of new dunes in the Dutch Delta: nature compensation and 'building with nature', *Journal of coastal conservation* 18, 505–513.

Van der Putten, W. H., Van Dijk, C., and Troelstra, S. R. (1988). Biotic soil factors affecting the growth and development of Ammophila arenaria, *Oecologia* 76, 313–320.

Van der Putten, W. H., Van Dijk, C., and Peters, B. A. M. (1993). Plant-specific soil-borne diseases contribute to succession in foredune vegetation, *Nature* 362, 53–56.

Van der Wal, D. (2004). Beach-dune interactions in nourishment areas along the Dutch coast, *Journal of Coastal Research* pp. 317–325.

Van der Weerd, A. J. and Wijnberg, K. M. (2016). Aeolian sediment flux derived from a natural sand trap, *Journal of coastal research* 75, 338–342.

van Dorp, D., Boot, R., and van der Maarel, E. (1985). Vegetation succession on the dunes near Oostvoorne,

The Netherlands, since 1934, interpreted from air photographs and vegetation maps, *Vegetatio* 58, 123–136.

Van Duin, M., Wiersma, N., Walstra, D., Van Rijn, L., and Stive, M. (2004). Nourishing the shoreface: observations and hindcasting of the Egmond case, The Netherlands, *Coastal Engineering* 51, 813–837.

Van Egmond, E. M., van Bodegom, P. M., Berg, M. P., Wijsman, J. W., Leewis, L., Janssen, G. M., and Aerts, R. (2018). A mega-nourishment creates novel habitat for intertidal macroinvertebrates by enhancing habitat relief of the sandy beach, *Estuarine, Coastal and Shelf Science* 207, 232–241.

Van Genuchten, M. T. (1980). A closed-form equation for predicting the hydraulic conductivity of unsaturated soils, *Soil Science Society of America Journal* 44, 892–898.

Van Koningsveld, M. and Mulder, J. P. M. (2004). Sustainable coastal policy developments in the Netherlands. A systematic approach revealed, *Journal of Coastal Research* pp. 375–385.

Van Koningsveld, M., Otten, C., Mulder, J., et al. (2007). Dunes: the Netherlands soft but secure sea defences, in: Proceedings 18th World dredging congress, Florida USA, WODA.

Van Puijenbroek, M. E. (2017). *Dunes, above and beyond*, Ph.D. thesis, Wageningen University.

Van Puijenbroek, M. E., Limpens, J., de Groot, A. V., Riksen, M. J., Gleichman, M., Slim, P. A., van Dobben, H. F., and Berendse, F. (2017a). Embryo dune development drivers: beach morphology, growing season precipitation, and storms, *Earth Surface Processes and Landforms* 42, 1733–1744.

Van Puijenbroek, M. E., Nolet, C., De Groot, A. V., Suomalainen, J. M., Riksen, M. J., Berendse, F., and Limpens, J. (2017b). Exploring the contributions of vegetation and dune size to early dune development using unmanned aerial vehicle (UAV) imaging, *Biogeosciences* 14, 5533.

Van Rijn, L. C. (1997). Sediment transport and budget of the central coastal zone of Holland, *Coastal Engineering* 32, 61–90.

Van Slobbe, E., De Vriend, H., Aarninkhof, S., Lulofs, K., De Vries, M., and Dircke, P. (2013). Building with Nature: in search of resilient storm surge protection strategies, *Natural hazards* 66, 1461–1480.

Vellinga, P. (1982). Beach and dune erosion during storm surges, *Coastal Engineering* 6, 361–387.

Vergiev, S., Filipova-Marinova, M., Trifonova, E., Kotsev, I., and Pavlov, D. (2013). The impact of sea water immersion on the viability of psammophilous species Leymus racemosus subsp. sabulosus and Ammophila arenaria, *CR Acad Bulg Sci* 66, 212–216.

Verhulst, P.-F. c c. o. (1838). Notice on the law that the population follows in its growth, *Corresp. Math. Phys.* 10, 113–126.

Vinent, O. D. and Moore, L. J. (2015). Barrier island bistability induced by biophysical interactions, *Nature Climate Change* 5, 158–162.

Von Kármán, T. (1930). Mechanische ahnlichkeit und turbulenz, *Math.-Phys. Klasse* .

Wal, A. and McManus, J. (1993). Wind regime and sand transport on a coastal beach-dune complex, Tentsmuir, eastern Scotland, *Geological Society, London, Special Publications* 72, 159–171.

Webb, N. P., Okin, G. S., and Brown, S. (2014). The effect of roughness elements on wind erosion: The importance of surface shear stress distribution, *Journal of Geophysical Research: Atmospheres* 119, 6066–6084.

Weidong, L., Baret, F., Xingfa, G., Qingxi, T., Lanfen, Z., and Bing, Z. (2002). Relating soil surface moisture to reflectance, *Remote sensing of environment* 81, 238–246.

Werner, B. (1990). A steady-state model of wind-blown sand transport, *The Journal of Geology* 98, 1–17.

Werner, B. and Fink, T. (1993). Beach cusps as self-organized patterns, *Science* 260, 968–971.

Wesseling, J. G., Ritsema, C. J., Stolte, J., Oostindie, K., and Dekker, L. W. (2008). Describing the soil physical characteristics of soil samples with cubical splines, *Transport in Porous Media* 71, 289–309.

Westoby, M. J., Brasington, J., Glasser, N. F., Hambrey, M. J., and Reynolds, J. M. (2012). 'Structure-from-Motion' photogrammetry: A low-cost, effective tool for geoscience applications, *Geomorphology* 179,

300–314.

White, B. R. (1979). Soil transport by winds on Mars, *Journal of Geophysical Research: Solid Earth* 84, 4643–4651.

Wiggs, G., Baird, A., and Atherton, R. (2004). The dynamic effects of moisture on the entrainment and transport of sand by wind, *Geomorphology* 59, 13 – 30.

Wolman, M. G. and Miller, J. P. (1960). Magnitude and frequency of forces in geomorphic processes, *The Journal of Geology* 68, 54–74.

Wong, P. P., Losada, I. J., Gattuso, J.-P., Hinkel, J., Khattabi, A., McInnes, K. L., Saito, Y., Sallenger, A., et al. (2014). Coastal systems and low-lying areas, *Climate change* 2104, 361–409.

Wosten, J. and Van Genuchten, M. T. (1988). Using texture and other soil properties to predict the unsaturated soil hydraulic functions, *Soil Science Society of America Journal* 52, 1762–1770.

Wösten, J., Veerman, G., De Groot, W., and Stolte, J. (2001). Water retention and permeability characteristics of top and sub soils in the Netherlands: the Staring series, *Alterra, Wageningen* .

Yang, Y. and Davidson-Arnott, R. (2005). Rapid measurement of surface moisture content on a beach, *Journal of Coastal Research* 21, 447–452.

Yu, K., Lu, Z., and Stander, J. (2003). Quantile regression: applications and current research areas, *Journal of the Royal Statistical Society: Series D (The Statistician)* 52, 331–350.

Yuan, T., Maun, M., and Hopkins, W. G. (1993). Effects of sand accretion on photosynthesis, leaf-water potential and morphology of two dune grasses, *Functional Ecology* pp. 676–682.

Zarnetske, P. L., Hacker, S. D., Seabloom, E. W., Ruggiero, P., Killian, J. R., Maddux, T. B., and Cox, D. (2012). Biophysical feedback mediates effects of invasive grasses on coastal dune shape, *Ecology* 93, 1439–1450.

Zhang, L. and Baas, A. C. (2012). Mapping functional vegetation abundance in a coastal dune environment using a combination of LSMA and MLC: a case study at Kenfig NNR, Wales, *International journal of remote sensing* 33, 5043–5071.

Zhang, X. and Church, J. A. (2012). Sea level trends, interannual and decadal variability in the Pacific Ocean, *Geophysical Research Letters* 39.

Zingg, A. (1953). Wind tunnel studies of the movement of sedimentary material, in: Proceedings of the 5th Hydraulic Conference Bulletin, vol. 34, pp. 111–135.

Summary

Due to sea level rise, low-lying coastal zones across the globe are increasingly confronted with adverse impacts related to climate change, such as coastal erosion due to flooding and inundation or permanent submergence of previously subaerial land. The Netherlands is situated in the Rhine-Meuse delta along the North Sea coast, and about half of its approximately 500 km long sandy coastline is subject to structural marine erosion. With 26% of its surface area well below mean sea level, the Netherlands is particularly susceptible to large scale flooding, making flood risk management and adaptation policy to sea level rise essential for its existence. The focus of Dutch coastal policy has traditionally been on safety from flooding, but nowadays the focus has widened to also include preserving the spatial quality and natural values of the coastal zone. It was recognized that the beach and dunes, apart from flood defense, represent unique ecological and recreational values and often serve as an important source for drinking water supply. By acknowledging sand as 'the carrier of all coastal functions' the principal management practice since 1990 has been to nourish the coastline with sand whenever it was about to retreat beyond a defined reference position. A key component of such a dynamic preservation of the coastline involves utilizing natural processes to further redistribute the sand. By allowing marine and aeolian forces to gradually help shape the coastline, the aim of this building-with-nature engineering strategy is to counteract a negative sediment balance while minimizing adverse effects to the coastal ecosystem.

Dutch coastal safety policy in particular prioritizes creating favorable conditions for natural dune development, as over 75% of the Dutch coastline relies on its vegetated foredunes (the most seaward facing dune ridge parallel to the coastline) for flood defense against the sea. Coastal dunes are formed through a complex interaction between wind, waves, sand and vegetation and have the capacity (1) to reduce hydrodynamic impact from storm surges and (2) to keep up with sea-level rise by accumulating and stabilizing wind-blown sand. An essential element to coastal building-with-nature in the Netherlands is the utilization of European marram grass (*Ammophila arenaria*) to help stabilize and build up the foredunes. Compared to other (native) coastal pioneers that thrive on sandy soils, this beach grass is most effective at dune building because not only can it trap high amounts of wind-blown sand between its leaves and keep it in place within its roots, but it will in fact grow much more vigorously because of regular burial in sand. This introduces a reinforcing biogeomorphic feedback crucial to coastal dune development: trapping of wind-blown sand encourages marram grass to grow, which in turn enhances the capacity of marram grass to trap sand and build dunes.

Because of rising sea levels, the annual average sand nourishment volumes on the Dutch coast have increased from 0.4 M m^3 during the period 1952 until 1990, to 2.5 M m^3 between 1991 and 2000, and from 5 to approximately 12 M m^3 between 2001 until now, at an annual cost of around 25 million euro. Though, as sea level rise accelerates, it is anticipated that sand nourishments need to increase in volume or frequency to combat erosion and maintain the sandy coast. Within this context, an unprecedented mega-scale beach nourishment of 21.5 Mm^3 termed *Zandmotor* (or 'Sand Motor'), was constructed in 2011 along the Delfland coast just south of the city The Hague. The overall purpose of this mega-nourishment experiment is to test whether its benefits in terms if coastal safety, spatial quality and ecological values outweigh the extra costs involved and to determine to what extent such an approach can help cope with expected changes in the global climate. The *Zandmotor* has a hook-shaped design that aims to mirror the natural onshore migration of an intertidal sandbar. In line with the building-with-nature approach, natural dynamics are encouraged to redistribute the sand of the *Zandmotor* along the coastline, thereby broadening the adjacent foredunes and beach. However, because of its novel and experimental nature, the long-term effects of such a mega-scale beach nourishment on dune-building dynamics is unknown. The locally very high construction height (up to 7 m a.m.s.l.) in particular sets the *Zandmotor* apart from more traditionally nourished or natural coastlines.

This objective of this research is to provide field-based evidence and insight into how reinforcing biogeomorphic feedback drives dune development, on the *Zandmotor* and along nourished coastlines in general. A good insight into prevailing coastal aeolian dynamics is hereto essential, as wind-blown sand exerts direct control on foredune development. This insight, however, is challenged by a high degree of uncertainty in characterizing aeolian transport dynamics in coastal environments. This is foremost due to a lack of consensus about whether steady-state saltation (the principal mode of transport) is best described by a quadratic or cubic dependence to wind shear velocity (expression for the erosive force of the wind). But the saltation mass flux may often also not be in steady-state due to unsteady wind conditions or not be saturated to expected capacity due to meteorological and surficial conditions that limit the supply of sand to the aeolian transport system. Surface moisture, in particular, greatly increases the resistance of sand to entrainment, by binding sand grains together through cohesive and adhesive forces. While considerable effort has been undertaken to parameterize saltation equations to coastal environments, the spatial-temporal complexity of surface moisture and numerous other supply-limiting factors (e.g. beach armoring, cementation, shell layers) have been shown to significantly hamper their predictive quality.

Accurate and synchronous empirical measurements of aeolian sand transport and wind-forcing in coastal field experiments are very challenging to obtain. As a result, long-term continuous records of aeolian transport rates are not readily available. The challenge is to combine the advantages of passive trapping methods, i.e. direct measurement and long-term deployment, with the advantages of active sensor-based methods, i.e. automated operation at (very) high temporal resolutions. If accurate estimates of aeolian transport rates and subsequent estimates of available sand supply for dune building on the *Zandmotor* cannot be given, adequate predictions of dune development are also not possible. Moreover, relatively little empirical data are available on the mutually reinforcing dune-building interaction between marram grass

and sand deposition. Positive geomorphic feedback between the growth response of marram grass and burial by wind-blown sand is well documented and recognized to be fundamental to coastal dune development in temperate regions around the world. Field data, however, on plant response to sand burial, optimal and maximum burial levels and the capacity to deal with adverse conditions, are scarce. As a result, studies that model coastal dune development by incorporating positive feedback may be hampered by burial response growth functions that are not validated by empirical measurement.

It was examined to what extent the *Zandmotor* has contributed to creating accommodation space favorable for dune development, i.e. available space that is sheltered from frequent storm impacts and experiencing a steady accumulation of wind-blown sand. Compared to the rest of the Delfland coast, the supratidal beach of the *Zandmotor* provides very wide favorable accommodation space and therefore especially supports a high potential for new embryo dunes to develop. Comparing changes in dune cover by marram grass (from 2016 to 2017) to the average yearly change in dune height (between 2013 and 2017) revealed that dunes were almost exclusively present in accreting areas. This demonstrates the significance of positive biogeomorphic feedback in steering dune development. As such, even though its high construction height may not be optimal for successful marram grass establishment, the results highlight the overall importance of the *Zandmotor* to dune development potential. Because of persistent anthropogenic disturbances arising from recreation as well as nature management practices, however, dune development along this urbanized coastline may not reach its full potential.

Using a newly developed automated sand trap in conjunction with detailed wind forcing measurements, a synchronous long-term record of saltation mass flux and shear velocity measurements has been constructed. Nonlinear quantile regression analysis indicates that the saltation mass flux may be better explained by a quadratic than a cubic dependence to shear velocity. Regression parameters obtained at the upper part of the response distribution are in line with parameters employed by the quadratic function of Kok et al. (2012), yielding more consistent saltation rates than predicted by the cubic function of Kawamura (1951). Fitting the quadratic and cubic function to the median response distribution indicates that saltation rates generated in (nourished) coastal environments may typically be two (for quadratic dependence) or three (for cubic dependence) orders of magnitude lower than predicted by transport equations of parameterized during wind tunnel experiments. The under-prediction of the saltation mass flux decreases when the quadratic and cubic functions are fitted to the observations made under optimal field conditions, but the still lower observed saltation rates indicate that coastal aeolian dynamics on the *Zandmotor* may be characterized by a persistent impact of supply-limiting conditions. Parameterizing the flux scaling parameter C of the quadratic and cubic saltation flux equations provides a measure to account for the overall impact of limiting factors, which can help ensue more realistic saltation mass flux predictions that are better applicable to conditions encountered on the *Zandmotor* and along nourished coastlines in general.

To improve the applicability of aeolian transport equations to the coastal environment it is critical to account for the control of surface moisture. An approach to accomplish this is by making the threshold shear velocity dependent on surface moisture conditions. It was shown

that, at particular wavelengths, optical remote sensing can be utilized to derive spatially extensive surface moisture maps with a high accuracy. The effect of surface moisture on spectral reflectance of coastal beach sand can be described by an optical as well as a soil physical model. The first model is grounded in optics and describes the proportional contribution of scattering and absorption of light by pore water in an unsaturated sand matrix. The second model is grounded in soil physics and links the hydraulic behavior of pore water in an unsaturated sand matrix to its optical properties. Near- and short-wave infrared wavelengths are most effective for relating surface moisture content to reflectance due to strong absorption of light in water, in particular at water absorption peaks of 1470 and 1940 nm. But, because of strong absorption by the atmosphere, an active remote sensing technique is required at these wavelengths. This research shows that a terrestrial laser scanner operating at $\lambda = 1550$ nm is capable of deriving accurate surface moisture maps at high spatio-temporal resolutions, which can help provide better insight into the control of surface moisture on coastal aeolian dynamics.

European marram grass (*Ammophila arenaria*) possesses two traits that are uniquely advantageous to dune-building: (1) a very high tolerance to burial by wind-blown sand, and (2) more vigorous growth due to positive feedback to sand burial. Using high-resolution geospatial data (i.e. elevation models and near-infrared imagery) acquired with an unmanned aerial vehicle (UAV) and nonlinear quantile regression analysis, it is demonstrated that the growth response of marram grass to sand burial by wind, expressed by changes in Normalized Difference Vegetation Index (Δ NDVI) and vegetation cover (Δ Cover), can be described by a Gaussian response model. The regression curves indicate an optimal burial rate for marram grass of 0.31 meter of sand per growing season, and suggest (by extrapolation of the data) a maximum burial tolerance between 0.78 and 0.96 meter of sand per growing season. The growth response parameters found in this research are specific to the *Zandmotor* and are likely not generically applicable to describe growth response of marram grass to sand burial by wind. The parameters may, however, be representative for many of the dunes found along the Dutch coastline, as the deposition rates on which the function parameters are based were representative for Dutch nourished coasts.

During this research, empirical measurements of aeolian transport and foredune evolution have been obtained synchronously, such that it has been possible to directly relate aeolian transport to coastal dune development. Sand budget analysis showed that typically only a small amount of sand blown towards the foredunes along the *Zandmotor* is deposited persistently and thus made available for dune development. The highest amount of deposition occurred around the seaward facing vegetation boundary of marram grass, highlighting the importance of marram grass accumulate and stabilize wind-blown sand. While positive biogeomorphic feedback between marram grass and aeolian dynamics may ultimately be the most important driver for coastal dune development, it is often also the least considered component of the coastal aeolian transport-dune system. Putting more focus on the dune-building capacity of marram grass is advantageous to coastal management in the Netherlands: dune development is directly related to the growth response of marram grass to sand burial, thus maximizing the potential of marram grass to grow maximizes the potential of coastal dunes to develop and provide coastal safety.

Samenvatting

Als gevolg van de stijging van de zeespiegel worden kustgebieden over de hele wereld in toenemende mate geconfronteerd met nadelige gevolgen van klimaatverandering, met kusterosie door stormvloeden of permanente inundatie van laaggelegen land als gevolg. Nederland maakt deel uit van de Rijn-Maasdelta langs de Noordzeekust. De helft van de ongeveer 500 km lange zandige kustlijn is onderhevig aan structurele mariene erosie. En omdat een kwart van het landoppervlak onder zeeniveau ligt, is Nederland bijzonder blootgesteld aan grootschalige overstromingen. Overstromingsrisico beheer en aanpassingsbeleid aan de zeespiegelstijging zijn daarom essentiële onderdelen van Nederlands water- en kustbeleid. De focus van het kustbeleid lag van oudsher op veiligheidsgarantie tegen overstromingen, maar tegenwoordig is de focus verbreed naar het behoud van de ruimtelijke kwaliteit en natuurwaarden van de kustzone. Het wordt tegenwoordig breed erkend dat strand en duinen, naast waterkering, ook unieke ecologische en recreatieve waarden vertegenwoordigen en als een belangrijke bron voor drinkwatervoorziening dienen. Door zand te aan te wijzen als 'de drager van alle kustfuncties', richt het kustbeleid zich sinds 1990 voornamelijk op het suppleren van de kustlijn met zand wanneer deze gaat afwijken van een bepaalde referentie positie. Een belangrijk onderdeel van een dergelijk dynamisch behoud van de kustlijn, is het gebruik van natuurlijke processen om het zand verder te herverdelen langs de kust. Door gebruik te maken van mariene en eolische processen om geleidelijk de kustlijn te vormen, is het doel van deze bouwen-met-natuur strategie om een negatieve zandbalans tegen te gaan en de nadelige effecten voor het kust-ecosysteem te minimaliseren.

Het Nederlandse kustbeleid geeft prioriteit aan het creëren van gunstige omstandigheden voor natuurlijke duinontwikkeling, aangezien meer dan 75 % van de Nederlandse kustlijn vertrouwt op de voorduinen (de meest zeewaartse duinrug parallel aan de kustlijn) als belangrijkste bescherming tegen de zee. Kustduinen worden gevormd door een complexe interactie tussen wind, golven, zand en vegetatie en hebben de capaciteit om (1) de hydrodynamische impact van stormvloeden te verminderen en om (2) mee te groeien met de zeespiegelstijging door continue stuivend zand in te vangen en te stabiliseren. De eigenschap van Nederlandse voorduinen om stuivend zand in te vangen en te stabiliseren wordt vooral mogelijk gemaakt door Europees helmgras (*Ammophila arenaria*). Dit strandgras is een zeer effectieve duinbouwer: het kan niet alleen grote hoeveelheden stuivend zand invangen en vasthouden met zijn dicht opeengepakte bladeren en lange wortelstelsels, het gaat ook veel krachtiger groeien wanneer het regelmatig bedolven wordt door stuivend zand. Dit introduceert een zelfversterkende bio-geomorfologische feedback die cruciaal is voor de ontwikkeling van kustduinen: het invangen van stuivend zand

stimuleert helmgras om te groeien, wat op zijn beurt het vermogen vergroot van helmgras om zand in te vangen en duinen te bouwen.

Door zeespiegelstijging zijn de jaarlijkse gemiddelde zandsuppletievolumes aan de Nederlandse kust gestegen van 0,4 Mm^3 in de periode 1952 tot 1990 tot 2,5 Mm^3 tussen 1991 en 2000, en van 5 tot ongeveer 12 Mm^3 tussen 2001 tot nu, tegen jaarlijkse kosten van ongeveer 25 miljoen euro. De verwachting is, naarmate de zeespiegelstijging versnelt, dat zandsuppleties in volume of frequentie gaan toenemen om erosie tegen te gaan en de zandige kustlijn in stand te houden. In dit kader is in 2011 net ten zuiden van Den Haag een ongekend grote zandsuppletie van 21,5 Mm^3 aangelegd. Het algemene doel van dit megasuppletie-experiment, genaamd de Zandmotor, is om te testen of de baten in termen van kustveiligheid, ruimtelijke kwaliteit en natuurwaarden, opwegen tegen de extra kosten die ermee gemoeid zijn. Daarnaast is het doel ook om te bepalen in hoeverre een dergelijke aanpak kan helpen bij het opvangen van verwachte veranderingen in het klimaat. De Zandmotor heeft een haakvormig ontwerp dat de natuurlijke landwaartse migratie een intergetijde zandbank moet nabootsten. In lijn met de bouwen-met-natuur benadering worden natuurlijke transport processen toegelaten om het zand van de Zandmotor langs de kustlijn verder te verdelen en zo de aangrenzende voorduinen en strand te verbreden. Vanwege het nieuwe en experimentele karakter zijn de langetermijneffecten van een dergelijke megasuppletie op de dynamiek van kustduinen echter onbekend. Vooral door de lokaal zeer hoge topografie (tot 7 m boven de zeespiegel) onderscheidt de Zandmotor van meer traditioneel gevoede of natuurlijke kusten.

Het doel van dit onderzoek is om inzicht te verschaffen in hoe duinontwikkeling, op de Zandmotor en langs suppleerde kustlijnen, wordt gestimuleerd door de zelfversterkende bio-geomorfologische terugkoppeling (*positieve feedback*) tussen eolisch zandtransport en de groeireactie van Europees helmgras op stuivend zand. Een goed inzicht in de heersende eolische dynamiek aan de kust is hierbij essentieel, aangezien zonder aanbod van stuivend zand de voorduinen zich niet kunnen ontwikkelen. Dit inzicht wordt echter uitgedaagd door een hoge mate van onzekerheid in het karakteriseren van eolische transportdynamiek in kustgebieden. Dit komt in de eerste plaats door een gebrek aan consensus of saltatie, de dominante vorm van zandtransport door de wind, het best kan worden beschreven door een kwadratische of kubische afhankelijkheid van de schuifsnelheid van de wind. Schuifsnelheid is de windsnelheid net boven de grond, wat gebruikt wordt om de erosieve kracht van de wind uit te drukken. Maar daarnaast zijn eolische zandtransport processen vaak ook erg instabiel vanwege het turbulente karakter van de wind en wordt de beschikbaarheid van zand om te gaan stuiven vaak beperkt door ongunstige meteorologische condities en/of omgevingsfactoren. Natte stranden in het bijzonder verhogen de weerstand van zand om te gaan stuiven aanzienlijk, omdat zandkorrels door cohesieve en adhesieve krachten aan elkaar worden gebonden. Hoewel veel inspanningen zijn geleverd om zandtransport vergelijkingen geschikt te maken voor kustgebieden, blijven de ruimtelijk-temporele complexiteit van bodemvocht en tal van andere beperkende factoren de voorspellende kwaliteit dergelijke vergelijkingen ernstig belemmeren.

Nauwkeurige en gelijktijdige empirische metingen van eolisch transport (saltatie) en windsnelheid aan de grond (schuifsnelheid) zijn zeer lastig om te verkrijgen in kustgebieden. Als gevolg hiervan zijn onafgebroken lange-termijn meetreeksen van eolisch zandtransport niet di-

rect beschikbaar. De uitdaging is om de voordelen van passieve meet methoden, d.w.z. directe meting en langdurige inzet, te combineren met de voordelen van methoden die gebaseerd zijn op actieve (digitale) sensoren, d.w.z. geautomatiseerde werking op (zeer) hoge temporele resoluties. Als nauwkeurige schattingen van eolische zandtransport, en daaraan gerelateerde schattingen van beschikbare hoeveelheden zand voor duinopbouw op de Zandmotor niet kunnen worden gegeven, zijn adequate voorspellingen van duinontwikkeling ook niet mogelijk. Bovendien zijn er relatief weinig empirische gegevens beschikbaar over de elkaar versterkende wisselwerking tussen de groei van helmgras en stuivend zand. Veld metingen, aan de reactie van helmgras op het begraven van zand, wat optimale of maximale begraving niveaus zijn, of wat het vermogen is om met ongunstige om te gaan, zijn schaars of incompleet. Als gevolg hiervan kunnen studies, die de ontwikkeling van kustduinen modelleren en daarbij rekening houden met positieve feedback, worden belemmerd door het gebruik van groei functies voor helmgras die niet zijn gevalideerd door metingen in het veld.

Het is onderzocht in hoeverre de Zandmotor bijdraagt aan het creëren van zgn. accommodatie ruimte die gunstig is voor duinontwikkeling, d.w.z. beschikbare ruimte voor duinontwikkeling dat is beschut tegen frequente stormvloeden en een gestage ophoping van stuivend zand kent. Vergeleken met de rest van de Delflandse kust biedt het strand van de Zandmotor zeer brede gunstige accommodatie ruimte en ondersteunt het daarmee vooral een hoog potentieel voor de ontwikkeling van nieuwe embryonale duinen. Door veranderingen in bedekking van duinen door helmgras (2016 t/m 2017) te vergelijken met de gemiddelde jaarlijkse verandering in duinhoogte (2013 t/m 2017), bleek dat duinen vrijwel uitsluitend aanwezig zijn in gebieden die gekenmerkt worden met een positief zandbudget. Dit toont het belang aan van positieve bio-geomorfologische feedback bij het sturen van duinontwikkeling. Hoewel de hoge constructie hoogte misschien niet optimaal is voor een succesvolle vestiging van helmgras, onderstrepen de resultaten het algemene belang van de Zandmotor voor het ontwikkelingspotentieel van duinen. Echter, vanwege aanhoudende antropogene verstoringen als gevolg van zowel recreatie als natuurbeheer, bereikt duinontwikkeling langs deze verstedelijkte kustlijn mogelijk niet zijn volledige potentieel.

Met behulp van een nieuw ontwikkelde geautomatiseerde stuifzandvanger, in combinatie met gedetailleerde windsnelheid metingen, is een onafgebroken lange-termijn meetreeks van eolisch zandtransport (saltatie massaflux) en windkracht aan de grond (schuifsnelheid) opgesteld. Niet-lineaire kwantielregressieanalyse geeft aan dat de saltatie massaflux beter verklaard kan worden door een kwadratische dan een kubische afhankelijkheid van de schuifsnelheid. Regressie-parameters, verkregen in de bovenste percentielen van de meetverdeling, zijn in overeenstemming met de parameters die worden gebruikt door de kwadratische functie van Kok et al. (2012), wat resulteert in meer consistente saltatie schattingen dan voorspeld door de kubische functie van Kawamura (1951). Regressie van de kwadratische en kubieke functies door de mediaan van de meetverdeling laat zien dat schattingen van saltatie op (gesuppleerde) stranden doorgaans twee ordes (voor kwadratische afhankelijkheid) of drie ordes (voor kubische afhankelijkheid) van grootte lager kunnen zijn dan geschat door traditionele zandtransport vergelijkingen. De onderschatting van de saltatie massaflux neemt af wanneer de kwadratische en kubische functies worden aangepast aan de waarnemingen gedaan onder optimale veldomstandigheden, maar de nog steeds lagere waargenomen hoeveelheden saltatie geven aan dat

eolisch transportdynamiek op de Zandmotor kan worden gekenmerkt door een aanhoudende invloed van zandtransport beperkende omstandigheden. Het parameteriseren van de massaflux parameter C van zowel de kwadratische als de kubische vergelijking, levert een maatstaf om rekening te houden met de algehele impact van dergelijke beperkende factoren. Dit maakt een meer realistische schatting van de saltatie massaflux mogelijk, dat beter de omstandigheden reflecteert die van invloed zijn op zandtransport op de Zandmotor en gesuppleerde stranden in het algemeen.

Om de toepasbaarheid van eolische zandtransport vergelijkingen beter toepasbaar te maken voor kustgebieden, is het van cruciaal belang om rekening te houden met de invloed van de natheid van het het strand. Een benadering om dit te bereiken is door de drempelwaarde voor schuifsnelheid waarop zand kan gaan stuiven afhankelijk te maken van de mate van de natheid van het strandoppervlak. Het is tijdens dit onderzoek aangetoond dat, bij bepaalde golflengten, optische remote sensing gebruikt kan worden om ruimtelijk patronen van oppervlakkig bodemvocht met een hoge nauwkeurigheid af te leiden. Het effect van bodemvocht op de spectrale reflectie van strandzand kan zowel met een optisch als een bodem-fysisch model worden beschreven. Het eerste model is gebaseerd op optica en beschrijft de proportionele bijdrage van verstrooiing en absorptie van licht in water dat in de poriën zit van een onverzadigde zand matrix. Het tweede model is gebaseerd op bodem-fysica en koppelt het hydraulische gedrag van poriënwater in een onverzadigde zandmatrix aan zijn optische eigenschappen. Golflengtes in het (nabij) infrarood blijken het meest effectief om het vochtgehalte aan het oppervlak te relateren aan reflectie. Dit is vanwege de sterke absorptie van licht in water, met name op de waterabsorptiepieken rond 1470 en 1940 nm. Vanwege de sterke absorptie van zonlicht door de atmosfeer is een actieve remote sensing techniek echter vereist bij deze golflengtes. Dit onderzoek toont aan dat een terrestrische laserscanner, die opereert op de golflengte $\lambda = 1550$ nm, in staat is om nauwkeurige oppervlaktevochtkaarten af te leiden met een hoge ruimtelijke en temporele resoluties. Dit kan helpen om een beter inzicht te krijgen in de controle die de natheid van het het strandoppervlak uitoefent op de eolische zandtransport dynamiek.

Europees helmgras (*Ammophila arenaria*) bezit twee eigenschappen die op unieke wijze bijdragen aan de ontwikkeling van kustduinen: (1) een zeer hoge tolerantie voor begraving in stuivend zand, en (2) een krachtigere groei door een positieve terugkoppelingsreactie op begraving door stuivend zand. Met behulp van zeer gedetailleerde ruimtelijke gegevens (hoogtemodellen en nabij-infraroodbeelden) die zijn verkregen met een drone en geanalyseerd m.b.v. niet-lineaire kwantielregressie, is aangetoond dat de groeireactie van helmgras op begraving door stuivend zand, uitgedrukt door veranderingen in vegetatiestatus (zgn. Normalized Difference Vegetation Index (Δ NDVI)) en vegetatiebedekking (Δ Cover), kan worden beschreven met een Gaussische functie. De regressiecurves geven een optimale begraving voor helmgras aan van 0,31 meter zand per groeiseizoen, en suggereren (door extrapolatie van de gegevens) een maximale begravingstolerantie tussen 0,78 en 0,96 meter zand per groeiseizoen. De groeifunctie parameters die in dit onderzoek zijn gevonden, zijn specifiek voor de Zandmotor en zijn waarschijnlijk niet algemeen toepasbaar om de groeireactie van helmgras op begraving van stuifzand te beschrijven. De parameters kunnen echter wel representatief zijn voor veel duinen die langs de Nederlandse kust worden aangetroffen, aangezien de hoeveelheden instuivend zand

waarop de functieparameters zijn gebaseerd representatief zijn voor Nederlandse gesuppleerde kusten.

Tijdens dit onderzoek zijn veld metingen aan stuivend zand en de topografie van voorduinen synchroon verkregen, zodat het mogelijk was om eolisch zandtransport direct te relateren aan duinontwikkeling. Zandbudgetanalyse toont aan dat over het algemeen slechts een kleine hoeveelheid stuivend zand dat vanaf de Zandmotor naar de duinen wordt geblazen, blijvend wordt afgezet in de duinen en zo beschikbaar komt voor duinontwikkeling. De grootste hoeveelheid zandafzetting vond plaats rond de zeewaarts gerichte vegetatiegrens van helmgras, wat het belang onderstreept van helmgras om stuivend zand in te vangen en te stabiliseren. Hoewel positieve bio-geomorfologishe terugkoppeling tussen de groeireactie van helmgras op stuivend zand van fundamenteel belang is duinontwikkeling, blijft het vaak een onderbelicht en daardoor onbekend component binnen het kust-duin systeem. Meer aandacht besteden aan het vermogen van helmgras om duinen te ontwikkelen is gunstig voor het kustbeheer in Nederland: door stranden zodanig te suppleren dat het de groeireactie van helmgras op stuivend zand maximaliseert, wordt het potentieel van kustduinen om zich te ontwikkelen en kustveiligheid te bieden ook maximaal benut.

Acknowledgements

Obviously I would not have been able do this work all by myself; accomplishing a PhD is very much a team effort and I owe a debt of gratitude to a lot of people. First of all I want to thank Coen en Michel for giving me their confidence to start this journey and supporting me throughout the way. I know I must have tested your patience these last few years, waiting on me to (finally!) finish my thesis. Marinka, I very much enjoyed working closely with you and have fond memories of all the field trips we took to Texel, Terschelling and the Zandmotor. I just like to forget that one time I put gasoline in a diesel engine and we had to be towed to a garage to get the car repaired. Also lets not talk about those two times I accidentally drove onto the Afsluitdijk and we had to drive an extra 30 km to reach our destination. And yes, it was me who scared that seal away, sorry about that :) Also, you are right; vegetarian meals are not that boring.

All the time spent in the office would quickly have gotten very dull without my colleagues and office mates of the chair group. Joep, Ate, Sija, Celia, Niels, Rens and all others, many thanks for all the fun & games during work hours, including those long wandering walks around the campus. I don't think we left any stone unturned during our discussions, whether it was about science or sillier things in life. I want to especially thank Harm, Piet, Dirk, and Gerben for all their technical support and scientific feedback. Without you it would have been very difficult to get all the equipment up and running and carry out the field experiments. For the support I got from my co-authors, thank you for your indispensable contributions and critical feedback.

The Unmanned Aerial Remote Sensing Facility of WUR has been instrumental for doing my research. Besides it being a lot of fun, I found it very inspiring to be a member of the team. Lammert, Juha, Jappe, Henk, Sander and Saskia, thank you for making this possible! As part of the NatureCoast research project, I worked with a large interdisciplinary team of people studying the Zandmotor. Guys, I very much enjoyed our time together and learning to see the Zandmotor from all these different perspectives!

And last not but not least, Coleen, thanks for always having my back. Without your insight and encouragement I may not have reached the finish line. Now onto our next adventures!

About the author

Corjan Nolet was born on December 26, 1980 in Oud-Beijerland, the Netherlands. Most of his childhood he lived in the small coastal village Burgh-Haamstede, where his attachment to the beach and dunes was shaped from an early age. He obtained his Master's degree in International Land and Water Management at Wageningen University in 2011. For his internship, he went to the Dutch Antilles Island of Bonaire to investigate the emission and deposition of fine dust from various environmental sources. He studied the effect of surface moisture on aeolian transport processes for his thesis. After graduating he briefly worked at an organic farm.

From late 2013, Corjan embarked on his PhD research with the Soil Physics and Land Management Group at Wageningen University. His research focused on coastal aeolian processes and dune vegetation dynamics. He combined his interest for tinkering with electronics with his research, for example by designing his own automated sand traps and using near-infrared drone flights to study the evolution of the foredunes along the Zandmotor. Through his research Corjan has gained considerable experience in remote sensing techniques and geospatial data analysis.

Corjan is now focusing on remote sensing and GIS for Water Resources Management with FutureWater, a research and consultancy company based in Wageningen. Here he continues

to develop valuable technical skills, related to statistical analysis of large spatial climate data sets, as well as teaching skills, for example by conducting training courses of the use of open-source GIS software and supervising students during their internship.

Corjan currently lives in Wageningen with his partner Coleen and their two-year old daughter Elis. A cat named Momo has also decided that she is part of the family.

Peer-reviewed journal publications

Carranza, C., Nolet, C., Pezij, M., and van der Ploeg, M. J. (2020). Estimating root zone soil moisture with Random Forests, journal of Hydrology X, accepted

Nolet, C. and Riksen, M. J. (2019). Accommodation space indicates dune development potential along an urbanized and frequently nourished coastline, *Earth Surface Dynamics* 7, 129–145

Goossens, D., Nolet, C., Etyemezian, V., Duarte-Campos, L., Bakker, G., and Riksen, M. (2018). Field testing, comparison, and discussion of five aeolian sand transport measuring devices operating on different measuring principles, *Aeolian research* 32, 1–13

Nolet, C., van Puijenbroek, M., Suomalainen, J., Limpens, J., and Riksen, M. (2018). UAV-imaging to model growth response of marram grass to sand burial: Implications for coastal dune development, *Aeolian Research* 31, 50–61

Van Puijenbroek, M. E., Nolet, C., De Groot, A. V., Suomalainen, J. M., Riksen, M. J., Berendse, F., and Limpens, J. (2017b). Exploring the contributions of vegetation and dune size to early dune development using unmanned aerial vehicle (UAV) imaging, *Biogeosciences* 14, 5533

Nolet, C., Poortinga, A., Roosjen, P., Bartholomeus, H., and Ruessink, G. (2014). Measuring and modeling the effect of surface moisture on the spectral reflectance of coastal beach sand, *PloS one* 9, e112 151

PE&RC Training and Education Statement

With the training and education activities listed below the PhD candidate has complied with the requirements set by the C.T. de Wit Graduate School for Production Ecology and Resource Conservation (PE&RC) which comprises of a minimum total of 32 ECTS (= 22 weeks of activities)

Review of literature (4.5 ECTS)

- How positive plant-sand feedback interaction drives coastal dune development (2014)

Writing of project proposal (4.5 ECTS)

- Bio-geomorphology of primary coastal dunes (2013)

Post-graduate courses (3.6 ECTS)

- Introduction to R for statistical analysis; PE&RC (2013)
- Sampling for mapping; PE&RC (2015)
- Geo-statistics; PE&RC (2015)
- R for big data; PE&RC (2017)

Laboratory training and working visits (3.3 ECTS)

- BNUC-L RPAS license; EuroURC ILT (2014)
- Application of remote sensing techniques at the Zandmotor and Argus video monitoring (2014)

Invited review of (unpublished) journal manuscript (2 ECTS)

- Environmental Monitoring and Assessment: Relationship between spectral reflectance and hydraulic conductivity of fluvial sediments (2017)
- Geomorphology: Biogeomorphological responses of nebkhas to historical long-term land uses in an arid coastal aeolian sedimentary system (2020)

Competence strengthening / skills courses (1.7 ECTS)

- Data management version control; Deltares (2013)
- Hands-on training on course development teaching: geometrical processing and analysis of UAV data; Capita Selecta RS with UAV's (2015)
- Media training camera presentation; STW NatureCoast (2016)
- Management for data files and documents; Library WUR (2016)
- Reviewing a scientific paper; WGS (2017)

PE&RC Annual meetings, seminars and the PE&RC weekend (1.5 ECTS)

- PE&RC First years weekend (2013)
- PE&RC Last years weekend (2017)

Discussion groups / local seminars / other scientific meetings (5.3 ECTS)

- Greenvision lunch meeting: computer-vision and robotics researchers; Environmental Science Group (2014-2015)
- Unmanned aerial remote sensing facility; Wageningen University and Research Centre (2015-2017)
- Lunch discussion meetings; Soil Physics and Land Management Group (2015-2018)

International symposia, workshops and conferences (9.2 ECTS)

- Desertland II conference on desertification and land degradation; oral presentation; Ghent, Belgium (2015)
- The unmanned systems expo conference; oral presentation; The Hague, the Netherlands (2015)
- 9th International conference on aeolian research; oral presentation; Mildura, Australia (2016)
- Annual conference by Netherlands Centre for Coastal Research; poster presentation; Ouddorp, the Netherlands (2016)
- The sand motor conference; poster presentation; The Hague, the Netherlands (2016)

Lecturing / supervision of practical's / tutorials (17.4 ECTS)

- Design in land and water management (2013-2016)
- Introduction to land degradation and remediation (2013-2016)
- Hydrogeology: groundwater Modelling (2013-2017)
- Fundamentals of land management (2015-2017)
- Practicum water (2016)

Supervision of BSc and MSc students (6 ECTS)

- Dynamics of dune development: effects of plants on sand trapping
- Biogeomorphology of dune formation: the mutual interest of the trapping of sand

The research was carried out within the program Nature-driven nourishment of coastal systems (NatureCoast) and funded by technology foundation TTW (grant 12686), applied science division of the Netherlands Organization for Scientific Research (NWO).

Cover design by Stijn